Investigation of Steel-Stringer Bridges: Superstructures and Substructures, Volume I

Final Report
October 2007

Sponsored by
the Iowa Highway Research Board (Project TR-522)
and the Iowa Department of Transportation (CTRE Project 04-184).

ctre
Center for Transportation
Research and Education

IOWA STATE
UNIVERSITY

Iowa State University's Center for Transportation Research and Education is the umbrella organization for the following centers and programs: Bridge Engineering Center • Center for Weather Impacts on Mobility and Safety • Construction Management & Technology • Iowa Local Technical Assistance Program • Iowa Traffic Safety Data Service • Midwest Transportation Consortium • National Concrete Pavement Technology Center • Partnership for Geotechnical Advancement • Roadway Infrastructure Management and Operations Systems • Statewide Urban Design and Specifications • Traffic Safety and Operations

About the Bridge Engineering Center

The mission of the Bridge Engineering Center is to conduct research on bridge technologies to help bridge designers/owners design, build, and maintain long-lasting bridges.

Disclaimer Notice

The contents of this report reflect the views of the authors, who are responsible for the facts and the accuracy of the information presented herein. The opinions, findings and conclusions expressed in this publication are those of the authors and not necessarily those of the sponsors.

The sponsors assume no liability for the contents or use of the information contained in this document. This report does not constitute a standard, specification, or regulation.

The sponsors do not endorse products or manufacturers. Trademarks or manufacturers' names appear in this report only because they are considered essential to the objective of the document.

Nondiscrimination Statement

Iowa State University does not discriminate on the basis of race, color, age, religion, national origin, sexual orientation, gender identity, sex, marital status, disability, or status as a U.S. veteran. Inquiries can be directed to the Director of Equal Opportunity and Diversity, (515) 294-7612.

Technical Report Documentation Page

1. Report No. IHRB Project TR-522	2. Government Accession No.	3. Recipient's Catalog No.	
4. Title and Subtitle Investigation of Steel-Stringer Bridges: Superstructures and Substructures, Volume I		5. Report Date October 2007 6. Performing Organization Code	
7. Author(s) Terry J. Wipf, F. Wayne Klaiber, David J. White, Jeremy Koskie		8. Performing Organization Report No. CTRE Project 04-184	
9. Performing Organization Name and Address Center for Transportation Research and Education Iowa State University 2901 South Loop Drive, Suite 3100 Ames, IA 50010-8634		10. Work Unit No. (TRAIS) 11. Contract or Grant No.	
12. Sponsoring Organization Name and Address Iowa Department of Transportation 800 Lincoln Way Ames, IA 50010		13. Type of Report and Period Covered Final Report 14. Sponsoring Agency Code	
15. Supplementary Notes			

16. Abstract

There are hundreds of structurally deficient or functionally obsolete bridges in the state of Iowa. With the majority of these bridges located on rural county roads where there is limited funding available to replace the bridges, diagnostic load testing can be utilized to determine the actual load carrying capacity of the bridge. One particular family or fleet of bridges that has been determined to be desirable for load testing consists of single-span bridges with non-composite, cast-in-place concrete decks, steel stringers, and timber substructures.

Six bridges with poor performing superstructure and substructure from the aforementioned family of bridges were selected to be load tested. The six bridges were located on rural roads in five different counties in Iowa: Boone, Carroll, Humboldt, Mahaska, and Marshall. Volume I of this report presents diagnostic load tests on the superstructure of the six bridges. The results of the diagnostic load tests were used to calibrate analytical models of the bridges for rating purposes. All of the bridges were independently rated by three rating agencies using a codified approach. Those ratings were then compared to ratings calculated using a bridge model calibrated to the actual response of the bridge due to the load test. The calibrated bridge model was then used to rate the bridges and determine whether an increase in the initial codified bridge ratings was feasible.

Volume I of this report focuses on evaluating the superstructure for this family of bridges. This volume discusses the behavior characteristics that influence the load carrying capacity of this fleet of bridges. In particular, the live load distribution, partial composite action, and bearing restraint were investigated as potential factors that could influence the bridge ratings. Implementing fleet management practices, the bridges were analyzed to determine if the load test results could be predicted to better analyze previously untested bridges. For this family of bridges it was found that the ratings increased as a result of the load testing demonstrating a greater capacity than determined analytically. Volume II of this report focuses on evaluating the timber substructure for this family of bridges. In this volume, procedures for detecting pile internal decay using nondestructive ultrasonic stress wave techniques, correlating nondestructive ultrasonic stress wave techniques to axial compression tests to estimate deteriorated pile residual strength, and evaluating load distribution through poor performing timber substructure elements by instrumenting and load testing the abutments of the six selected bridges are discussed. Also, in this volume pile repair methods for restoring axial and bending capacities of pile are developed and evaluated.

17. Key Words field testing— diagnostic load testing—load rating— non-composite steel girder bridge		18. Distribution Statement No restrictions.	
19. Security Classification (of this report) Unclassified.	20. Security Classification (of this page) Unclassified.	21. No. of Pages 191	22. Price NA

Form DOT F 1700.7 (8-72) **Reproduction of completed page authorized**

INVESTIGATION OF STEEL-STRINGER BRIDGES: SUPERSTRUCTURES AND SUBSTRUCTURES, VOLUME I

Final Report
October 2007

Principal Investigator
F. Wayne Klaiber
Professor, Department of Civil, Construction, and Environmental Engineering
Iowa State University

Co-Principal Investigators
David J. White
Associate Professor, Department of Civil, Construction, and Environmental Engineering
Iowa State University

Terry J. Wipf
Professor, Department of Civil, Construction, and Environmental Engineering
Iowa State University

Research Assistants
Jeremy Koskie
Mohamed Mekkawy

Sponsored by
the Iowa Highway Research Board
(IHRB Project TR-522)

Preparation of this report was financed in part
through funds provided by the Iowa Department of Transportation
through its research management agreement with the
Center for Transportation Research and Education
CTRE Project 04-184.

Center for Transportation Research and Education
Iowa State University
2901 South Loop Drive, Suite 3100
Ames, IA 50010-8632
Phone: 515-294-8103
Fax: 515-294-0467
www.ctre.iastate.edu

TABLE OF CONTENTS

ACKNOWLEDGMENTS XV

EXECUTIVE SUMMARY XII

1. INTRODUCTION 1

2. LITERATURE REVIEW 3

2.1 Bridge Rating and Posting 3
2.1.1 Iowa Department of Transportation Rating Vehicles 3
2.1.2 ASD Rating 6
2.1.3 LFD Rating 6
2.1.4 LRFR Rating 7
2.2 Load Testing 7
2.2.1 Load Testing in the United States and Abroad 7
2.2.2 Methodology 8
2.3 Benefits of Load Testing 9
2.3.1 Girder Distribution Factors 10
2.3.2 Material Properties 10
2.3.3 Curbs and Railings 10
2.3.4 Bearing Restraint 10
2.3.5 Partial Composite Action 11
2.4 Load Rating Using Load Test Results 13
2.4.1 Extrapolation 13
2.4.2 Lichtenstein's Approach 14
2.4.3 Barker's Approach 16
2.4.4 BDI Approach 19
2.5 Load Testing Examples 20
2.5.1 Overweight Load Responses (Schultz et al., 1998). 20
2.5.2 Economical Bridge Testing (Chajes et al. 1996) 21
2.5.3 Short – Span Steel Bridges (Stallings and Yoo, 1997) 21

3. BOONE COUNTY BRIDGE (BCB) 24

3.1 Bridge Description 24
3.2 Test Setup 27
3.2.1 Test Truck 27
3.2.2 Testing Plan and Instrumentation 27
3.3 Bridge Analysis 30
3.3.1 Neutral Axis and Partial Composite Action 30
3.3.2 Load Distribution 38
3.3.3 Moment of Inertia 39

3.4 BDI Optimization 41
3.5 Bridge Rating 48
3.5.1 Conventional Rating 48
3.5.2 Rating Using Optimized Parameters From BDI Software 49

4. MARSHALL COUNTY BRIDGE (MCB) 51

4.1 Bridge Description 51
4.2 Test Setup 53
4.2.1 Test Truck 53
4.2.2 Testing Plan and Instrumentation 53
4.3 Bridge Analysis 55
4.3.1 Neutral Axis and Partial Composite Action 55
4.3.2 Load Distribution 63
4.3.3 Moment of Inertia 66
4.4 BDI Optimization 66
4.5 Bridge Rating 72
4.5.1 Conventional Rating 72
4.5.2 Rating Using Optimized Parameters From BDI Software 73

5. MAHASKA (350) COUNTY BRIDGE (KCB1) 75

5.1 Bridge Description 75
5.2 Test Setup 77
5.2.1 Test Truck 77
5.2.2 Testing Plan and Instrumentation 78
5.3 Bridge Analysis 80
5.3.1 Neutral Axis and Partial Composite Action 80
5.3.2 Load Distribution 85
5.3.3 Moment of Inertia 86
5.4 BDI Optimization 87
5.5 Bridge Rating 92
5.5.1 Conventional Rating 92
5.5.2 Rating Using Optimized Parameters From BDI Software 93

6. CARROLL COUNTY BRIDGE (CCB) 95

6.1 Bridge Description 95
6.2 Test Setup 97
6.2.1 Test Truck 97
6.2.2 Testing Plan and Instrumentation 97
6.3 Bridge Analysis 100
6.3.1 Neutral Axis and Partial Composite Action 100
6.3.2 Load Distribution 107
6.3.3 Moment of Inertia 108
6.4 BDI Optimization 109

6.5 Bridge Rating 113
6.5.1 Conventional Rating 113
6.5.2 Rating Using Optimized Parameters From BDI Software 113

7. MAHASKA (380) COUNTY BRIDGE (KCB2) 115

7.1 Bridge Description 115
7.2 Test Setup 117
7.2.1 Test Truck 117
7.2.2 Testing Plan and Instrumentation 118
7.3 Bridge Analysis 120
7.3.1 Neutral Axis and Partial Composite Action 120
7.3.2 Load Distribution 127
7.3.3 Moment of Inertia 128
7.4 BDI Optimization 128
7.5 Bridge Rating 133
7.5.1 Conventional Rating 133
7.5.2 Rating Using Optimized Parameters From BDI Software 134

8. HUMBOLDT COUNTY BRIDGE (HCB) 136

8.1 Bridge Description 136
8.2 Test Setup 138
8.2.1 Test Truck 138
8.2.2 Testing Plan and Instrumentation 138
8.3 Bridge Analysis 141
8.3.1 Neutral Axis and Partial Composite Action 141
8.3.2 Load Distribution 148
8.3.3 Moment of Inertia 150
8.4 BDI Optimization 150
8.5 Bridge Rating 154
8.5.1 Conventional Rating 154
8.5.2 Rating Using Optimized Parameters From BDI Software 154
8.6 Superstructure Response to Destructive Substructure Testing 155
8.6.1 Test Setup 156
8.6.2 Destructive Testing Sequence 157
8.6.3 Destructive Test Results 158

9. SUMMARY OF LOAD TESTING RESULTS 163

9.1 Factors Influencing Bridge Response and Ratings 163
9.1.1 Live Load Distribution Summary 163
9.1.2 Partial Composite Action Summary 164
9.1.3 Bearing Restraint Summary 165
9.2 Bridge Rating Summary 165

10. CONCLUSIONS AND RECOMMENDATIONS 167

10.1 Summary 167
10.2 Conclusions 167
10.3 Recommendations 168

REFERENCES 169

LIST OF FIGURES

Figure 2.1. Iowa DOT Design Vehicles. 4
Figure 2.2. Load-Deflection Curve for a Girder With Composite Action. 12
Figure 2.3. Partially Composite Girder Stress Profile. 18
Figure 2.4. Girder - Concrete Stress Profile. 18
Figure 3.1. BCB Alignment View Looking South. 24
Figure 3.3. Typical Girder Bearing. 25
Figure 3.4. BCB Deterioration. 26
Figure 3.5. BCB Repairs. 26
Figure 3.6. Cross Section of BCB Looking North. 27
Figure 3.7. BCB Test Truck. 28
Figure 3.8. BCB Test Truck Dimensions. 28
Figure 3.9. Plan View of Loading Lanes Used in BCB Test 29
Figure 3.10. Location of BCB Quarter Points and Abutment Centerlines. 29
Figure 3.11. BCB Truck Tandem Centroid Centered Over Abutment. 30
Figure 3.12. Instrumentation Near Abutment of BCB 31
Figure 3.13. BCB North and South End Transducer Locations Looking North 31
Figure 3.14. BCB Midspan Transducer Locations Looking North. 31
Figure 3.15. Concrete and Steel Mounted Transducers at Midspan of BCB. 32
Figure 3.16. BCB Lane 1 Strains and Deflections 33
Figure 3.17. BCB Lane 2 Strains and Deflections 34
Figure 3.18. BCB Lane 3 Strains and Deflections 35
Figure 3.19. BCB Neutral Axis Locations. 37
Figure 3.20. Effective Section. 40
Figure 3.21. BCB Effective Moments of Inertia. 41
Figure 3.22. BCB Girder 1 Optimized Strain Comparison. 43
Figure 3.23. BCB Girder 2 Optimized Strain Comparison. 43
Figure 3.24. BCB Girder 3 Optimized Strain Comparison. 44
Figure 3.25. BCB Girder 4 Optimized Strain Comparison. 44
Figure 3.26. BCB Girder 5 Optimized Strain Comparison. 45
Figure 3.27. BCB Girder 6 Optimized Strain Comparison. 45
Figure 3.28. BCB Spring Constant Comparison for Lane 1 Girder 1. 47
Figure 3.29. BCB Girder 1 Lane 1 Maximum Strain for Varying Spring Constants. 47
Figure 4.1. MCB Alignment View Looking North. 51
Figure 4.2. MCB Girder 2 Deterioration and Delamination. 52
Figure 4.3. MCB Core Locations and Retrieved Core Specimen. 52
Figure 4.4. Cross Section of MCB Looking North. 53
Figure 4.5. MCB Test Truck. 54
Figure 4.6. MCB Test Truck Dimensions. 54
Figure 4.7. Plan View and Loading Lanes Used in MCB Test. 55
Figure 4.8. Instrumentation Near Abutment of MCB. 56
Figure 4.9. MCB North and South End Transducer Locations Looking North. 56
Figure 4.10. MCB Midspan Transducer Locations Looking North. 56
Figure 4.11. MCB Removal of Excess Corrosion for Transducer Application. 57
Figure 4.12. MCB Lane 1 Strains and Deflections. 58

Figure 4.13. MCB Lane 2 Strains and Deflections. 59
Figure 4.14. MCB Lane 3 Strains and Deflections. 60
Figure 4.15. MCB Lane 4 Strains and Deflections. 61
Figure 4.16. MCB Neutral Axis Locations. 62
Figure 4.17. Exposed Top Flanges After MCB Deck Demolition. 63
Figure 4.18. MCB Effective Moments of Inertia. 67
Figure 4.19. MCB Girder 1 Optimized Strain Comparison. 69
Figure 4.20. MCB Girder 2 Optimized Strain Comparison. 69
Figure 4.21. MCB Girder 3 Optimized Strain Comparison. 70
Figure 4.22. MCB Girder 4 Optimized Strain Comparison. 70
Figure 4.23. MCB Girder 5 Optimized Strain Comparison. 71
Figure 4.24. MCB Girder 6 Optimized Strain Comparison. 71
Figure 5.1. KCB1 Alignment View Looking North. 75
Figure 5.2. KCB1 Poor Concrete Consolidation. 76
Figure 5.3. KCB1 Deck Crack. 76
Figure 5.4. KCB1 Cross Section Looking North. 77
Figure 5.5. KCB1 Test Truck. 77
Figure 5.6. KCB1 Test Truck Dimensions. 78
Figure 5.7. KCB1 Plan View Loading Lanes Used in KCB1 Test. 79
Figure 5.8. KCB1 North and South End Transducer Locations Looking North. 79
Figure 5.9. KCB1 Midspan Transducer Locations Looking North. 79
Figure 5.10. KCB1 Lane 1 Strains and Deflections. 81
Figure 5.11. KCB1 Lane 2 Strains and Deflections. 82
Figure 5.12. KCB1 Lane 3 Strains and Deflections. 83
Figure 5.13. KCB1 Neutral Axis Locations. 84
Figure 5.14. KCB1 Effective Moments of Inertia. 87
Figure 5.15. KCB1 Girder 1 Optimized Strain Comparison. 89
Figure 5.16. KCB1 Girder 2 Optimized Strain Comparison. 90
Figure 5.17. KCB1 Girder 3 Optimized Strain Comparison. 90
Figure 5.18. KCB1 Girder 4 Optimized Strain Comparison. 91
Figure 5.19. KCB1 Girder 5 Optimized Strain Comparison. 91
Figure 6.1. CCB Alignment View Looking North. 95
Figure 6.2. Asphalt Patches in CCB Concrete Deck. 96
Figure 6.3. CCB Cross Section Looking North. 96
Figure 6.4. CCB Test Truck Dimensions. 97
Figure 6.5. CCB Plan View Loading Lanes. 98
Figure 6.6. CCB Bearing Transducer Locations. 99
Figure 6.7. CCB North End and Quarter Point Transducer Locations Looking North. 99
Figure 6.8. CCB Midspan Transducer Locations Looking North. 99
Figure 6.9. CCB South End Transducer Locations Looking North. 100
Figure 6.10. CCB Lane 1 Strains and Deflections. 101
Figure 6.11. CCB Lane 2 Strains and Deflections. 102
Figure 6.12. CCB Lane 3 Strains and Deflections. 103
Figure 6.13. CCB Lane 4 Strains and Deflections. 104
Figure 6.14. CCB Lane 5 Strains and Deflections. 105
Figure 6.15. CCB Neutral Axis Locations. 106

Figure 6.16. CCB Girder 1 Optimized Strain Comparison. 111
Figure 6.17. CCB Girder 2 Optimized Strain Comparison. 111
Figure 6.18. CCB Girder 3 Optimized Strain Comparison. 112
Figure 6.19. CCB Girder 4 Optimized Strain Comparison. 112
Figure 7.1. KCB2 Alignment View Looking Northwest. 115
Figure 7.2. KCB2 Pile Deterioration. 116
Figure 7.3. KCB2 Railing Damage. 116
Figure 7.4. Cross Section of KCB2 Looking Northwest. 117
Figure 7.5. KCB2 Test Truck. 117
Figure 7.6. KCB2 Test Truck Dimensions. 118
Figure 7.7. Plan View of Loading Lanes Used in KCB2 Test. 119
Figure 7.8. KCB2 Northeast, Southwest, and Quarter Point Transducer Locations Looking Northwest. 119
Figure 7.9. KCB2 Midspan Transducer Locations Looking Northwest. 119
Figure 7.10. KCB2 Lane 1 Strains and Deflections. 121
Figure 7.11. KCB2 Lane 2 Strains and Deflections. 122
Figure 7.12. KCB2 Lane 3 Strains and Deflections. 123
Figure 7.13. KCB2 Lane 4 Strains and Deflections. 124
Figure 7.14. KCB2 Lane 5 Strains and Deflections. 125
Figure 7.15. KCB2 Neutral Axis Locations. 126
Figure 7.16. KCB3 Girder 1 Optimized Strain Comparison. 130
Figure 7.17. KCB2 Girder 2 Optimized Strain Comparison. 131
Figure 7.18. KCB2 Girder 3 Optimized Strain Comparison. 131
Figure 7.19. KCB2 Girder 4 Optimized Strain Comparison. 132
Figure 7.20. KCB2 Girder 5 Optimized Strain Comparison. 132
Figure 8.1. HCB Alignment View Looking West. 136
Figure 8.2. HCB Elevation View of Bridge Looking North. 137
Figure 8.3. Cross Section of HCB Looking West. 137
Figure 8.4. HCB Test Truck Crossing Bridge After Pier Removal. 138
Figure 8.5. HCB Test Truck Dimensions 139
Figure 8.6. HCB Plan View Loading Lanes 139
Figure 8.7. HCB Test Truck in Lane 3. 140
Figure 8.8. HCB East End and Quarter Point Transducer Locations Looking West. 140
Figure 8.9. HCB Midspan Transducer Locations Looking West. 141
Figure 8.10. HCB West End Transducer Locations Looking West. 141
Figure 8.11. HCB Lane 1 Strains and Deflections. 142
Figure 8.12. HCB Lane 2 Strains and Deflections. 143
Figure 8.13. HCB Lane 3 Strains and Deflections. 144
Figure 8.14. HCB Lane 4 Strains and Deflections. 145
Figure 8.15. HCB Lane 5 Strains and Deflections. 146
Figure 8.16.HCB Neutral Axis Locations. 147
Figure 8.17. HCB Girder 1 Optimized Strain Comparison. 152
Figure 8.18. HCB Girder 2 Optimized Strain Comparison. 152
Figure 8.19. HCB Girder 3 Optimized Strain Comparison. 153
Figure 8.20. HCB Girder 4 Optimized Strain Comparison. 153
Figure 8.21. HCB East Abutment Cross Section. 156

Figure 8.22. Photograph Showing Sections of Piles 3 and 7 Removed from HCB.....157
Figure 8.23. Photograph Showing Sections of Piles 6 and 7 Removed from HCB.....158
Figure 8.24. HCB Lane 1 Destructive Testing Strain Profile at Midspan.....159
Figure 8.25. HCB Lane 3 Destructive Testing Strain Profile at Midspan.....159
Figure 8.26. HCB Lane 5 Destructive Testing Strain Profile at Midspan.....160
Figure 8.27. HCB Destructive Testing Lane 1 Strain Profile at East Abutment.....160
Figure 8.28. HCB Destructive Testing Lane 3 Strain Profile at East Abutment.....161
Figure 8.29. HCB Destructive Testing Lane 5 Strain Profile at East Abutment.....161

LIST OF TABLES

Table 2.1. Values for K_{b1}. 15
Table 2.2. Values for K_{b2}. 15
Table 2.3. Values for K_{b3}. 15
Table 2.4. Error Functions. 19
Table 3.1. BCB Test Truck Weights. 27
Table 3.2. BCB Maximum Strains Obtained. 36
Table 3.3. BCB Midspan Strains. 36
Table 3.4. BCB Induced Truck Moments. 38
Table 3.5. BCB Maximum Single Lane Percent Distributions. 38
Table 3.6. BCB Calculated Distribution Factors. 39
Table 3.7. BCB Distribution Ratios. 39
Table 3.8. BCB Moments of Inertia (in^4). 40
Table 3.9. BCB Optimization Parameters. 42
Table 3.10. BCB Optimized Parameters Using All Steel Transducers. 42
Table 3.11. BCB Bottom Flange Strain Scale Error and Correlation. 46
Table 3.12. BCB Analytical Ratings. 48
Table 3.13. BCB Optimized Ratings. 49
Table 3.14. BCB Operating Rating Percent Increase After Optimization 50
Table 4.1. MCB Truck Weights. 53
Table 4.2. MCB Induced Truck Moments. 64
Table 4.3. MCB Maximum Single Lane Strain Based Percent Distributions. 64
Table 4.4. MCB Maximum Single Lane Deflection Based Percent Distributions. 65
Table 4.5. MCB Calculated Distribution Factors. 65
Table 4.6. MCB Distribution Ratios. 65
Table 4.7. MCB Moments of Inertia (in^4). 66
Table 4.8. MCB Optimization Parameters. 68
Table 4.9. MCB Optimized Parameters Using All Steel Transducers 68
Table 4.10. MCB Bottom Flange Strain Scale Error and Correlation. 72
Table 4.11. MCB Analytical Bridge Ratings. 73
Table 4.12. MCB Optimized Ratings. 74
Table 4.13. MCB Operating Rating Percent Increase After Optimization. 74
Table 5.1. KCB1 Truck Weights. 78
Table 5.2. KCB1 Induced Truck Moments. 85

Table 5.3. KCB1 Maximum Single Lane Percent Distributions. 85
Table 5.4. KCB1 Calculated Single Lane Distribution Factors. 86
Table 5.5. KCB1 Distribution Ratios. 86
Table 5.6. KCB1 Moments of Inertia (in^4) 86
Table 5.7. KCB1 Optimization Parameters. 88
Table 5.8. KCB1 Optimized Parameters Using All Steel Transducers. 88
Table 5.9. KCB1 Bottom Flange Strain Scale Error and Correlation. 89
Table 5.10. KCB1 Analytical Bridge Ratings 92
Table 5.11. KCB1 Optimized Ratings. 94
Table 5.12. KCB1 Operating Rating Percent Increase After Optimization. 94
Table 6.1. CCB Truck Weights. 97
Table 6.2. CCB Induced Truck Moments 107
Table 6.3. CCB Maximum Single Lane Percent Distributions. 107
Table 6.4. CCB Calculated Distribution Factors. 108
Table 6.5. CCB Distribution Ratios. 108
Table 6.6. CCB Optimization Parameters. 109
Table 6.7. CCB Optimized Parameters Using All Steel Transducers. 110
Table 6.8. CCB Bottom Flange Strain Scale Error and Correlation. 110
Table 6.9. CCB Analytical Ratings. 113
Table 6.10. CCB Optimized Ratings. 114
Table 6.11. CCB Operating Rating Percent Increase After Optimization. 114
Table 7.1. KCB2 Truck Weights. 118
Table 7.2. KCB2 Induced Truck Moments. 127
Table 7.3. KCB2 Maximum Single Lane Percent Distributions. 127
Table 7.4. KCB2 Calculated Single Lane Distribution Factors. 128
Table 7.5. KCB2 Distribution Ratios. 128
Table 7.6. KCB2 Optimization Parameters. 129
Table 7.7. KCB2 Optimized Parameters Using All Steel Transducers. 129
Table 7.8. KCB2 Bottom Flange Strain Scale Error and Correlation. 130
Table 7.9. KCB2 Analytical Bridge Ratings. 133
Table 7.10. KCB2 Optimized Ratings. 135
Table 7.11. KCB2 Operating Rating Percent Increase After Optimization. 135
Table 8.1. HCB Truck Weights. 138
Table 8.2. HCB Induced Truck Moments 148
Table 8.3. HCB Maximum Single Lane Percent Distributions 148
Table 8.4. HCB Calculated Lane Distribution Factors. 149
Table 8.5. HCB Distribution Ratios. 149
Table 8.6. HCB Optimization Parameters. 151
Table 8.7. HCB Optimized Parameters Using All Steel Transducers. 151
Table 8.8. HCB Bottom Flange Strain Scale Error and Correlation. 151
Table 8.9. HCB Analytical Bridge Ratings 154
Table 8.10. HCB Optimized Ratings. 155
Table 8.11. HCB Operating Rating Percent Increase After Optimization. 156
Table 9.1. Summary of Live Load Distribution Ratios. 163
Table 9.2. Live Load Distribution Ratio Average and Standard Deviation. 163
Table 9.3. Summary of Partial Composite Action 164

Table 9.4. Percent Increase in Operating Bridge Ratings. 165

ACKNOWLEDGMENTS

The investigation presented in this final report was conducted by the Iowa State University Bridge Engineering Center under the auspices of the Center for Transportation Research and Education at Iowa State University. The research was sponsored by the Project Development Division of the Iowa Department of Transportation and Iowa Highway Research Board under Research Project TR-522

The authors wish to thank the various Iowa DOT engineers who helped with this project and provided their input and support. A special thanks is accorded to the following counties and their respective county engineers for their cooperation and assistance with the field tests: Boone County: David Anthony, Carroll County: David Paulson, Humboldt County: Paul Jacobson, Mahaska County: Jerome Nusbaum, and Marshall County: Royce Fitchner.

A special thanks are extended to Mr. Doug Wood, manager of the ISU Structural Engineering Laboratory and the numerous civil engineering graduate and undergraduate students for thir assistance in various aspects of the project.

EXECUTIVE SUMMARY

There are hundreds of structurally deficient or functionally obsolete bridges located within the state if Iowa. With the majority of these bridges located on rural county roads where there is limited funding available to replace the bridges, diagnostic load testing can be utilized to determine the actual load carrying capacity of the bridge. One particular family or fleet of bridges that has been determined to be desirable for load testing consists of single span bridges with non-composite, cast-in-place concrete decks, steel stringers, and timber substructures. This family of bridges is desirable for load testing because the codified ratings are often overly conservative due to the non-composite section properties and assumed simply supported boundary conditions. Furthermore, timber abutments are subjected to physical and biological deterioration, which is difficult to detect and quantify. This deterioration influences the load carrying capacity of timber substructures and thus affects the overall performance of the bridge system.

Six bridges with poor performing superstructure and substructure from the aforementioned family of bridges were selected to be load tested. The six bridges were located on rural roads in five different counties in Iowa: Boone, Carroll, Humboldt, Mahaska, and Marshall. Volume I of this report presents diagnostic load tests on the superstructure of the six bridges. The results of the diagnostic load tests were used to calibrate analytical models of the bridges for rating purposes. All of the bridges were independently rated by three rating agencies using a codified approach. Those ratings were then compared to ratings calculated using a bridge model calibrated to the actual response of the bridge due to the load test. Volume I of this report focuses on evaluating the superstructure for this family of bridges. This volume discusses the behavior characteristics that influence the load carrying capacity of this fleet of bridges. In particular, the live load distribution, partial composite action, and bearing restraint were investigated as potential factors that could influence the bridge ratings. Implementing fleet management practices, the bridges were analyzed to determine if the load test results could be predicted to better analyze previously untested bridges.

Three rating agencies, Iowa Department of Transportation, a private consulting firm, and the research team at Iowa State University, calculated similar bridge ratings base on the load factor rating method. In order to determine the bridge ratings, each of the bridges were modeled and optimized using the load test results. The optimization process aided in the evaluation of the behavior characteristics.

For one of the bridges there was an opportunity to determine the effect of deteriorated substructure elements on the superstructure. The research team was provided the opportunity to perform some destructive testing on the substructure of one of the bridges by removing some of the piles. The removal of the pile sections had no effect on the strains observed in the superstructure. The load distribution in the girders did not change with the removal of the piles.

1. INTRODUCTION

There are over 25,000 bridges in Iowa, and nearly 7,000 of these bridges are structurally deficient or functionally obsolete (National Bridge Inventory, 2004). Structurally deficiency indicates that a structure can no longer carry the required live load due to the deterioration of one or more of the bridge components, whereas functionally obsolete indicates that a bridge is inadequate due to factors such as its width or vertical clearance. A functionally obsolete bridge essentially hinders traffic due to its geometry however primary load carrying members are structurally adequate. Of the nearly 7,000 structurally deficient or functionally obsolete bridges, 86% are located on county roads.

One particular family of bridges that has been determined to be structurally deficient is simply supported, non-composite, steel stringer bridges, with cast-in-place concrete decks. This is a common type of bridge on low volume county highways in Iowa. There are a total of 913 structurally deficient or functionally obsolete composite or non-composite bridges in Iowa (National Bridge Inventory, 2003). This family of bridges is also a good candidate for field testing as it has frequently been determined to have larger capacities than can be determined theoretically. For the safety of the public and to prevent large loads these bridges cannot support, they are often posted. In order to remove or increase bridge postings, load testing can be utilized to determine whether the bridge has additional capacity and thus does not require posting or can be posted at a higher limit.

There are two main types of load testing: diagnostic and proof load testing. A proof load test consists of loading a bridge until a certain predetermined stress or deflection is observed in the bridge. Once the proof load has been determined, the bridge is then rated for that particular load. A diagnostic load test consists of loading a bridge with a predetermined load and measuring the response of the bridge or critical bridge component(s). The response to the diagnostic load test is then used, along with analytical bridge models, to determine the bridge rating. Proof load testing tends to be more costly and time consuming and since it was not implemented in this project it will not be discussed any further.

In this project, six non-composite, single-span bridges on low volume roads in the previously described family were tested. The bridges that were tested were located in Boone, Marshall, Mahaska, Carroll, and Humboldt counties. The objective of the load testing was to determine the behavior characteristics that were similar in all of the bridges such as live load distribution, partial composite action, and bearing restraint. Quantifying these behavior characteristics allows for the extrapolation of predicted behaviors to previously untested bridges. By predicting the behavior of a family of bridges, it becomes possible to modify the rating of the bridge to take advantage of the behavior characteristics. Using the load test results, a computer model of the bridge can be calibrated to determine the bridge ratings for the Iowa Department of Transportation (DOT) rating vehicles. The ratings determined from the calibrated model can then be compared to codified ratings to determine if there is any correlation with codified ratings. This idea of using the results of load testing to apply to previously untested bridges in order to maintain a particular fleet of bridges is referred to as fleet management.

This family of bridges was not limited to the number of girders comprising the superstructure. The Iowa DOT developed a set V-Series of standard plans beginning in the mid 1920's; some of these original V-Series plans ranging from the V1 Series up through the V14 Series were still available. Starting in 1950, a significant change in the V-Series occurred though; in the V9 Series, the Iowa DOT began putting shear lugs, welded angles, on the top of the girders. On top of the welded angle, another bar was welded parallel to the top flange of the girder. Installing the shear lugs created composite action between the concrete deck and the steel girder. As previously mentioned, the family of bridges that was selected for this project were specifically non-composite, therefore the bridges selected for testing were likely from the Iowa DOT V1 to the V8 Series. Plan sets obtained from the Iowa DOT only included the following: V1, V3, V5, and V8 Series.

A procedure for load testing timber pile abutments is provided in Volume II of this report. The V Series bridges consisted of both timber and concrete substructures; however, two different substructure types were not used in the same standard Series. Of the four sets of V Series plans obtained from the Iowa DOT, only the V3 Series had the concrete abutments; it also was the only set to have concrete parapet railings as opposed to the steel railings that were found in the other V Series plans. Only bridges with timber substructures and steel railings were selected for testing; this type of bridge was found only in the V1, V5, and V8 Series.

Of the six bridges selected for load testing, there were two four-girder bridges, two five-girder bridges, and two six-girder bridges. All of the six bridges tested had timber pile abutments supporting the superstructure. The two five-girder bridges were located in Mahaska County and were designed using the V5 Series for an 18-foot roadway width. It is important to differentiate the roadway width, as the 18-foot roadway width was designed using five girders and the 20 foot roadway width was designed using six girders. Another bridge from the V5 series was located in Marshall County; this bridge consisted of six girders and was a modified V5 Series design. It was modified to have a roadway width of 24 feet instead of the specified 20 feet from the standard design. Original plans for this bridge were obtained from the Marshall County Engineers Office. Original plans for the other six girder bridge, located in Boone County, were not found, however the bridge resembled the V5 Series with a 20 foot roadway width. The two four-girder bridges were located in Carroll and Humboldt Counties and were designed using the V8 Series. Two of the bridges that were tested, one from Marshall County and one from Humboldt County, have been removed from service and replaced with a new bridge and a box culvert, respectively.

The Humboldt bridge removal provided an opportunity to do some destructive testing on the substructure. Because of this opportunity, it was decided to determine if the removal of any of the substructure components would result in a change in the load distribution in the superstructure. Piles were removed from one of the abutments of the Humboldt county bridge to determine the load transfer to the other pile elements as well as the effect on the superstructure. Both the piles and the girders were instrumented to determine the change in the load path due to the removal of the substructure elements.

2. LITERATURE REVIEW

2.1 Bridge Rating and Posting

Before any load testing is undertaken, a visual inspection of the bridge must first be completed. Any noticeable deterioration or damage should be documented. Critical bridge components and locations of critical areas on these components should also be determined during the bridge inspection. A bridge obviously should not be tested if catastrophic failure due to loading, such as the yielding of steel girders or failure of a critical member is of any concern. Bridges susceptible to catastrophic failure lack redundancy of major load carrying members or have fracture critical members. In the case of these members, failing the entire structure would result. If a bridge has significant deterioration and cannot support even a light test vehicle, the bridge should also not be tested for fear of catastrophic failure during load testing (Lichtenstein, 1993).

Once the bridge has been inspected, the bridge can be rated using a number of different rating procedures. There are three different rating procedures: an allowable stress design (ASD) rating, a load factor design (LFR) rating, and a load and resistance factor rating (LRFR). The rating equations for ASD, LFR, and LRFR generally have the same form:

$$RF = \frac{\text{Available Capacity For The Live Load Effect}}{\text{Rating Vehicle Load Demand}} \quad (1)$$

where RF is the rating factor for a particular bridge element and the capacity is the theoretical capacity less the dead load effect. Depending on the rating procedure, the capacity differs and is either the factored theoretical capacity or the allowable stress of the bridge component being rated. The dead load is calculated from assumed material properties of the bridge elements that are supported by the bridge component being rated. Material properties typically used for the structural elements are 150 pcf for concrete and 490 pcf for steel. The demand from a rating vehicle on the bridge component that is being rated is determined by placing the vehicle on the bridge where the maximum effect occurs.

There are two types of ratings for bridges, inventory rating and operating rating, where the inventory rating is defined as the vehicle weight that the bridge can support for an indefinite period of time and the operating rating is essentially the maximum vehicle weight that the bridge can support. Inventory ratings often use the same member capacities or allowable stresses as those used in design whereas the member capacities or stresses in the operating rating are often larger than those used in design.

2.1.1 Iowa Department of Transportation Rating Vehicles

The wheel spacing and loading for the HS20 and Tandem trucks that are used in designing bridges from the AASHTO LRFD Bridge Design Specifications are shown in Figure 2.1. These trucks are the same as the HL93 design truck and consists of three point loads with variable spacing from 14 to 30 feet for the back axle (AASHTO LRFD Bridge Design

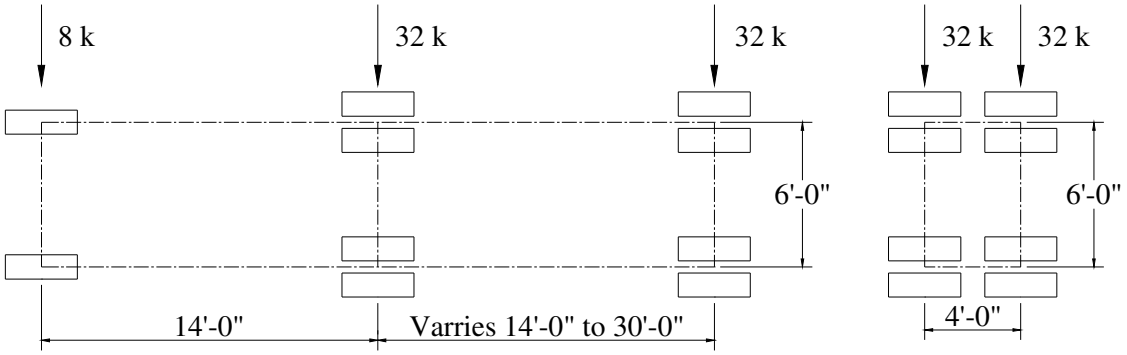

(a) HS20

(b) Tandem

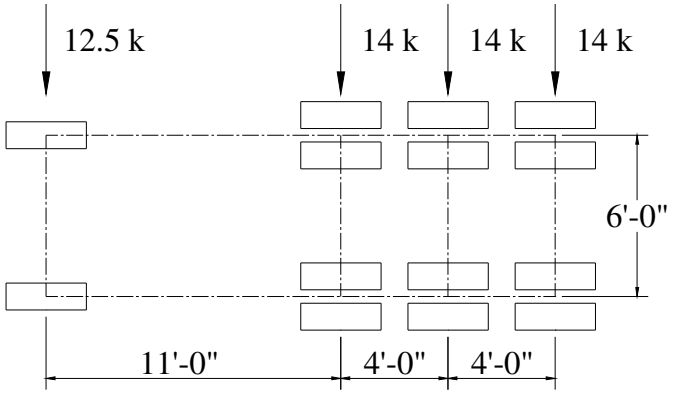

(c) Type 4

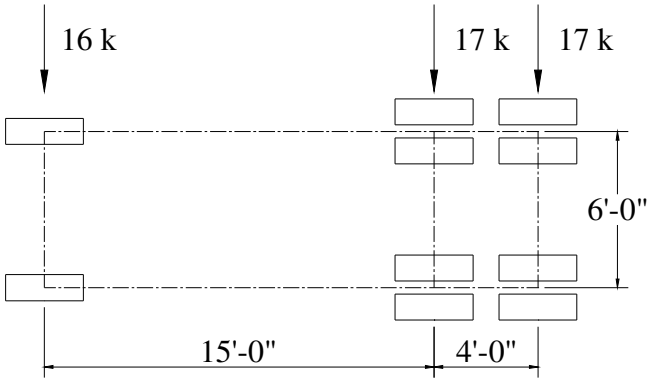

(d) Type 3

Figure 2.1. Iowa DOT Design Vehicles.

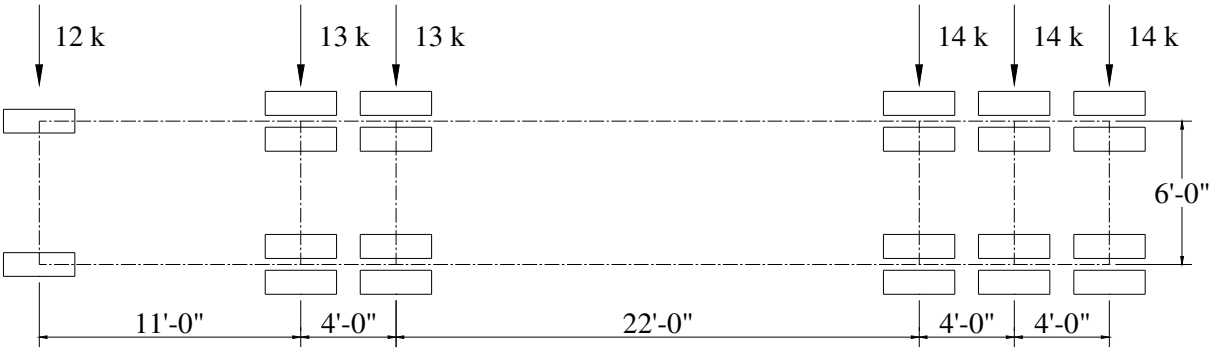

(e) Type 3S3

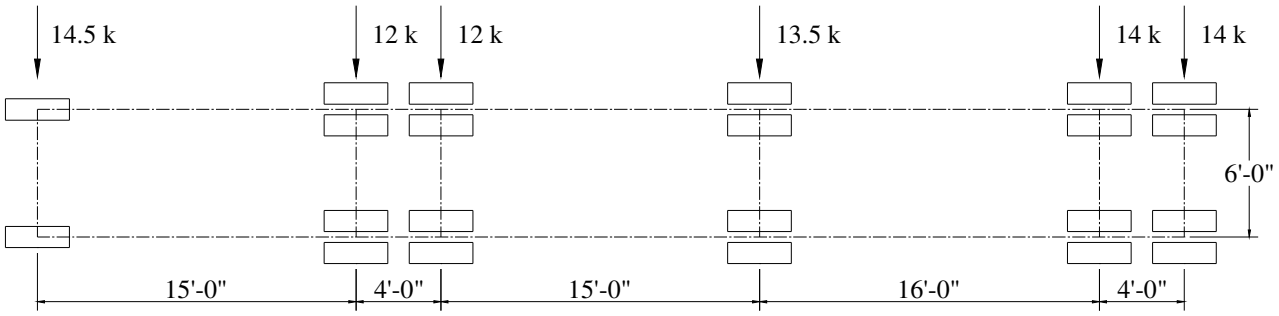

(f) Type 3-3

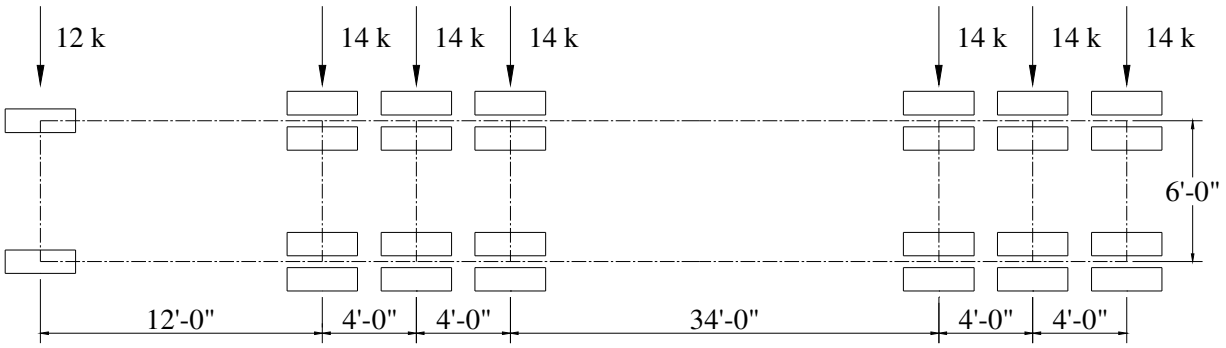

(g) Type 4S3

Figure 2.1. Continued.

Specifications, 2004). The rating vehicle consists of the three axle truck shown in Figure 2.1(a) and the tandem axle loading shown in Figure 2.1(b) and the wheel configuration, truck or tandem, that provides the maximum live load moment, is to be used. A lane loading of 640 lb/ft is used for design but is not used for rating calculations. For short span bridges, the design Tandem, with two axles, often controls the rating but is not used by the Iowa DOT in their ratings.

Other vehicles used in bridge ratings by the Iowa DOT are also shown in Figure 2.1. Any legal loads specified by a particular state DOT should also be included with the rating vehicles. According to the Iowa DOT, the maximum gross weight for livestock and construction vehicles on non-interstate highways is 96,000 pounds for a vehicle with seven axles and 62-foot wheel spacing. A chart listing the legal vehicle weights for vehicles based on the number of axles and their spacing can be found on the Iowa DOT website. Bridge ratings for single-span bridges between 30 and 40 feet in length are typically governed by the HS20 rating vehicle because two of the axles are positioned on the bridge simultaneously. For short span bridges, less than 30 foot spans, the Type 3 or Type 4 vehicles could potentially control due to their rear axle grouping and relatively shorter overall lengths, whereas the HS20 design vehicle would be reduced to having one axle on the bridge for spans less than approximately 30 feet in length and therefore would not govern the rating.

2.1.2 ASD Rating

Allowable stress design philosophy is based on maintaining structural integrity through the use of factors of safety on the capacity of the member being designed. The allowable stress rating uses the same approach by limiting the capacity, or allowable stress, of the member and ensuring that the live load effect due to the rating vehicle does not exceed the capacity of the bridge component. Equation 2 is used to determine the rating of a bridge based on the allowable stress design method:

$$RF = \frac{R - D}{L(1 + I)} \tag{2}$$

where: R is the allowable stress of the member, D is the effect of the dead loads, L is the nominal live-load effect of the rating vehicle, and I is the impact factor for the live-load.

2.1.3 LFD Rating

Load Factor Design does not only place factors of safety on the capacity but also on the loads applied to the structure. The load factors are based on statistics and a pre-selected probability against failure. Equation 3 is used to determine the rating of a bridge based on the load factor design method:

$$RF = \frac{\phi R_n - \gamma_D D}{\gamma_L L(1 + I)} \tag{3}$$

where: ϕR_n is the nominal resistance of the member, and γ_D and γ_L are dead and live load factors, respectively.

2.1.4 LRFR Rating

A Load and Resistance Factor Rating (LRFR) has been developed as a Guide Specification by AASHTO. The LRFR procedure factors both the applied loads as well as the resistance of the structural components using factors determined through statistical analyses to ensure the reliability of the structure against failure. Equation 4 is used to determine the rating of a bridge component based on the load and resistance factor rating method:

$$RF = \frac{C - (\gamma_{DC})(DC) - (\gamma_{DW})(DW) \pm (\gamma_P)(P)}{\gamma_L (LL + IM)} \quad (4)$$

where: C is the capacity equal to:

$C = \phi_c \phi_s \phi R_n$ for the strength limit states.

$C = f_R$ for the service limit states.

where: f_R is the allowable stress specified in the LRFD code, ϕ_c is a condition factor, ϕ_s is a system factor, ϕ is an LRFD resistance factor, R_n is the nominal member resistance (as inspected), γ_{DC} is the load factor for the structural components and attachments, DC is the dead-load effect due to structural components and attachments, γ_{DW} is the load factor for wearing surfaces and utilities, DW is the dead-load effect due to wearing surface and utilities, γ_P is the load factor for permanent loads other than dead loads = 1.0, P is the permanent loads other than dead loads, γ_L is the evaluation live-load factor, LL is the live-load effect, and IM is the dynamic load allowance.

Rating vehicles are assumed to occupy all of the possible lanes to produce the maximum live load effect on the structure. This assumption has allowed Equations 2, 3, and 4 to be shown in their simplified form and allows for the use of the girder distribution factors and a two-dimensional analysis of the bridge. A rating factor of less than one means that the member is not sufficient for the live load specified. Similarly a rating factor greater than or equal to one means that the member is sufficient for the live load specified. The member or bridge component with the lowest rating factor will govern the load rating for the bridge.

2.2 Load Testing

2.2.1 Load Testing in the United States and Abroad

In 1999, Schiff and Philbrick conducted a review of current experimental technologies and practices and found that there were several states that conducted load testing on bridges for load capacity calculations including: Texas, Connecticut, New York, Michigan, North Carolina, and Alabama (Schiff, 1999). In these states, the state department of transportation are the major source of funding for the research and testing.

Load testing being performed in Texas is primarily on slab bridges and pan and girder bridges.

These bridges required an extensive amount of instrumentation which required up to two days to install; the reason instrumentation installation took so long was because the gages were mounted on the reinforcing steel which required the removal of concrete. Mounting strain transducers on the surface of the concrete was found to be unreliable in the past while mounting them directly on the steel was found to be a viable solution. The test results indicated that the bridges had a significantly higher capacity than determined analytically and based on the results, thefollowing are recommendations provided by the Texas DOT:

- Strain gages should be mounted directly on the steel reinforcement.
- Transducers mounted to the concrete in tensile regions are too dependant upon transducer location as crack locations are highly influential on the strains measured.
- The measured strains in bridge members are significantly lower than those calculated by theoretical and design methods.
- Dynamic load effects are responsible for, at most, a 10 percent increase above semi-static load effects.

Though initially thought to conduct load testing on bridges for load capacity calculations, Connecticut and North Carolina were determined to be using in place monitoring systems for bridge assessment to determine whether there is a need to replace the bridge.

New York, Michigan, and Alabama use bridge testing in the assessment and rating of their bridges. New York has increased the load rating of bridges as a result of load testing. It was found in one particular bridge tested that the contributions from the end restraint of the girders to the strength of the bridge was quite substantial. Based on testing data, Michigan has found a significant reserve capacity in the bridges tested. Alabama has been implementing load testing for rating purposes since 1990 and has performed 46 load tests.

There has also been extensive work done by the Ontario Ministry of Transportation in Canada. Canada primarily performs proof load tests to determine the load carrying capacity of existing bridges. Switzerland also performs proof load tests on their bridges but are usually done after the bridges have been constructed to ensure that their capacities will be sufficient. The bridges are then accepted by the government (Moses et al., 1994).

2.2.2 Methodology

Loads can be applied to a bridge in many different ways depending on the type of test being conducted and the results desired from the load test. Loads can be applied statically by use of concrete blocks or other stationary weights that are placed on the bridge by a crane. The stationary load can also be applied using hydraulic jacks positioned below the bridge. The hydraulic jacks would need to react against either substructure bridge elements or anchors placed in the soil below the bridge. Movable loading can also be applied using vehicles of known weight and dimensions. The movable load can be placed in different transverse paths across the bridge to simulate actual loading conditions. The applied test load for the diagnostic test should be large enough to ensure the physical behavior of the bridge at the load rating level. The physical behavior of the bridge should remain linear between the diagnostic test load and the rating level (Lichtenstein, 1993).

There are three main types of measurements that should be taken during a load test: strains, displacements, and rotations. The strains measured in the critical members of the bridge are needed to determine if the bridge is has any reserve capacity beyond the test loads. The displacements and strains in the bridge are needed to ensure that the bridge undergoes elastic behavior during loading and to ensure full recovery after loading. The deflections of the various members at the mid-span of the bridge are typically all that are needed. Differential deflections between the top and bottom flanges of heavily deteriorated girders may be useful as well to ensure the integrity of the section during loading. Measuring the rotation of the stringers at the support will help in the determination of the presence of bearing restraint (Lichtenstein, 1993).

Once the bridge is instrumented at its critical locations, it can be tested. The test vehicle should be brought slowly onto the bridge so as not to induce a dynamic load on the bridge. Each load case should be conducted a minimum of two times to ensure repeatability of results. The loading should be gradually increased and the responses to each of the loadings should be recorded. Each loading shall remain on the bridge for a minimum of five minutes to ensure the measured deflections and strains have stabilized. The observed behavior of the bridge is then compared to the analytical model, and discrepancies between the observed and predicted behavior is noted. The bridge model is then modified to represent the observed characteristics of the bridge and a rating for the bridge is calculated (Pinjarkar et al., 1990).

The analytical model for the bridge is modified to account for the responses observed during the load testing. In the case of the bridge rating increasing as a result of a load test, careful consideration must be taken to account for the impact of larger service loads on the response observed during the load test. If the conditions of the revised analytical model change with an increased load, or the resistance decreases with increased loading, the bridge rating should be revised as well (Pinjarkar, et al. 1990).

Any results obtained from load testing must be able to be repeated. The differences between analytical model results and actual results must be explained before the results of the load test can be used to increase a rating for a given bridge. Extrapolating results of a diagnostic load test beyond the loads used during the test is quite risky and is not recommended unless the linear behavior under loading can be proven to continue for the higher loads (Lichtenstein, 1993).

2.3 Benefits of Load Testing

The rating factor can be quite conservative when the capacity of the bridge is determined theoretically. The capacity of the bridge determined using distribution factors, assumed material properties, simply supported conditions, non-composite action, and zero additional stiffness from curbs and railings can often be conservative as these factors could increase the capacity of the bridge. The capacity of a bridge is often, but not always, determined to be much larger through load testing than can be determined theoretically. A bridge rating could be lowered as a result of load testing due to severe deterioration of major load carrying members. The capacity of a bridge can increase by calculating the actual stiffness of the

bridge components and by determining the three dimensional response under loading. Analytical models make conservative assumptions on the load distribution in the girders and the material properties. They also do not take into account increased stiffness from the presence of curbs and railings on the bridge. The assumed bridge geometry can also differ from what is actually present. Geometry assumptions like simply supported end conditions for the girders and non-composite action are often different from what is actually observed through load testing. Determining the load distribution, material properties, bearing restraint, amount of composite action, and increased stiffness, if any, from curbs and railings will give a more precise estimate of the bridge's capacity.

2.3.1 Girder Distribution Factors

The load distribution to each of the girders can be determined directly through load testing. Using the measured strains in each girder during a load test, the percentage of the load that each girder supports can be calculated. Knowing the percentage of the load that is transferred through the deck to each girder can increase the capacity of the overall bridge as a global system. Both the longitudinal and transverse stiffness of the deck will affect the capacity of the bridge.

2.3.2 Material Properties

Determining the actual material properties of a bridge can also increase the capacity of the structure, however it can be rather expensive to determine the actual material properties of the concrete and steel. The benefits of knowing the actual material properties may be insignificant provided the materials have not deteriorated over time. In the bridge rating process, the assumed material strength of the various bridge components has been found to be generally conservative compared to the actual strength. The compressive strength of the concrete is typically higher than the specified strength. The yield strength of the reinforcing steel as well as the steel girders is also typically higher than specified. If significant deterioration is observed and is expected to continue, an increase in the load rating of that bridge is not recommended.

2.3.3 Curbs and Railings

The participation of the concrete parapet barriers can provide added flexural resistance to the bridge at service loads. At higher loads, the contribution of the barriers decreases. The participation of the concrete curbs is obviously less than the larger concrete parapets. The participation of steel railings can also provide added flexural resistance to the bridge at service loads. Their participation often leads to larger stiffness in the exterior girders than was initially assumed.

2.3.4 Bearing Restraint

Single span bridges are typically designed assuming simply supported conditions, however this condition is seldom observed during a load test. The end bearings of the girders have been found to resist the moment. This bearing restraint frequently results in a negative moment at

the supports which in turn reduces the maximum positive moment at or near the mid-span of the bridge.

Bearing restraint, resulting in a net decrease in the positive moment at the mid-span of the bridge observed during service loads, cannot be relied upon at larger loads. The restraint could be due to a frozen bearing and increased loading could free the bearing thus releasing any support restraint observed under service loads.

2.3.5 Partial Composite Action

Unintended partial composite action has been found in steel stringer-concrete slab bridges built without mechanical shear connectors. Very few bridges were built with mechanical shear connections prior to 1950. The non-composite bridges have been found to exhibit partial composite action at service loads, but at larger loads the degree of composite action can decline resulting in the bridge performing as a non-composite bridge. The loss of composite action can be detected during loading by the nonlinear nature of the load-strain and/or load-deflection curves. This does not allow the composite action observed at lower service loads to be extrapolated linearly to larger loads.

Limiting bond stresses at the steel-concrete interface for composite and non-composite behavior has been proposed by Lichtenstein. For slabs that are cast on top of the stringers, he recommends the limiting the bond stress to 70 psi for concrete with a compressive strength of 3 ksi. For slabs that are cast with the top flange of the stringer embedded into the slab, a limiting bond stress of 100 psi for a concrete compressive strength of 3 ksi is recommended. As long as the horizontal shear stress at the concrete-steel interface is less than the specified bond strength the behavior of the bridge can be assumed to be composite, otherwise it is non-composite. If partial composite action can be determined, the bridge will have increased strength as well as a greater ability to transfer loads transversely.

As the load increases during a proof load test, the location of the neutral axis of the girder moves toward the compression region of the girder. This indicates that the girder is loosing stiffness with increased loading. A portion of this loss in stiffness is due to the deterioration of the composite action with the increased loading. The deterioration does not occur at low load levels, but begins at a certain load level. Once the composite action deterioration begins, it is almost directly proportional to the load level. The load-strain curve is repeatable for similar loadings proving the transfer of the horizontal shear from the stringer to the deck is elastic.

This partial composite action is presumed to be attributed to two conditions. The friction between the girder and slab has been found to be insignificant and therefore not the cause of partial composite action. The other possibility is the bond created between the concrete and the steel due to the chemical bond created during curing process. This bond may also be attributed to the aggregate interlocking between the concrete deck and a delaminated strip of concrete chemically bonded to the girder.

The only way to determine if a bond exists between the deck and girders is to perform a load

test, however the bond resistance from girder to girder on a particular bridge is usually not uniform. A non-composite bridge tested to failure by Bakht and Jaeger (Bakht and Jaeger, 1992) was found to exhibit partial composite action in the interior girders but act non-compositely in the exterior girders.

In order to estimate the degree of composite action that can be relied upon beyond the loads applied during a diagnostic load test, the load-deflection curve for an actual load test must be analyzed. During the initial stages of loading, the load-deflection curve is linear and follows that of the predicted fully composite section. The linear region labeled in Figure 2.2 shows two lines; the line with the larger slope corresponds to a load-deflection curve for a composite girder. The observed load deflection line follows that of a composite section then, once the bond between the concrete and steel becomes compromised, the behavior is nonlinear. It is important to note though, that once the bond has been compromised a sudden increase in deflection is not observed, but rather there is a gradual decrease in the slope of the load-deflection curve. In other words, the bond strength is not completely compromised but gradually "deteriorates" with increased loading. Also, it is important to note that the "deterioration" of the bond strength under high load levels is not permanent. Lichtenstein proposed a load-deflection curve for an analytical model, as shown in Figure 2.2, having a linear relationship following the curve of a composite girder. This linear relationship terminates when the bond strength is compromised. At that point, the load-deflection curve is linear with the same slope as that of a non-composite section. Determining the load at which the bond strength becomes compromised is found through load testing.

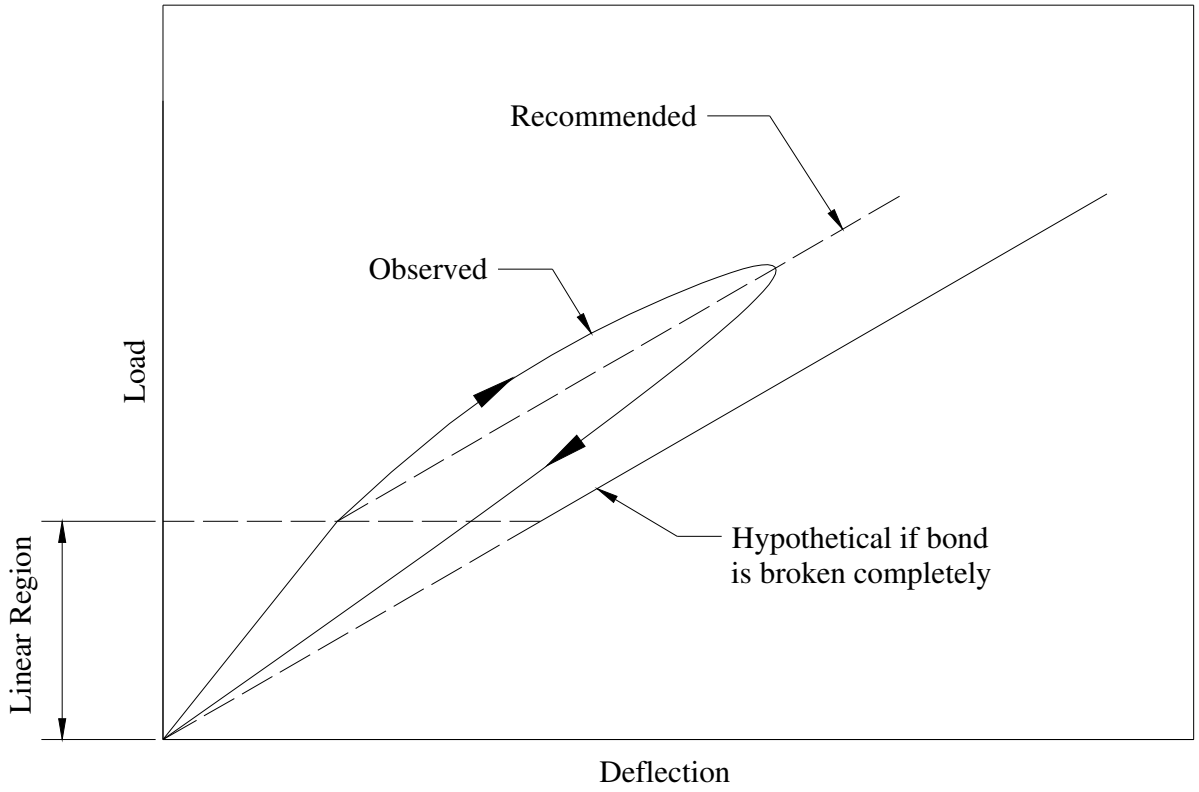

Figure 2.2. Load-Deflection Curve for a Girder With Composite Action.

Empirical formulas have been developed by Lichtenstein to estimate the bond strength at a steel-concrete interface. A bond strength of $0.1\sqrt{f'_c}$ has been proposed (the bond strength for 4,000 psi concrete would be about 75 psi), where f'c is the compressive strength of the concrete deck in MPa. The use of the empirical formula for determining the bond strength can only be used in association with the results of a diagnostic load test which confirms the presence of composite action. The empirical bond strength is conservative as bond strengths exceeding 145 psi have been observed.

2.4 Load Rating Using Load Test Results

2.4.1 Extrapolation

The test vehicle is rarely the same as the rating vehicles shown in Figure 2.1. In most cases, the test vehicle does not weigh as much as the rating vehicles so determining the bridge rating from the test vehicle cannot be performed directly. One way to determine the rating is to extrapolate the results from the test vehicle using Equation 5:

$$\sigma_{rat}^{m} = \frac{\sigma_{rat}}{\sigma_{test}} \sigma_{test}^{m} \tag{5}$$

where: σ_{test}^{m} is the measured live load stress resulting from the test vehicle, σ_{rat}^{m} is the live load stress of rating vehicle interpreted from σ_{test}^{m}, and σ_{rat} and σ_{test} are analytical live load stresses due to the rating vehicle and the test vehicle, respectively. Using this equation, the initial rating factor, RF_i (from Equation 2) can be modified resulting in Equation 6 as follows:

$$RF = \frac{\sigma_{test}}{\sigma_{test}^{m}} \times RF_i \tag{6}$$

where L from Equation 2 is the same as σ_{rat} in Equation 5. Caution should be taken when using these rating equations for loads larger than the test loads as it is not certain that the bridge will remain linear beyond the test load and a linear extrapolation at the ultimate state is not possible for most bridges (Cai and Shahawy, 2001).

Another way to calculate the bridge rating through extrapolation is by extrapolating the live load moment stress to the maximum allowable stress in the girders using Equation 7:

$$M_{cap} = M_{test}\left[\frac{\sigma_{all} - \sigma_{DL}}{(1+I)\sigma_T}\right] \tag{7}$$

where: σ_T is the maximum live-load stress produced by the test trucks, M_{test} is the moment applied during the test, M_{cap} is the theoretical moment capacity, σ_{all} is the allowable stress, and σ_{DL} is the dead load stress. The rating factor is simply the moment capacity (M_{cap}) divided by the absolute maximum moment created by one wheel line of the standard vehicle loading.

This equation yields the highest rating factors for the bridges tested because it utilizes all of the added benefits not accounted for in the AASHTO equations like the three-dimensional characteristics of the bridge, unintended composite action, support restraint, and the stiffness of the curbs and guardrails. It is important that the strains measured during the load test remain linear to ensure that a linear extrapolation can be performed. It is also important that there is a linear response during removal of the load (Moses et al. 1994).

2.4.2 Lichtenstein's Approach

Lichtenstein has developed an adjustment factor (K) that can be used in the rating equations to allow for incorporating the load test results. Equation 8 is the adjustment factor that was developed by Lichtenstein to determine the new load rating:

$$K = 1 + K_a \times K_b \tag{8}$$

where: K_a is a factor based on any benefits derived from the load test and the section factor found to resist the test load. K_b accounts for the relationship between the load test results and those predicted analytically as well as the type and frequency of follow-up inspections and the presence or absence of special features such as non-redundant framing and fatigue prone details. K_a is of the form provided in Equation 9, and the general equation for K_b is provided in Equation 10:

$$K_a = \frac{\varepsilon_c}{\varepsilon_T} - 1 \tag{9}$$

$$K_b = K_{b1} \times K_{b2} \times K_{b3} \tag{10}$$

where: ε_T is the maximum member strain measured during the load test and ε_c is the corresponding theoretical strain due to the test vehicle and its position on the bridge which produced ε_T. K_{b1} takes into account the analysis performed by the load test team and their understanding and explanations of the possible enhancements to the load capacity observed during the test; the range of values for K_{b1} are 0 to 1.0 with zero indicating that the test team is not able to explain the test behavior or validate the test results and a value of 1.0 indicating that the test measurements can be directly extrapolated to performance at higher loads corresponding to the rating levels. K_{b2} is a reduction factor that takes into account the frequency and type of inspection for the bridge. K_{b3} is a reduction factor that takes into account the bridge geometry and its susceptibility to catastrophic failure. Equation 11 provides the relationship for ε_c:

$$\varepsilon_c = \frac{L_T}{(SF)E} \tag{11}$$

where: L_T is the calculated theoretical load effect in the member corresponding to the measured strain ε_T, SF is the member's appropriate section factor (area, section modulus, etc.) and E is the member modulus of elasticity.

Presented in Table 2.1are typical values for K_{b1}, where: T is the test vehicle effect and W is the gross rating load effect. The reason for knowing whether the member behavior can be extrapolated to $1.33W$ is to ensure that the structure has adequate reserve capacity beyond its rating load level (W). This can be established either through proof load testing or by calculation. Typical values for K_{b2} and K_{b3} are provided in Table 2.2 and Table 2.3, respectively. When deciding upon a value of K_{b3} to use, it is important to ensure that components requiring reduction be considered only once in the ratings.

If K is equal to one, then either there was not a load test performed or the load test results agree exactly with those predicted analytically. If K is less than one, then the analytical prediction overestimated the actual capacity of the bridge. Finally, if K is greater than one, then the bridge has benefited from the load test as the capacity is greater than that predicted analytically.

Table 2.1. Values for K_{b1}.

Can member behavior be extrapolated to 1.33 W?		Magnitude of test load			K_{b1}
Yes	No	$\frac{T}{W} < 0.4$	$0.4 \le \frac{T}{W} \le 0.7$	$\frac{T}{W} > 0.7$	
✓		✓			0
✓			✓		0.8
✓				✓	1.0
	✓	✓			0
	✓		✓		0
	✓			✓	0.5

Table 2.2. Values for K_{b2}.

INSPECTION		K_{b2}
Type	Frequency	
Routine	Between 1 and 2 years	0.8
Routine	Less than 1 year	0.9
In-Depth	Between 1 and 2 years	0.9
In-Depth	Less than 1 year	1.0

Table 2.3. Values for K_{b3}.

Fatigue Controls?		Redundancy		K_{b3}
No	Yes	No	Yes	
	✓	✓		0.7
	✓		✓	0.8
✓		✓		0.9
✓			✓	1.0

2.4.3 Barker's Approach

The main problem with the increasing the rating of a bridge based on measured strains being lower than the theoretical strains is that the reason for such an increase is not clearly defined (Goble et al. 2000). The procedure provided by Lichtenstein does not quantify the amount of reserve capacity nor does it explain how the increased capacity was achieved which increases the risk associated with the use of the rational equations developed. This problem has been addressed by Barker in "Quantifying Field-Test Behavior for Rating Steel Girder Bridges" (Barker 2001).

An experimental load test provides the bridge capacity as a total of the individual contributions from various sources. If some of the increased capacity for the bridge cannot rely on all of the individual contributions, then some of the sources of increased flexural resistance should be omitted; the factors contributing to the increased stiffness must be defined. In other words, all of the increased capacity from a bridge test should not be used so the bridge capacity needs to be divided into its various components. The experimental rating equation can be expanded into its components as shown in Equation 12:

$$RF_{EXP} = \frac{(0.55F_y - \sigma_{D)}}{Im_E \times \left[\frac{\frac{M_{RVW}}{M_{TRK}} \times \frac{M_E}{M_{LE}} \times \frac{M_{LE}}{DF_E} \times \frac{M_T}{M_E}}{\frac{S_E}{S_A^{ADIM}} \times S_A^{ADIM}} \right] \times DF_E} \tag{12}$$

Equation 12 is used to determine the experimental inventory rating. Dividing Equation 12 by the Equations 2, 3, or 4 yields Equation 13:

$$\frac{RF_{EXP}}{RF_{ANY}} = \left[\left(\frac{Im_A}{Im_E} \right) \times \left(\frac{M_E}{M_T} \right) \times \left(\frac{M_{LE}}{M_E} \right) \times \left(\frac{DF_A}{DF_E} \right) \times \left(\frac{M_{WL}}{\frac{M_W}{DF_E} \times \frac{M_{RVW}}{M_{TRK}}} \right) \times \left(\frac{S_A^{ADIM}}{S_A} \right) \times \left(\frac{S_E}{S_A^{ADIM}} \right) \right] \tag{13}$$

where: (Im_A/Im_E) is the contribution from the impact factor; (M_E/M_T) is the contribution from the bearing restraint force effects; (M_{LE}/M_E) is the contribution from longitudinal distribution of moment; (DF_A/DF_E) is the contribution from the lateral distribution; $(M_{WL}/[(M_W/DF_E) \times M_{RVW}/M_{TRK}])$ is the contribution from additional system stiffness, i.e. curbs, railings, etc.; (S_A^{ADIM}/S_A) is the contribution from actual section dimensions for section modulus; and (S_E/S_A^{ADIM}) is the contribution for unintended or additional composite action. Using this equation, various factors of the increased rating can be omitted so as to not account for their contribution in the overall rating.

The experimental lateral distribution factor can be determined by measuring the bottom flange

strains across the midspan of the bridge under loading. Equation 14 provides the relationship of the experimental lateral distribution factor, DF_E, to the measured strains:

$$DF_E = \frac{2 \times (\sigma_i \times S_{Ai})_{CriticalGirder}}{\sum (\sigma_i \times S_{Ai})} \tag{14}$$

where σ_i is the bottom flange stress for girder i and S_{Ai} is either the actual section or nominal design section modulus for girder i.

To determine the bearing force at the abutment, Equation 15 can be used:

$$\text{Bearing Force} = A_{bf} \text{ x } \sigma_{bf} \tag{15}$$

where A_{bf} is the area of the bottom flange at the bearing and σ_{bf} is the calculated stress on the bottom flange at the bearing from the measured strain.

The bearing force causing a decreased moment at the midspan also induces an axial stress in the girder that may want to be discounted in the bridge capacity. To remove this axial force, Equations 16 and 17 can be used:

$$\sigma_{axial} = \frac{\text{Bearing Force}}{A_{comp}} \tag{16}$$

$$A_{comp} = A_{steel} + \frac{A_{conc}}{n} \tag{17}$$

where A_{comp} is the equivalent steel composite area, A_{steel} is the nominal or measured area of the steel section, A_{conc} is the nominal or measured area of effective concrete, and n is the ratio of Young's Modulus of steel to that of concrete. The axial force is subtracted from the linear girder stress profile as shown in Equation 18:

$$\sigma = -\frac{1}{Slope} \times \frac{d}{2} + \frac{Intrcpt}{Slope} - \sigma_{axial} \tag{18}$$

where σ is the stress at a depth d above the bottom flange, $Slope$ is the slope of the stress profile, and $Intrcpt$ is the neutral axis location from the bottom flange as shown in Figure 2.3.

The total measured moment for a girder, M_T and slab section can be divided into three parts: 1) bending about the steel neutral axis, M_L, 2) bending about the concrete neutral axis, M_U, and 3) a couple representing the composite action, $N \times a$, as shown in Figure 2.4. To calculate the total moment, M_T, Equations 19 to 22 can be used.

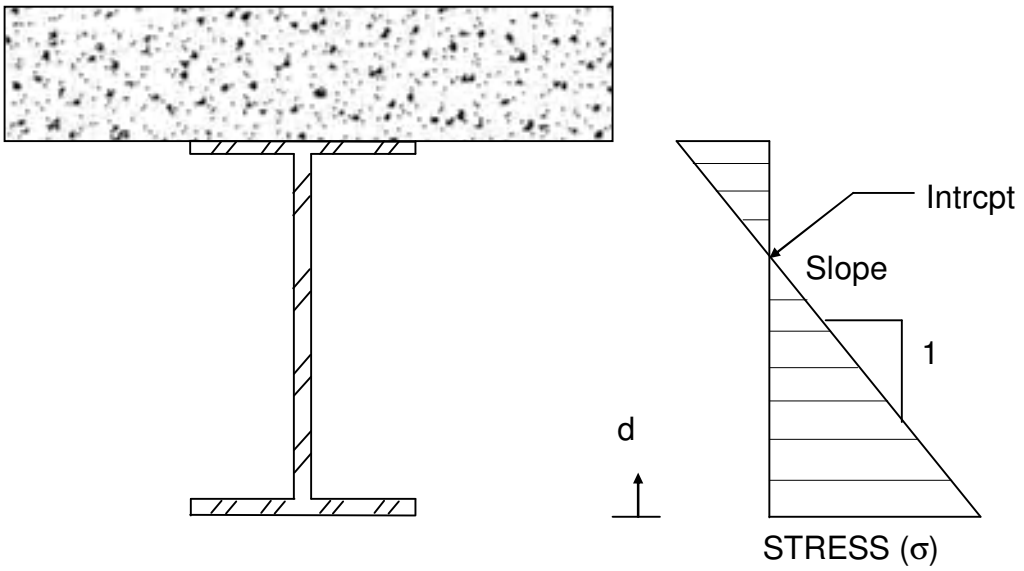

Figure 2.3. Partially Composite Girder Stress Profile.

$$M_T = M_U + M_L + N_a \tag{19}$$

$$M_L = (\sigma_o - \sigma_{CG}) s_{steel}^{ADIM} \tag{20}$$

$$M_U = \frac{E_{conc} I_{conc}}{E_{steel} I_{steel}^{ADIM}} \times M_L \tag{21}$$

$$N_a = \sigma_{CG} A_{steel}^{ADIM} a \tag{22}$$

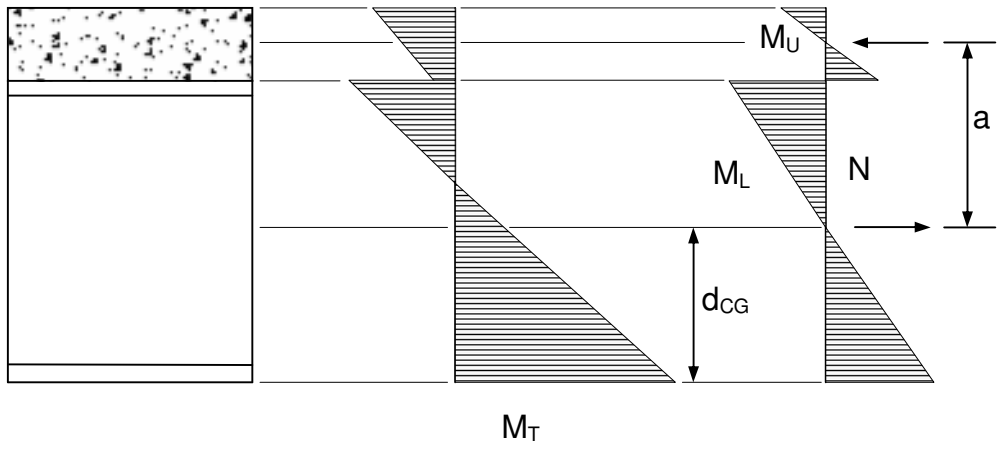

Figure 2.4. Girder - Concrete Stress Profile.

2.4.4 BDI Approach

Bridge Diagnostics Inc. (BDI) has developed hardware and software packages for use in bridge testing. The system includes hardware for the structural testing system (STS) and a software packet with data presentation (WinGRF), model generation (WinGEN), and structural analysis (WinSAC) programs. The structural testing system that is used in the field testing process consists of four main elements: BDI intelliducers, a BDI STS unit, an Autoclicker, and a power unit. The BDI intelliducers are attached directly to individual bridge elments to measure the strains induced by the loading vehicle. The STS unit is used to collect the data provided from the intelliducers. The autoclicker can be used to reference the truck location to the strain measurements as the test vehicle proceeds over the bridge. Finally, the power unit provides power to the system (Wipf et al., 2003).

The data presentation software WinGRF allows for a graphical presentation of the strain versus position relationship during the load test. The neutral axis location can also be plotted as the load progresses across the bridge. Once the data have been collected, using the bridge dimensions, a finite element model can be generated using WinGEN. The strain data from the test can be input into the software along with the corresponding transducer locations to calibrate the bridge model. The model should be calibrated to include the actual boundary conditions. A truck simulating the test vehicle is used to calibrate the calculated strains so that they are the "same" as the measured strains from the test. Using the generated model from WinGEN, WinSAC can be used to refine the model. This software uses an iterative approach to find a solution by changing user defined parameters like boundary conditions or material properties. Once the model has been calibrated, a standard rating equation from AASHTO, Equations 2, 3, or 4, are used to determine the rating with the appropriate rating vehicle applied to the structure to determine the live load effect.
The model calibration reduces the error between the results obtained through load testing and the theoretical results. The optimization reduces the error by computing four different error values: absolute error, percent error, scale error, and the correlation coefficient. Error function equations are provided in Table 2.4. Error Functions.Table 2.4.

Table 2.4. Error Functions.

Error Function	Equation
Absolute Error	$\sum \lvert \varepsilon_m - \varepsilon_c \rvert$
Percent Error	$\frac{\sum (\varepsilon_m - \varepsilon_c)^2}{\sum (\varepsilon_m)^2}$
Scale Error	$\frac{\sum \max \lvert \varepsilon_m - \varepsilon_c \rvert_{gage}}{\sum \max \lvert \varepsilon_m \rvert_{gage}}$
Correlation Coefficient	$\frac{\sum (\varepsilon_m - \bar{\varepsilon}_m)(\varepsilon_c - \bar{\varepsilon}_c)}{\sum \sqrt{(\varepsilon_m - \bar{\varepsilon}_m)^2 (\varepsilon_c - \bar{\varepsilon}_c)^2}}$

where: ε_m is the measured strain, ε_c is the calculated strain, and $\bar{\varepsilon}_m$ and $\bar{\varepsilon}_c$ are the average measured and calculated strains, respectively (Bridge Diagnostics Inc., 1999).

2.5 Load Testing Examples

A number of states have utilized load testing to determine the capacity and ratings of various bridge types. The summaries from four different reports on bridge testing from the late 1990's are provided as examples of what has been done in the past in regards to bridge load testing.

2.5.1 Overweight Load Responses (Schultz et al., 1998)

Three different bridge types were load tested, prior to a permit load crossing over the structures, to determine the result of the permit load on the structure and to compare the actual stiffness of the bridges to analytical models that had been created for each bridge. The three types of bridges that were tested included: a reinforced concrete slab bridge, a reinforced concrete T-girder bridge, and a composite welded plate steel girder bridge with a concrete deck. All three bridges were continuous over three spans. In the following paragraphs, only the results from the steel girder bridge test will be summarized. Only the positive moment region of the center span of the three span bridge was designed to be composite; the end spans were non-composite.

The load tests were conducted using a three-axle tandem dump truck weighing 63.02 kip positioned on three different load paths: east shoulder, east lane, and west lane, to establish the lateral load transfer characteristics. The strain data were collected continuously along with the corresponding truck location; each load test was performed two times in each of the load paths to ensure the repeatability of the results. Once the tests using the test truck were completed, the permit truck was allowed to cross the structure. The permit truck had a gross weight of 285.38 kip. This truck crossed the structure only once during which strain data and the corresponding truck location were collected and recorded.

In the non-composite region of the bridge, the strains observed in the top and bottom flanges were not equal, indicating that partial composite action existed in this region. The partial composite action was found to be reproducible under the same loading. The effective flange width was smaller in the exterior girders than for the interior girders, however the neutral axis locations in the interior and exterior girders were approximately the same. The same neutral axis location was attributed to the additional resistance provided by the curbs over the exterior girders. The effects of the permit load were 27 and 116 percent higher in the positive and negative moment regions respectively, than the test truck. Using the test results, the analytical model was modified to better represent the actual stiffness of the bridge.

Through load testing, the girder was found to be 22 percent stiffer in the composite regions than previously calculated. The partial composite action observed was not linear and varied from girder to girder, and the supports were found to only partially restrain rotation. The modification of the bridge model after the test load resulted in very close predictions of the strains that were observed with the permit load.

2.5.2 Economical Bridge Testing (Chajes et al. 1996)

A three span bridge built in 1940 with nine non-composite steel stringers was load tested to determine its actual capacity. Each of the three spans were simply supported with the top flanges of the girders embedded into the concrete deck making the bottom surface of the top flange flush with the bottom of the deck. Minor repairs have been made to the bridge over its lifetime including the welding of steel plates over the corrosion damaged areas and the welding of the girders to their bearing plates thus restraining their rotation. The bridge was initially designed with an 8.5 inch deck and a future wearing surface of 2 inches; however, the actual wearing surface on the bridge was 11 inches. The bridge had been posted due to a substandard rating factor obtained using the BRASS program. The 64-foot center span was the controlling span for the posting and thus was the only span instrumented in the load test.

A load test using a 50-kip truck was conducted with the truck traveling along three different paths two times each to ensure the repeatability of the results. The load tests revealed that there was partial composite action, some degree of support restraint, and the actual distribution factors for the girders. The partial composite action was calculated by determining the neutral axis of the girders from the top and bottom flange strains. The degree of support restraint was determined by assuming the rotation was resisted by springs whose spring stiffness was determined by comparing the unrestrained theoretical rotations to the longitudinal strain distribution observed. The analytical model was calibrated using the strains measured during the load tests.

Based on the fact that the bridge had been in service for over 50 years and the slab-stringer interface exhibited no visual deterioration, it was decided to rely on the partial composite action in determining the rating factor for the bridge. It also helped to know that the bridge had a high degree of redundancy reducing the risk in the decision to rely on the observed composite action. A relatively frequent inspection of the bridge, particularly the slab-girder interface, to ensure the partial composite action has not deteriorated was recommended. The rating factors determined for the bridge using the revised parameters in the BRASS analysis were found to be within seven percent of those found using the finite element model.

2.5.3 Short – Span Steel Bridges (Stallings and Yoo, 1997)

Four single span, simply supported bridges, each with four girders, were load tested for the purpose of determining their capacity. The bridges consisted of steel stringers with cast in place concrete decks. The cast in place concrete was placed in such a manner as to embed the top flange of the girders in the deck making the bottom of the top flange of the girder flush with the bottom of the deck. Two of the bridges had been posted and the goal of the load test was to remove such posting while the reason for testing the other two bridges was to help determine the bridge characteristics like partial composite action, connection forces, and girder distribution factors.

The moments calculated using the measured strains were smaller than the moment calculated based upon the loading of the bridge and the assumed bridge parameters, i.e. simply supported, non-composite, etc. The cause of the observed moments being smaller than the

calculated moments is due to restraining moment at the supports. The results obtained are believed to be consistent among similar bridges of comparable age.

Determining the wheel-load distribution factors for the girders has been conducted based upon the strain measurements taken from the girder bottom flanges. The distribution factor has been assumed to be equal to the ratio of the strain in the girder to the sum of the strains in all of the girders. Another way to determine the distribution factors is to use a weighted sum of the bottom flange strains in order to account for possible edge stiffening effects from the curb or barrier. Distribution factors are highly dependant upon the material properties or weight factors of the structure. The larger of the distribution factors calculated using multiple and single lane loadings is used, however the distribution factors calculated for single and two lane loadings were found to be quite close for the bridges tested. The loading condition that was used to calculate the distribution factors was a static condition where measurements were taken with the test vehicle(s) stationary.

The strains that were measured during the load test were found to be between 27 and 52 percent lower than the higher calculated strains, which are believed to be caused by the bearing restraint. Some of the reduction can be attributed to partial composite action but this cannot account for all of the reduction in strain in the girders.

Impact factors for bridges can be calibrated by determining the ratios of the strains determined for a moving (dynamic) load to the strain determined for a static load. Sound judgment is required when determining the impact factors based on the actual response of the bridge to dynamic loading. For one of the bridges tested, the ratio of dynamic strain to static strain for an exterior girder was found to be 5.33, which is not practical. The reason for the high impact factor is due to the very small static strain in this particular girder compared to the strain in the interior girders. Due to the impractical results obtained for the exterior girder, an impact factor was determined for a critical interior girder. An alternative approach is to find a weighted sum of the dynamic and static strains in all four girders. Comparing the impact factors obtained incorporating the weight factors to those where the weight factors are assumed to be one indicates that the impact factors are not very dependent upon the weight factors, i.e. the section moduli. The impact factors calculated using a weighted sum of all of the girders tend to be larger than those calculated using the most critical girder. In three out of the four bridges, the measured impact factors are less than the AASHTO factors with the fourth bridge only having a slightly larger measured impact factor than the AASHTO value.

2.5.4 Diagnostic Testing Concrete Bridges (Klaiber et al. 1997)

Four types of reinforced concrete bridges were diagnostically tested for the purpose of comparing the results from the load test to the rating of the bridge, calculated using empirical formulas. The bridges were rated using the procedure developed by Lichtenstein to compare the results of the load test to the analytical model. The four types of bridges tested are: reinforced concrete open spandrel arch, reinforced concrete filled spandrel arch, reinforced concrete slab, and reinforced concrete stringer.

It was found that the open spandrel arch, though slightly deteriorated, performed better than

what was predicted. The strain observed under loading was less than half that predicted, 143 microstrain and 399 microstrain, respectively.

One reason for the capacity of the bridge being larger than predicted is due to the compressive strength of the concrete. The assumed compressive strength was 3,000 psi and the average compressive strength of the concrete obtained from core samples was 4,320 psi. The yield strength of the structural steel was also larger than what was predicted. The average yield strength was 41,400 psi and the assumed yield strength was only 30,000 psi for structural steel used between 1905 and 1936. The same was true for the reinforcing steel with the average actual yield strength being 33,900 psi compared to the assumed value of 30,000 psi.

Each component of the bridge was initially rated to find the minimum overall rating for the bridge. As a result of the load test, the rating of the girder and hangers supporting the deck from the arches increased; the rating of the arches however decreased. The decrease in the rating of the arches is explained by the presence of a greater load distribution to other parts of the bridge than what was predicted by the analytical model. The overall rating of the bridge was governed by the deck though. There was not any strain data obtained for the deck during the load testing for this bridge and so the theoretical load rating could not be modified. Similar results were found for similar bridges, with the deck governing the rating of the bridge.

A slab bridge that was diagnostically load tested also resulted in lower measured strains than those that were calculated analytically. The reason for the increased capacity in the slab bridge was due to the increased stiffness from the concrete barriers. The contribution to the overall capacity of the bridge from the barriers is neglected in the analytical model. It was found, however, that barriers significantly contributed to the stiffness of the bridge.

The results from the diagnostic load test of a reinforced concrete stringer bridge decreased the rating of the bridge. The bridge was two spans and consisted of three reinforced concrete stringers and a reinforced concrete deck. The discrepancy in the rating of the bridge was a result of the calculated effective flange width of the T-girder being larger than the actual effective flange width. In this case, the rating calculated empirically was larger than the rating calculated using the test results. The decrease in rating for the Type 3 vehicle was from a predicted 51 tons to an actual 30 tons.

2.5.5 Lessons Learned From Previous Load Testing Examples

Bridges designed with steel girders and cast-in-place concrete decks typically have higher load carrying capacities than theoretically determined. Not all diagnostic load tests will result in an increase in the load rating of the bridge as was the case of one of the bridges tested by Klaiber et al. 1997. The load testing provided viable results for determining the capacity of the bridges that could not have been determined using analytical models.

3. BOONE COUNTY BRIDGE (BCB)

3.1 Bridge Description

One of the bridges from the aforementioned family of bridges load tested is located in Boone County, IA. The bridge (FHWA ID: 77110), henceforth referred to as the BCB, is located on G Avenue approximately 8.5 miles south of Ogden, IA and one mile west of USH 169. Shown in Figure 3.1 is an alignment view of the BCB which was built in 1900 as a 36-foot simple-span, non-composite bridge with six steel girders, a concrete deck, and no skew crossing Little Beaver Creek. The substructure consists of seven timber piles with a double C-channel cap and a timber back wall. A photograph of a typical pile cap configuration for this family of bridges is shown in Figure 3.2 with a close up of the typical girder bearing shown in Figure 3.3. Currently not posted, the BCB was given a sufficiency rating of 49 when it was last inspected in June of 2004.

Figure 3.1. BCB Alignment View Looking South.

The superstructure appears to be in good condition with some minor rust in areas as shown in Figure 3.4(a). Typical decay that was found in some of the piles is shown in Figure 3.4(b). There were minor repairs made to the bridge in 1993 when the south bridge approach was washed away; the repairs consisted of the installation of a sheet pile wall behind the existing timber back wall and then filling the void with concrete. Shown in Figure 3.5(a) is the sheet pile wall while the concrete behind the top of the timber backwall is shown in Figure 3.5(b).

Figure 3.2. Typical Pile Cap Configuration.

Figure 3.3. Typical Girder Bearing.

(a) Minor rust on girders **(b) Rotten pile**

Figure 3.4. BCB Deterioration.

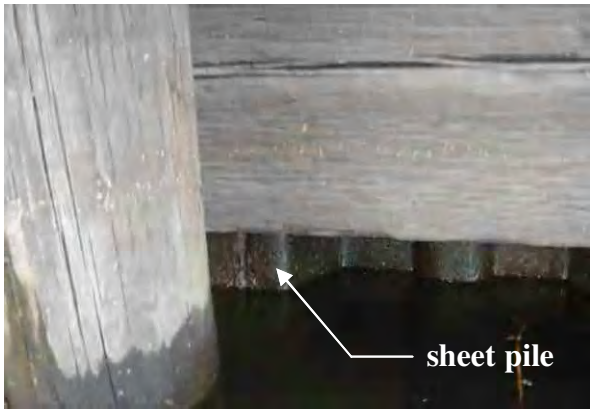

Figure 3.5. BCB Repairs.

The superstructure, a cross section of which is shown in Figure 3.6, consists of six W21x68 girders with a 7.5-inch thick concrete deck. There are C-channel diaphragms at the 1/3 points of the bridge as shown in Figure 3.4(a). On both sides of the bridge there are concrete curbs eight inches wide twelve inches deep as well as a steel railing.

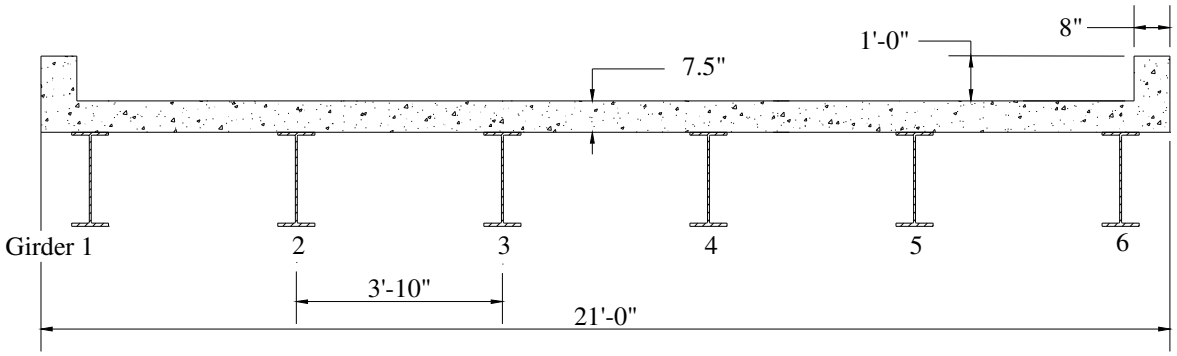

Figure 3.6. Cross Section of BCB Looking North.

3.2 Test Setup

3.2.1 Test Truck

There were three incremental loads, referred to as: an empty truck, a half full truck, and a full truck, used to test the bridge. The incremental loads refer to the amount of material, in this case gravel, the truck was carrying with the full truck increment being close to the maximum amount the truck could legally carry. The truck used for the load test was provided by the county and was a standard maintenance tandem dump truck. A photograph of the test truck crossing the bridge during a load test is provided in Figure 3.7 with its axle weights and dimensions presented in Table 3.1 and Figure 3.8, respectively.

Table 3.1. BCB Test Truck Weights.

Truck Loading	Axle Weights (kip)			Gross Weight (kip)
	A	B	C	
Empty	10.82	5.98	5.98	22.86
Half Full	13.12	11.73	11.73	36.86
Full	15.08	17.19	17.19	49.86

3.2.2 Testing Plan and Instrumentation

There were three paths or lanes, shown in Figure 3.9, selected for the truck to follow as it crossed the bridge. Each lane was tested twice for each load increment to check repeatability of the test results. Measurements (strains and deflections) were taken when the centroid of the tandem was at the centerline of each abutment and at each quarter point (see Figure 3.9). The location of the centerline of the abutments and each quarter point were painted on the bridge as shown in Figure 3.10; the location of the tandem axle centroid in relation to one of the transverse lines painted on the bridge is shown in Figure 3.11.

Figure 3.7. BCB Test Truck.

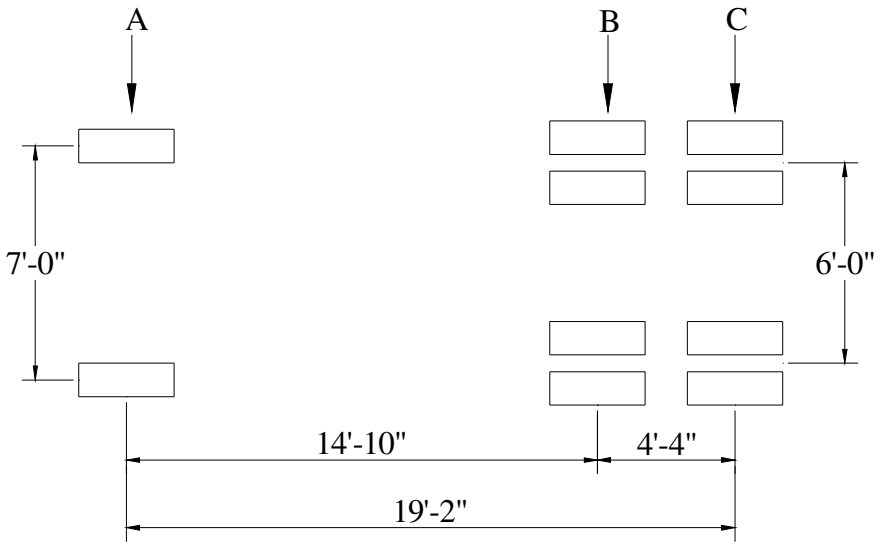

Figure 3.8. BCB Test Truck Dimensions.

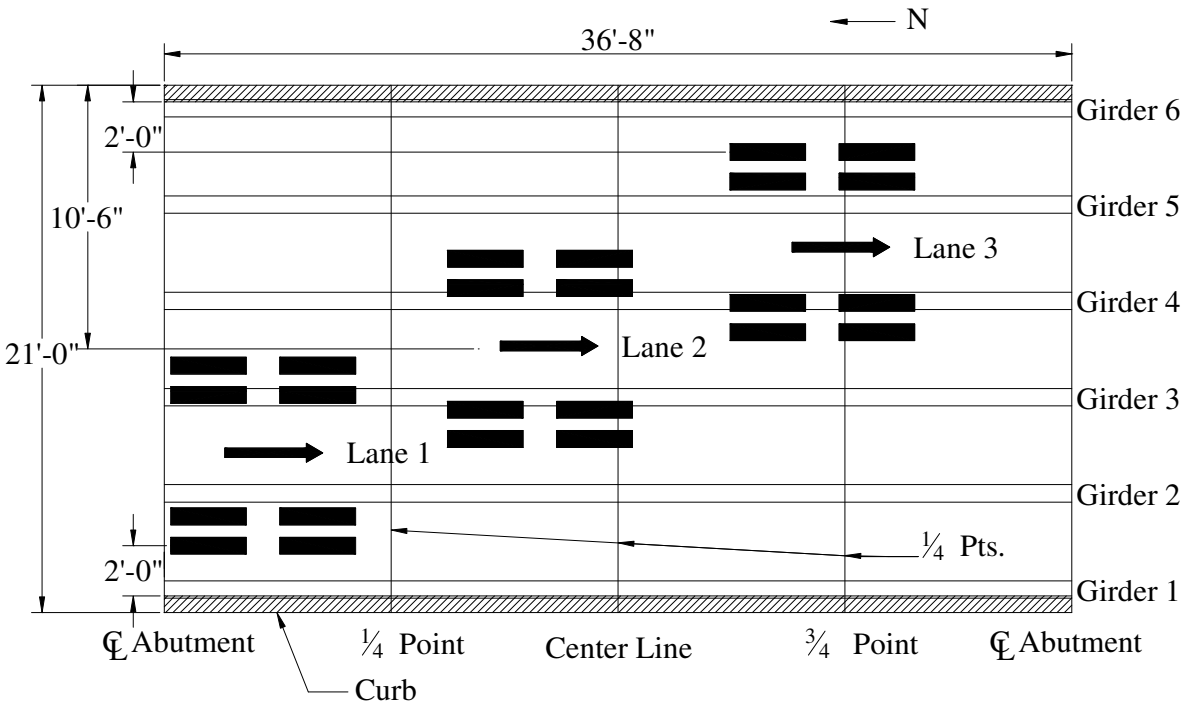

Figure 3.9. Plan View of Loading Lanes Used in BCB Test.

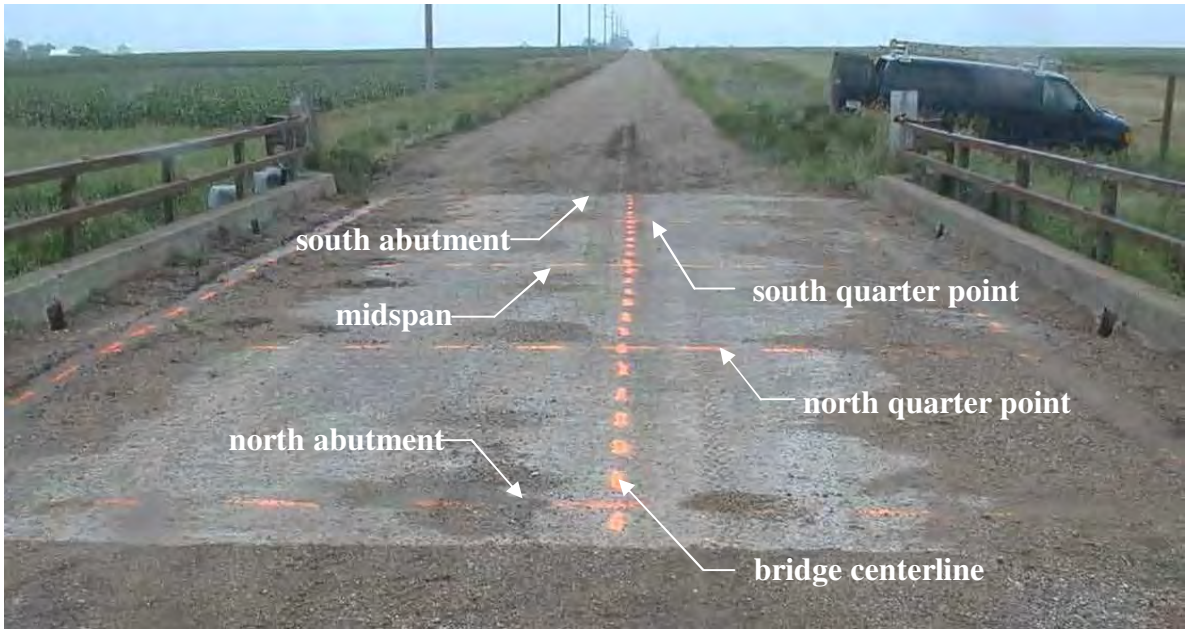

Figure 3.10. Location of BCB Quarter Points and Abutment Centerlines.

Figure 3.11. BCB Truck Tandem Centroid Centered Over Abutment.

The bridge was instrumented six inches (see Figure 3.12) from the edge of the bearing at each abutment and at the midspan. Strain transducers were installed on the top and bottom flanges of Girders 1, 3, and 5 near each abutment as shown in Figure 3.13. At the midspan, strain transducers were attached on the top and bottom flanges of each of the girders as well as on the underside of the concrete deck near Girders 1, 3, and 5 near each abutment as shown in Figure 3.14. Also, shown in Figure 3.14 are the locations of the deflection transducers installed at the midspan on all of the girders. There were a total of 24 strain transducers and six deflection transducers installed on the bridge for the load test. Strain transducers installed on the concrete had extensions attached to increase the gage length from the standard three inches to nine inches. A photograph of a concrete mounted strain transducer as well as a transducer on the bottom surface of the top flange of one of the girders is presented in Figure 3.15.

3.3 Bridge Analysis

3.3.1 Neutral Axis and Partial Composite Action

The bridge was designed as a non-composite simple span bridge. As is common with most bridges of this type, there were some unintended responses from the bridge that could increase the flexural capacity of the bridge. Shown in Figure 3.16 through Figure 3.18 are the top and bottom flange strains and the deflections with the loading in Lane 1, Lane 2, and Lane 3, respectively. In the three figures, TF and BF refers to the top and bottom flange strains,

Figure 3.12. Instrumentation Near Abutment of BCB

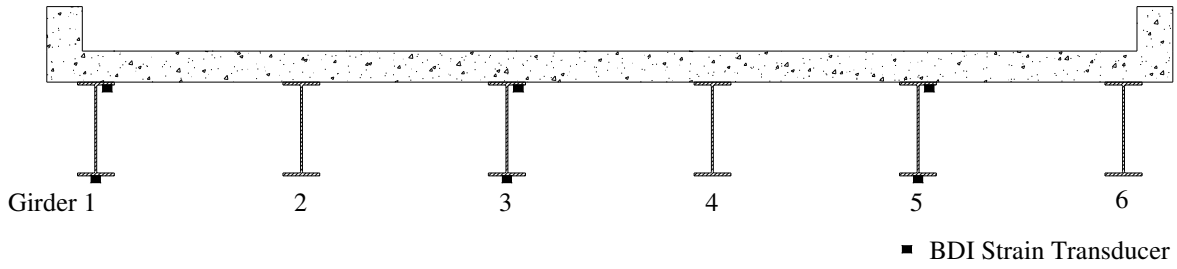

Figure 3.13. BCB North and South End Transducer Locations Looking North

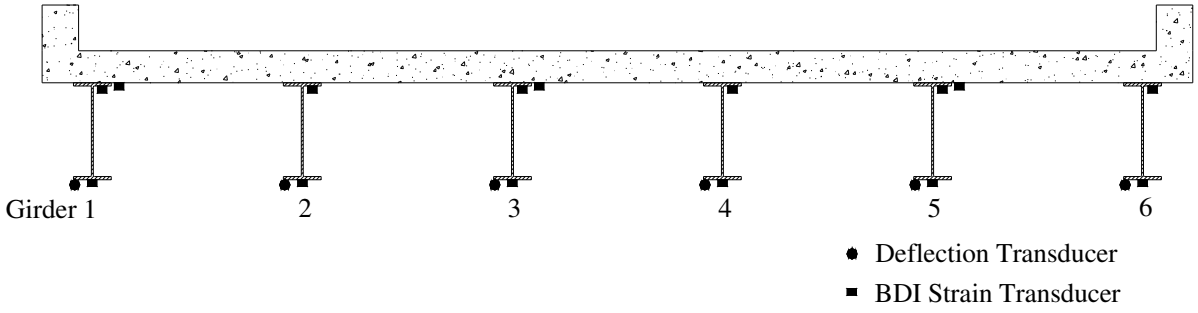

Figure 3.14. BCB Midspan Transducer Locations Looking North.

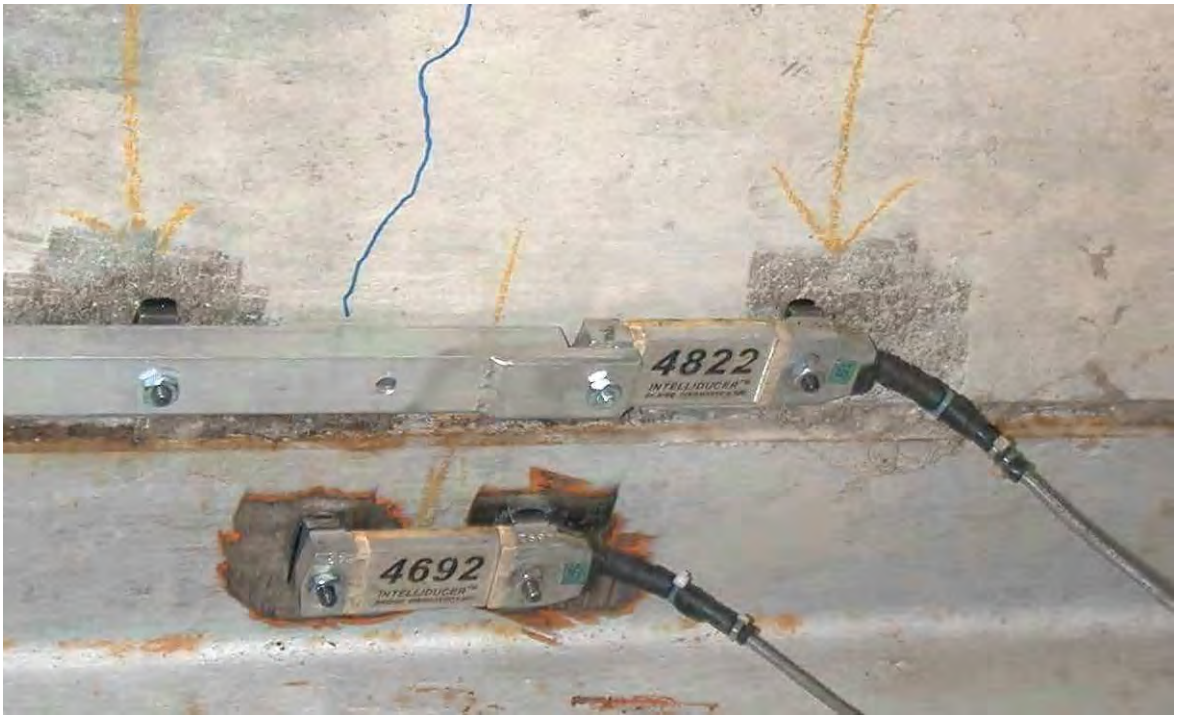

Figure 3.15. Concrete and Steel Mounted Transducers at Midspan of BCB.

respectively. The deflection profiles follow the same general shape as the bottom flange strain profiles. As can be seen in Figure 3.17, there was symmetry in the deflection and strain profiles for the truck centered on the bridge. The maximum tensile strains observed in Lane 1, Lane 2, and Lane 3 were 119, 104, and 134 microstrain, respectively and the maximum deflections were 0.147, 0.125, 0.150 inches, respectively.

The strain values plotted are not the maximum values obtained during the various tests but are the values obtained when the centroid of the truck tandem was directly over the midspan of the bridge. Maximum strains in each girder did not occur when the truck was at the same longitudinal position on the bridge; so for uniformity, the longitudinal truck position producing strain values close to the maximum values was selected as the centroid of the truck tandem coinciding with the midspan location of the bridge. The absolute maximum top and bottom flange strains observed for the full truck at varying longitudinal positions are shown in Table 3.2 and the values plotted with the previously noted truck position are presented in Table 3.3.

The following descriptions are used to differentiate the locations of the BDI transducers. The first character describes its location: N for north abutment, M for midspan, and S for south abutment, while the second character identifies which girder the BDI was on. The third character is used to identify the location of the BDI on the girder: B for the bottom flange, T for the top flange, and C for the concrete on the underside of the deck. For example, M3B would indicate a BDI located at the midspan on the bottom flange of Girder 3.

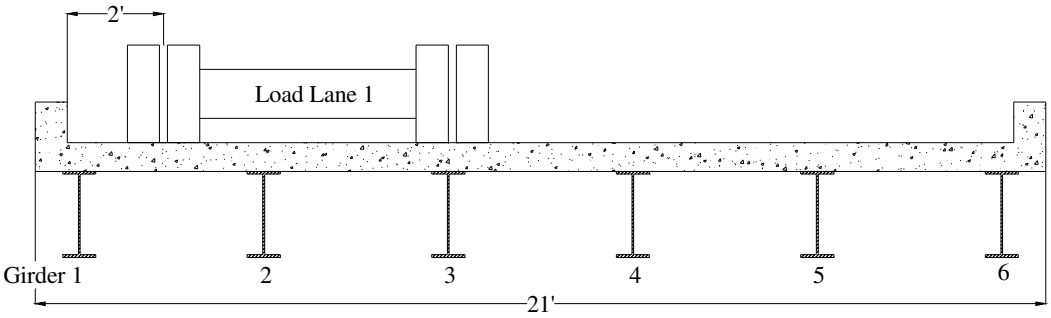

(a) Lane 1 Loading

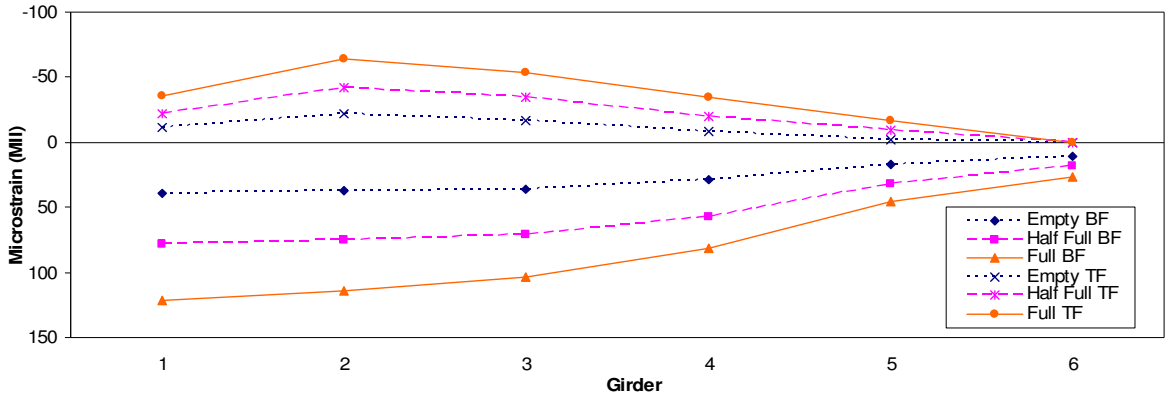

(b) Strain Profile

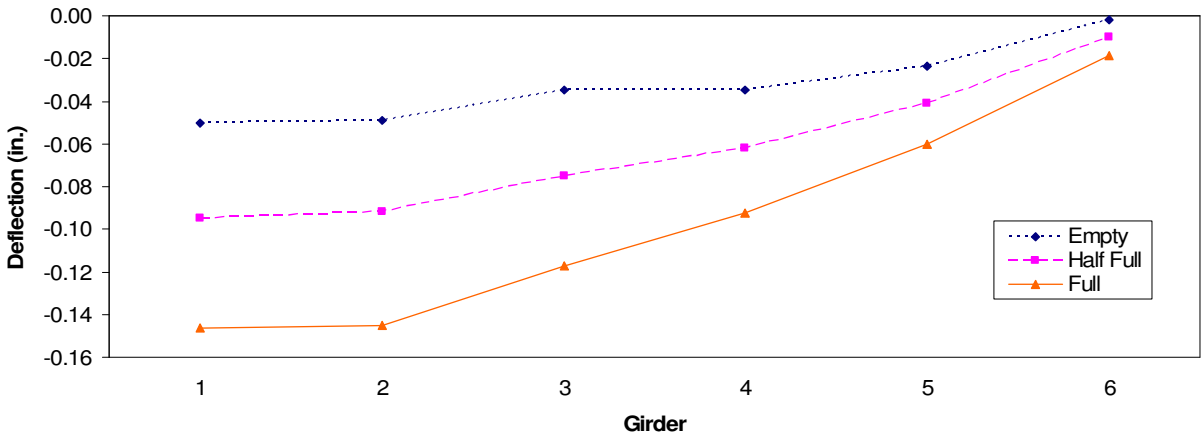

(c) Deflection Profile

Figure 3.16. BCB Lane 1 Strains and Deflections

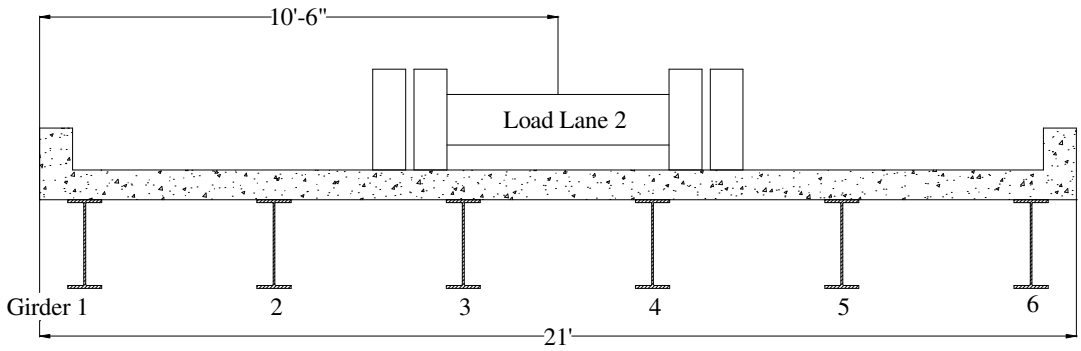

(a) Lane 2 Loading

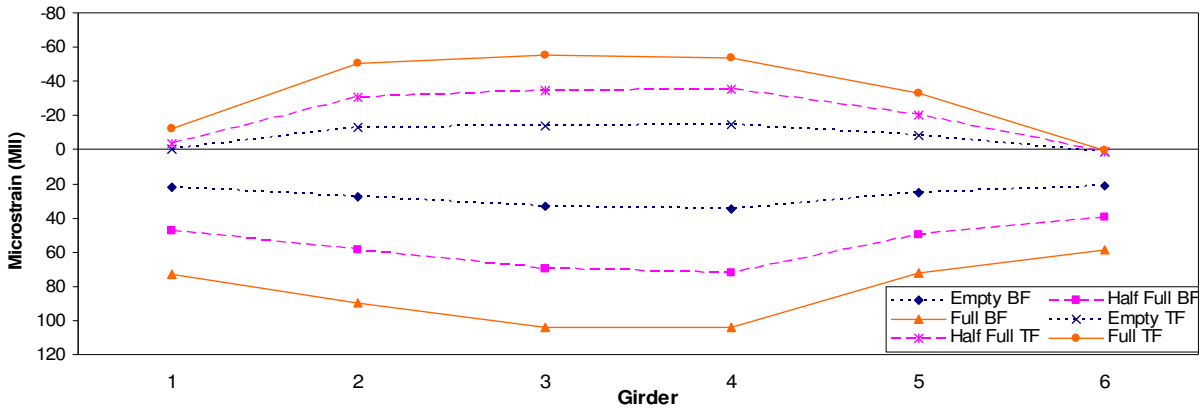

(b) Strain Profile

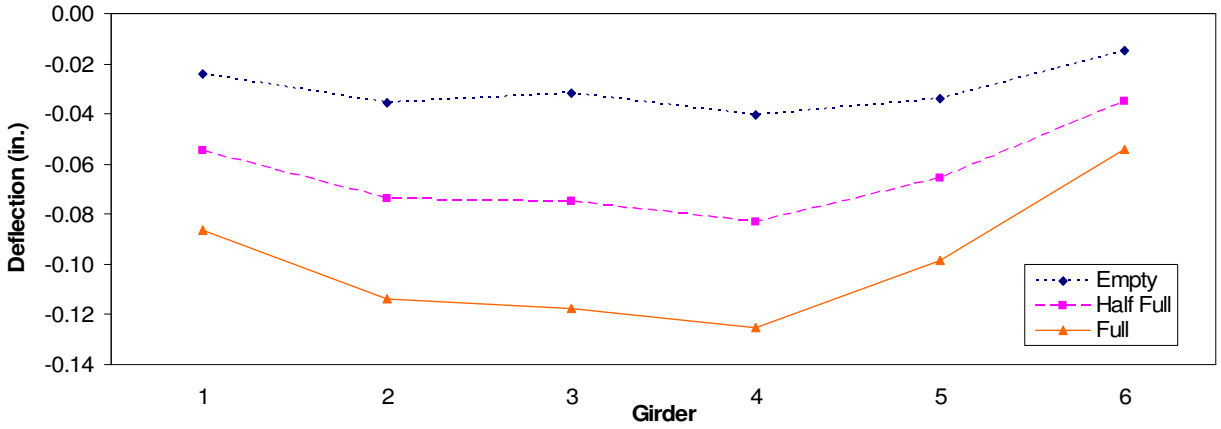

(c) Deflection Profile

Figure 3.17. BCB Lane 2 Strains and Deflections

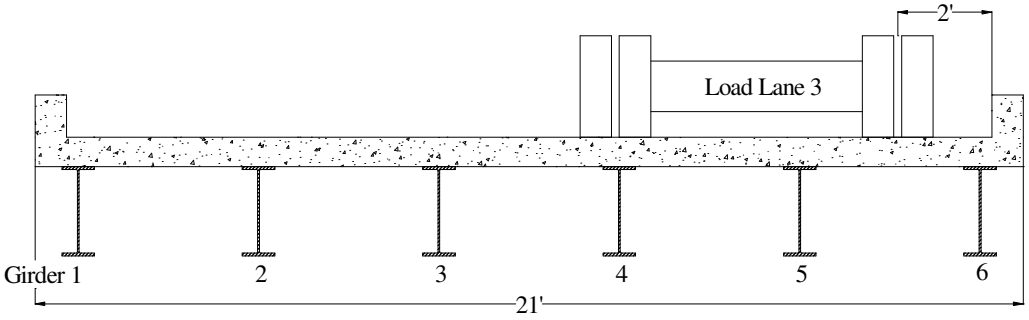

(a) Lane 3 Loading

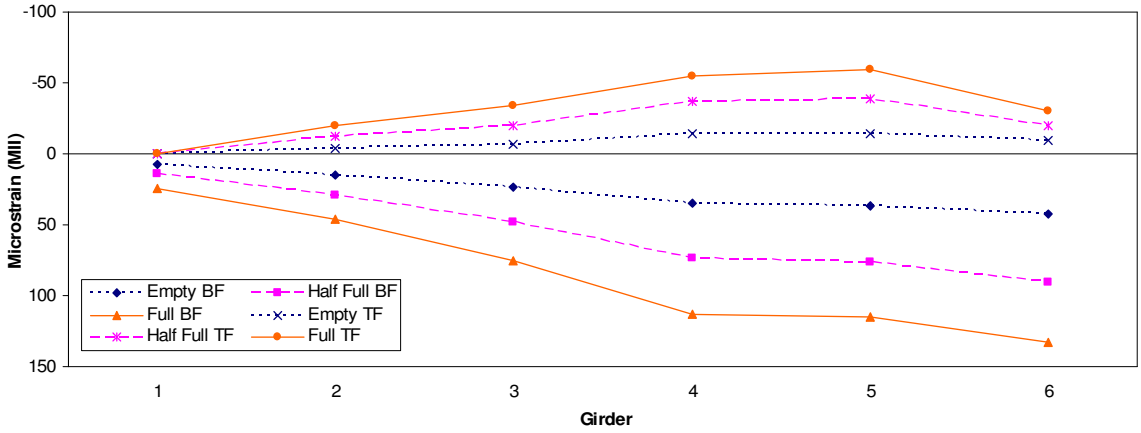

(b) Strain Profile

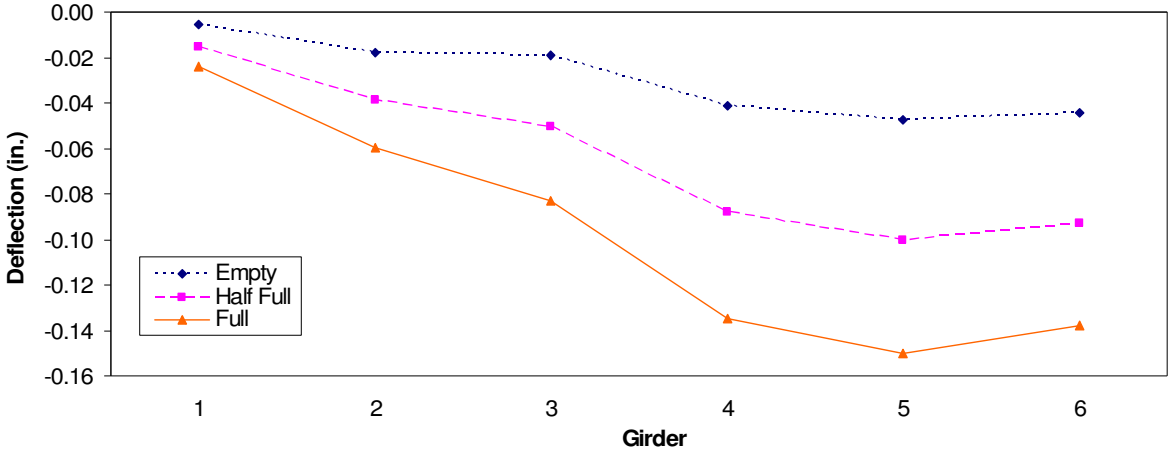

(c) Deflection Profile

Figure 3.18. BCB Lane 3 Strains and Deflections

Table 3.2. BCB Maximum Strains Obtained.

Lane	Microstrain (MII)											
	M1B	M2B	M3B	M4B	M5B	M6B	M1T	M2T	M3T	M4T	M5T	M6T
1	124	116	105	83	47	28	-36	-65	-55	-35	-17	-1
2	75	90	105	106	75	61	-12	-50	-57	-55	-33	-2
3	26	48	76	113	118	136	0	-21	-34	-57	-63	-31

Table 3.3. BCB Midspan Strains.

Lane	Microstrain (MII)											
	M1B	M2B	M3B	M4B	M5B	M6B	M1T	M2T	M3T	M4T	M5T	M6T
1	119	112	104	80	45	26	-34	-63	-54	-34	-17	1
2	72	89	104	104	72	58	-12	-49	-56	-54	-33	0
3	24	46	76	112	115	134	0	-20	-33	-56	-60	-29

The largest difference in strains occurred in the Lane 1 loading for the M1B BDI transducer where there was a difference of 5 microstrain which is a 4.9% difference. With the very small discrepancy between the maximum values and those plotted, only the values obtained when the centroid of the truck tandem was at the midspan of the bridge will be reported for the remaining five bridge tests.

The neutral axis locations, shown in Figure 3.19, were determined by interpolating between the top and bottom flange strains to determine the location on the girder where the strain was equal to zero. Partial composite action, shown simply by the location of the neutral axes being located between the theoretical composite and non-composite neutral axis locations, was observed in all of the girders for each of the three lanes loaded. The partial composite action deteriorated with increased loading; this can be seen in Figure 3.19 by the neutral axis location moving toward the non-composite neutral axis location with the increased loading.

A neutral axis location above the top flange, as observed in Figure 3.19(a) and (b) for Girder 6, indicates the neutral axis for the girder was located in the concrete deck. The two exterior girders exhibited considerably higher stiffnesses than the interior girders as determined by a much higher neutral axis location which is indicative of a composite section. When directly loaded, the neutral axis of the exterior girders was close to that of a fully composite girder, but when the load was on the opposite side of the bridge, the neutral axis location was above the theoretical composite neutral axis location. This can be attributed to the very small top flange strain values (1 and 0 microstrain in Lane 1 and Lane 3, respectively as displayed in Table 3.3) observed in the girders that were on the opposite side of the bridge as the loading. The increased stiffness can be attributed to the concrete curb and the steel railing which were not included in the calculation of the composite neutral axis location. Neutral axis profiles for Lane 1 and Lane 3 were close to the mirror images of each other which demonstrate bridge symmetry.

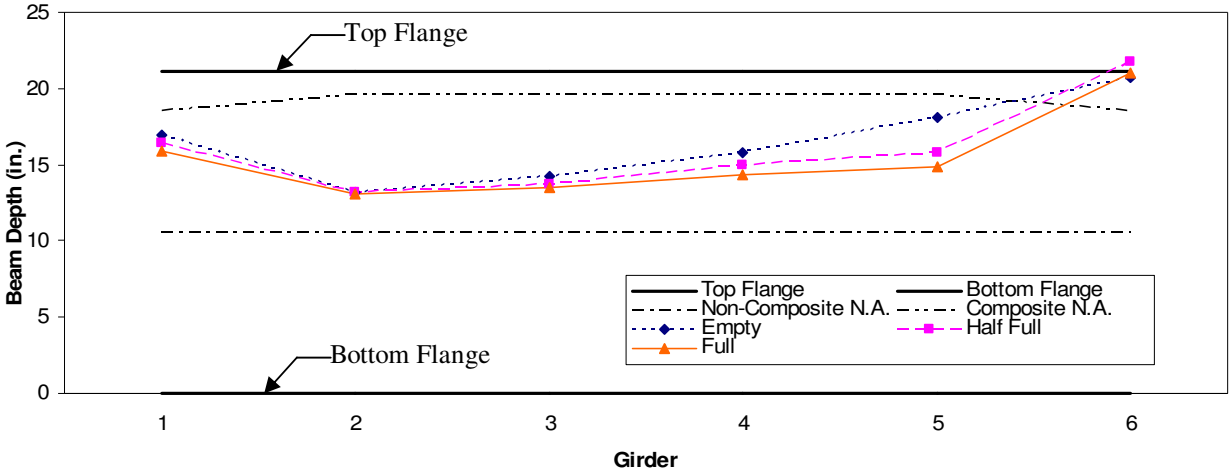

(a) Lane 1

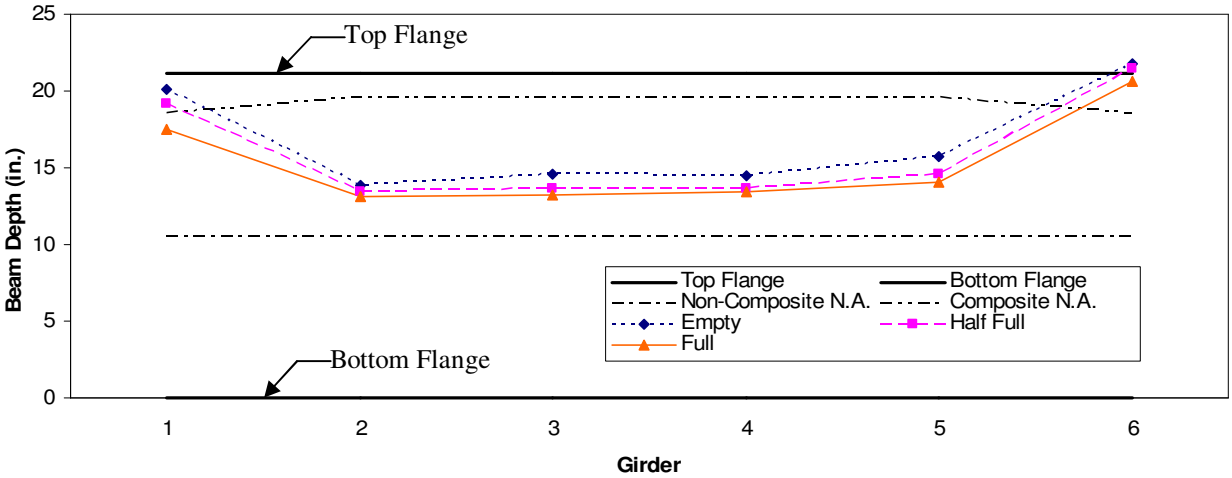

(b) Lane 2

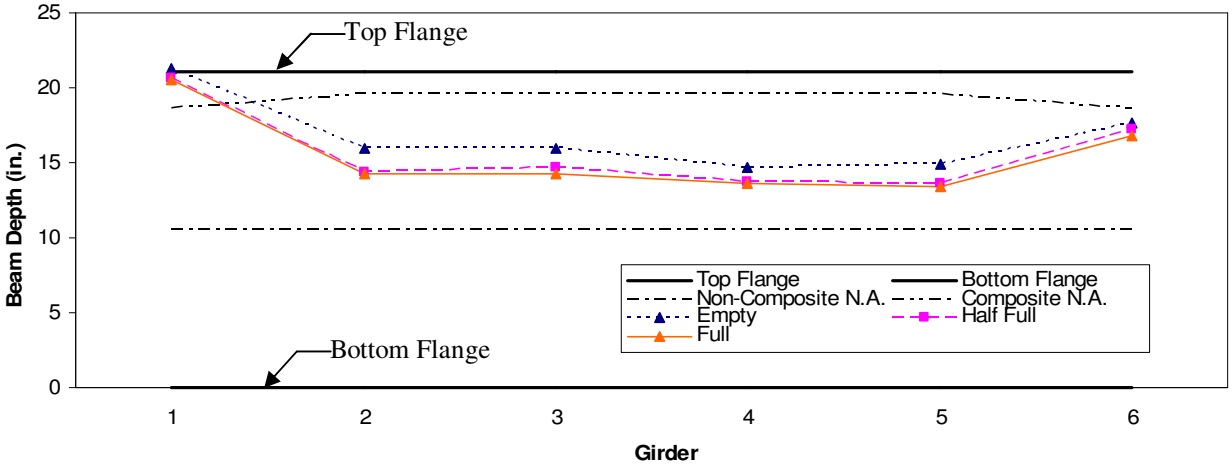

(c) Lane 3

Figure 3.19. BCB Neutral Axis Locations.

3.3.2 Load Distribution

Using the previously described truck locations, the theoretical moment induced in the bridge, assuming simply supported conditions, was calculated for each loading; these are presented in Table 3.4. As may be seen in this table, there was an 88% increase in moment from empty to half full and a 174% increase in moment from empty to full.

Table 3.4. BCB Induced Truck Moments.

Load	Moment (in-k)
Empty Truck	1250
Half Full Truck	2355
Full Truck	3425

The live load distribution factor equations have been modified during the past ten years but the new, more complex distribution factors are seldom used by county engineers who use the more conservative "s-over" equations. From the 1998 AASHTO Standard Specifications for Highway Bridges, the distribution factors for a bridge with a concrete deck on steel I-girder girders are S/7.0 and S/5.5 for one and two traffic lanes, respectively. Using the bottom flange strains, the percent distributions were calculated as the ratio of the individual girder strain to the sum of all six girder strains. With each of the three load increments producing slightly different load distribution percentages, the maximum values, summarized in Table 3.5, were selected for each of the three lanes. Note that the values are the maximum percentage values of the three load cases and therefore do not sum to 100%. As may be seen, the maximum distribution percentages occurred in the exterior girders when directly loaded. Girders 3 and 4 had distribution percentages very close to each other for Lane 2 loading further displaying the bridge symmetry observed in the bottom flange strain profile shown in Figure 3.17.

Table 3.5. BCB Maximum Single Lane Percent Distributions.

Lane \ Girder	1	2	3	4	5	6
1	24.5	23.1	21.5	17.0	10.2	6.7
2	14.5	17.9	20.8	21.3	15.6	12.8
3	5.0	9.2	14.9	22.1	23.5	27.3

As previously noted, the percent distribution are provided in Table 3.5; however in order to compare the load distribution to the AASHTO distribution factors, the values must be multiplied by two to obtain the distribution of a single wheel line. The maximum distribution factors from the percent distributions summarized in Table 3.5 are provided in Table 3.6. Using superposition, Lanes 1 and 3 were used to determine the distribution factors, also shown in Table 3.6, for two lanes. As previously noted, the partial composite action deteriorated with increased loading as shown by the neutral axis locations moving toward the non-composite neutral axis location; therefore, calculating multiple lane distribution factors using superposition is not a conservative approach.

Table 3.6. BCB Calculated Distribution Factors.

Lane \ Girder	1	2	3	4	5	6
1	0.49	0.46	0.43	0.34	0.20	0.13
2	0.29	0.36	0.42	0.43	0.31	0.26
3	0.10	0.18	0.30	0.44	0.47	0.55
1&3	0.59	0.65	0.73	0.78	0.67	0.68

The maximum distribution factors for the interior and exterior girders for the single lane loading are 0.47 and 0.55, respectively, while the AASHTO distribution factor for the single lane loading with a girder spacing of 3'-10" using the aforementioned equation of S/7.0 is 0.55. The maximum distribution factors for the interior and exterior girders for the two lane loading are 0.78 and 0.68, respectively, while the AASHTO distribution factor for multiple lane loading using the aforementioned equation of S/5.0 is 0.70. Values obtained by dividing the AASHTO distribution factors by the experimental distribution factors are summarized in Table 3.7.

Table 3.7. BCB Distribution Ratios.

	Single Lane	Two Lanes
Interior Girder Distribution	0.47	0.78
Exterior Girder Distribution	0.55	0.68
AASHTO Distribution Factor	0.55	0.70
Interior Factor Ratio	1.17	0.89
Exterior Factor Ratio	1.00	1.03

The distribution ratios for the single lane show that the AASHTO equations are slightly conservative as the ratios exceed 1.0. For the two lane loading case though, the ratios indicate that the actual load distribution is smaller than predicted using the AASHTO equation for the interior girders. The exterior girder load distribution is very close to the factors predicted using the AASHTO equations with the ratios being very close to 1.0.

3.3.3 Moment of Inertia

The moment of inertia is not the same for each girder due to the varying amount of partial composite action. In order to calculate the moment of inertia for each girder, the neutral axis was determined from the top and bottom flange strains for each load case which moved the neutral axis toward the top flange of the girder. Once the neutral axis location was determined from the strain data, a composite section with an effective concrete width necessary to move the neutral axis from the non-composite location to that calculated from the strain data was determined. Knowing the effective width of concrete allows a theoretical partial composite moment of inertia to be determined. A diagram of the effective girder section is shown in Figure 3.20. The neutral axis locations for each girder are close to the same for the three load increments. Moments of inertia in each girder for the three load increments were averaged and are provided in Table 3.8.

The non-composite moment of inertia for the steel girder is 1,480 in4 and the composite moment of inertia for the girder with an effective flange width equal to the girder spacing is 4,230 in4 for the interior girders and 3,890 in4 for the exterior girders. The moment of inertia for the exterior girders does not consider the curb or the railing in the calculation. Including the curb alone would result in a moment of inertia for the exterior girders larger than that of the interior girders. The interior girders had moments of inertia that were between those calculated for the composite and non-composite sections; the exterior girders had considerably higher moments of inertia than those calculated for the composite section. As was the case with the neutral axis locations in the exterior girders that did not have the load directly above them, the relatively small strains observed in the top flanges of the girders caused the moment of inertia to be larger than those calculated from the larger strain values. The increased stiffness of the curb and railing that were not accounted for in the composite moment of inertia calculations account for the difference. The moments of inertia for each girder and lane loading are shown graphically in Figure 3.21 along with the values for the non-composite and composite neutral moments of inertia. An average moment of inertia for the three lane loadings is also provided in this figure.

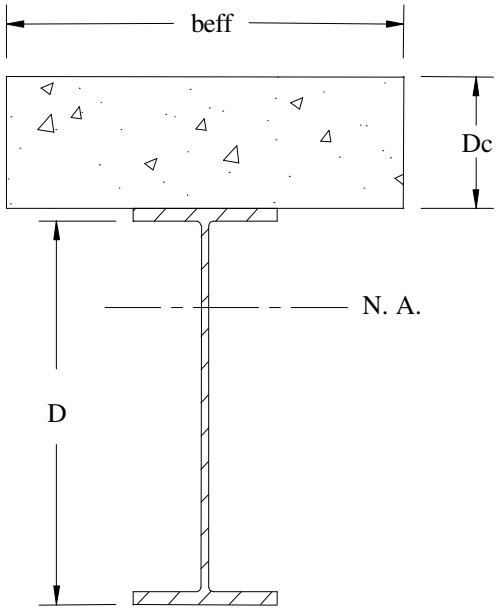

Figure 3.20. Effective Section.

Table 3.8. BCB Moments of Inertia (in^4).

Lane \ Girder	1	2	3	4	5	6
1	3220	2245	2435	2800	3175	4800
2	4010	2340	2450	2465	2735	4830
3	4665	2745	2785	2500	2495	3465
Average	3965	2445	2555	2590	2800	4365

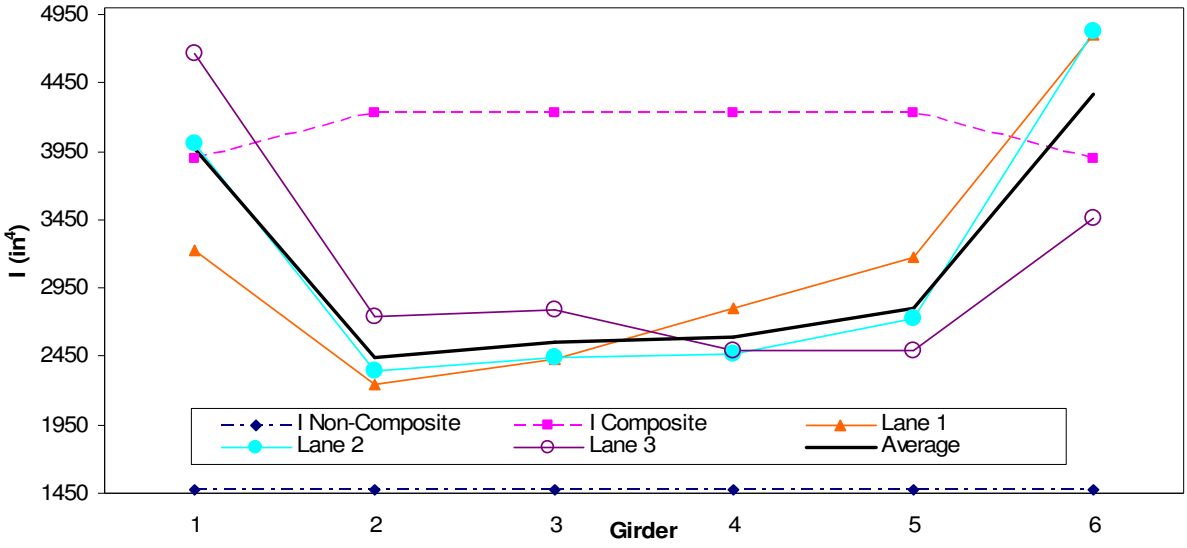

Figure 3.21. BCB Effective Moments of Inertia.

3.4 BDI Optimization

The bridge was modeled using software (WinGEN) provided by Bridge Diagnostics Inc. that utilizes the actual test data to create a model that is close to the actual bridge based on the response of the structure to the truck loadings. This bridge model modeled each girder separately allowing the moment of inertia for each girder to be optimized separately. This was important due to the partial composite action differences in each of the girders. The deck was modeled using plate elements, while the girders were modeled using girder elements. Rotational springs were attached to the ends of each of the girders. There were four rotational springs used: one for the north end of the exterior girders, one for the north end of the interior girders, and two more for the interior and exterior girders on the south end of the bridge.

As a starting point for the model generation, the average values presented in Table 3.8 were used for the initial girder moments of inertia. The initial value assumed for all of the spring constants was 1000 kip-in/rad and the initial Young's modulus for concrete was determined by assuming a concrete strength of 3,000 psi. Using an empirical formula, the initial value for the modulus of concrete was determined to be 3,150 ksi.

Only the strains measured on the steel girders were input into the model; concrete slab strains were not input into the model because there were large variations in the concrete strains measured due to the random location of cracks. After the model was generated using WinGEN, it was then analyzed using WinSAC. WinSAC compares the actual strains induced by the test truck to those produced by a theoretical truck with the same dimensions and wheel loads crossing the modeled bridge in the same lanes. Theoretical girder strains determined

using the initial input values for the girder moments of inertia, concrete modulus of elasticity, and rotational spring stiffness yielded a scale error of 21.4%.

With the scale error being so large, the model needed to be optimized. The parameters that were optimized included the moments of inertia for each girder, the rotational spring stiffness, and the deck modulus of elasticity. Upper and lower bounds selected for the optimization parameters are presented in Table 3.9. The upper and lower bound for the moment of inertia of the girders corresponded to 120% of the composite and 80% of the non-composite moments of inertia, respectively. Optimizing the bridge using the parameters in Table 3.9 yielded a scale error of 9.3%; the optimized values are provided in Table 3.10.

The procedure outlined in Section 3.3.3 where an attempt to obtain initial moments of inertia for the girders was not successful as the optimized values did not correlate with the initial values presented in Table 3.10. The apparent symmetry observed in the neutral axis, deflection profile, and strain profile plots previously presented was not observed in the optimized girder moments of inertia. For example, the symmetry in strain and deflection responses for Girders 3 and 4 displayed in Figure 3.17 did not result in similar optimized moments of inertia as the moments of inertia in Girders 3 and 4 were 1,875 and 3,010 in^4, respectively. The lack of symmetry in the optimized values can also be observed in the values obtained for the spring constants. A symmetrical bridge would presumably have the same spring constants for both ends of a bridge; however, the optimized values for the rotational springs on the north side of the bridge were lower than those for the south side of the bridge. A deck modulus of 4,745 ksi corresponds to a concrete compressive strength of about 6,800 psi, more than double the initial assumed concrete strength of 3,000 psi. A graphical comparison of the optimized strains for each loading path to the actual strain values induced by the test truck for Girder 1 through Girder 6 are presented in Figure 3.22 through Figure 3.27, respectively.

Table 3.9. BCB Optimization Parameters.

Optimization Parameter	Lower Bound	Upper Bound
Moment of Inertia (in^4)	1185	4780
Rotational Spring Stiffness (kip-in/rad)	0	1,000,000
Modulus of Concrete (ksi)	2500	5500

Table 3.10. BCB Optimized Parameters Using All Steel Transducers.

Optimized Parameter	Initial Value	Optimized Value
Girder 1 I_y (in^4)	3965	4525
Girder 2 I_y (in^4)	2445	3590
Girder 3 I_y (in^4)	2555	1875
Girder 4 I_y (in^4)	2590	3010
Girder 5 I_y (in^4)	2800	3580
Girder 6 I_y (in^4)	4365	3835
North Exterior Rotational Spring (kip-in/rad)	1000	239,200
North Interior Rotational Spring (kip-in/rad)	1000	138,400
South Exterior Rotational Spring (kip-in/rad)	1000	671,300
South Interior Rotational Spring (kip-in/rad)	1000	243,600
Deck Modulus (ksi)	3150	4745

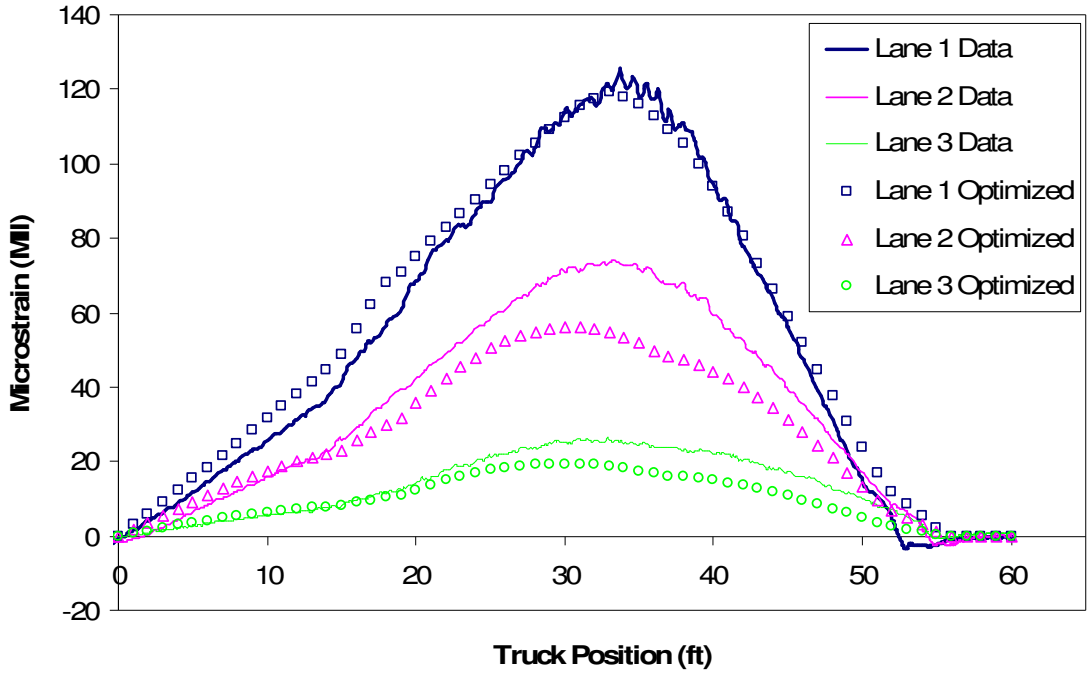

Figure 3.22. BCB Girder 1 Optimized Strain Comparison.

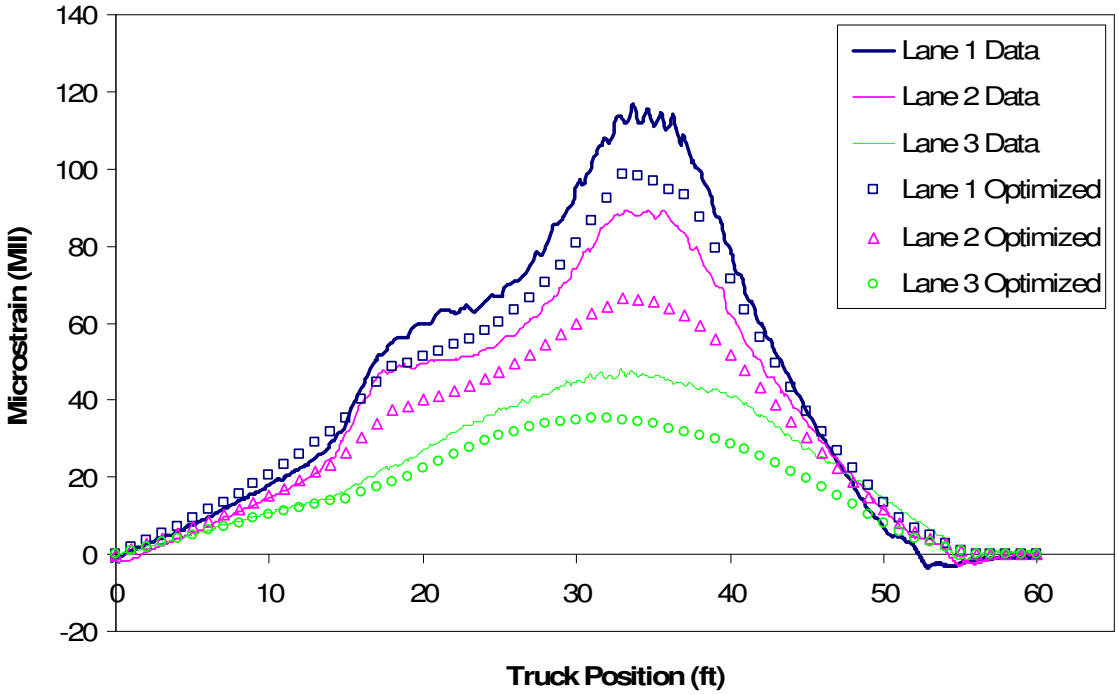

Figure 3.23. BCB Girder 2 Optimized Strain Comparison.

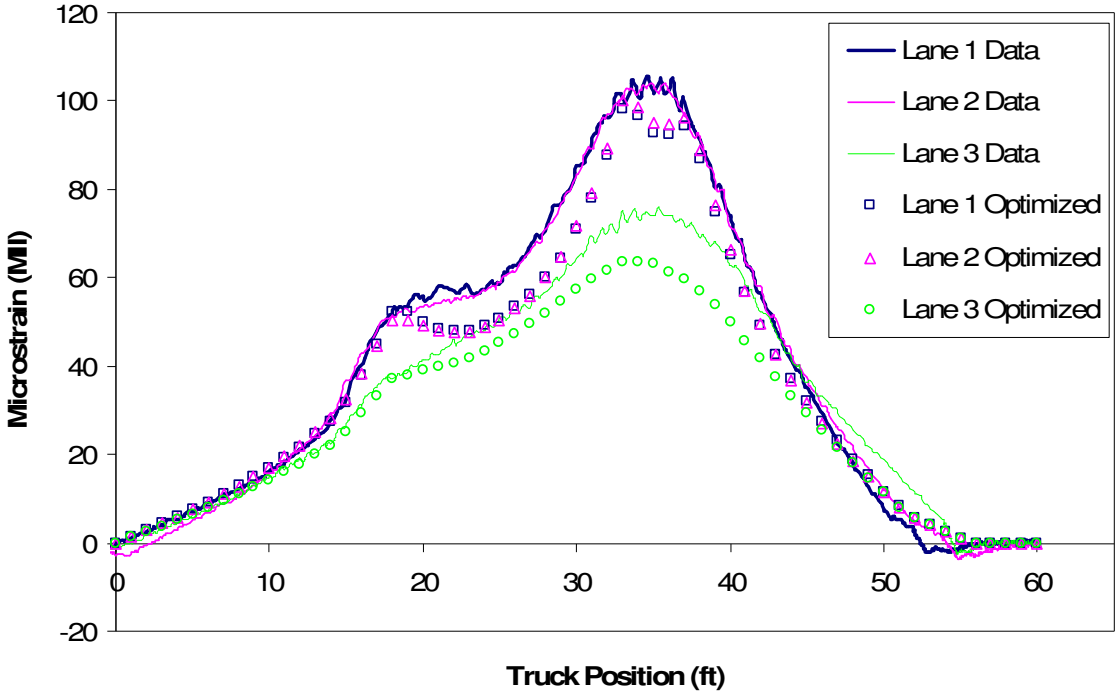

Figure 3.24. BCB Girder 3 Optimized Strain Comparison.

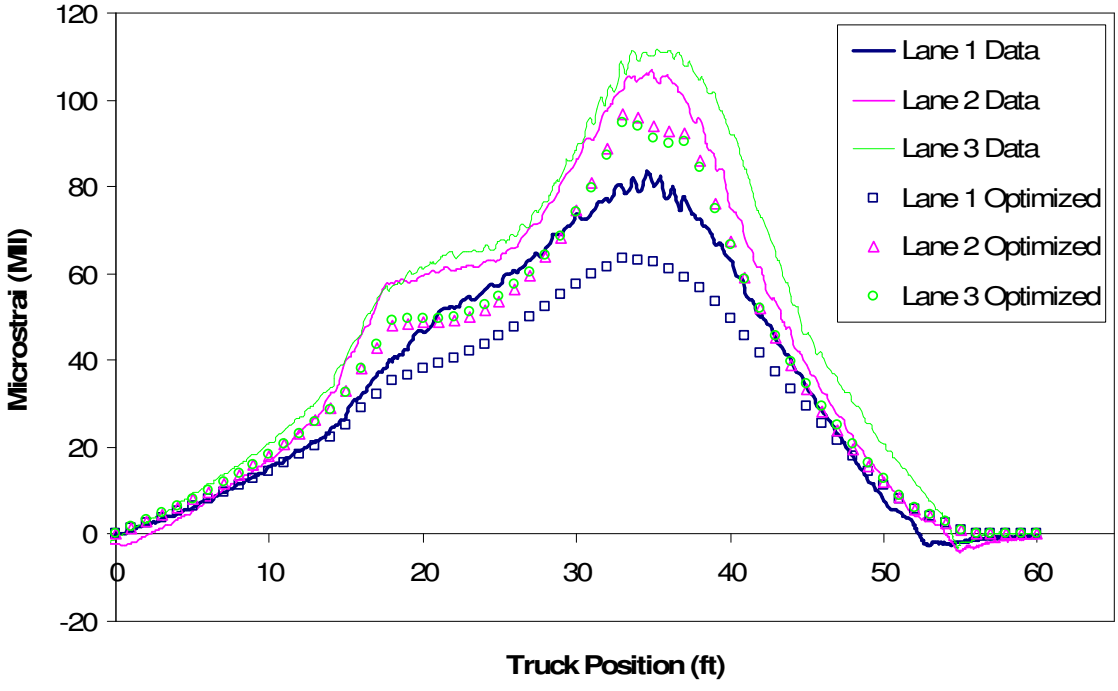

Figure 3.25. BCB Girder 4 Optimized Strain Comparison.

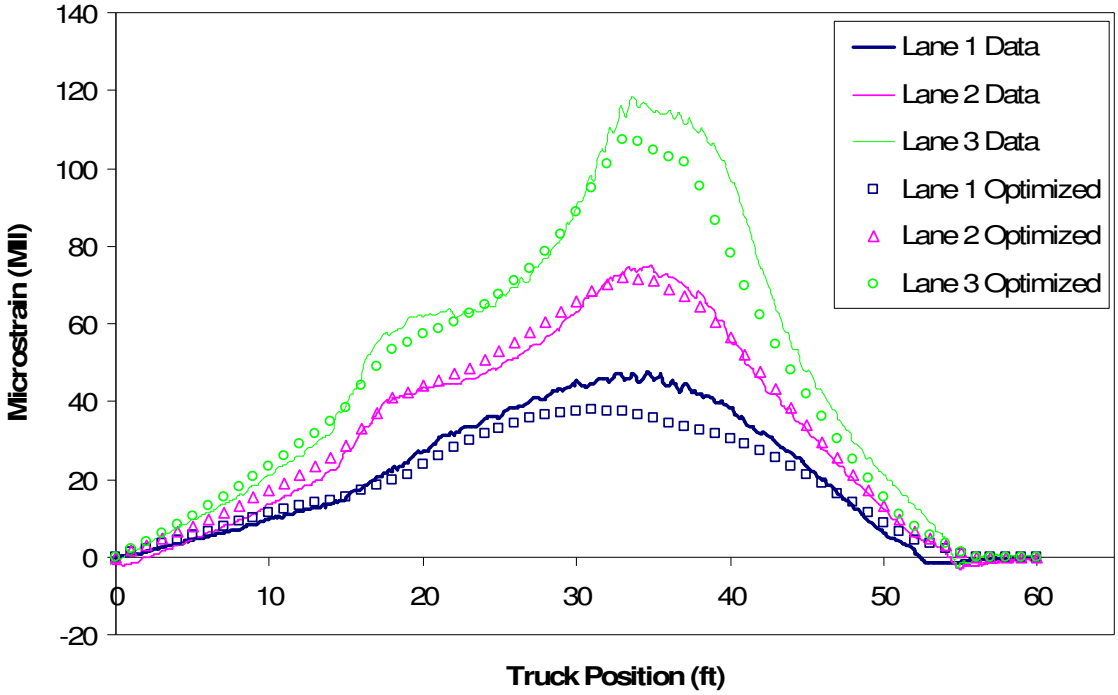

Figure 3.26. BCB Girder 5 Optimized Strain Comparison.

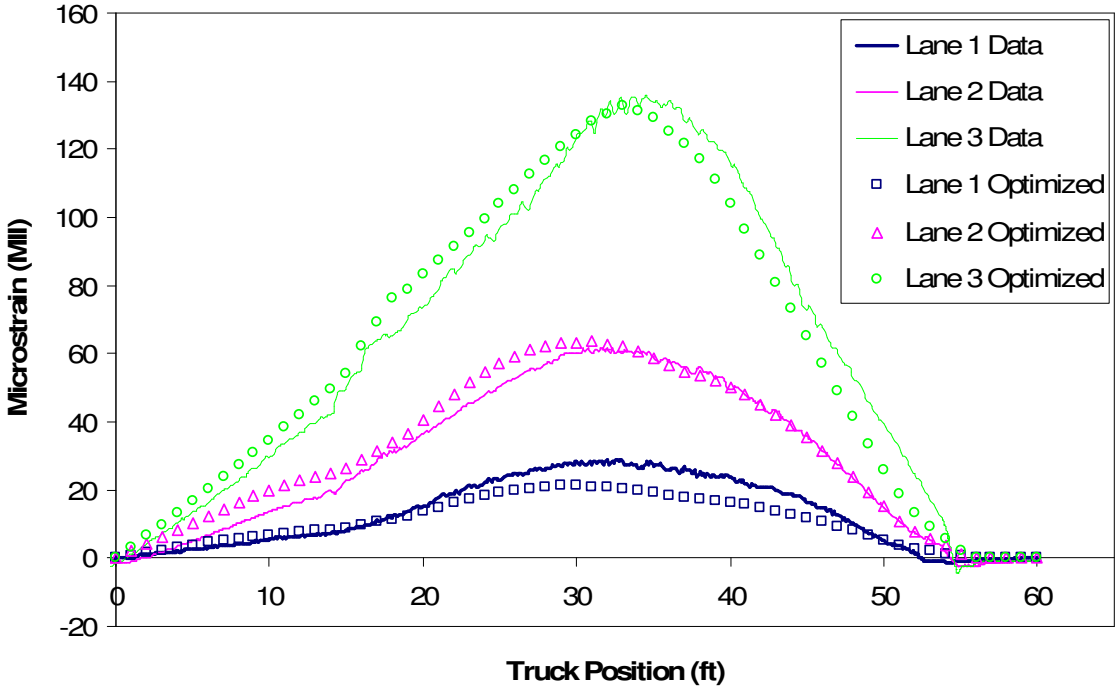

Figure 3.27. BCB Girder 6 Optimized Strain Comparison.

In almost all cases, the optimized strain values were close to the actual strain values from the test truck. The correlation between the optimized strains and the actual strains are summarized in Table 3.11. The scale error ranged from 0.4 to 2.8 and the correlation ranged from 0.833 to 0.974. A scale error of 0 and a correlation of 1.0 represent a perfect fit between the theoretical results produced with the WinGEN model and the actual load test results.

Table 3.11. BCB Bottom Flange Strain Scale Error and Correlation.

Girder	1	2	3	4	5	6	Average
Scale Error	1.7	0.4	1.1	1.2	2.2	2.8	1.6
Correlation	0.890	0.845	0.833	0.863	0.903	0.974	0.885

In an attempt to decrease the overall scale error, the strains measured near the supports were removed from the bridge optimization model. The previous optimized values were input into a model that had only the girder midspan strains in an attempt to quantify the effect of the bearing transducers on the scale error. This model was analyzed and resulted in a scale error of only 2.3%, a 7% reduction from the optimized model using all of the girder strains. The correlation values provided in Table 3.11 did not change in the new analysis.

To obtain a better understanding as to the effect of the rotational springs on the bridge performance, the optimized concrete deck modulus of elasticity and the moments of inertia for each girder were input into the model. Then, using the modified model, the spring constants for all spring locations were held constant and simultaneously increased from 0 kip-in/rad to 1 billion kip-in/rad. A separate bridge analysis, using the original BCB test truck crossing the bridge, was conducted for each spring constant increment. The comparison between the spring constants to the actual and optimized test data for the Lane 1 loading in Girder 1 is provided in Figure 3.28. Note that the aforementioned optimized spring constants were not the same on both the north and south ends of each girder but were the same for this investigation. A log based graphical representation comparing the maximum strain observed to the spring constant is provided in Figure 3.29.

The optimized spring constants show that the bridge is neither completely simply supported nor completely fixed. Based on the results for the spring constant comparison, a value of 10 million kip-in/rad for the spring constant represents a condition of 95% fixity and the increase from a spring constant of 100 million to 1 billion kip-in/rad was insignificant. This was determined by comparing the maximum strain in the bridge with a spring constant of 10 million to the maximum strain for a spring constant of zero and the maximum strain for a spring constant equal to 1 billion. From Figure 3.29, it can be observed that the optimized spring constants result in a condition of 35% fixity; therefore, the optimized model will produce midspan strains lower than those calculated assuming simply supported end conditions on the girders.

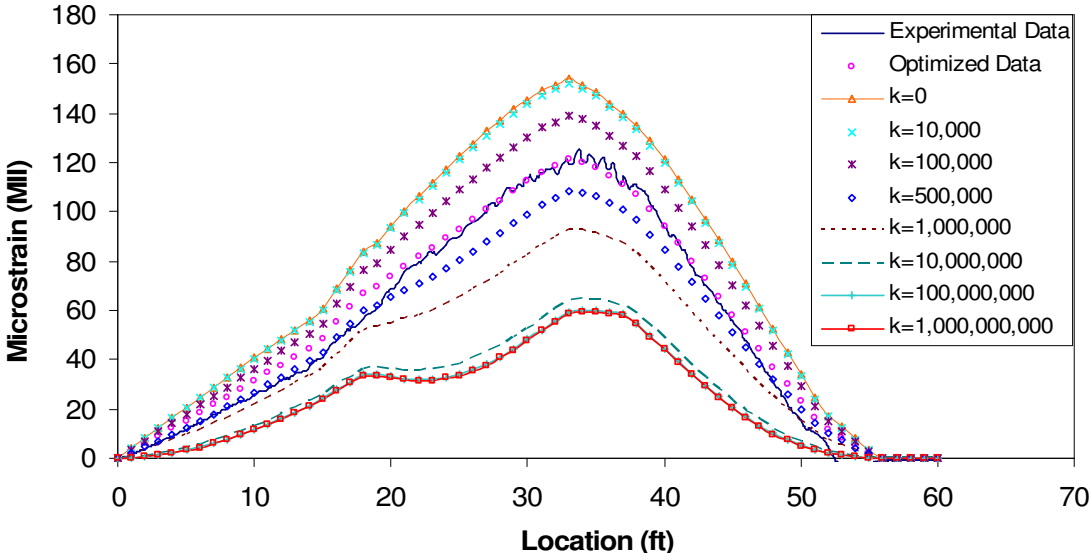

Figure 3.28. BCB Spring Constant Comparison for Lane 1 Girder 1.

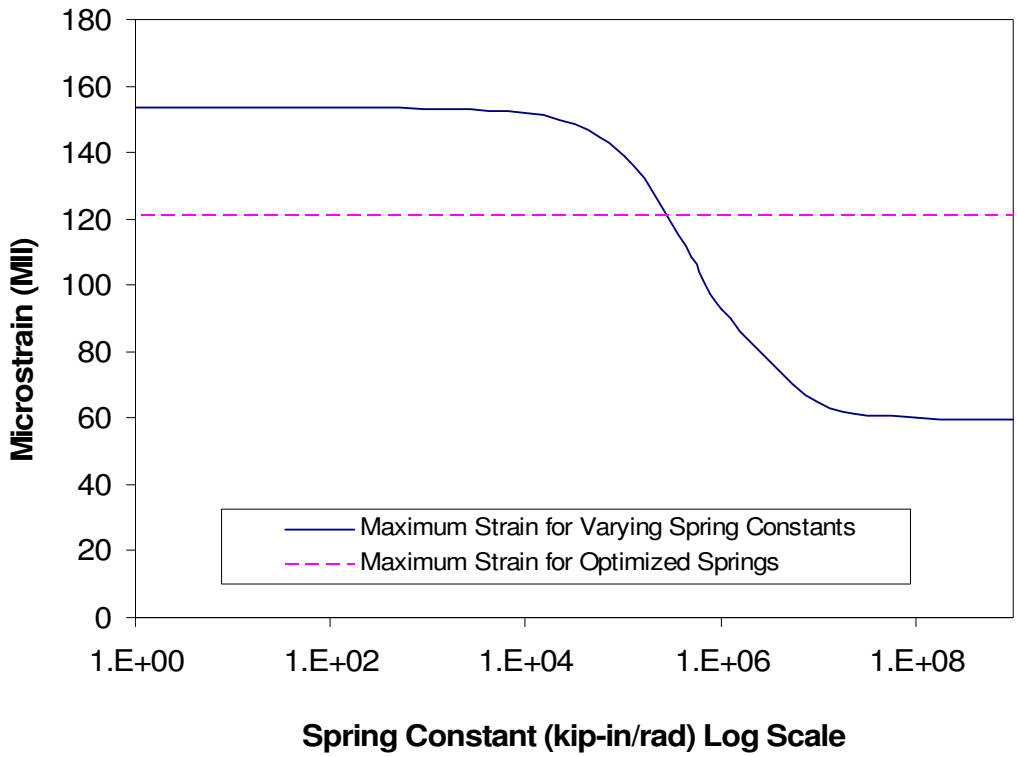

Figure 3.29. BCB Girder 1 Lane 1 Maximum Strain for Varying Spring Constants.

3.5 Bridge Rating

3.5.1 Conventional Rating

The bridge was rated using the Load Factor Rating (LFR) approach. This analytical rating, in which both the interior and exterior girders were rated, was performed assuming a non-composite design with simply supported conditions. The bridge was also independently rated by both the Iowa DOT and a private consulting firm (PCF). Ratings calculated by the three different rating agencies are provided in Table 3.12.

Table 3.12. BCB Analytical Ratings.

Interior Girders						
	ISU		PCF		Iowa DOT	
Vehicle	Operating	Inventory	Operating	Inventory	Operating	Inventory
HS20 (36 ton)	55.1	33.0	51.4	30.8	46.8	28.1
Type 4 (27.25 ton)	45.3	27.1	43.0	25.8	38.6	23.2
Type 3-3 (40 ton)	80.6	48.3	77.1	46.8	69.2	41.5
Type 3S3 (40 ton)	70.7	42.3	68.1	40.8	61.1	36.7
Exterior Girders						
	ISU		PCF		Iowa DOT	
Vehicle	Operating	Inventory	Operating	Inventory	Operating	Inventory
HS20 (36 ton)	55.1	33.0	53.7	32.2	44.6	26.6
Type 4 (27.25 ton)	45.3	27.1	44.9	26.9	36.8	22.1
Type 3-3 (40 ton)	80.6	48.3	80.5	48.2	66.0	39.6
Type 3S3 (40 ton)	70.7	42.3	71.1	42.6	58.4	35.2

The ratings calculated by ISU are slightly less conservative than those calculated by PCF for the interior girders but the exterior girders are nearly identical. The major difference occurs from the calculation of the dead load for each girder. For the ISU ratings, the dead load was calculated for the entire bridge including curbs railings and diaphragms. The total dead load for the bridge was then divided by the number of girders, six, and then divided by the length of the bridge to determine the load per unit length of the bridge. In contrast, PCF and the Iowa DOT calculated the dead load for each girder as the girder weight and the tributary amount of concrete supported by each girder. Compared to the values calculated by ISU, this resulted in a slightly lower dead load for the interior girders and a slightly higher dead load for the exterior girders.

The Iowa DOT ratings were significantly more conservative than those calculated by ISU and PCF. The Iowa DOT found the controlling bridge rating to be governed by serviceability criterion. Article 10.57 of the AASHTO Standard Specifications for Highway Bridges states that the operating rating for the steel stringer bridge shall not be greater than the ratio of the difference of the unfactored dead load and 80% of the girder moment capacity to the unfactored live load. The provision is for overload vehicles with girder moment capacity at

80% the yield strength of the steel for non-composite sections and the girder moment capacity at 95% the yield strength of the steel for composite sections. The inventory rating is similar to the operating rating except that the live load is factored by 1.67, thus reducing the rating. According to the experience of the Iowa DOT rating engineers, the provision rarely controls the rating of composite sections but it will often control the rating of non-composite sections. Neither PCF nor ISU checked this provision during their rating calculations. Even though the Iowa DOT ratings were more conservative than the other two rating agencies, their inventory ratings for the interior and exterior girders were still sufficient for legal loads.

3.5.2 Rating Using Optimized Parameters From BDI Software

Utilizing the strains measured during the load test, the BDI software (WinGEN) was used to determine the bridge rating using the bridge model updated with the optimized parameters. Using the modified bridge model, the bridge was rated using the same rating vehicles as the analytical ratings. The rating vehicles were input into the WinGEN software and traversed across the bridge in pre-selected lanes to produce maximum strains in the girders. Both single lane loading and double lane loading cases were analyzed using the WinSAC software. With the optimized moments of inertia for each girder being different, each girder must be rated separately using the BDI software. The load factor rating method was once again used for the ratings using the optimized bridge parameters. The operating and inventory ratings were calculated for each girder and are summarized in Table 3.13.

Table 3.13. BCB Optimized Ratings.

Operating Rating (ton)						
	Girder					
Vehicle	1	2	3	4	5	6
HS20 (36 ton)	85.3	105.5	213.5	134.6	104.0	97.9
Tandem (25 ton)	54.0	64.3	136.3	82.8	64.0	61.8
Type 3 (25 ton)	73.0	89.0	193.0	115.3	88.5	83.8
Type 4 (27.25 ton)	68.7	85.6	185.0	112.8	84.7	78.5
Type 3-3 (40 ton)	124.0	157.2	344.8	205.2	155.6	142.4
Type 3S3 (40 ton)	108.8	133.2	291.6	172.0	132.0	124.4
Type 4S3 (48 ton)	122.9	152.6	337.0	198.7	151.2	140.6
Inventory Rating (ton)						
	Girder					
Vehicle	1	2	3	4	5	6
HS20 (36 ton)	51.1	63.0	127.8	80.6	62.3	58.7
Tandem (25 ton)	32.5	38.5	81.8	49.5	38.5	37.0
Type 3 (25 ton)	43.8	53.3	115.5	69.0	53.0	50.0
Type 4 (27.25 ton)	40.9	51.2	113.4	66.8	50.7	46.9
Type 3-3 (40 ton)	74.4	105.2	206.4	123.2	93.2	85.2
Type 3S3 (40 ton)	65.2	79.6	174.8	103.2	79.2	74.4
Type 4S3 (48 ton)	73.4	91.2	201.6	119.0	90.7	84.0

The ratings calculated using the optimized parameters were much higher than the ratings calculated using the analytical rating equations. Using the response of the test truck to calibrate the model increased the rating for the HS20 test vehicle from 55.1 ton to a minimum of 85.3 ton in Girder 1 resulting in a 55% increase. The percentage increase from the ISU analytical ratings to the optimized ratings for the operating level is provided in Table 3.14. The range for the increased ratings after optimization for the HS20 rating vehicle was 55 for an exterior girder (Girder 1) to 287% for an interior girder (Girder 3).

Table 3.14. BCB Operating Rating Percent Increase After Optimization

	Girder					
Vehicle	1	2	3	4	5	6
HS20 (36 ton)	55	91	287	144	89	78
Type 4 (27.25 ton)	52	89	308	149	87	73
Type 3-3 (40 ton)	54	95	328	155	93	77
Type 3S3 (40 ton)	54	88	312	143	87	76

4. MARSHALL COUNTY BRIDGE (MCB)

4.1 Bridge Description

The second bridge (FHWA ID: 243470) that was tested is located in Marshall County, IA on Summit Road approximately 3 miles northwest of Marshalltown, IA. The bridge, henceforth referred to as the MCB, is a 40-foot simple-span, non-composite bridge with six steel girders, a concrete deck with a five-inch thick asphalt overlay, and no skew crossing a creek. An alignment view of the MCB looking north is shown in Figure 4.1. The substructure consists of seven timber piles with a double C-channel cap and a timber back wall. At the time of testing, the bridge was posted at 20 ton for a straight truck and 30 ton for a truck and trailer combination vehicle. When it was last inspected in December of 2003, the bridge was given a sufficiency rating of 2 due to significant deterioration of the superstructure components.

Figure 4.1. MCB Alignment View Looking North.

There was heavy rust on most of the girders with the most significant deterioration causing delamination in some of the steel girders. This delamination was the most significant on the north end at approximately the 1/3rd point of the bridge where there were C-channel diaphragms between the girders. Some of the deterioration and delamination can be seen in Figure 4.2 where one of the delaminated areas has been circled for clarity.

The asphalt overlay, which was heavily cracked and trapped water between the concrete deck and the overlay, also caused some major deterioration in the concrete deck. On this bridge, with the average daily traffic around 940 (2001), the repeated loading and the trapped water caused about two inches of the concrete deck to completely deteriorate. During the bridge inspection, three coring holes shown in Figure 4.3, were noticed; only one of the cores continued all the way through the concrete deck.

Figure 4.2. MCB Girder 2 Deterioration and Delamination.

Figure 4.3. MCB Core Locations and Retrieved Core Specimen.

The superstructure, a cross section of which is shown in Figure 4.4, consists of six W24x80 girders with an 8-inch thick concrete deck. There are C-channel diaphragms at the 1/3 points of the bridge one of which is shown in Figure 4.2, and concrete curbs (eight inches wide by one foot tall) as well as a steel railing on both sides of the bridge (see Figure 4.3).

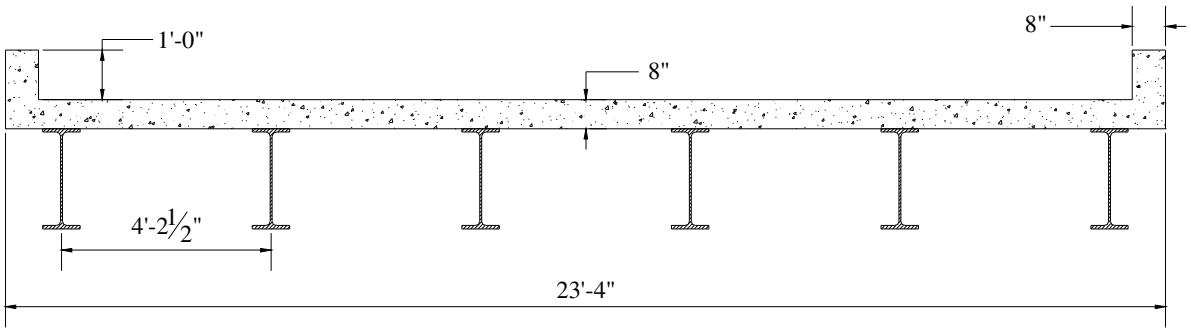

Figure 4.4. Cross Section of MCB Looking North.

4.2 Test Setup

4.2.1 Test Truck

Three incremental loads (function of the amount of gravel the truck is carrying), referred to as: an empty truck, a half full truck, and a full truck were once again selected for the bridge tests. The truck used for the load test was provided by the county and was a standard maintenance tandem dump truck. A photograph of the test truck as it is crossing the bridge during a load test is shown in Figure 4.5; its axle weights are presented in Table 4.1, and its dimensions are shown in Figure 4.6.

Table 4.1. MCB Truck Weights.

Truck Loading	Axle Weights (kip)			Gross Weight (kip)
	A	B	C	
Empty	10.60	6.65	6.65	24.90
Half Full	14.05	13.80	13.40	41.25
Full	17.05	17.80	16.75	51.60

4.2.2 Testing Plan and Instrumentation

There were four paths or lanes, shown in Figure 4.7, selected for the truck to follow as it crossed the bridge. Each lane was tested twice for each load increment to check repeatability of the test results. Measurements (strains and deflections) were taken when the centroid of the tandem was at the centerline of each abutment and at each quarter point (See Figure 4.7). The locations of the abutment centerlines and the quarter points were painted on the bridge in a manner similar to that used in the BCB test.

Figure 4.5. MCB Test Truck.

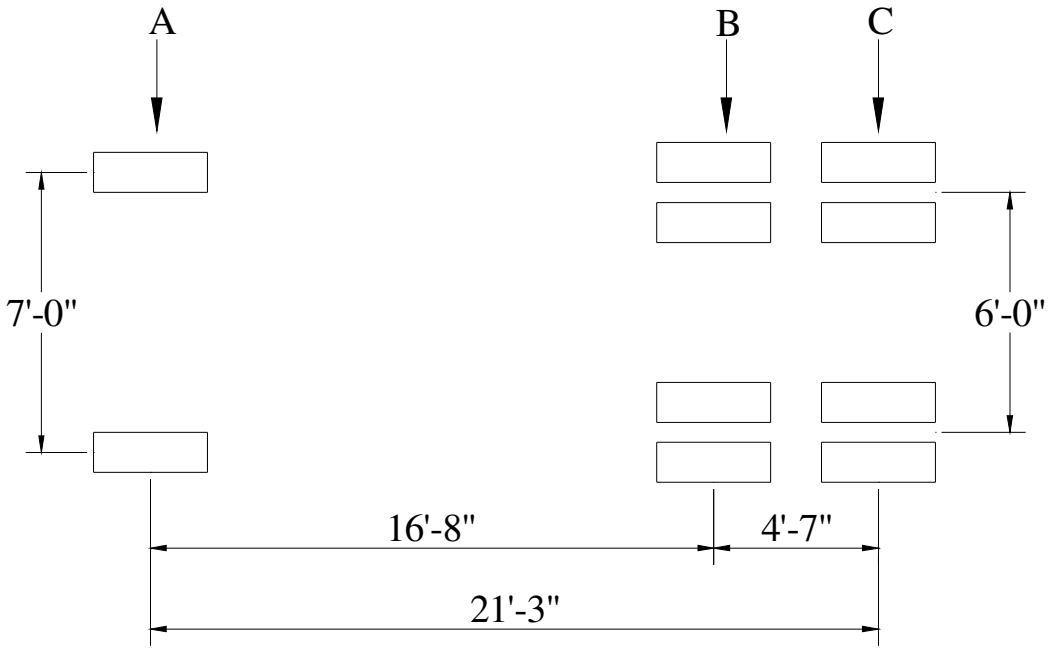

Figure 4.6. MCB Test Truck Dimensions.

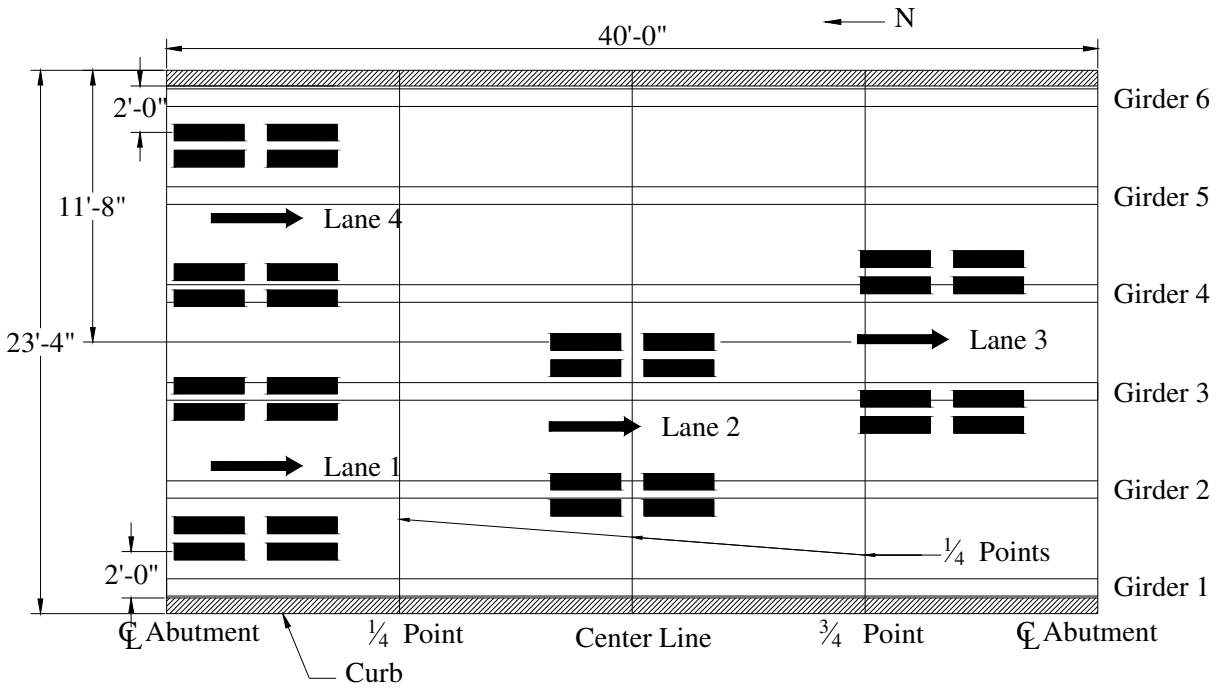

Figure 4.7. Plan View and Loading Lanes Used in MCB Test.

The bridge was instrumented six inches from the edge of the bearing as shown in Figure 4.8; strain transducers were also installed on the top and bottom flanges of Girders 1, 3, and 5 near the abutments as shown in Figure 4.9. At the midspan, strain transducers were attached on the top and bottom flanges on each of the girders as well as on the underside of the concrete deck near Girders 1, 3, and 5, between Girders 1 and 2, and between Girders 3 and 4 as shown in Figure 4.10. One strain transducer was located on the top of each of the two railings at the midspan as well. There were also deflection transducers installed at the midspan on all of the girders as also shown in Figure 4.10; for the tests, there were a total of 32 strain transducers and six deflection transducers installed.

Due to the high amount of deterioration, as previously mentioned and illustrated in Figure 4.2, some of the transducers required extensive removal of corrosion and the delaminated material to ensure the transducers would properly measure the girder strains. This problem is shown in the close up photograph (see Figure 4.11) of one of transducers mounted on the top flange of one of the girders at the midspan.

4.3 Bridge Analysis

4.3.1 Neutral Axis and Partial Composite Action

The bridge was designed as a non-composite simple span bridge. As is common with most bridges of this type, there were some details in the bridge that could increase the flexural capacity of the bridge. Shown in Figure 4.12 through Figure 4.15 are the top and bottom flange strains and the deflections with the loading in Lane 1 through Lane 4, respectively.

Figure 4.8. Instrumentation Near Abutment of MCB.

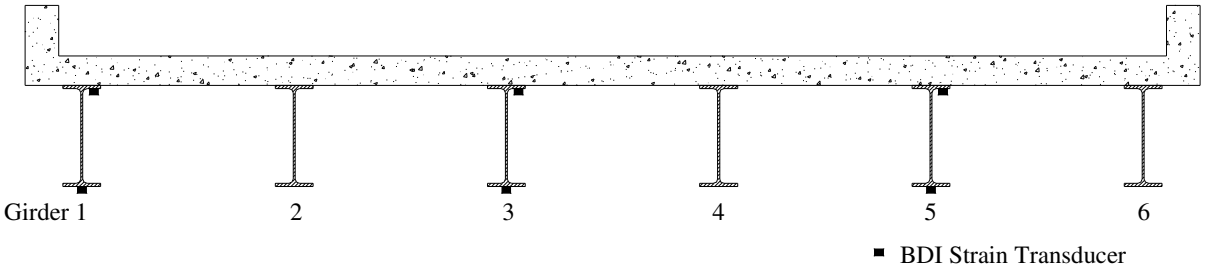

Figure 4.9. MCB North and South End Transducer Locations Looking North.

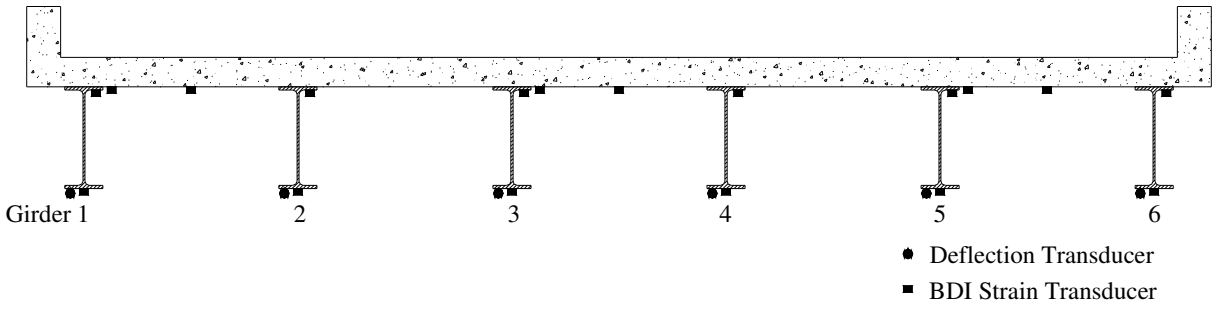

Figure 4.10. MCB Midspan Transducer Locations Looking North.

Figure 4.11. MCB Removal of Excess Corrosion for Transducer Application

In the four figures, TF and BF refers to the top and bottom flange strains, respectively. The deflection profiles follow the same general shape as the bottom flange strain profiles. As can be seen in Figure 4.14, there was symmetry in the strain profile for the truck centered on the bridge and, with the exception of the deflection in Girder 3, the deflection profile also exhibited symmetry. Based on a visual inspection of Girder 3, Girder 3 strains relative to the strains in the other girders and the Girder 3 deflections relative to the deflections in the other girders seem to be less than they should be. Quantification of the observed difference in the deflection profile will be discussed in more detail in the load distribution section (Section 4.3.2). The maximum tensile strains observed in Lane 1, Lane 2, Lane 3, and Lane 4 were 96, 88, 87, and 104 microstrain, respectively and the maximum deflections measured were 0.100, 0.090, 0.086, and 0.107 inches, respectively. The neutral axis locations for each lane and load increment are provided in Figure 4.16.

Once again the strain values plotted are not the maximum values obtained during the various tests but are the values obtained when the centroid of the truck tandem was directly over the midspan of the bridge, thus fixing the longitudinal truck position for all load increments.

The neutral axis locations, shown in Figure 4.16, were determined by interpolating between the top and bottom flange strains to determine the location on the girder where the strain was equal to zero. Composite action, shown simply by the location of the neutral axes above the theoretical composite neutral axis location, was observed in all of the girders for each of the lanes loaded. The amount of composite action did not change with the increased loading as

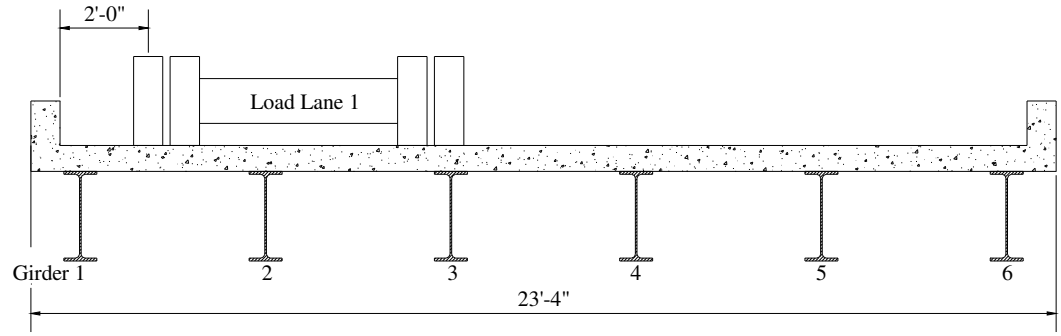

(a) Lane 1 Loading

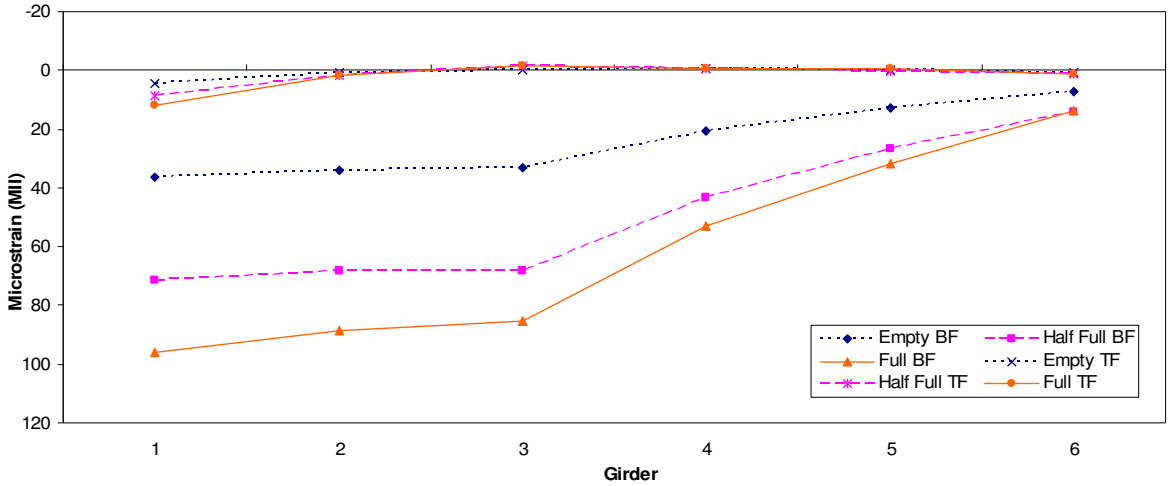

(b) Strain Profile

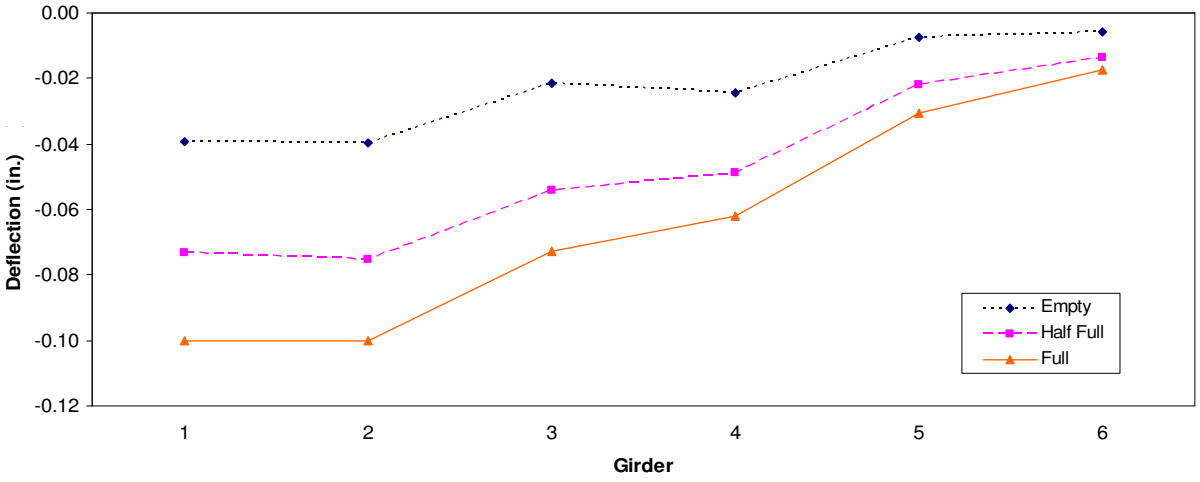

(c) Deflection Profile

Figure 4.12. MCB Lane 1 Strains and Deflections.

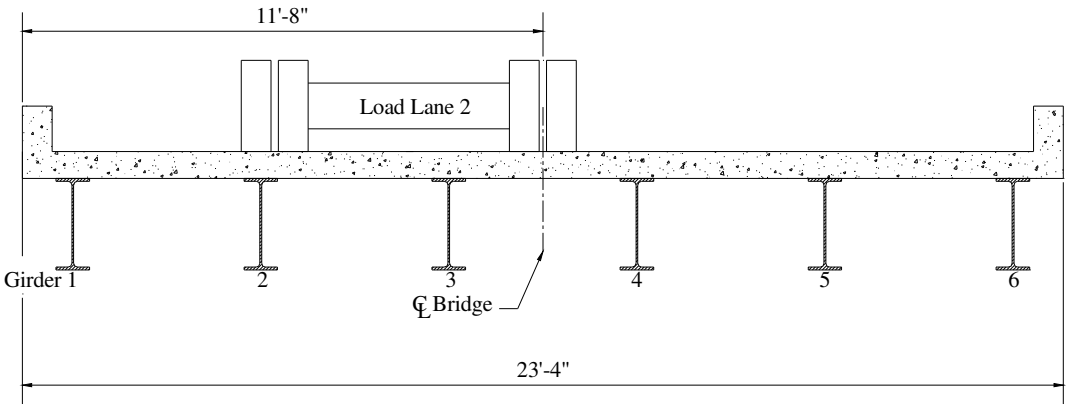

(a) Lane 2 Loading

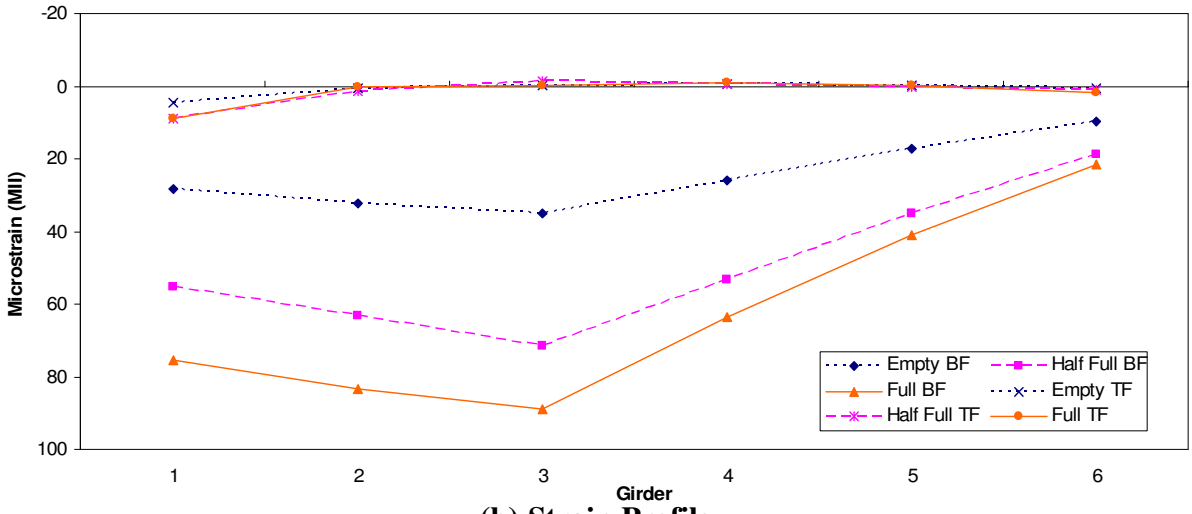

(b) Strain Profile

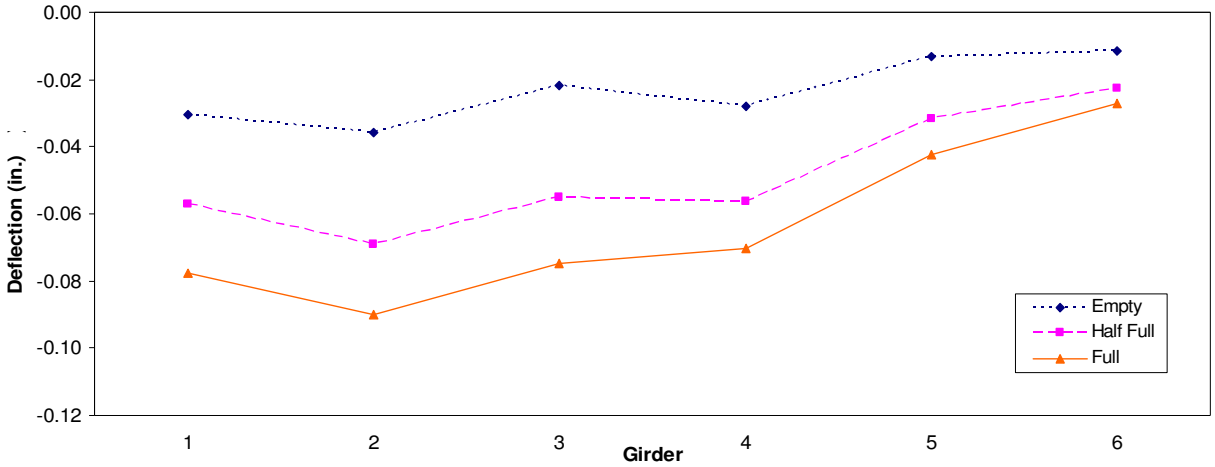

(c) Deflection Profile

Figure 4.13. MCB Lane 2 Strains and Deflections.

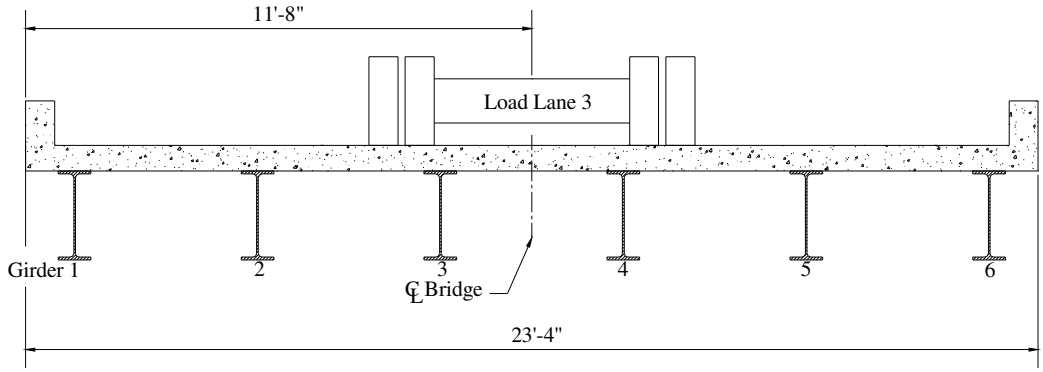

(a) Lane 3 Loading

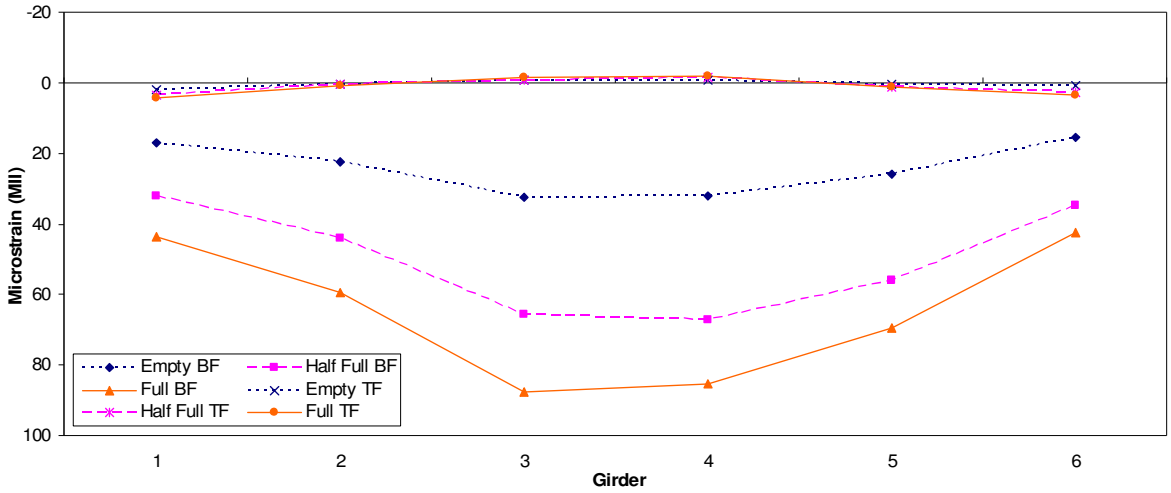

(b) Strain Profile

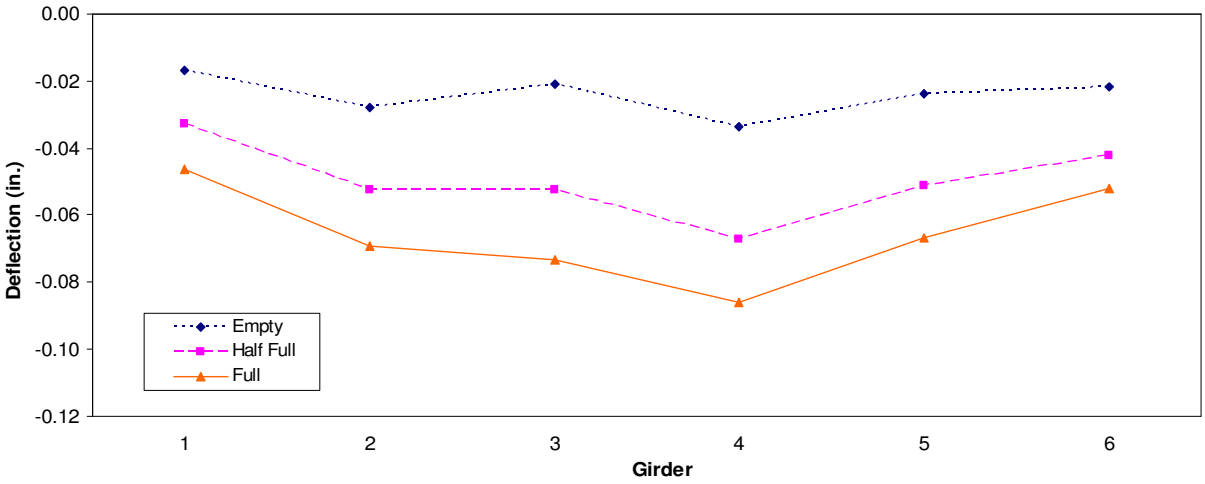

(c) Deflection Profile

Figure 4.14. MCB Lane 3 Strains and Deflections.

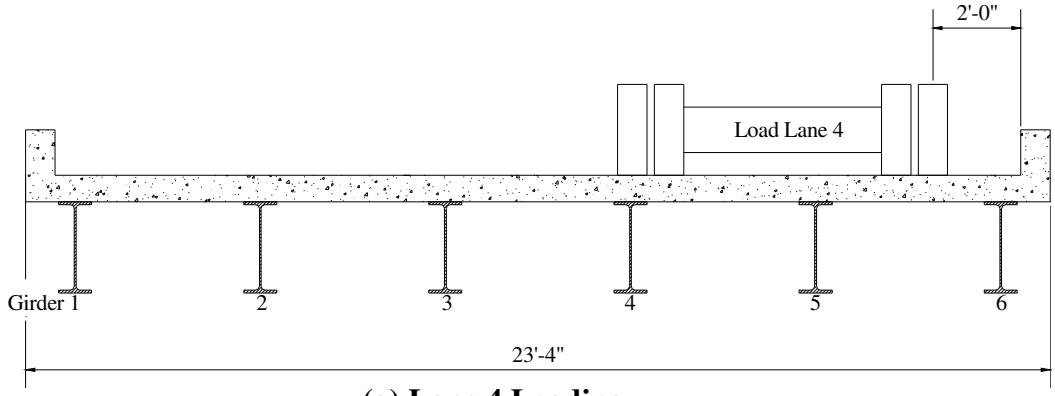

(a) Lane 4 Loading

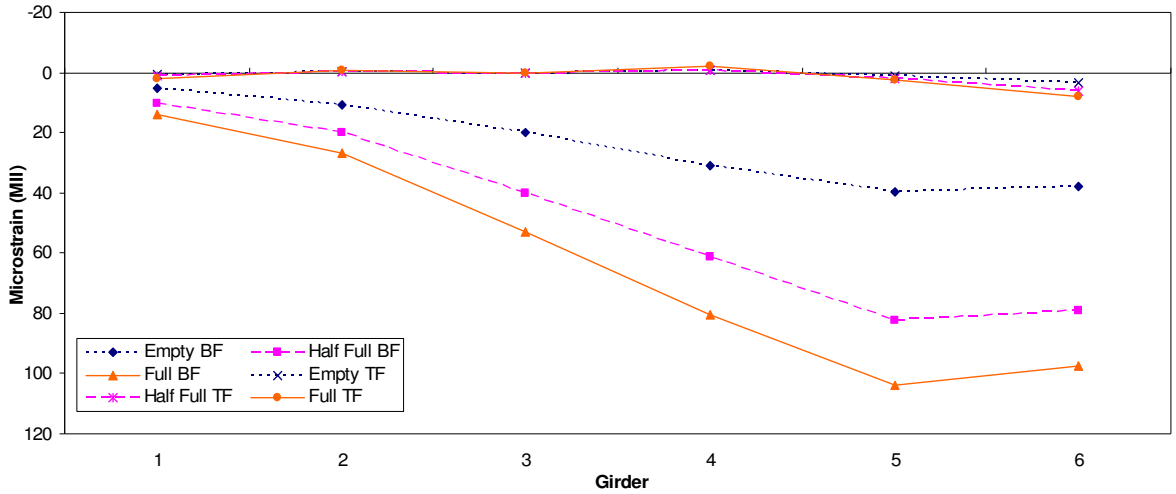

(b) Strain Profile

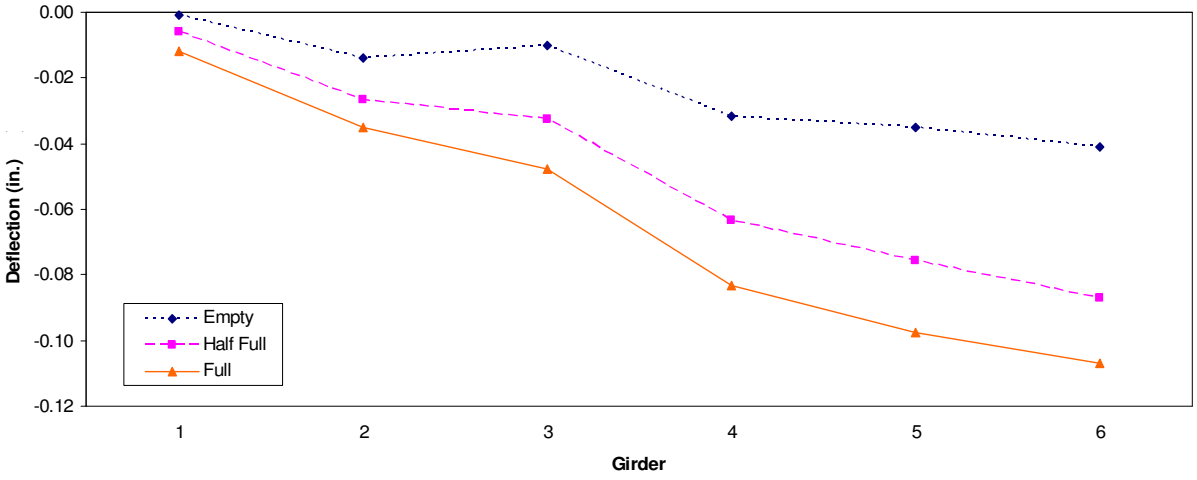

(c) Deflection Profile

Figure 4.15. MCB Lane 4 Strains and Deflections.

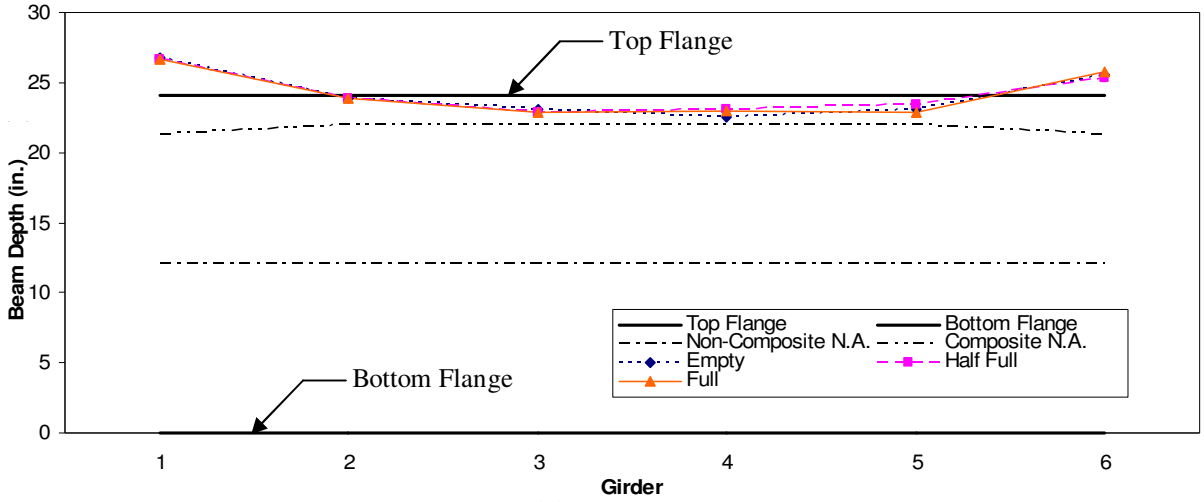

(a) Lane 1

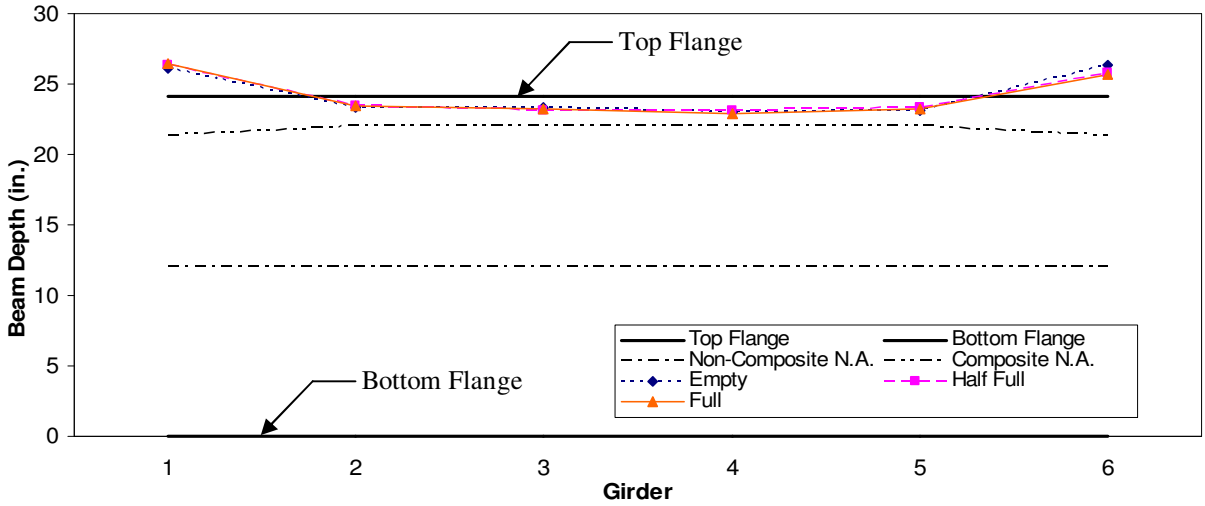

(b) Lane 3

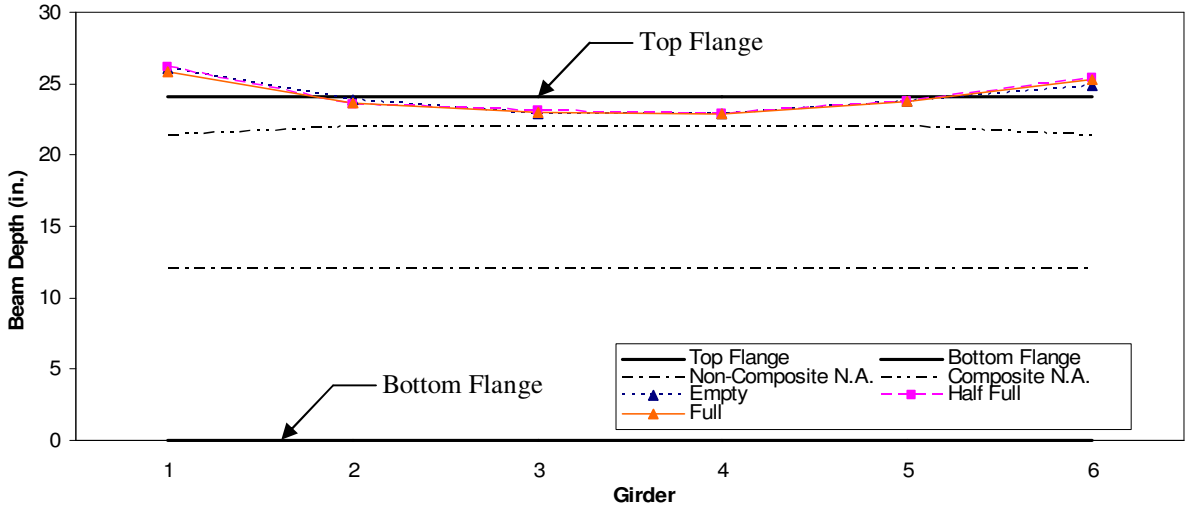

(c) Lane 4

Figure 4.16. MCB Neutral Axis Locations.

was the case with the BCB, but instead the neutral axis locations are all very close to being the same. All of the interior girders had neutral axis locations between the top of the top flange and the calculated composite neutral axis location, while the exterior girders had neutral axis locations above the top flange of the girders and therefore into the concrete deck.

The bottom flange strains increased with increased loading but the top flange strains remained relatively constant as shown in Figure 4.12 through Figure 4.15; therefore, the top flange of the girder did not take the compressive bending stresses but rather the girder and concrete deck acted in a composite manner with the deck taking the compressive bending stresses. Based on the neutral axis locations and the top flange strains, it appeared that there may have been some kind of shear connection between the girders and the concrete deck creating the composite action even though no such a connection appeared on the plans provided. Approximately two weeks after testing this bridge it was removed and replaced with a new bridge. The bridge demolition provided little explanation as to why this composite action occurred as the top flanges were completely free of any kind of mechanical shear connector as shown in Figure 4.17.

Figure 4.17. Exposed Top Flanges After MCB Deck Demolition.

4.3.2 Load Distribution

Using the previously described truck locations, the theoretical moment induced in the bridge, assuming simply supported conditions, was calculated for each loading; these are presented in Table 4.2. As may be seen in this table, there was a 99% increase in moment from empty to half full and a 153% increase from empty to full.

Table 4.2. MCB Induced Truck Moments.

Load	Moment (in-k)
Empty Truck	1485
Half Full Truck	2960
Full Truck	3760

Using the bottom flange strains, the percent distributions were calculated as the ratio of the individual girder strain to the sum of the six girder strains. With each of the three load increments producing slightly different load distribution percentages, the maximum values, summarized in Table 4.3, were selected for each of the three lanes. Note that the values are the maximum percentage values of the three load cases and therefore do not sum to 100%. As may be seen, the maximum distribution percentages occurred in the exterior girders when directly loaded with the exception of Girder 5 for Lane 4 loading which had a slightly larger distribution percentage than that of Girder 6. Girders 3 and 4 had distribution percentages very close to each other for Lane 3 loading which demonstrates symmetry in the bottom flange strains. Symmetry in the bottom flange strains can also be observed by comparing the Girder 1 distribution for Lane 1 to the Girder 6 distribution for Lane 4.

Table 4.3. MCB Maximum Single Lane Strain Based Percent Distributions.

Lane \ Girder	1	2	3	4	5	6
1	26.0	24.0	23.5	14.8	9.1	5.1
2	20.2	22.3	24.1	18.0	11.8	6.6
3	11.8	15.5	22.5	22.4	18.7	11.6
4	3.7	7.3	14.1	21.5	28.1	27.0

As previously noted, the deflection profile did not appear to follow the same shape as the bottom flange strain profile for Girder 3. To better quantify the perceived discrepancy between the strain and deflection profiles, the maximum percent distributions were calculated based on the girder deflections and are presented in Table 4.4. Comparing the results for the strain and deflection based percent distributions for Lane 1 loading, it can be seen that not only was the percent distribution for Girder 3 based on deflections lower by 4.5% but the percent distribution for Girder 2 was 4.8% higher. A change in load distribution from 24% to 29% is equivalent to a change in the load supported by the girder for a 72,000 lb vehicle of 3,600 lbs. In terms of the girder capacity, a 5% difference in load distribution would result in a change in the induced moment for the full truck load increment of 190 in-kip. The available moment capacity (available moment capacity being the difference in the capacity of the girder and the unfactored dead load carried by the girder) for one girder is 5,005 in-kips and the total moment induced on the bridge for the full truck loading was 3,760 in-kips. The effect of the 5% difference in the load distribution on the available moment capacity of the girder results in a total change of 3.8%. For the maximum test load increment, the 5% change in load distribution is negligible for this bridge but with larger loads the distribution becomes more significant. Since the bridge ratings are dependent upon the moment capacity of the girders and the deflections are small, and thus of minimal concern, only load distributions determined from the girder strains will be discussed.

Table 4.4. MCB Maximum Single Lane Deflection Based Percent Distributions.

Lane \ Girder	1	2	3	4	5	6
1	28.5	28.8	19.0	17.7	8.0	4.8
2	21.8	25.5	19.6	19.9	11.1	8.1
3	11.8	19.2	18.7	23.2	17.2	15.1
4	3.1	10.6	12.4	23.8	26.3	30.9

As previously noted, the percent distributions are provided in Table 4.3; however in order to compare the load distribution to the AASHTO distribution factors the values must be multiplied by two to obtain the distribution of a single wheel line. The maximum distribution factors from the percent distributions summarized in Table 4.3 are provided in Table 4.5. Using superposition, Lanes 2 and 4 were used to determine the distribution factors, also shown in Table 4.5, for two lanes.

Table 4.5. MCB Calculated Distribution Factors.

Lane \ Girder	1	2	3	4	5	6
1	0.52	0.48	0.47	0.30	0.18	0.10
2	0.40	0.45	0.48	0.36	0.24	0.13
3	0.24	0.31	0.45	0.45	0.37	0.23
4	0.07	0.15	0.28	0.43	0.56	0.54
2&4	0.48	0.59	0.76	0.79	0.80	0.67

The maximum distribution factors for the interior and exterior girders for the single lane loading are 0.56 and 0.54, respectively, while the AASHTO distribution factor for the single lane loading with a girder spacing of 4'-2.5" using the equation of S/7.0 is 0.60. The maximum distribution factors for the interior and exterior girders for the two lane loading are 0.80 and 0.67, respectively, while the AASHTO distribution factor for multiple lane loading using the equation of S/5.0 is 0.77. Values obtained by dividing the AASHTO distribution factors by the actual experimental distribution are summarized in Table 4.6.

Table 4.6. MCB Distribution Ratios.

	Single Lane	Two Lanes
Interior Girder Distribution	0.56	0.80
Exterior Girder Distribution	0.54	0.67
AASHTO Distribution Factor	0.60	0.77
Interior Factor Ratio	1.07	0.96
Exterior Factor Ratio	1.11	1.14

The distribution ratios for the single lane show that the AASHTO equations are slightly conservative as the ratios exceed 1.0. For the two lane loading case though, the ratios indicate that the actual load distribution is smaller than predicted using the AASHTO equation

for the interior girders. The exterior girder load distribution is very close to the factors predicted using the AASHTO equations with the ratios being very close to 1.0. In general, the AASHTO distribution factors are verified by the field test results.

4.3.3 Moment of Inertia

The moment of inertia is not the same for each girder due to the varying amount of composite action. The moment of inertia for each girder was calculated following the same procedure outlined in Section 3.3.3 for the BCB. With the neutral axis locations for each girder being close to the same for the three load increments, it would follow that the moments of inertia, presented in Table 4.7, for the three load increments would be very close. An average moment of inertia for each girder from the three load increments is also provided in Table 4.7.

Table 4.7. MCB Moments of Inertia (in^4).

Lane \ Girder	1	2	3	4	5	6
1	9500	7415	6965	6920	7055	8420
2	9060	7190	7110	6995	7095	8725
3	8830	7320	6980	6945	7375	8200
4	9355	6955	7165	6935	7475	8300
Average	9185	7220	7055	6950	7250	8410

The non-composite moment of inertia for the girder is 2,370 in^4 and the composite moment of inertia for the girder with an effective flange width equal to the girder spacing is 6,680 in^4 for the interior girders and 6,220 in^4 for the exterior girders for which neither the curb nor railing were considered in the calculation. With the location of the neutral axis being higher than the theoretical composite neutral axis location, the calculated moments of inertia for each girder are also larger than those calculated assuming a composite section. A graphical comparison of the moments of inertia for each girder to the theoretical composite and non-composite moments of inertia is provided in Figure 4.18. Also shown in Figure 4.18 is the average moment of inertia for each girder. The moments of inertia for the interior girders are very close to the same with an overall average of 7,120 in^4 and a standard deviation of 185 in^4. There is more scatter in the calculated moments of inertia for the exterior girders with an average of 8,800 in^4 and a standard deviation of 480 in^4. The edge stiffness observed in the exterior girders of the BCB was also observed in this bridge with much larger moments of inertia in the exterior girders.

4.4 BDI Optimization

The bridge was once again modeled using software (WinGEN) provided by Bridge Diagnostics Inc. that utilizes the actual test data to create a model that is close to the actual bridge based on the response of the structure to the truck loadings. This bridge model consisted of modeling each girder separately so that the moment of inertia for each girder could be optimized. Even though the interior girders had moments of inertia close to the same as previously noted, it was important to model each girder separately to verify the similarity

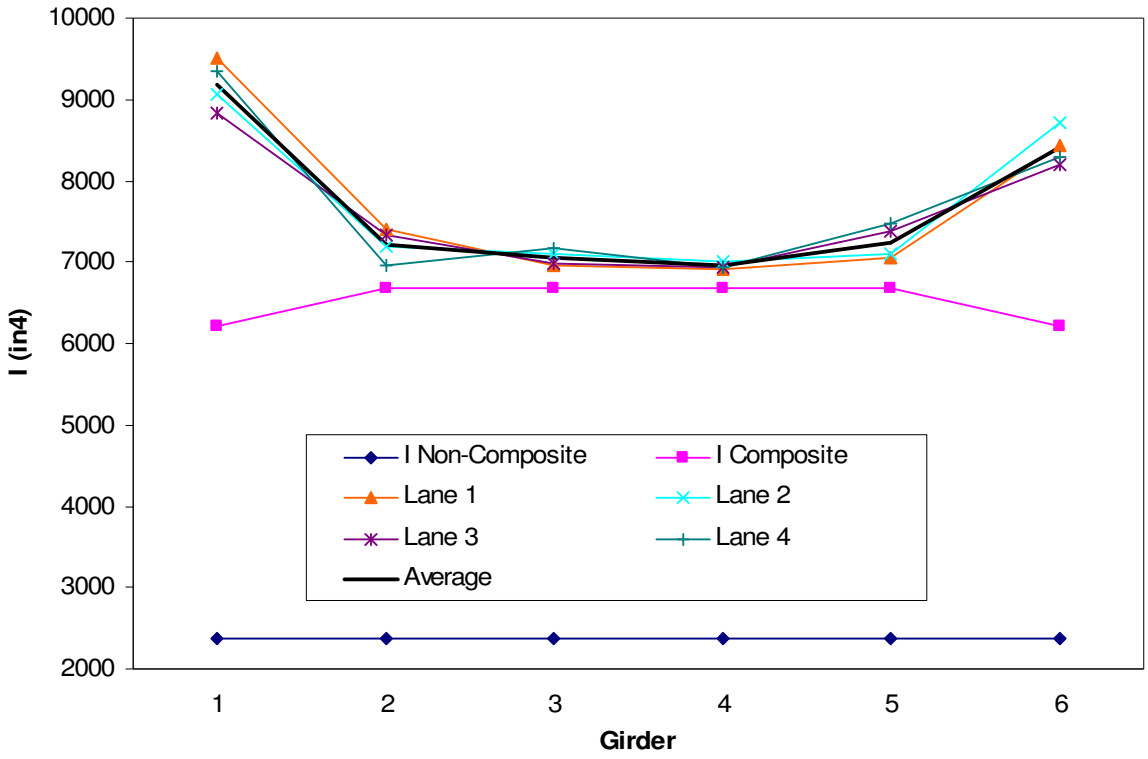

Figure 4.18. MCB Effective Moments of Inertia.

after the optimization of the girder moments of inertia. Modeling each girder separately also increases the correlation between the actual test data and the theoretical response after optimization. As before, the deck was modeled using plate elements, while the girders were modeled using beam elements. Rotational springs were attached to the ends of each of the girders: one for the north end of the exterior girders, one for the north end of the interior girders, and two more for the interior and exterior girders at the south end of the bridge.

As a starting point for the model generation, the initial girder moments of inertia were the average values presented in Table 4.7. The initial values for all of the spring constants was 10,000 kip-in/rad and the initial value of the Young's modulus for concrete was once again selected as 3,150 ksi corresponding to a compressive strength of 3,000 psi. Only the steel girder strains were input into the model; those attached to the bottom of the concrete slab were not input into the model because of a large variation in the strains measured. After the model was generated in WinGEN, it was analyzed using WinSAC. WinSAC compares the actual strains induced by test truck to those produced by a theoretical truck with the same dimensions and wheel loads as the test truck.

Initial values for the model parameters did not produce strains that correlated with the actual strains obtained from the load test so the bridge was optimized. The parameters that were optimized included the moments of inertia for each girder, the rotational spring stiffness, and the modulus of elasticity for the concrete deck. Upper and lower bounds for the optimization parameters are presented in Table 4.8. The upper and lower bounds for the moment of inertia

of the girders corresponded to 120% of the composite and 80% of the non-composite neutral axis locations, respectively. Optimizing the bridge using the parameters in Table 4.8 yielded a scale error of 10.3%; the optimized values are provided in Table 4.9.

Table 4.8. MCB Optimization Parameters.

Optimization Parameter	Lower Bound	Upper Bound
Moment of Inertia (in^4)	1813	10,000
Rotational Spring Stiffness (kip-in/rad)	0	1,000,000
Modulus of Concrete (ksi)	2500	5500

Table 4.9. MCB Optimized Parameters Using All Steel Transducers

Optimized Parameter	Initial Value	Optimized Value
Girder 1 I_y (in^4)	9185	7610
Girder 2 I_y (in^4)	7220	9260
Girder 3 I_y (in^4)	7055	4330
Girder 4 I_y (in^4)	6950	7425
Girder 5 I_y (in^4)	7250	5440
Girder 6 I_y (in^4)	8410	9225
North Exterior Rotational Spring (kip-in/rad)	10,000	221,800
North Interior Rotational Spring (kip-in/rad)	10,000	233,200
South Exterior Rotational Spring (kip-in/rad)	10,000	179,800
South Interior Rotational Spring (kip-in/rad)	10,000	220,400
Deck Modulus (ksi)	3150	5465

The procedure outlined in Section 4.3.3 where an attempt to obtain initial moments of inertia for the girders was again not successful as the optimized values did not correlate with the initial values as displayed in Table 4.9. The apparent symmetry observed in the neutral axis, deflection profile and strain profile plots previously presented was not observed in the optimized girder moments of inertia. Comparing the optimized moment of inertia in the geometrically symmetric Girders 2 and 5 shows that the optimization was not symmetrical as the optimized values were 9,260 and 5,440 in^4, respectively. Optimized values obtained for the spring constants were relatively close to each other. A deck modulus of elasticity of 5,465 ksi corresponds to a concrete compressive strength of 9,000 psi, three times the initial assumed strength of 3,000 psi. A graphical comparison of the optimized strains for each loading path are compared to the actual strains induced by the test truck for Girder 1 through Girder 6 are presented in Figure 4.19 through Figure 4.24.

In almost all cases, the optimized strain values were close to the actual strains from the test truck. The correlation between the optimized strain values and the actual strain values are summarized in Table 4.10. The scale error ranged from 0.6 to 5.3 and the correlation ranged from 0.890 to 0.950.

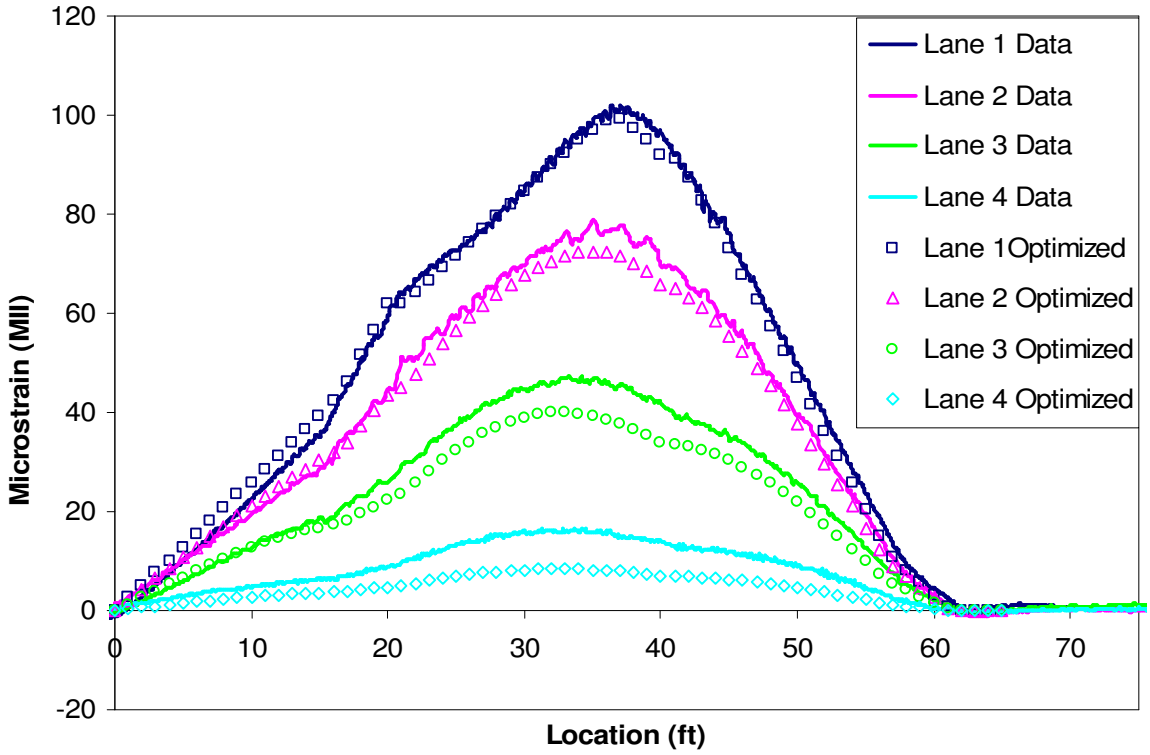

Figure 4.19. MCB Girder 1 Optimized Strain Comparison.

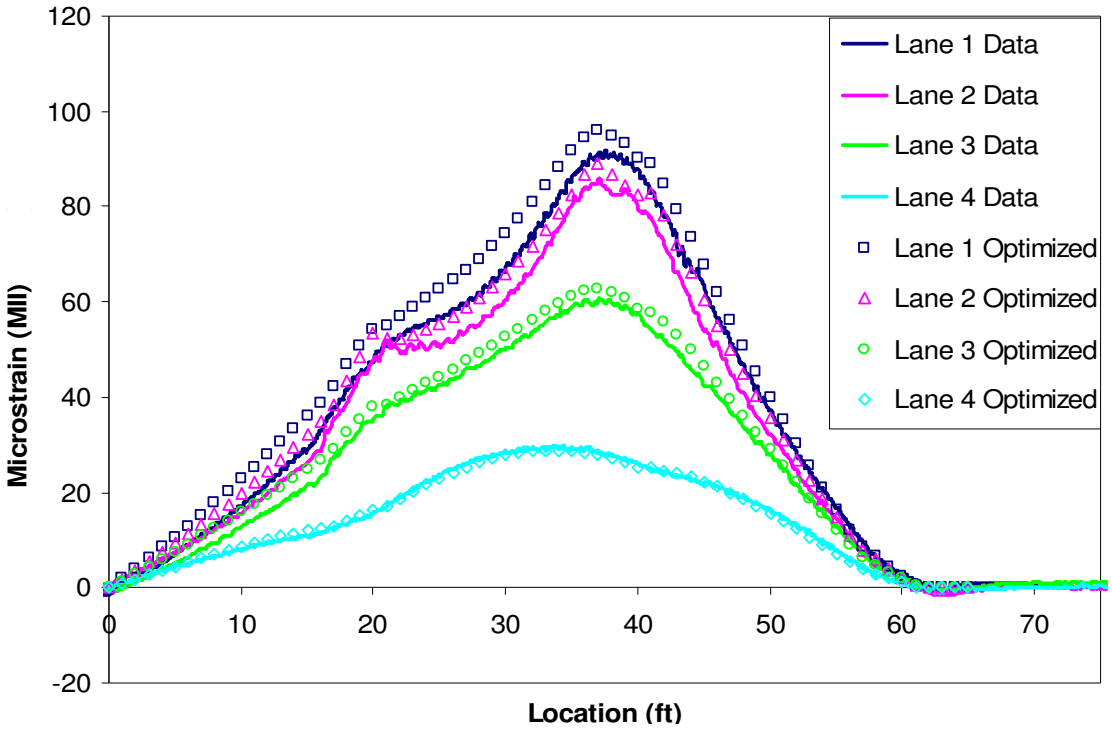

Figure 4.20. MCB Girder 2 Optimized Strain Comparison.

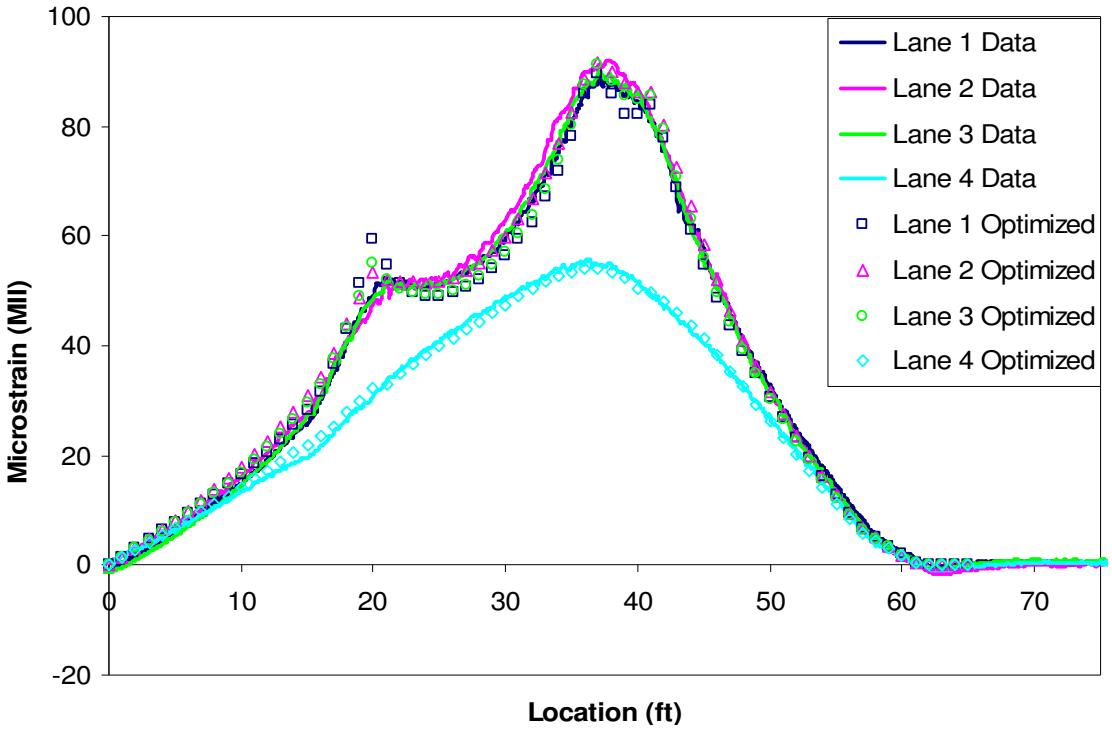

Figure 4.21. MCB Girder 3 Optimized Strain Comparison.

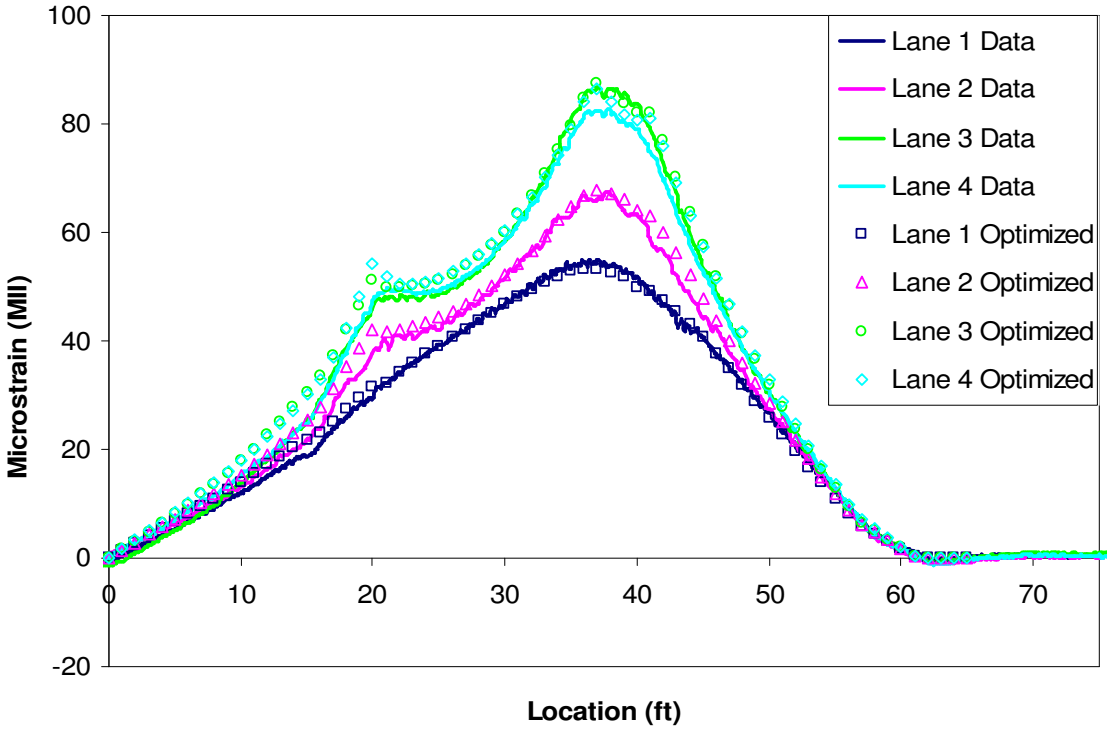

Figure 4.22. MCB Girder 4 Optimized Strain Comparison.

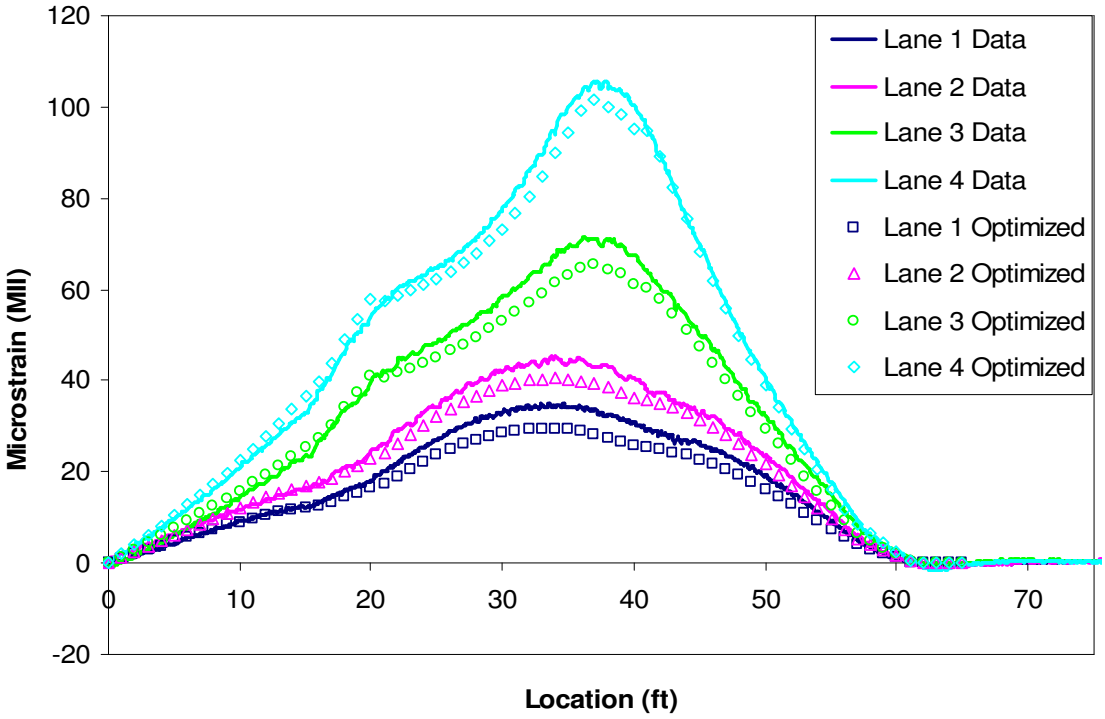

Figure 4.23. MCB Girder 5 Optimized Strain Comparison.

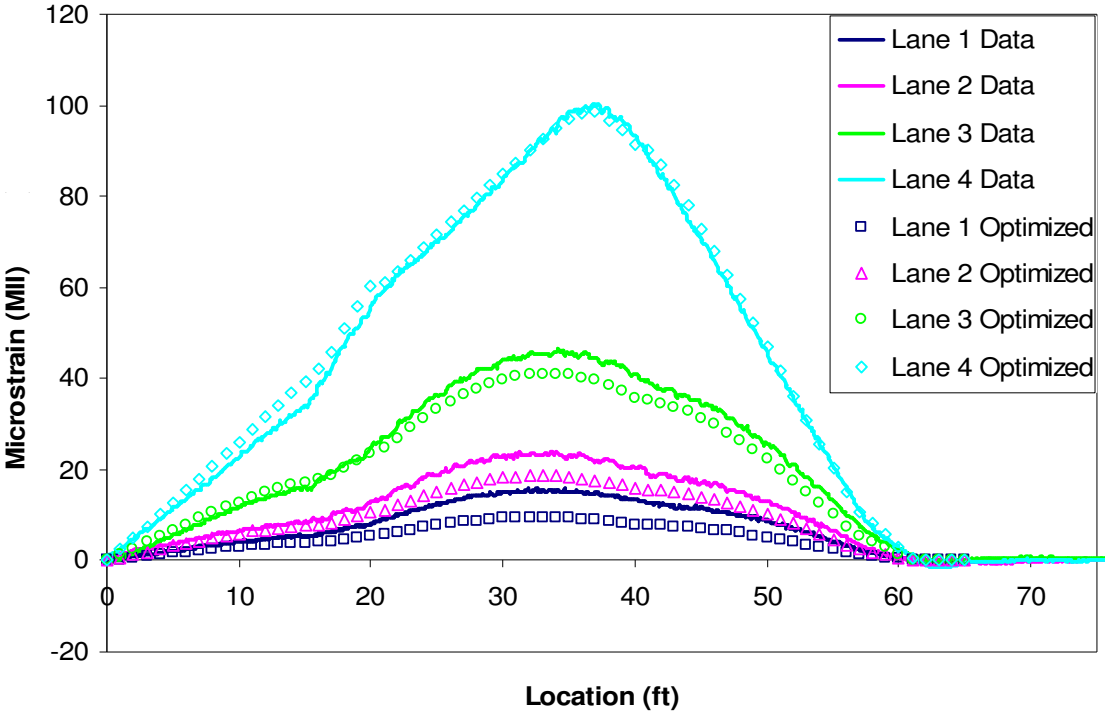

Figure 4.24. MCB Girder 6 Optimized Strain Comparison.

Table 4.10. MCB Bottom Flange Strain Scale Error and Correlation.

Girder	1	2	3	4	5	6	Average
Scale Error	0.6	5.3	3.7	5.1	1.4	0.9	2.8
Correlation	0.950	0.926	0.890	0.892	0.913	0.935	0.918

In an attempt to quantify the effect of the strains near the abutment on the overall scale error, the values from the bridge optimization were input into a model that compared the optimized strains to the actual strains using only the midspan strains. This model was analyzed and resulted in a scale error of only 2.8%, a 7.5% reduction from the original optimization model using all of the steel girder strains. The correlation values provided in Table 4.10 did not change in the new analysis.

An investigation of the effect of changing the spring constants on the midspan strains was not conducted on this bridge. All of the bridges are similar in length and their support conditions are very similar. For the BCB a spring constant of 100,000 resulted in a condition of 15% fixity of the support and a spring constant of 500,000 resulted in a condition of 48% fixity. The spring stiffness optimization for the MCB yielded optimized spring stiffness coefficients very close to each other and were in the range of 100,000 and 500,000 kip-in/rad. An average optimized spring constant for the MCB of around 200,000 kip-in/rad would be comparable to a condition of about 23% for the BCB.

4.5 Bridge Rating

4.5.1 Conventional Rating

The bridge was rated once again using the Load Factor Rating (LFR) approach. This analytical rating, in which both the interior and exterior girders were rated, was performed assuming a non-composite design with simply supported conditions. The bridge was also independently rated by both the Iowa DOT and PCF. Ratings calculated by the three different rating agencies are summarized in Table 4.11.

The ratings calculated by ISU and PCF for the interior girders are once again very close. The ratings for the exterior girders that were calculated by ISU are somewhat more conservative than those calculated by PCF. The dead load calculations for the exterior girders is the main cause of the discrepancy in the in the exterior girders. For both the interior and exterior girders, the operating ratings exceeded the required vehicle loads. The inventory ratings for the interior and exterior girders were less than the legal load for all of the rating vehicles.

The serviceability criterion once again controlled the ratings for this bridge causing the rating calculations performed by the Iowa DOT to be more conservative than those calculated by ISU and PCF. The Iowa DOT and ISU found the exterior and interior girder ratings to be the same whereas PCF found the ratings for the interior girders to control the bridge rating.

Table 4.11. MCB Analytical Bridge Ratings.

Interior Girders						
	ISU		PCF		Iowa DOT	
Vehicle	Operating	Inventory	Operating	Inventory	Operating	Inventory
HS20 (36 ton)	46.7	28.0	45.4	27.5	40.0	24.0
Type 4 (27.25 ton)	39.3	23.6	39.1	23.4	34.1	20.5
Type 3-3 (40 ton)	66.7	40.0	66.8	40.0	58.2	34.9
Type 3S3 (40 ton)	62.7	37.6	62.9	37.7	54.9	32.9
Exterior Girders						
	ISU		PCF		Iowa DOT	
Vehicle	Operating	Inventory	Operating	Inventory	Operating	Inventory
HS20 (36 ton)	46.7	28.0	50.1	30.0	40.0	23.8
Type 4 (27.25 ton)	39.3	23.6	42.7	25.6	34.1	20.4
Type 3-3 (40 ton)	66.7	40.0	72.9	43.7	58.0	34.8
Type 3S3 (40 ton)	62.7	37.6	68.7	41.2	54.8	32.8

4.5.2 Rating Using Optimized Parameters From BDI Software

Utilizing the strains measured during the load test, the BDI software (WinGEN) was once again used to determine the bridge rating using the bridge model with the optimized parameters. Using the modified bridge model, the bridge was rated using the same rating vehicles as were used in the analytical ratings. The rating vehicles were input into the WinGEN software and traversed across the bridge in pre-selected lanes to produce maximum strains in the girders. Both single lane loading and double lane loading cases were analyzed using the WinSAC software. With the optimized moments of inertia for each girder being different, each girder must be rated separately using the BDI software. The load factor rating method was once again used for the ratings using the optimized bridge parameters. The operating and inventory ratings were calculated for each girder and are summarized in Table 4.12.

As with the previous bridge, the ratings calculated using the optimized parameters were much higher than the ratings calculated using the analytical rating equations. The limiting girder was Girder 2 having the lowest operating rating with a limit of 34 tons for a HS20 rating vehicle; the same girder had a limit of 23 ton using the analytical rating equations. The inventory ratings were larger than the legal loading for the rating vehicles with Girder 2 having the lowest rating. The inventory rating for Girder 2 with the HS20 rating vehicle was 40.6 ton, just slightly above the vehicle weight of 36 ton. The inventory ratings for Girder 6 were very close to those for Girder 2 and were also slightly larger than the legal load. A table representing the percentage increase from the ISU analytical ratings to the optimized ratings for the operating level is provided in Table 4.13. The range for the increased ratings after optimization for the HS20 rating vehicle was 45% for interior Girder 2 to 279% for interior Girder 3.

Table 4.12. MCB Optimized Ratings.

Operating Rating (ton)						
	Girder					
Vehicle	1	2	3	4	5	6
HS20 (36 ton)	91.8	67.7	176.8	95.0	125.6	70.6
Tandem (25 ton)	62.3	43.8	116.3	60.5	82.0	47.5
Type 3 (25 ton)	81.8	59.0	158.5	82.8	111.0	62.8
Type 4 (27.25 ton)	77.1	56.7	154.8	79.6	107.6	58.9
Type 3-3 (40 ton)	129.2	102.0	278.8	144.0	193.6	99.2
Type 3S3 (40 ton)	124.0	88.4	239.6	123.6	167.6	94.8
Type 4S3 (48 ton)	146.9	102.7	275.5	142.1	192.0	105.6
Inventory Rating (ton)						
	Girder					
Vehicle	1	2	3	4	5	6
HS20 (36 ton)	55.0	40.6	105.9	56.9	75.3	42.3
Tandem (25 ton)	37.3	26.2	69.6	36.2	49.1	28.5
Type 3 (25 ton)	49.0	35.4	95.0	49.6	66.5	37.6
Type 4 (27.25 ton)	46.0	34.0	92.7	47.7	64.5	35.3
Type 3-3 (40 ton)	77.4	61.1	167.0	86.3	116.0	59.4
Type 3S3 (40 ton)	74.3	53.0	143.5	74.1	100.4	56.8
Type 4S3 (48 ton)	88.0	61.5	165.1	85.1	115.0	63.3

Table 4.13. MCB Operating Rating Percent Increase After Optimization.

	Girder					
Vehicle	1	2	3	4	5	6
HS20 (36 ton)	97	45	279	103	169	51
Type 4 (27.25 ton)	96	44	294	103	174	50
Type 3-3 (40 ton)	94	53	318	116	190	49
Type 3S3 (40 ton)	98	41	282	97	167	51

5. MAHASKA (350) COUNTY BRIDGE (KCB1)

5.1 Bridge Description

The third bridge that was tested is located in Mahaska County, IA on Rutledge Avenue approximately 5 miles northeast of Oskaloosa, IA. The bridge (FHWA ID: 237350), henceforth referred to as the KCB1, is a 33.3-foot simple-span, non-composite bridge with five steel girders, a concrete deck, and no skew crossing a creek. The substructure consists of five timber piles with a double C-channel cap and a timber back wall. The bridge, an alignment view of which is shown in Figure 5.1, is currently posted at 20 ton for a straight truck and 30 ton for a truck and trailer combination vehicle and was given a sufficiency rating of 45 when it was last inspected in April of 2004.

Figure 5.1. KCB1 Alignment View Looking North.

The superstructure was in relatively good condition with only minor rust on the girders. Signs of poor concrete consolidation during the construction of the deck were observed on the underside of the deck where there were large voids near the midspan. The poor consolidation caused some of the reinforcing steel to be exposed as shown in Figure 5.2. There was also a large crack in the concrete deck located at the midspan of the bridge, a photograph of which is provided in Figure 5.3.

Figure 5.2. KCB1 Poor Concrete Consolidation.

Figure 5.3. KCB1 Deck Crack.

The superstructure, a cross section of which is shown in Figure 5.4, consists of five W21x62 girders with a 7.5-inch thick concrete deck. There are C-channel diaphragms at the 1/3 points of the bridge, concrete curbs eight inches wide by one foot tall, and steel railing on both sides of the bridge. The bridge was relatively narrow and only capable of allowing a single lane of traffic.

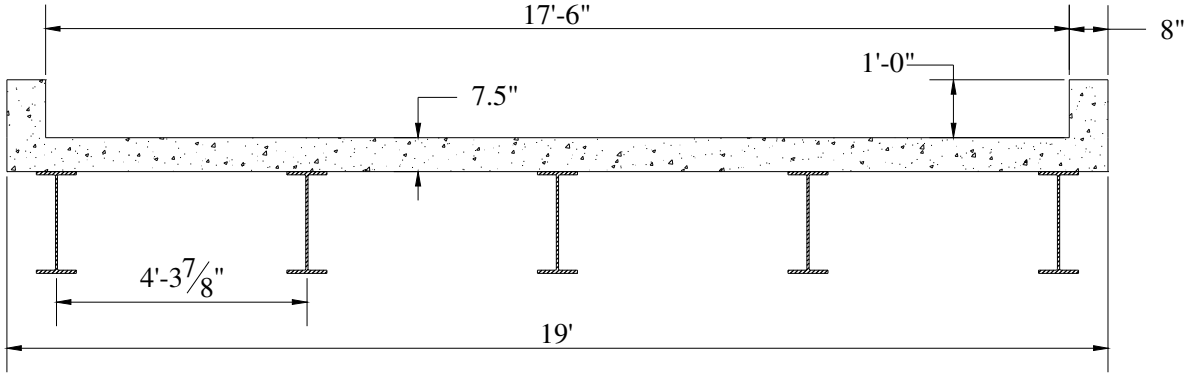

Figure 5.4. KCB1 Cross Section Looking North.

5.2 Test Setup

5.2.1 Test Truck

There were three incremental loads, referred to as: an empty truck, a half full truck, and a full truck, used to test the bridge. The truck used for the load test was provided by the county and was a standard maintenance tandem dump truck. A photograph of the test truck as it crossed the bridge during a load test is shown in Figure 5.5, its axle weights are presented in Table 5.1, and its dimensions are presented in Figure 5.6.

Figure 5.5. KCB1 Test Truck.

Table 5.1. KCB1 Truck Weights.

Truck Loading	Axle Weights (kip)			Gross Weight (kip)
	A	B	C	
Empty	12.28	6.88	6.88	26.04
Half Full	15.96	13.57	13.57	43.10
Full	17.72	18.01	18.01	53.74

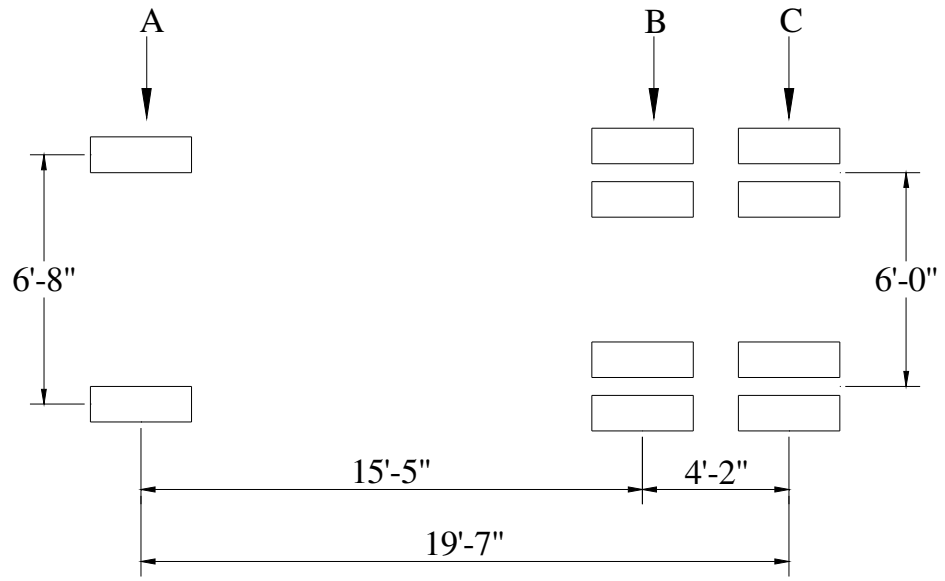

Figure 5.6. KCB1 Test Truck Dimensions.

5.2.2 Testing Plan and Instrumentation

There were three lanes selected for the truck to follow as it crossed the bridge. Each lane was loaded twice for each load level to ensure repeatability of the test results. Measurements (strains and deflections) were taken when the centroid of the tandem was at the centerline of each end bearing and at each one-quarter point as shown in Figure 5.7; the location of each of the three lanes the truck followed as it crossed the bridge are also shown in this figure.

The bridge was instrumented six inches from the edge of the bearing at each abutment and at the midspan. Strain transducers were installed on the top and bottom flanges of Girders 1, 3, and 5 near the abutments as shown in Figure 5.8. At the midspan, strain transducers were attached on the top and bottom flanges of each of the girders as well as on the underside of the concrete deck near Girders 1, 3, and 4 as shown in Figure 5.9. Also shown in Figure 5.9 are the locations of the deflection transducers installed at the midspan on all of the girders. One strain transducer was located on the top of each of the two railings at the midspan as well. There were a total of 27 strain transducers and five deflection transducers installed on the bridge for the load test.

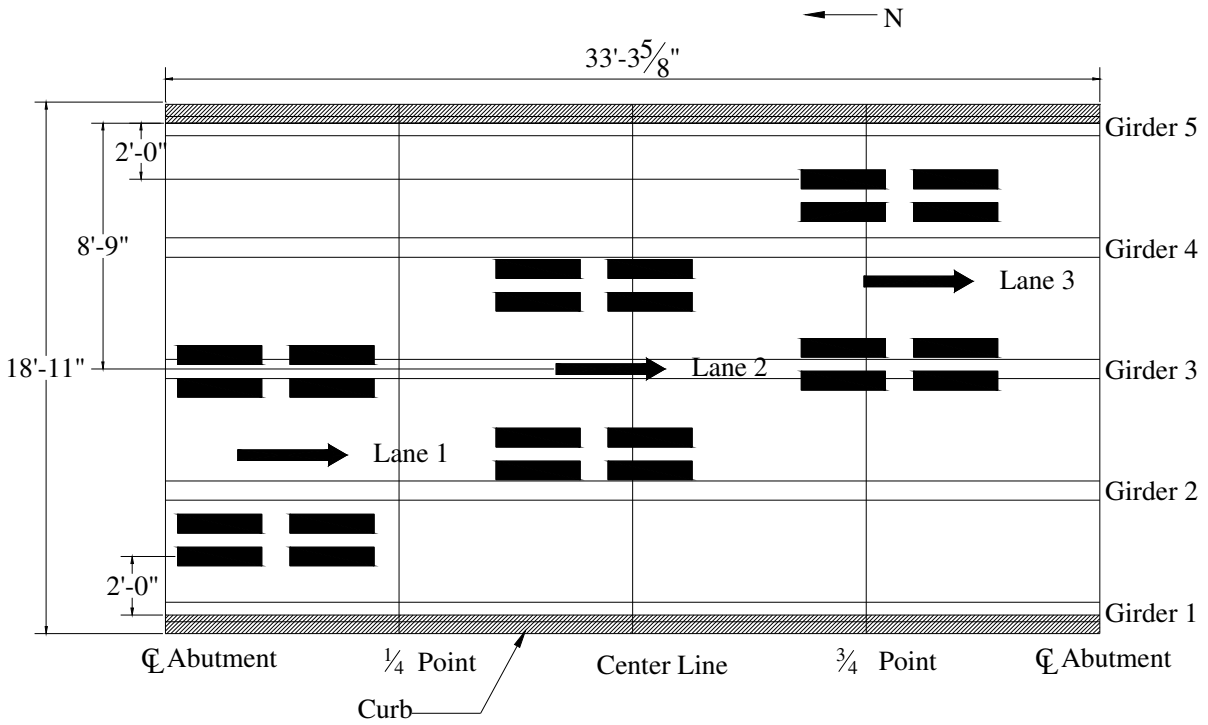

Figure 5.7. KCB1 Plan View Loading Lanes Used in KCB1 Test.

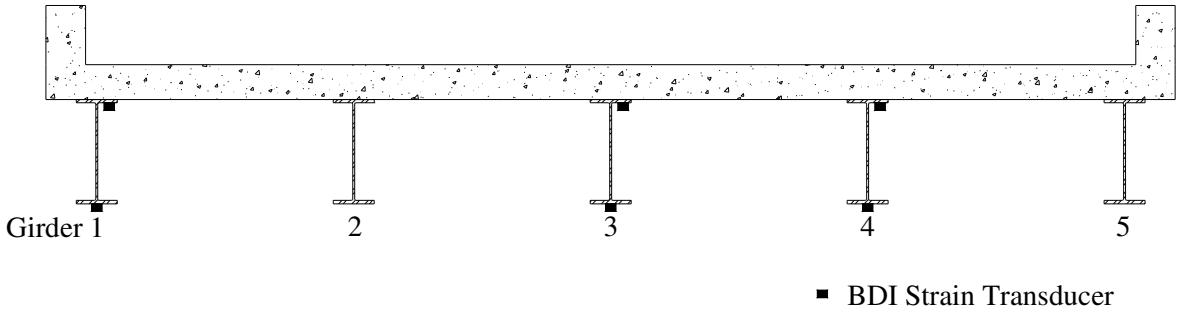

Figure 5.8. KCB1 North and South End Transducer Locations Looking North.

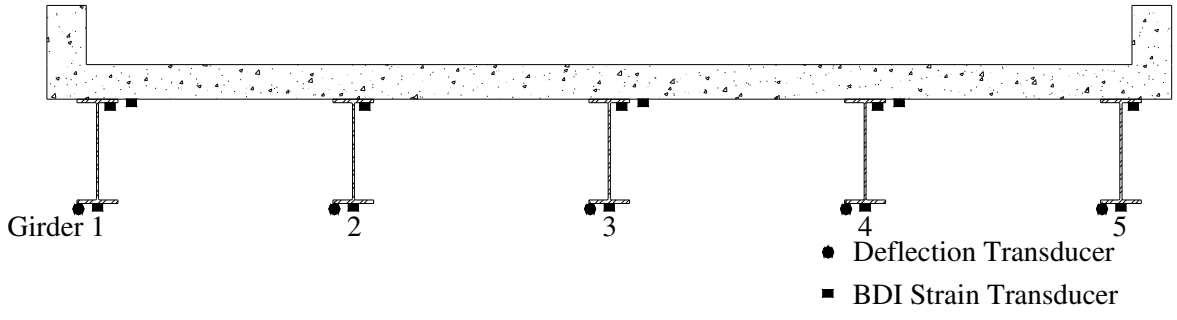

Figure 5.9. KCB1 Midspan Transducer Locations Looking North.

5.3 Bridge Analysis

5.3.1 Neutral Axis and Partial Composite Action

The bridge was designed as a non-composite simple span bridge and common with most bridges of this type, there were details that could increase the flexural capacity of the bridge. Shown in Figure 5.10 through Figure 5.12 are the top and bottom flange strains and deflections with the loading in Lane 1 through Lane 3, respectively. In the previous figures, TF and BF refers to the top and bottom flange strains, respectively. The deflection profile for the Lane 3 loading follows the same general shape as the bottom flange strain profiles; deflection profiles for Lanes 1 and 2, however, do not follow the same shape as the bottom flange strain profiles. Deflections for Girders 1 and 2 from Lanes 1 and 2 loading are roughly $1/3^{rd}$ the deflections of Girders 4 and 5 under Lane 2 and Lane 3 loading, respectively. The deflection in Girder 3 was the largest for Lane 1 loading but the maximum strain was observed in Girder 1 under the same loading. Girder 2 deflections were lower than the Girder 4 deflections under symmetrical loading whereas the strain profiles maintained symmetry under symmetrical loading as shown in Figure 5.11b. Both the top and bottom flange strain profiles exhibited symmetry as can be observed in Figure 5.11 as well as in Figure 5.10 and Figure 5.12 which are mirror images of each other. Other than the possibility of instrument error, it was not determined why Girder 2 deflections were so much smaller than those in the other girders.

Once again the strain values plotted are not the maximum values obtained during the various tests but are the values obtained when the centroid of the truck tandem was directly over the midspan of the bridge, which fixes the longitudinal truck position for all load increments.

The top flange strains in Girders 2 and 4 were larger than in any of the other girders when the KCB1 loading truck was in close proximity transversely to the girders. This bridge was a narrow bridge with only one lane of traffic and the partial composite action in these two girders could have experienced a larger amount of deterioration.

The neutral axis locations, shown in Figure 5.13, were determined by interpolating between the top and bottom flange strains to determine the location on the girder where the strain was equal to zero. Partial composite action, shown simply by the location of the neutral axes between the theoretical composite and non-composite neutral axis locations, was observed in all of the girders for each of the lanes loaded. The amount of partial composite action deteriorated with increased loading; this can be seen in Figure 5.13 where the neutral axis location shifts toward the non-composite neutral axis location with increased loading. The neutral axes of Girders 2 and 4 are also much closer to the non-composite neutral axis location than in the other girders.

The neutral axis locations for this bridge were closer to the non-composite neutral axis locations than was determined in the two previously tested bridges. Neutral axis locations in the exterior girders were also not as high as in the previously tested bridges but were higher than the interior girder neutral axis locations, thus displaying the edge stiffening effect that was prevalent in the previously tested bridge. The increased edge stiffness can be attributed

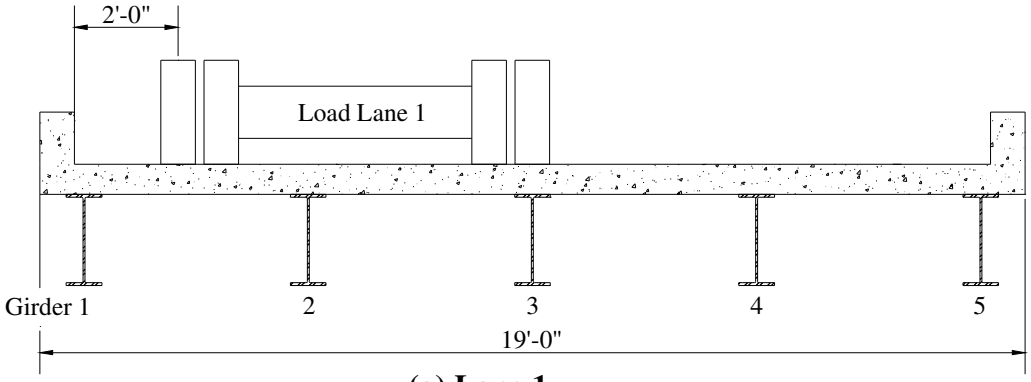

(a) Lane 1

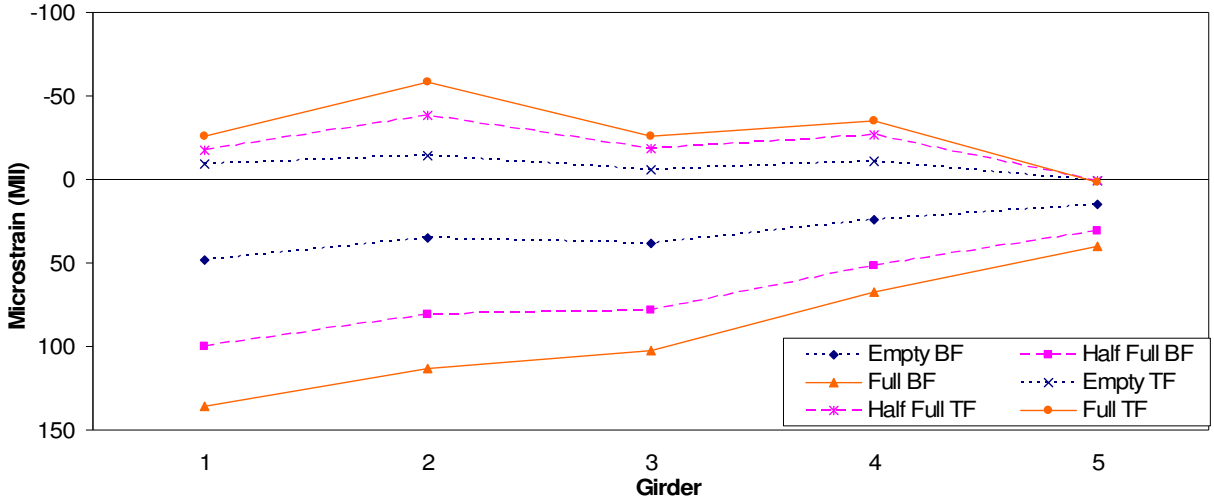

(b) Strain Profile

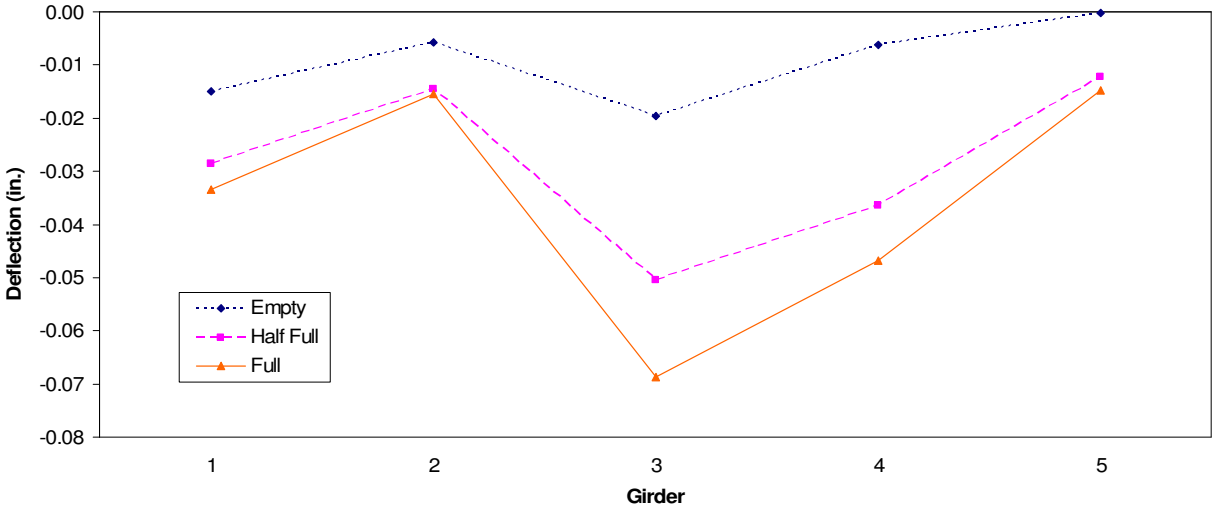

(c) Deflection Profile

Figure 5.10. KCB1 Lane 1 Strains and Deflections.

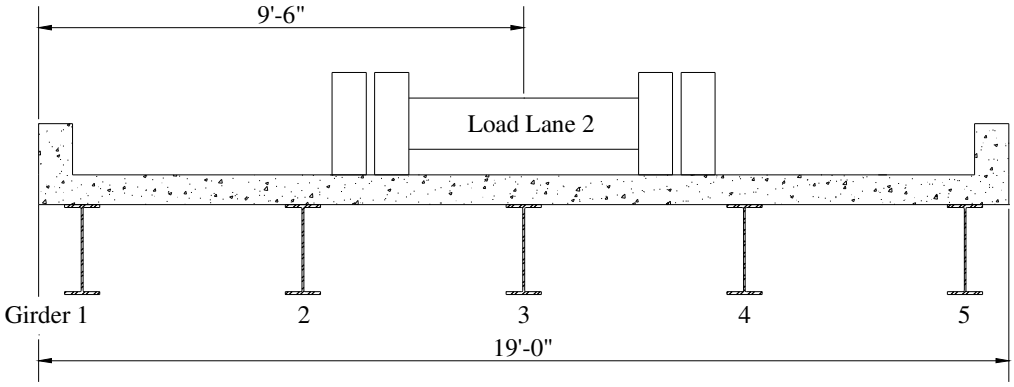

(a) Lane 2

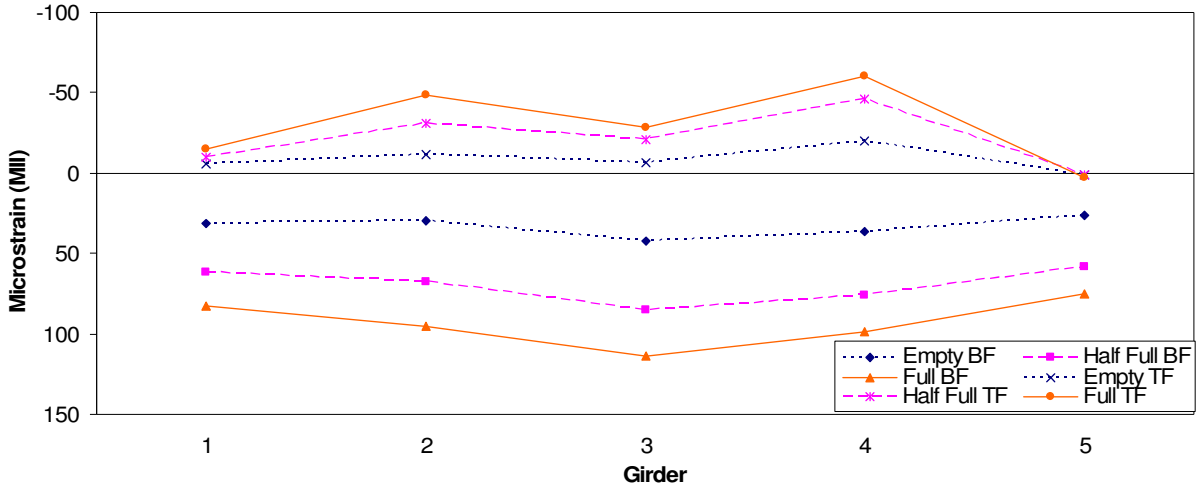

(b) Strain Profile

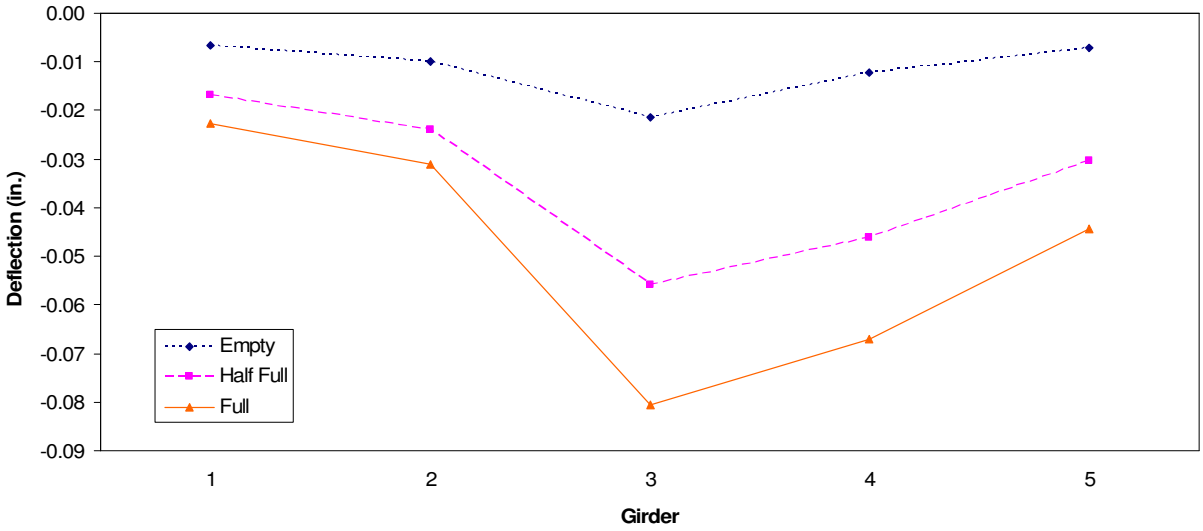

(c) Deflection Profile

Figure 5.11. KCB1 Lane 2 Strains and Deflections.

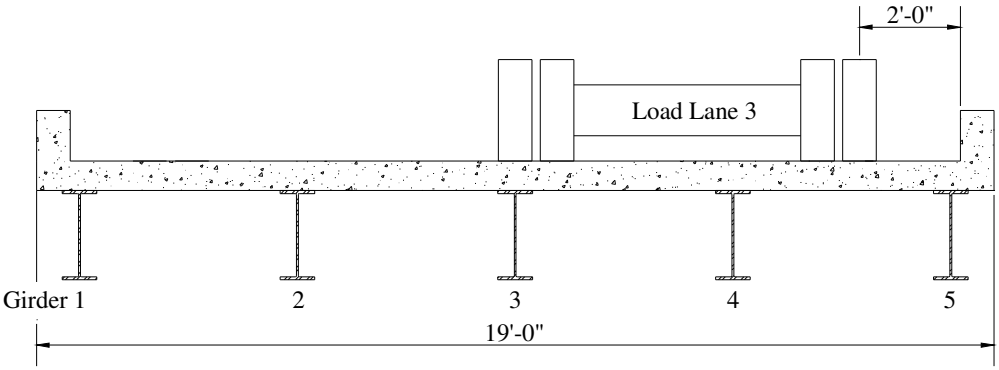

(a) Lane 3

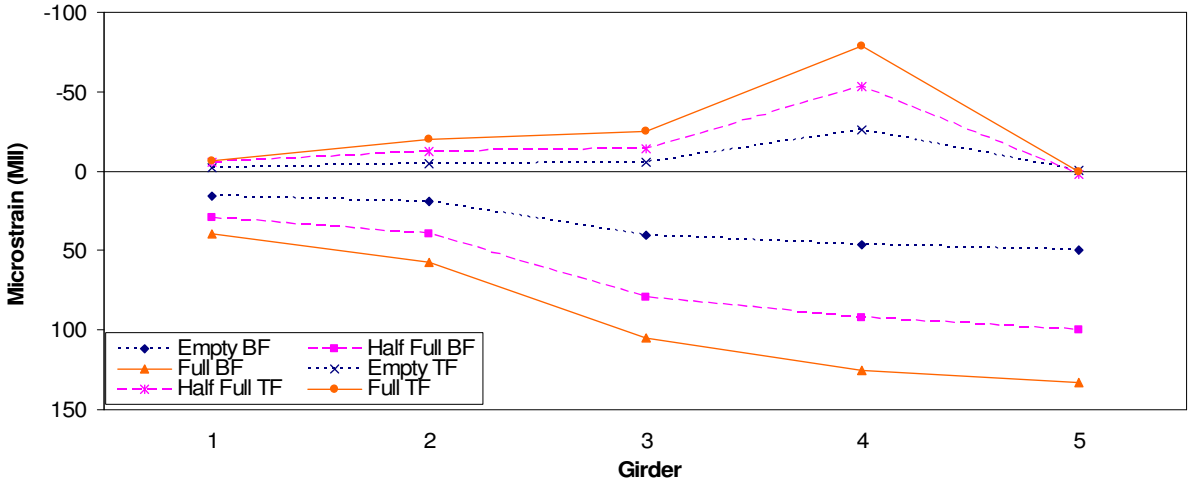

(b) Strain Profile

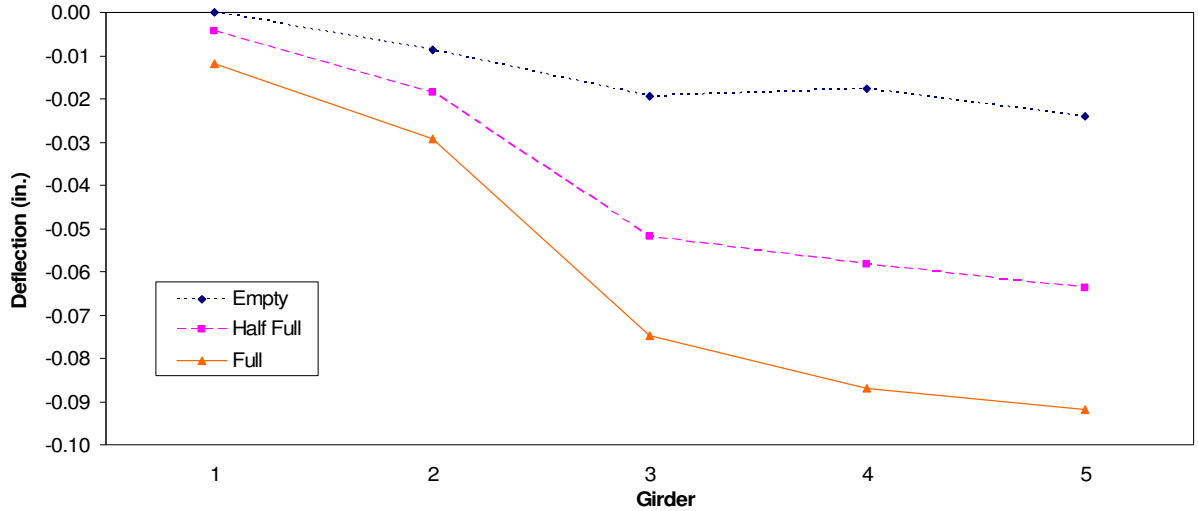

(c) Deflection Profile

Figure 5.12. KCB1 Lane 3 Strains and Deflections.

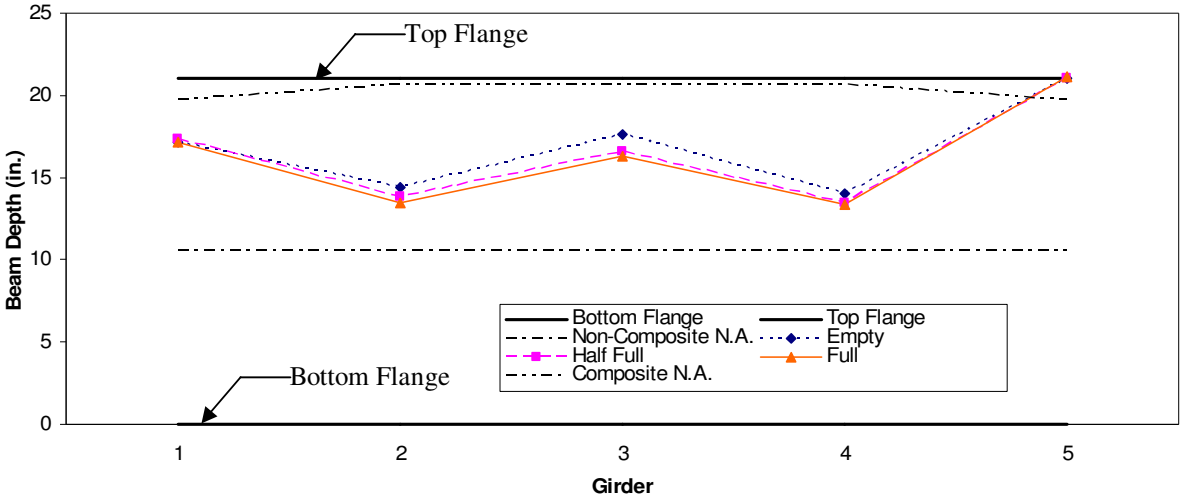

(a) Lane 1

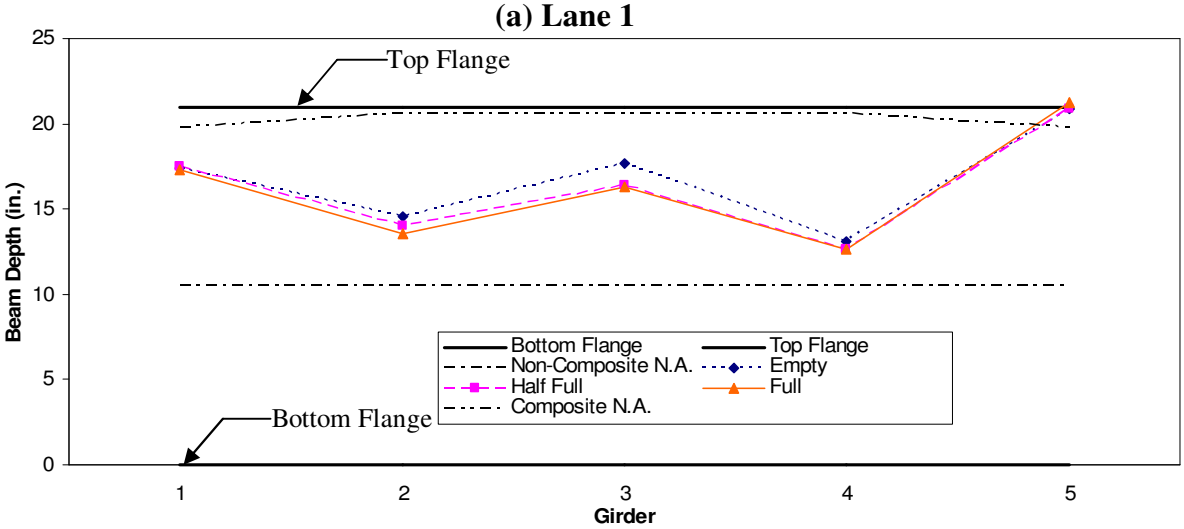

(b) Lane 2

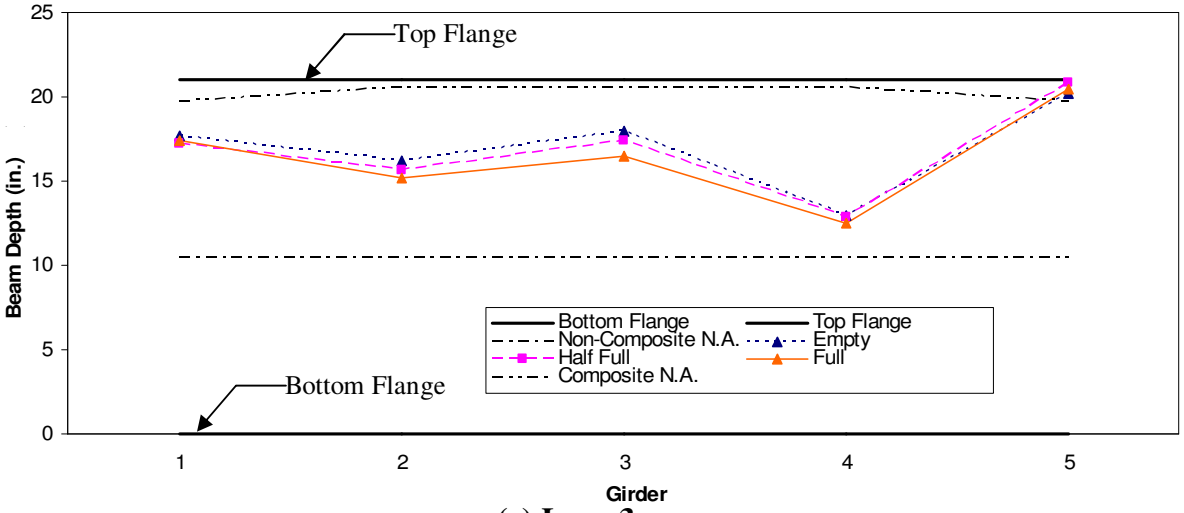

(c) Lane 3

Figure 5.13. KCB1 Neutral Axis Locations.

to the concrete curb and steel railing which were not included in the calculation of the composite neutral axis location. All of the neutral axis profiles are nearly identical indicating that the location of the neutral axis was not dependent upon the load distribution.

5.3.2 Load Distribution

Using the previously described truck locations, the theoretical moment induced in the bridge, assuming simply supported conditions was calculated for each loading; these are presented in Table 5.2. As may be seen in this table, there was a 97% increase in moment from empty to half full and a 162% increase in moment from empty to full.

Table 5.2. KCB1 Induced Truck Moments.

Load	Moment (in-k)
Empty Truck	1190
Half Full Truck	2345
Full Truck	3115

Using the bottom flange strains, the percent distributions were calculated as the ratio of the individual girder strain to the sum of the five girder strains. With each of the three load increments producing slightly different load distribution percentages, the maximum values, summarized in Table 5.3, were selected for each of the three lanes. Note that the values are the maximum percentage values of the three load cases and therefore do not sum to 100%. As may be seen, the maximum distribution percentages occurred in the exterior girders when directly loaded. Girders 2 and 4 had distribution percentages very close to each other for Lane 2 loading which demonstrates symmetry in the bottom flange strains. Symmetry in the bottom flange strains can be observed by comparing the Girder 1 distribution for Lane 1 loading to the Girder 5 distribution for Lane 3 loading.

Table 5.3. KCB1 Maximum Single Lane Percent Distributions.

Lane \ Girder	1	2	3	4	5
1	30.2	24.7	23.6	15.0	9.3
2	18.7	20.4	25.7	21.8	16.7
3	9.3	12.4	23.5	27.3%	29.3

As previously noted, the percent distributions are provided in Table 5.3; however in order to compare them to the AASHTO distribution factors the values must be multiplied by two to obtain the distribution of a single wheel line. The maximum distribution factors from the percent distributions summarized in Table 5.3 are provided in Table 5.4. The bridge was too narrow for there to be two lanes on it simultaneously so only single lane distribution factors were calculated.

The maximum distribution factors for the interior and exterior girders for the single lane loading are 0.55 and 0.60, respectively while the AASHTO distribution factor for the single lane loading with a girder spacing of 4'-3.875" using the aforementioned equation of S/7.0 is

0.62 for the interior girders. AASHTO stipulates that distribution factor for the exterior girders shall not be less than S/5.5 even though there is only one lane on the bridge which gives a distribution factor of 0.79 for the exterior girders. Values obtained by dividing the AASHTO distribution factors by the experimental distribution are summarized in Table 5.5.

Table 5.4. KCB1 Calculated Single Lane Distribution Factors.

Lane \ Girder	1	2	3	4	5
1	0.60	0.49	0.47	0.30	0.19
2	0.37	0.41	0.51	0.44	0.33
3	0.19	0.25	0.47	0.55	0.59

Table 5.5. KCB1 Distribution Ratios

	Single Lane
Interior Girder Distribution	0.55
Exterior Girder Distribution	0.60
AASHTO Interior Distribution Factor	0.62
AASHTO Exterior Distribution Factor	0.79
Interior Factor Ratio	1.13
Exterior Factor Ratio	1.31

The distribution ratios for the single lane show that the AASHTO equations are conservative as the ratios exceed 1.0. Load distribution factors calculated using the AASHTO equation are larger than the experimental distribution by 30% for the exterior girders. If the AASHTO equation for the interior girders of S/7 was used on the exterior girders, the exterior factor ratio would be 1.02, resulting in a much closer correlation. In general, the AASHTO distribution factors are verified by the field test results.

5.3.3 Moment of Inertia

The moment of inertia is not the same for each girder due to the varying amount of composite action. The moment of inertia for each girder was calculated following the same procedure outlined in Section 3.3.3 for the BCB. With the neutral axis locations for each girder being close to the same for the three load increments, it would follow that the moments of inertia, presented in Table 5.6, for the three load increments would be very close. An average moment of inertia for each girder from the three load increments is also provided in Table 5.6.

Table 5.6. KCB1 Moments of Inertia (in^4).

Lane \ Girder	1	2	3	4	5
1	3185	2270	3890	2185	4405
2	3250	2300	3075	1955	4375
3	3265	2755	3210	1960	4205
Average	3235	2440	3125	2035	4325

The non-composite moment of inertial for the girder is 1,330 in^4 and the composite moment of inertia for the girder with an effective flange width equal to the girder spacing is 4,235 in^4 for the interior girders and 3,955 in^4 for the exterior girders for which neither the moment of inertia, the curb, or the railing were considered in the calculation. With the location of the neutral axes for each girder between the non-composite and composite neutral axis locations, it is reasonable that the calculated moments of inertia are also between those of non-composite and composite sections. The moments of inertia for each girder and lane loading are shown graphically in Figure 5.14 along with the values for the non-composite and composite neutral axes. An average of the four lane loadings is also provided in Figure 5.14.

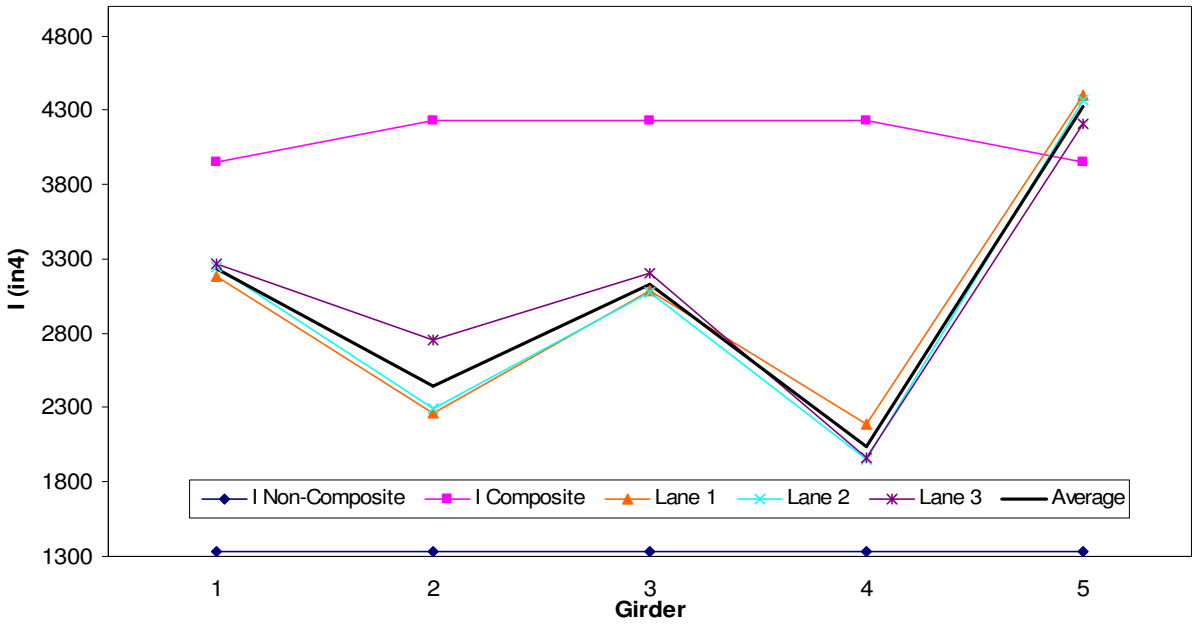

Figure 5.14. KCB1 Effective Moments of Inertia.

5.4 BDI Optimization

The bridge was once again modeled using software (WinGEN) provided by Bridge Diagnostics Inc. that utilizes the actual test data to create a model that is close to the actual bridge based on the response of the structure to the truck loadings. This bridge model consisted of modeling each girder separately so that the moments of inertia for each girder could be optimized. Modeling each girder separately increases the correlation between the actual test data and the theoretical response after optimization because the moment of inertia for each girder can be optimized. As before, the deck was modeled using plate elements, while the girders were modeled using beam elements. Rotational springs were attached to the ends of each of the girders: one for the north end of the exterior girders, one for the north end of the interior girders, and two more for the interior and exterior girders on the south end of the bridge.

As a starting point for the model generation, the initial girder moments of inertia were the average values provided in Table 5.6. The initial value for all of the spring constants was

1,000 kip-in/rad and the initial value of the Young's modulus for concrete was 3,150 ksi.

Only steel girder strains were input into the model; concrete slab strains were not input into the model because there were large variations in their magnitudes. After the model was generated using WinGEN, it was analyzed using WinSAC. WinSAC compares the actual strains induced by test truck to those produced by a theoretical truck with the same dimensions and wheel loads as the test truck. As before, strain comparisons in the girders using the initial input values for the girder moments of inertia, modulus of elasticity for the concrete in the deck, and rotational spring stiffness yielded a large scale error.

With the scale error being so large, the model needed to be optimized. The parameters that were optimized for the bridge included the moments of inertia for each girder, the rotational spring stiffness, and the modulus of elasticity for the concrete in the deck. Upper and lower bounds for the optimization parameters are presented in Table 5.7. The upper and lower bound for the moment of inertia of the girders corresponded to 120% of the composite and 80% of the non-composite neutral axis locations, respectively. Optimizing the bridge using the parameters in Table 5.7 still yielded a somewhat large scale error of 15.1%; the optimized values are provided in Table 5.8.

Table 5.7. KCB1 Optimization Parameters.

Optimization Parameter	Lower Bound	Upper Bound
Moment of Inertia (in^4)	1065	4405
Rotational Spring Stiffness (kip-in/rad)	0	1,000,000
Modulus of Concrete (ksi)	2500	6000

Table 5.8. KCB1 Optimized Parameters Using All Steel Transducers.

Optimized Parameter	Initial Value	Optimized Value
Girder 1 I_y (in^4)	3235	4205
Girder 2 I_y (in^4)	2440	2460
Girder 3 I_y (in^4)	3120	1970
Girder 4 I_y (in^4)	2040	1815
Girder 5 I_y (in^4)	4325	4405
North Exterior Rotational Spring (kip-in/rad)	1000	217,400
North Interior Rotational Spring (kip-in/rad)	1000	286,800
South Exterior Rotational Spring (kip-in/rad)	1000	251,000
South Interior Rotational Spring (kip-in/rad)	1000	332,100
Deck Modulus (ksi)	3150	5980

The procedure outlined in Section 5.3.3 where an attempt to obtain initial moments of inertia for the girders was again not successful as not all of optimized values correlated with the initial values displayed in Table 5.7. The apparent symmetry observed in the neutral axis, deflection profile and strain profile plots previously presented was not observed in the optimized girder moments of inertia. Comparing the optimized moment of inertia in the geometrically symmetric Girders 2 and 4 shows that the optimization was not symmetrical as the optimized values were 2,460 and 1,815 in^4, respectively. Optimized values obtained for

the spring constants were relatively close to each other ranging from about 220,000 to 330,000 kip-in/rad. The upper bound for the deck modulus of elasticity was increased to 6,000 ksi because the initial optimization yielded a modulus of elasticity very close to the initial upper bound of 5,500 ksi. As shown in Table 5.8, the concrete modulus of elasticity was still very close to the upper bound. It did not seem reasonable to continue increasing the upper bound for the modulus of elasticity for the concrete because a modulus of 6,000 ksi corresponds to a concrete compressive strength of nearly 11,000 psi. A graphical comparison of the optimized strains for each loading path are compared to the actual strains induced by the test truck for Girder 1 through Girder 5 are presented in Figure 5.15 through Figure 5.19, respectively.

In almost all cases, the optimized strains were close to the actual strains from the test truck. The correlation between the optimized strains and the actual strains are summarized in Table 5.9. The scale error ranged from 0.4 to 6.2 and the correlation ranged from 0.890 to 0.950.

Table 5.9. KCB1 Bottom Flange Strain Scale Error and Correlation.

Girder	1	2	3	4	5	Average
Scale Error	0.4	2.1	3.8	3.4	6.2	3.2
Correlation	0.912	0.895	0.865	0.900	0.923	0.899

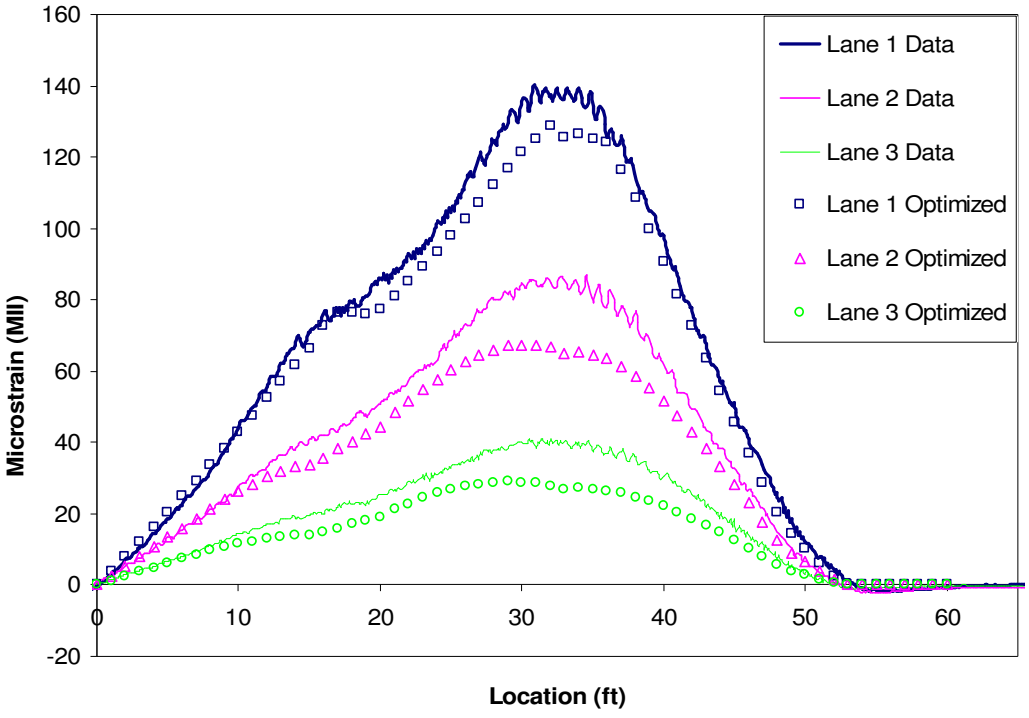

Figure 5.15. KCB1 Girder 1 Optimized Strain Comparison.

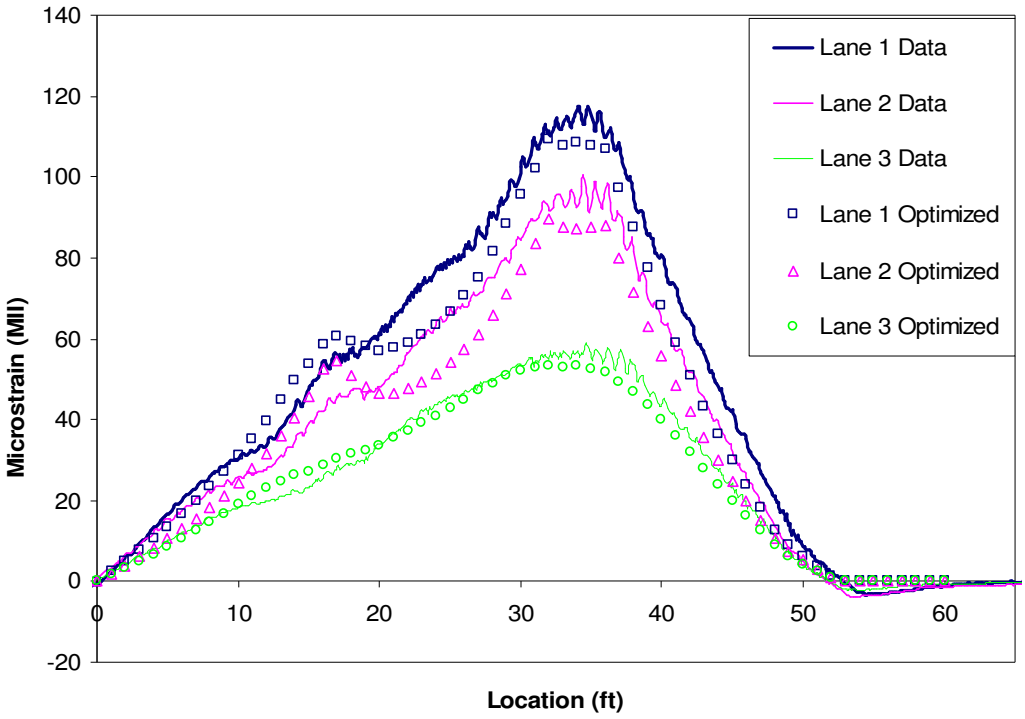

Figure 5.16. KCB1 Girder 2 Optimized Strain Comparison.

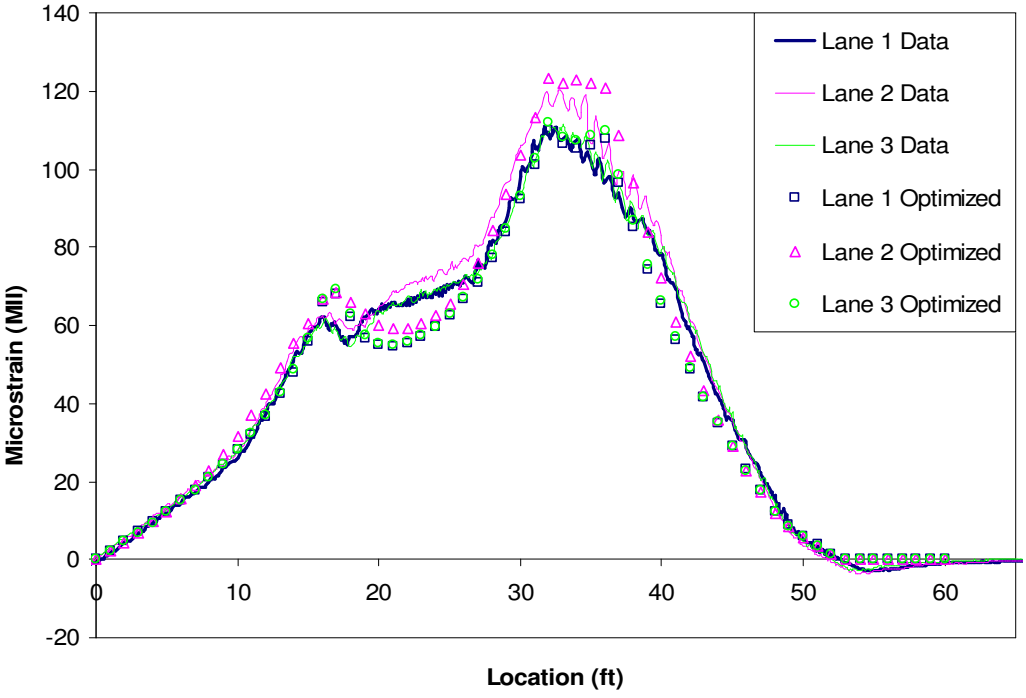

Figure 5.17. KCB1 Girder 3 Optimized Strain Comparison.

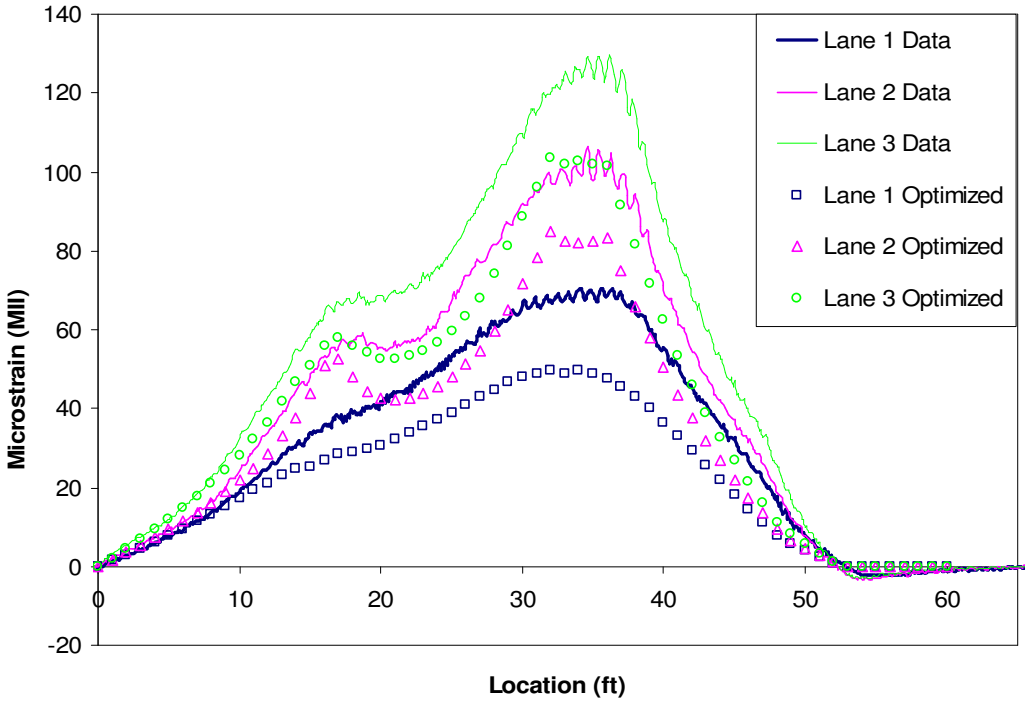

Figure 5.18. KCB1 Girder 4 Optimized Strain Comparison.

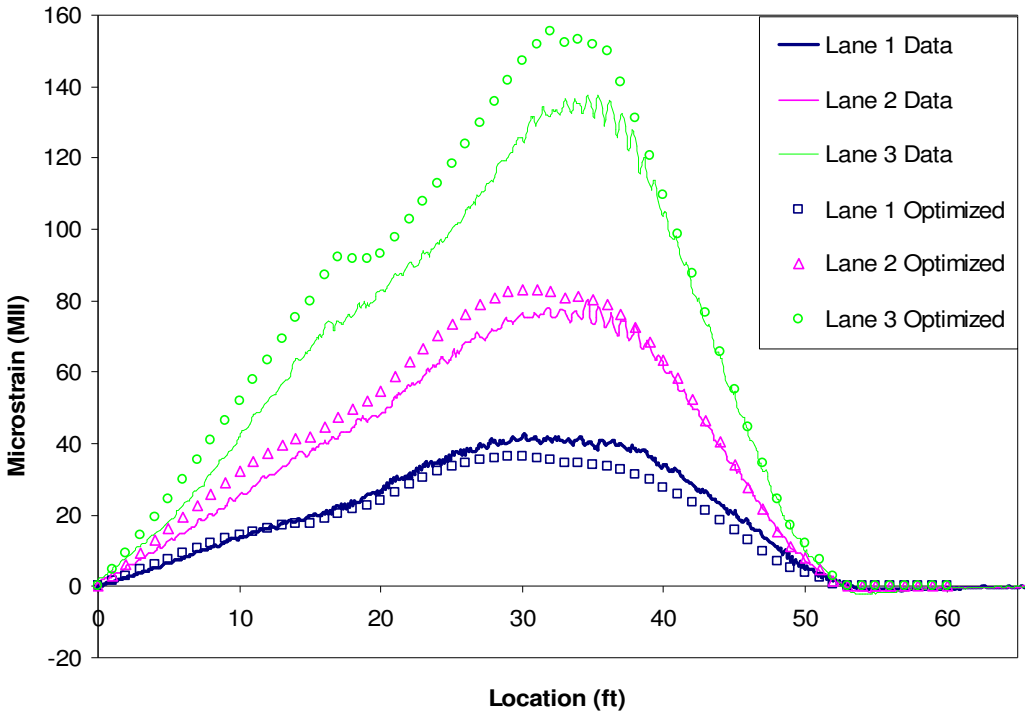

Figure 5.19. KCB1 Girder 5 Optimized Strain Comparison.

In an attempt to decrease the overall scale error, the strains measured near the supports were removed from the bridge optimization model. The previous optimized values were input into a model that had only the midspan strains in an attempt to quantify the effect of the bearing strains on the scale error. This model was analyzed and resulted in a scale error of only 3.2%, an 11.9% reduction from the original optimization model using all of the steel girder strains. The correlation values provided in Table 5.9 did not change in the new analysis.

5.5 Bridge Rating

5.5.1 Conventional Rating

The bridge was rated using the Load Factor Rating (LFR) approach. This analytical rating, in which both the interior and exterior girders were rated, was performed assuming a non-composite design with simply supported conditions. The bridge was also independently rated by both the Iowa DOT and PCF. Ratings calculated by the three different rating agencies are provided in Table 5.10.

Table 5.10. KCB1 Analytical Bridge Ratings.

Interior Girders						
	ISU		PCF		Iowa DOT	
Vehicle	Operating	Inventory	Operating	Inventory	Operating	Inventory
HS20 (36 ton)	66.4	39.8	64.3	38.5	56.5	33.9
Type 4 (27.25 ton)	52.8	31.6	52.3	31.3	46.7	28.0
Type 3-3 (40 ton)	94.3	56.5	94.2	56.4	80.2	50.5
Type 3S3 (40 ton)	80.3	48.1	80.4	48.2	73.4	44.0
Exterior Girders						
	ISU		PCF		Iowa DOT	
Vehicle	Operating	Inventory	Operating	Inventory	Operating	Inventory
HS20 (36 ton)	52.2	31.6	53.6	32.1	39.2	23.8
Type 4 (27.25 ton)	48.1	24.9	43.6	26.1	32.4	19.3
Type 3-3 (40 ton)	74.1	44.4	78.6	47.1	58.4	35.2
Type 3S3 (40 ton)	63.1	37.8	67.1	40.2	50.0	30.0

The ratings calculated by PCF correspond very closely to those calculated by ISU. The calculated ratings from ISU tend to be slightly more conservative than those calculated by PCF. Once again the Iowa DOT ratings were more conservative than those calculated by both ISU and PCF due to the serviceability criterion that they found to control the ratings. Operating ratings calculated for the bridge are sufficient for the legal loads and would not require the bridge to be posted. The exterior girders control the bridge ratings for all three rating agencies but were larger than the legal loads for the rating vehicles and therefore would not require the bridge to be posted at the operating level. The exterior girders fall slightly below the legal loading for the inventory ratings. Note that this bridge was posted prior to the load testing but that the ratings indicate that such posting is not necessary. The reason the

bridge was posted was not due to the superstructure elements though, but rather, the substructure elements. According to the 2002 inspection report obtained from the County Engineer's office, the north abutment piles were "rotting at the ground line" and thus the aforementioned bridge posting was recommended.

5.5.2 Rating Using Optimized Parameters From BDI Software

Utilizing the strains measured during the load test, the BDI software (WinGEN) was once again utilized to determine the bridge rating using the optimized parameters. Using the modified bridge model, the bridge was rated using the same rating vehicles as were used in the analytical ratings. The rating vehicles were input into the WinGEN software and traversed across the bridge in pre-selected lanes to produce maximum strains in the girders. Only a single lane loading was analyzed using the WinSAC software. With the optimized moments of inertia for each girder being different, each girder was rated separately using the BDI software. The load factor rating method was once again used for the ratings using the optimized bridge parameters. The operating and inventory ratings were calculated for each girder and are summarized in Table 5.11.

The optimized operating ratings for all of the rating vehicles were well above the legal loads for the bridge. The limiting girder was Girder 5 having the lowest operating rating with a limit of 88 tons for a HS20 rating vehicle, well above the legal weight of 36 ton. The inventory ratings were larger than the legal loading for the rating vehicles with Girder 2 having the lowest rating. The inventory rating for Girder 5 with the HS20 rating vehicle was 52.4 ton, well above the vehicle weight of 36 ton. A table presenting the percentage increase from the ISU analytical ratings to the optimized ratings for the operating level is presented in Table 5.12. The range for the increased ratings after optimization for the HS20 rating vehicle was 68% for exterior Girder 5 to 195% for interior Girder 3.

Table 5.11. KCB1 Optimized Ratings.

Operating Rating (ton)					
	Girder				
Vehicle	1	2	3	4	5
HS20 (36 ton)	101.2	153.0	195.8	193.0	87.5
Tandem (25 ton)	61.0	92.5	118.0	117.8	51.8
Type 3 (25 ton)	86.8	133.3	170.8	169.5	74.0
Type 4 (27.25 ton)	81.8	128.4	166.0	167.6	76.9
Type 3-3 (40 ton)	146.4	233.6	303.6	298.8	125.6
Type 3S3 (40 ton)	123.6	195.2	252.4	250.0	105.6
Type 4S3 (48 ton)	144.5	228.5	295.2	292.3	123.4
Inventory Rating (ton)					
	Girder				
Vehicle	1	2	3	4	5
HS20 (36 ton)	60.6	91.7	117.3	115.6	52.4
Tandem (25 ton)	36.5	55.4	70.7	70.5	31.0
Type 3 (25 ton)	52.0	79.8	102.2	101.5	44.3
Type 4 (27.25 ton)	49.0	76.9	99.4	100.4	46.0
Type 3-3 (40 ton)	87.7	139.9	181.9	179.0	75.2
Type 3S3 (40 ton)	74.1	116.9	151.2	149.8	63.3
Type 4S3 (48 ton)	86.6	136.9	176.9	175.1	73.9

Table 5.12. KCB1 Operating Rating Percent Increase After Optimization.

	Girder				
Vehicle	1	2	3	4	5
HS20 (36 ton)	94	130	195	191	68
Type 4 (27.25 ton)	70	143	214	217	60
Type 3-3 (40 ton)	98	148	222	217	70
Type 3S3 (40 ton)	96	143	214	211	67

6. CARROLL COUNTY BRIDGE (CCB)

6.1 Bridge Description

The fourth bridge that was load tested is located in Carroll County, IA on 245th Street just south of the city limits of Halbur, IA. The bridge (FHWA ID: 94680), henceforth referred to as the CCB, is a 33.3-foot simple-span, non-composite bridge with four steel girders, a concrete deck, and no skew crossing a creek. The substructure consists of six timber piles with a double C-channel cap and a timber back wall. Shown in Figure 6.1, the bridge is not currently posted and was given a sufficiency rating of 36 when it was last inspected in May of 2005.

Figure 6.1. CCB Alignment View Looking North.

The superstructure was in relatively good condition with only minor rust on the girders. The concrete deck however was in poor condition; there were areas of severe spalling on the wearing surface of the deck that had been patched with asphalt to create a smoother ride over the bridge. A photograph of the asphalt patches is shown in Figure 6.2.

Figure 6.2. Asphalt Patches in CCB Concrete Deck.

The superstructure, a cross section of which is shown in Figure 5.4, is a four girder system with two W21x63 exterior girders and two W24x87 interior girders with a 7.5 inch cast-in-place concrete deck. There are C-channel diaphragms at the 1/3 points of the bridge and a concrete curb (eight inches wide by 12 inches deep) as well as a steel railing located on both sides of the bridge.

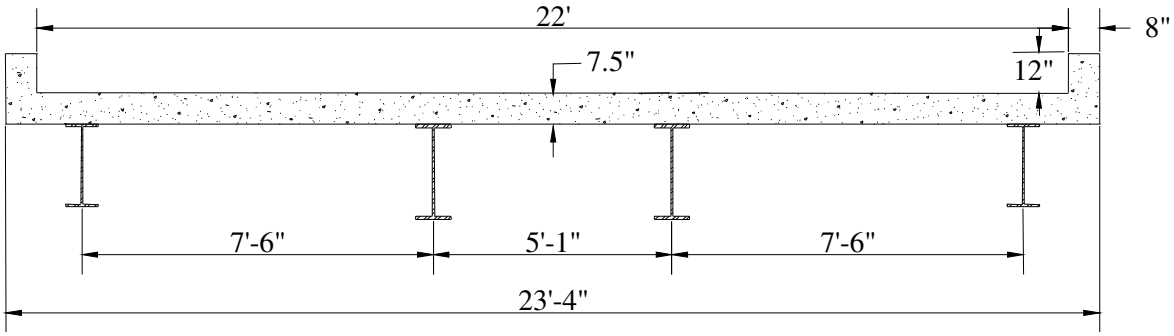

Figure 6.3. CCB Cross Section Looking North.

6.2 Test Setup

6.2.1 Test Truck

Two incremental loads, referred to as a half full truck and a full truck, were selected for loading in the bridge test. The incremental loads once again refer to the amount of material (gravel) the test truck was carrying during the load test. The truck used in the load test was provided by the county and was a standard maintenance tandem dump truck. Axle weights and dimensions of the test truck are provided in Table 6.1 and Figure 6.4, respectively.

Table 6.1. CCB Truck Weights.

Truck Loading	Axle Weights (kip)			Gross Weight (kip)
	A	B	C	
Half Full	12.95	13.80	13.50	40.25
Full	14.50	17.90	18.05	50.45

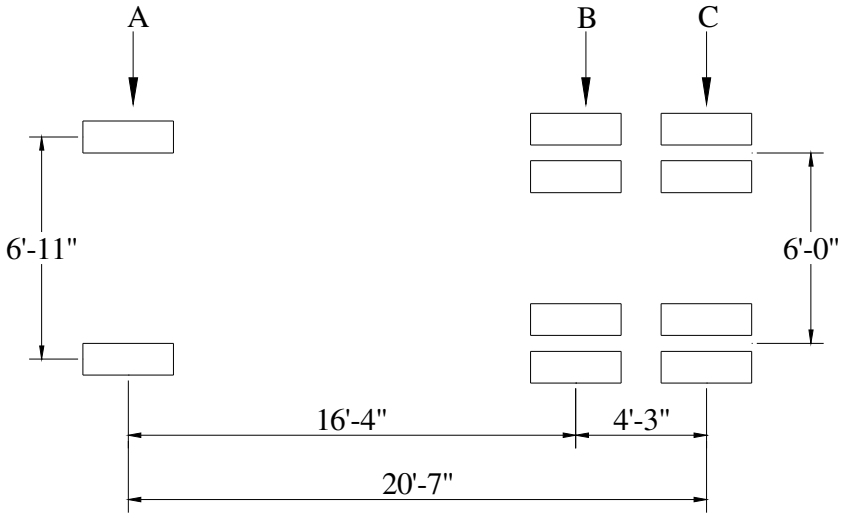

Figure 6.4. CCB Test Truck Dimensions.

6.2.2 Testing Plan and Instrumentation

There were five lanes, shown in Figure 6.5, selected for the truck to follow as it crossed the bridge. Each lane was tested twice for each load increment to check the repeatability of the test results. Measurements (strains and deflections) were taken when the centroid of the tandem was at the centerline of each end bearing and at each quarter point (see Figure 6.5).

The bridge was instrumented 24 inches from the edge of the bearing at each abutment, at the north quarter point, and at the midspan. Figure 6.6 is a photograph showing the location of the strain transducers 24 inches from the edge of the bearing. In this test, the strain transducers near the abutment were moved from six inches away from the edge of the abutment cap to 24 inches from the abutment cap in an attempt to reduce the chance of

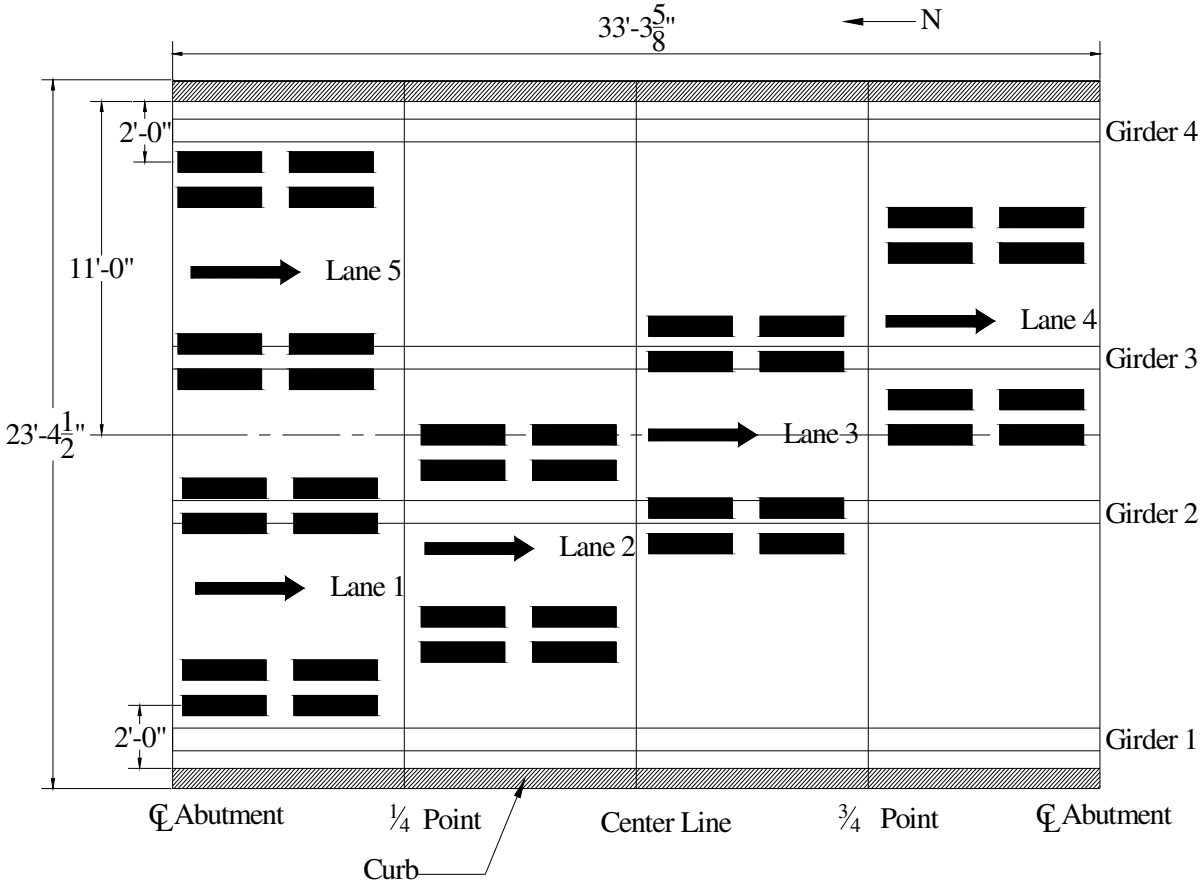

Figure 6.5. CCB Plan View Loading Lanes.

measuring stress concentrations that can be observed near the girder bearing. This would allow for a better understanding of the rotational restraint due to end conditions of the girders.

Strain transducers were installed on the top and bottom flanges of each girder near the north abutment and at the north quarter point as shown in Figure 6.7. Two strain transducers were positioned on the concrete at the midspan next to Girder 4 and directly between Girders 3 and 4. The locations of the strain and deflection transducers at the midspan on each girder and on the concrete are shown in Figure 6.8. Strain transducers were only installed on the top and bottom flanges of Girders 1 and 3 near the south abutment as shown in Figure 6.9. One strain transducer was located on the top of each of the two railings at the midspan as well. In total for testing this bridge, there were 32 strain transducers and four deflection transducers installed on the bridge.

Figure 6.6. CCB Bearing Transducer Locations.

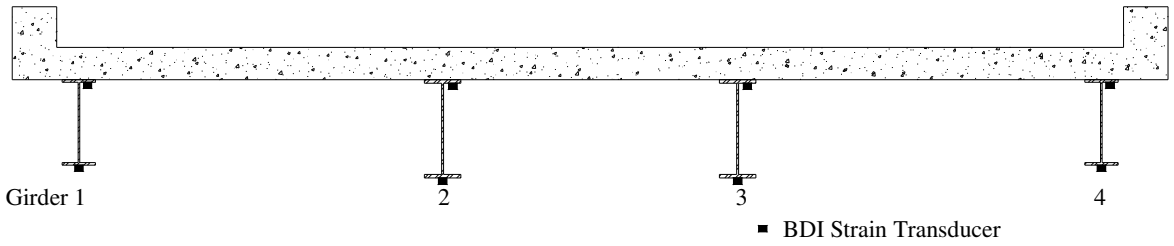

Figure 6.7. CCB North End and Quarter Point Transducer Locations Looking North.

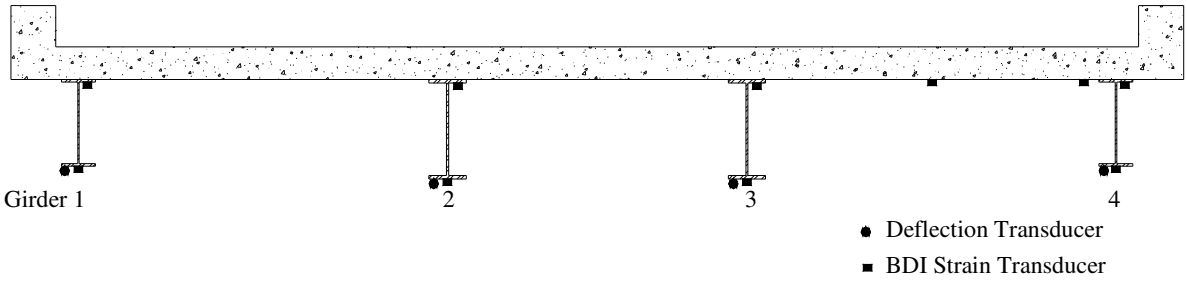

Figure 6.8. CCB Midspan Transducer Locations Looking North.

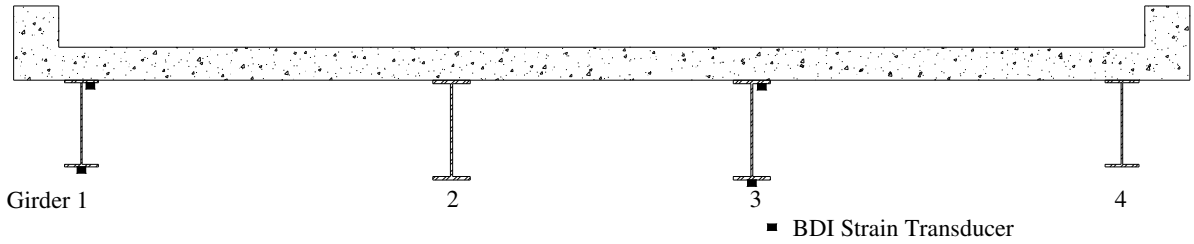

Figure 6.9. CCB South End Transducer Locations Looking North.

6.3 Bridge Analysis

6.3.1 Neutral Axis and Partial Composite Action

The bridge was designed as a non-composite simple span bridge and common with this type of bridge, there were some details that could increase the flexural capacity of the bridge. Shown in Figure 6.10 through Figure 6.14 are the top and bottom flange strains and deflections with the loading in Lane 1 through Lane 5, respectively. In these figures, TF and BF refers to the top and bottom flange strains, respectively. The deflection profile for the Lanes 4 and 5 loading follows the same general shape as the bottom flange strain profiles; deflection profiles for Lanes 1, 2, and 3, however, do not follow the same shape as the bottom flange strain profiles. The source of the difference in the profiles originates from the Girder 1 deflection which is roughly half of the deflection of Girders 4 during Lanes 1 and 5 loading, respectively. The deflections in Girder 2 were the largest for Lanes 1 and 2 loading but the maximum strain was observed in Girder 1 under the same loading. It was not determined why Girder 1 deflections were so much smaller than the deflections in the other girders.

The neutral axis locations, shown in Figure 6.15, were determined by interpolating between the top and bottom flange strains to determine the location where the strain was zero. Note that in Figure 6.15 the location of the top flange changes from the interior girders to the exterior girders due to the different depths of the two sections. Partial composite action, shown simply by the location of the neutral axes being located between the theoretical composite and non-composite neutral axis locations, was observed in all of the girders for each of the lanes loaded. The amount of partial composite action deteriorated with increased loading for Girder 3 only; this can be seen in Figure 6.15 by the neutral axis moving toward the non-composite neutral axis with increased loading. The neutral axis locations in Girders 1, 2, and 4 did not change with the change in load increment.

Neutral axis locations in the exterior girders were well within the concrete deck; this displays the edge stiffening effect that was prevalent in the previously tested bridge. The increased edge stiffness can be attributed to the concrete curb and steel railing which were not included in the calculations for determining the composite neutral axis location. The theoretical composite neutral axis locations, shown in Figure 6.15, were located within the concrete deck and within the top flange of the girder for the exterior and interior girders, respectively. All of the neutral axis profiles are nearly identical indicating that the location of the neutral axes

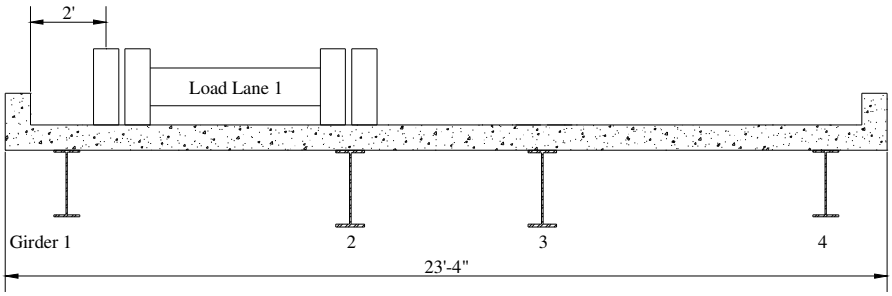

(a) Lane 1

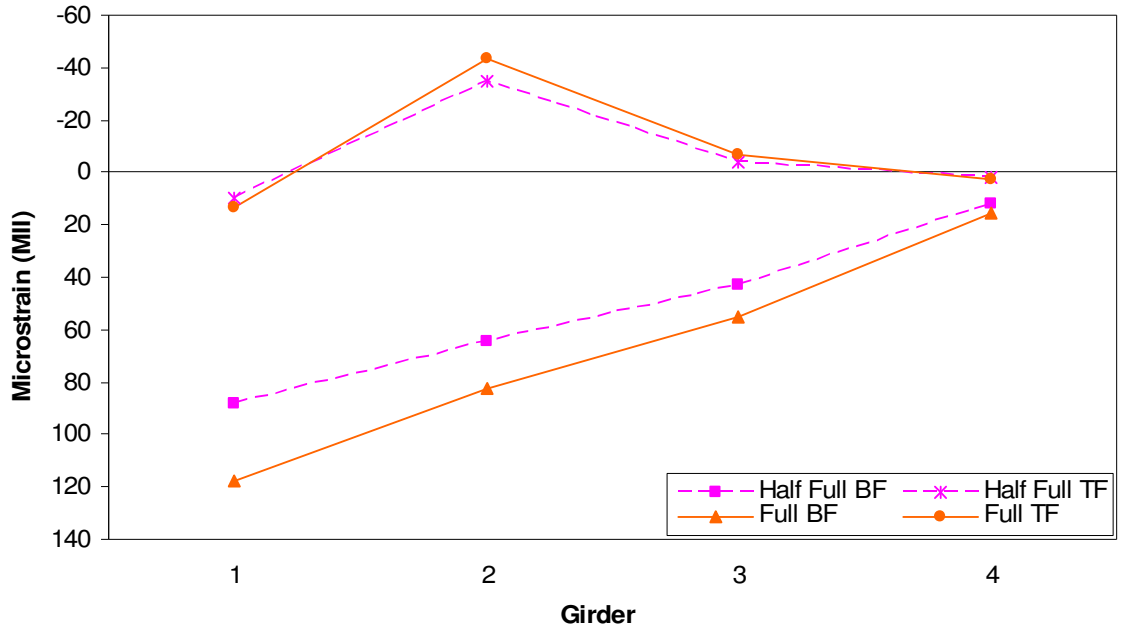

(b) Strain Profile

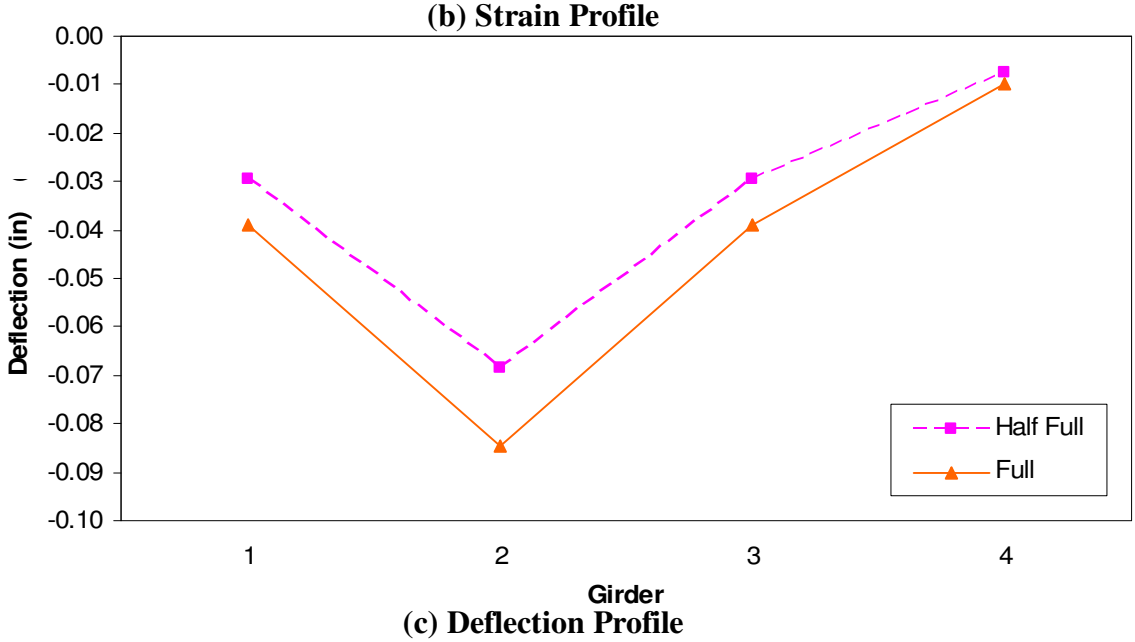

(c) Deflection Profile

Figure 6.10. CCB Lane 1 Strains and Deflections.

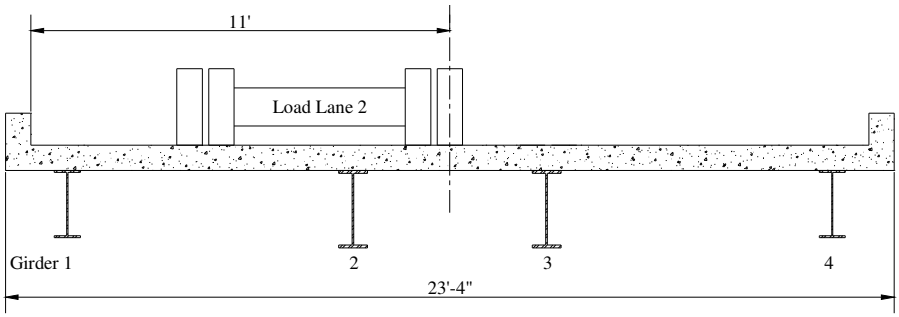

(a) Lane 2 Loading

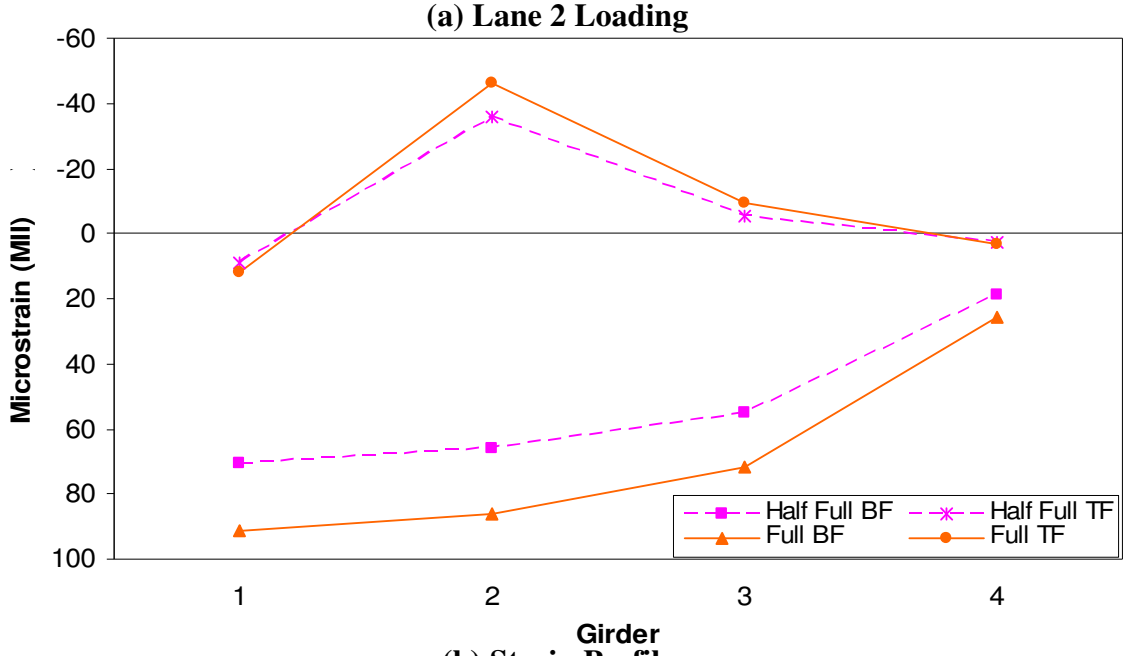

(b) Strain Profile

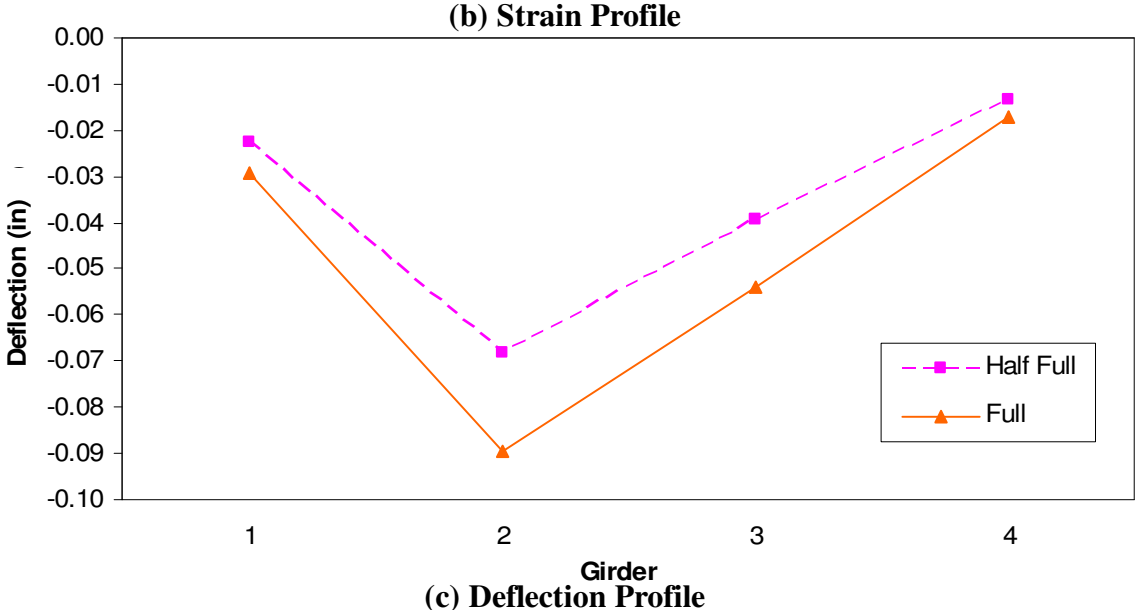

(c) Deflection Profile

Figure 6.11. CCB Lane 2 Strains and Deflections.

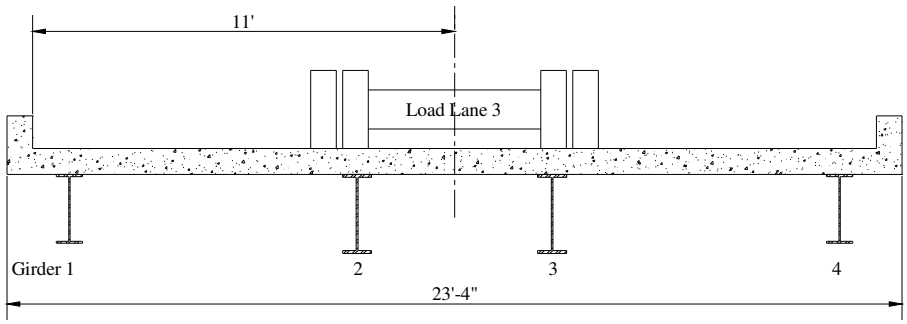

(a) Lane 3 Loading

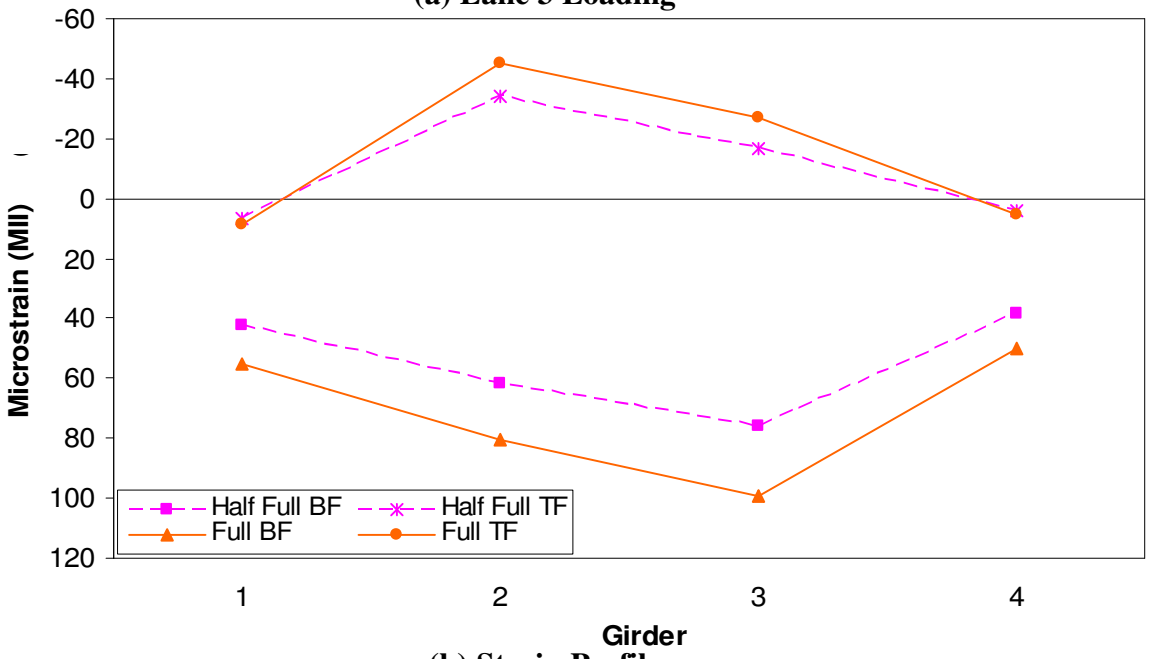

(b) Strain Profile

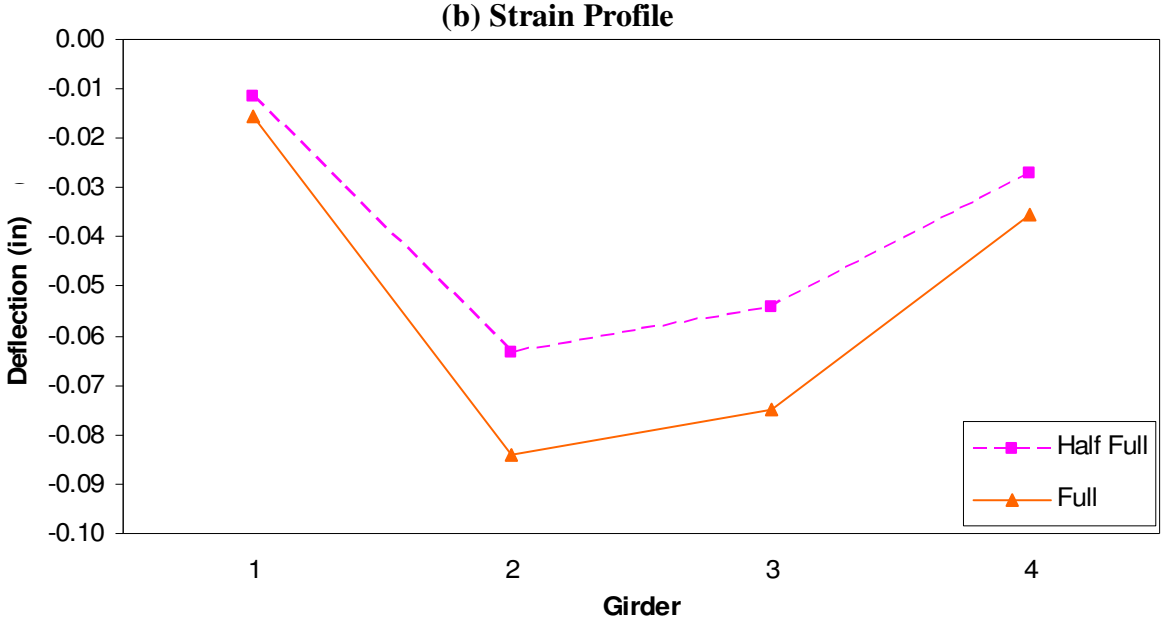

(c) Deflection Profile

Figure 6.12. CCB Lane 3 Strains and Deflections.

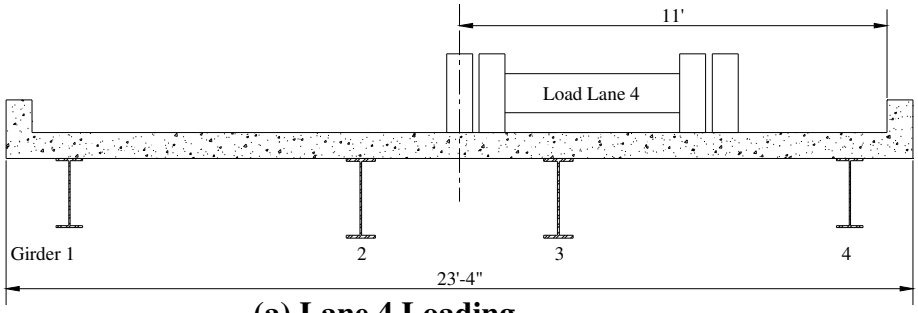

(a) Lane 4 Loading

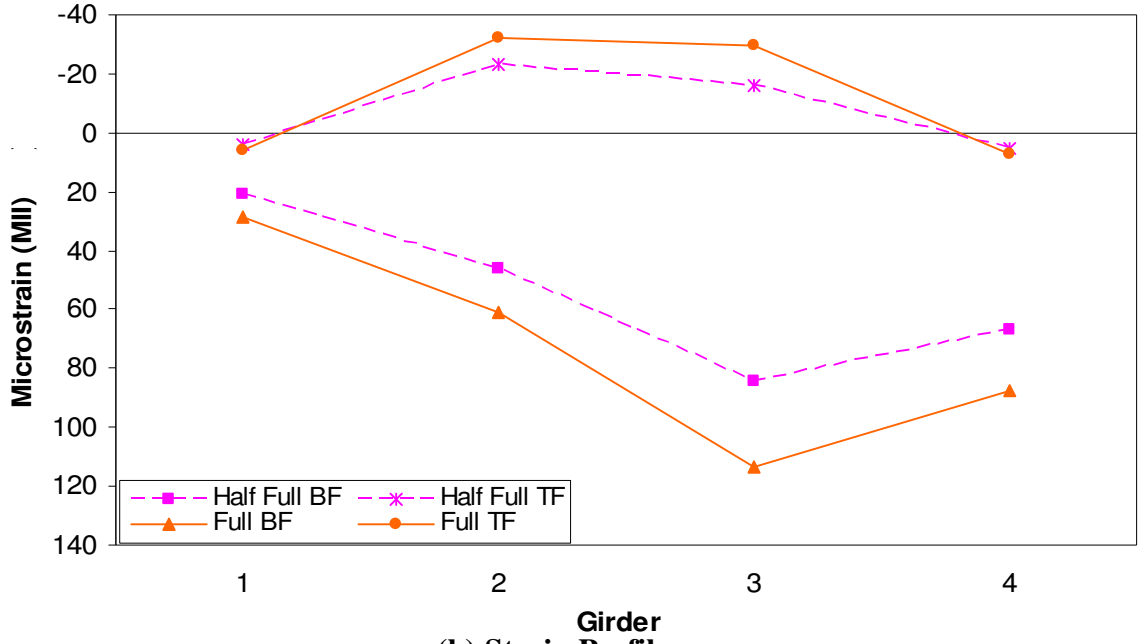

(b) Strain Profile

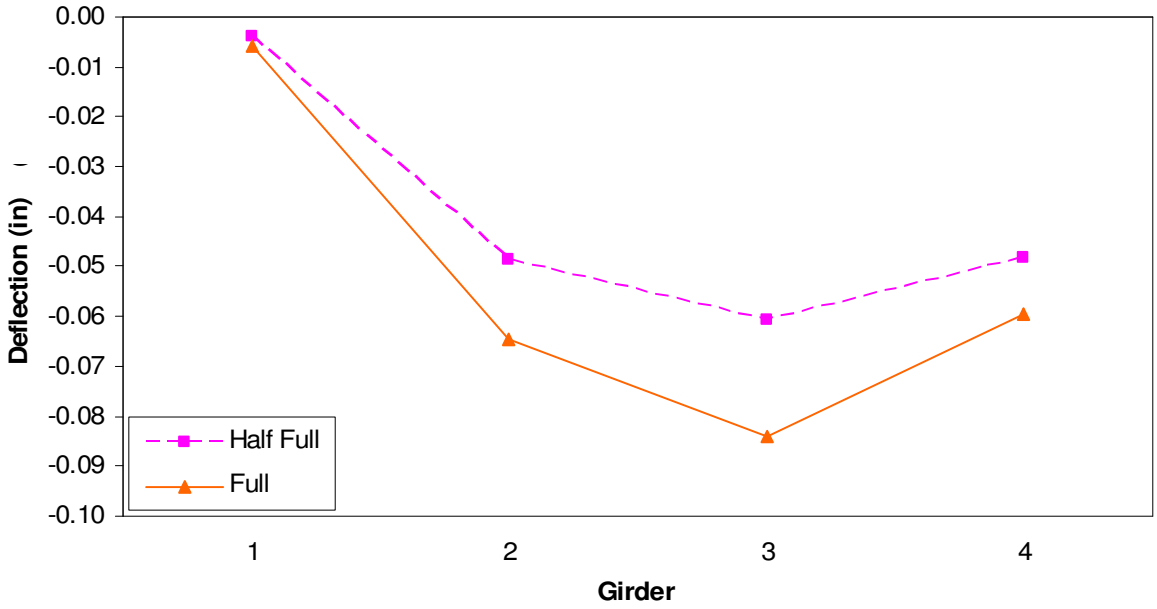

(c) Deflection Profile

Figure 6.13. CCB Lane 4 Strains and Deflections.

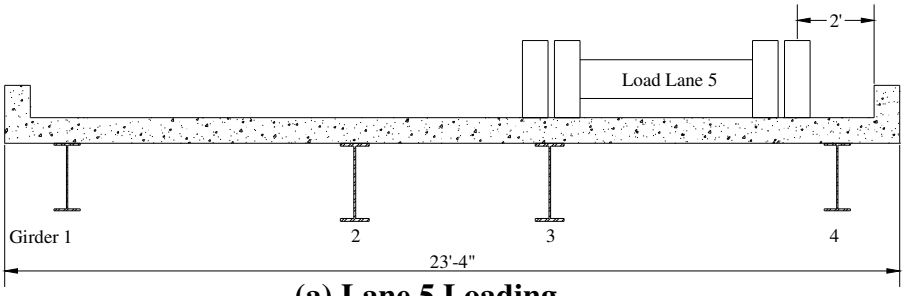

(a) Lane 5 Loading

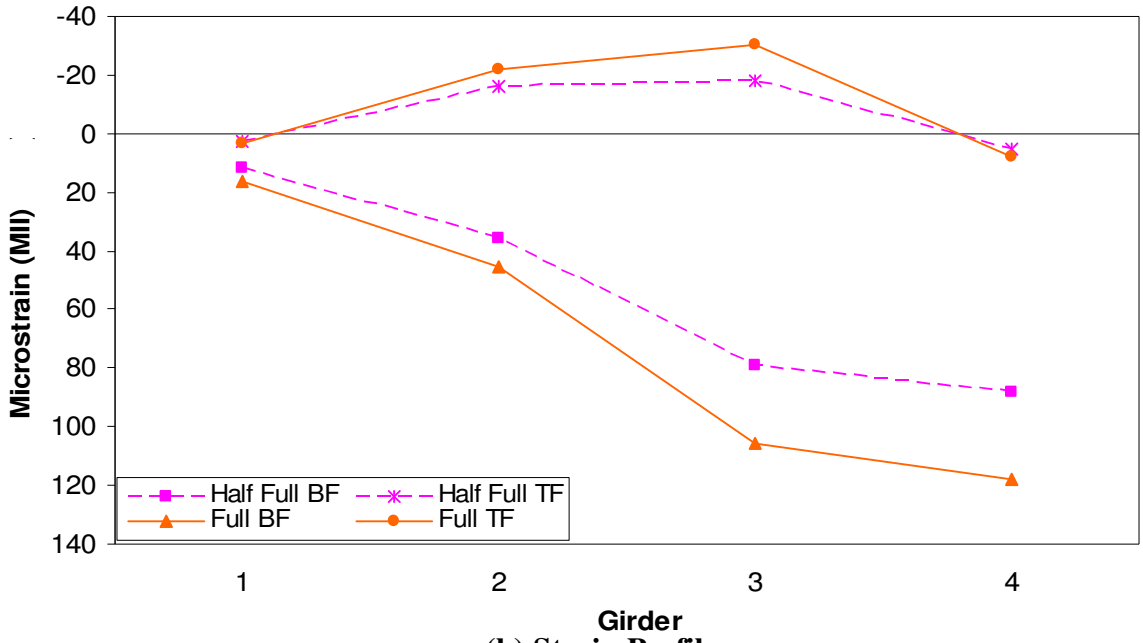

(b) Strain Profile

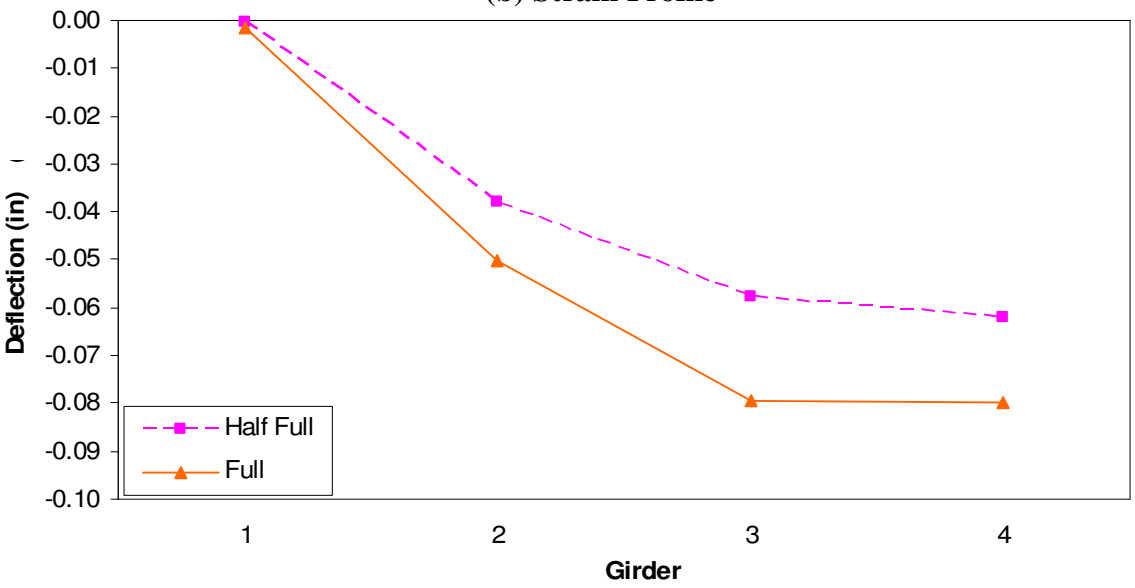

(c) Deflection Profile

Figure 6.14. CCB Lane 5 Strains and Deflections.

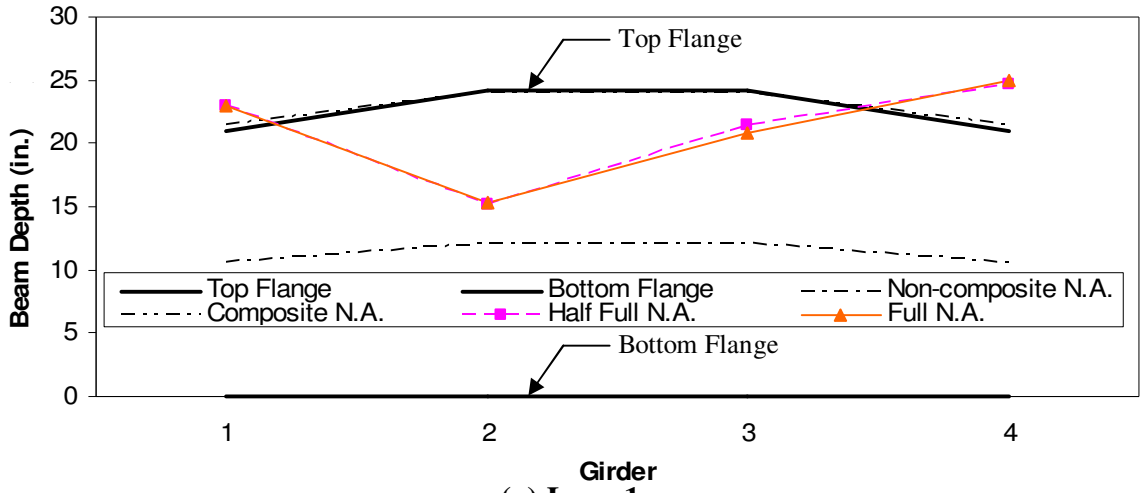

(a) Lane 1

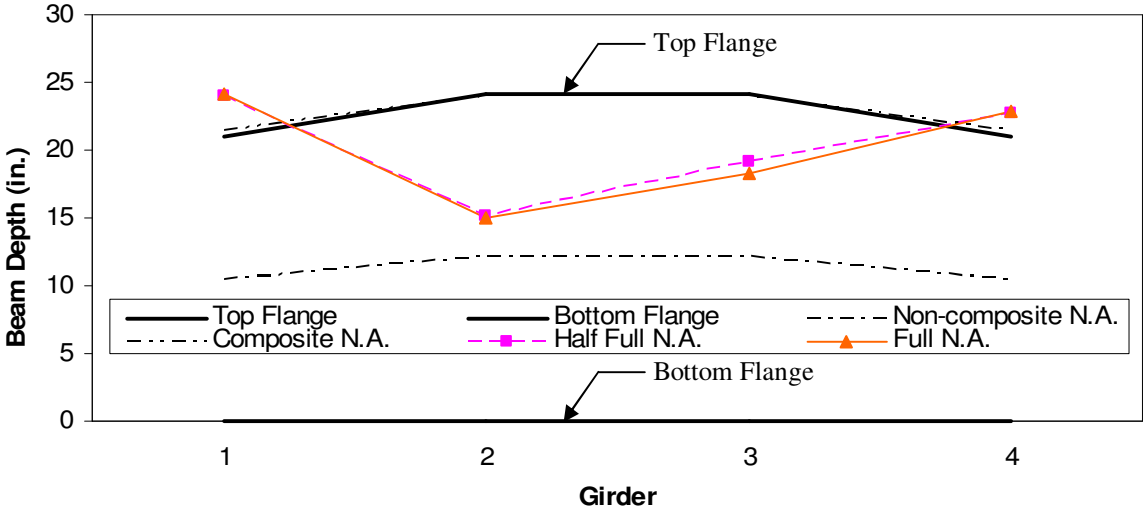

(b) Lane 3

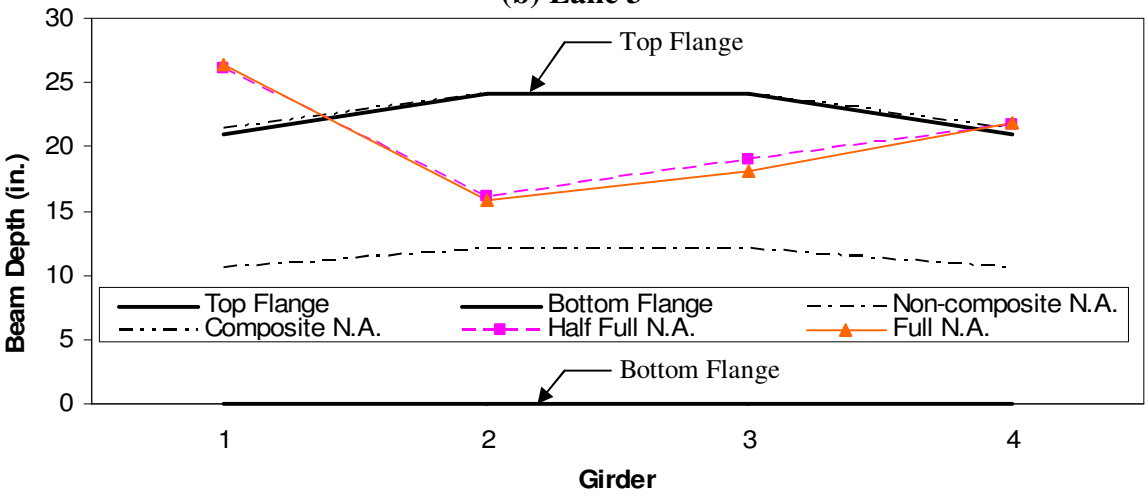

(c) Lane 5

Figure 6.15. CCB Neutral Axis Locations.

were not dependent upon the load distribution. The neutral axis locations for the exterior girders do increase slightly when the girders are not directly loaded. As mentioned in the BCB results, the high neutral axis locations result from the very small strain measurements in the top flange which are difficult to measure accurately. The neutral axis profiles were not symmetric; Girders 2 and 3 had significantly different neutral axis locations.

6.3.2 Load Distribution

Using the previously described truck locations, the theoretical moments in the bridge, assuming simply supported conditions, were calculated for each loading and are presented in Table 6.2. As may be seen in this table, there was a 37% increase in moment from a half full truck to a full truck.

Table 6.2. CCB Induced Truck Moments

Load	Moment (in-k)
Half Full Truck	2279
Full Truck	3133

Using the bottom flange strains, the percent distributions were calculated as the ratio of the weighted individual girder strain to the weighted sum of the four girder strains. The ratio was weighted to account for the different sections in the interior and exterior girders. With both of the load increments producing slightly different load distribution percentages, the maximum values, summarized in Table 6.3, were selected for each of the five lanes. Note that the values are the maximum percentage values of the two load cases and therefore do not sum to 100%. As may be seen, the maximum distribution percentages occurred in the exterior girders when directly loaded. Girders 1 and 4 had distribution percentages very close to each other for geometrically symmetric lane loadings (geometrically symmetric meaning mirror images of each other about the centerline of the bridge) which demonstrates symmetry in the bottom flange strains. The distribution for Girders 2 and 3 were not symmetrical with the test truck centered on the bridge in Lane 3. Only Girders 1 and 4 exhibited symmetry; Girders 2 and 3 did not.

Table 6.3. CCB Maximum Single Lane Percent Distributions.

Girder / Lane	1	2	3	4
Lane 1	33.4	37.9	25.2	4.4
Lane 2	24.9	37.4	31.1	7.0
Lane 3	14.1	32.8	40.4	12.8
Lane 4	7.3	24.7	45.9	22.6
Lane 5	4.3	20.0	45.0	31.3

As previously noted, the percent distributions are provided in Table 6.3; however in order to compare them to the AASHTO distribution factors the values must be multiplied by two to obtain the distribution of a single wheel line. The maximum distribution factors from the percent distributions summarized in Table 6.3 are provided in Table 6.4. Using superposition,

Table 6.4. CCB Calculated Distribution Factors.

Lane \ Girder	1	2	3	4
1	0.67	0.76	0.50	0.09
2	0.50	0.75	0.62	0.14
3	0.28	0.66	0.81	0.26
4	0.15	0.49	0.92	0.45
5	0.09	0.40	0.90	0.63
1 & 4	0.81	1.25	1.42	0.54
2 & 5	0.58	1.15	1.52	0.77

Lanes 1 and 4 and Lanes 2 and 5 were used to determine the distribution factors for two lanes. The two lane distribution factors are also provided in Table 6.4.

The maximum distribution factors for the interior and exterior girders for the single lane loading are 0.92 and 0.67, respectively, while the AASHTO distribution factor for the single lane loading with an average girder spacing of 6'-3.5" using the aforementioned equation of S/7.0 is 0.90 for the interior girders and for the exterior girders, with a spacing of 7'-6", is 1.07. The AASHTO distribution factors for the two lane loading case for the interior and exterior girders are 1.14 and 1.36, respectively. Values obtained by dividing the AASHTO distribution factors by the experimental distribution are summarized in Table 6.5.

Table 6.5. CCB Distribution Ratios.

	Single Lane	Double Lane
Interior Girder Distribution	0.92	1.52
Exterior Girder Distribution	0.67	0.81
Interior AASHTO Distribution Factor	0.90	1.14
Exterior AASHTO Distribution Factor	1.07	1.36
Interior Factor Ratio	0.98	0.75
Exterior Factor Ratio	1.60	1.68

The distribution ratios for the interior girders are less than 1.0 indicating that the field test results yielded a distribution factor higher than theoretically determined using the AASHTO equations. The exterior girder distribution ratios are both very large indicating the AASHTO distribution factors are conservative. Calculated exterior girder distributions based on the weighted girder strains are much lower than the distribution factors calculated using the ASHTO equations because the AASHTO equations do not allow for a change in the distribution factor based on the different girder sections.

6.3.3 Moment of Inertia

Using the previous method of determining a theoretical moment of inertia (see Section 3.3.3) produced very large and unrealistic moments of inertia for the exterior girders due to the relatively small top flange strains observed in the exterior girders. This observation has been discussed in the previously tested bridges when there was very small strains in the top flange

of the girders which in turn produced high neutral axis locations. The calculated moments of inertia prior to the model optimization for previous bridge tests did not correlate with the optimized moments of inertia. For these two reasons, the theoretical moments of inertia for this bridge are not provided.

6.4 BDI Optimization

The bridge was once again modeled using software (WinGEN) provided by Bridge Diagnostics Inc. and the actual test data were used to create a model that is close to the actual bridge based on the response of the structure to the truck loadings. This bridge model consisted of modeling each girder separately so that the moment of inertia for each girder could be optimized. This was important due to the partial composite action differences in each of the girders. As for all of the bridges, the deck was modeled using plate elements, while the girders were modeled using beam elements. Rotational springs attached to the ends of each of the girders: one for the north end of the exterior girders, one for the north end of the interior girders, and two more for the interior and exterior girders on the south end of the bridge.

Since moment of inertia calculations used on previous bridges were not performed on this bridge, the initial moment of inertia in each girder was assumed to be equal to the theoretical composite moment of inertia. The initial value for all of the spring constants was 1000 kip-in/rad, while the initial value for the modulus of elasticity for concrete was 3,200 ksi.

Only the steel girder strains were input into the model; the concrete slab strains were not input into the model because of the large variations in the measured strains due cracking. After the model was generated using WinGEN, it was then analyzed using WinSAC. WinSAC compares the actual strains induced by test truck to those produced by a theoretical truck with the same dimensions and wheel loads in the same location.

The initial model parameters produced a large scale error and the strains did not correlate very well with the actual strains obtained from the load test; therefore, the bridge was optimized. The parameters that were optimized included the moment of inertia for each girder, the rotational spring stiffness, and the concrete modulus of elasticity. Upper and lower bounds for the optimization parameters are presented in Table 6.6. The upper and lower bound for the moment of inertia of the girders corresponded to 133% of the composite and 80% of the non-composite neutral axis locations, respectively. Optimizing the bridge using the parameters in Table 6.6 yielded a scale error of 9.54%; the optimized values are provided in Table 6.7.

Table 6.6. CCB Optimization Parameters.

Optimization Parameter	Lower Bound	Upper Bound
Exterior Moment of Inertia (in^4)	1075	5900
Interior Moment of Inertia (in^4)	1975	9230
Rotational Spring Stiffness (kip-in/rad)	0	1,000,000
Modulus of Concrete (ksi)	2500	5700

Table 6.7. CCB Optimized Parameters Using All Steel Transducers.

Optimized Parameter	Initial Value	Optimized Value
Girder 1 I_y (in^4)	4440	5485
Girder 2 I_y (in^4)	7335	7865
Girder 3 I_y (in^4)	7335	7885
Girder 4 I_y (in^4)	4440	5435
North Exterior Rotational Spring (kip-in/rad)	1000	538,800
North Interior Rotational Spring (kip-in/rad)	1000	834,600
South Exterior Rotational Spring (kip-in/rad)	1000	876,600
South Interior Rotational Spring (kip-in/rad)	1000	576,600
Deck Modulus (ksi)	3200	5390

Though there was no symmetry in the neutral axis profile, deflection profile, nor strain profile plots, there was symmetry observed in the optimized girder moments of inertia. Comparing the optimized moment of inertia in the geometrically symmetric Girders 1 and 4 and geometrically symmetric Girders 2 and 3, shows that the optimization was symmetrical and only differed by 50 and 20 in^4, respectively. Optimized values obtained for the spring constants did not maintain the same symmetry ranging from about 550,000 to 850,000 kip-in/rad for both springs located on opposite sides of the bridge for both the interior and exterior girders. The upper bound for the deck modulus of elasticity was increased to 5,700 ksi because the initial optimization yielded a modulus of elasticity very close to the initial upper bound of 5,500 ksi but did not exceed 5,500 on a subsequent optimization. A graphical comparison of the optimized strains for each loading path are compared to the actual strains induced by the test truck in Girder 1 through Girder 4 are presented in Figure 6.16 through Figure 6.19, respectively.

In almost all cases, the optimized strains were very close to the actual strains resulting from the test truck. For the lower strain values, the optimization curves differed from the actual strains. The correlation between the optimized strains and the actual strains are summarized in Table 6.8; the scale error ranged from 0.3 to 5.0 and the correlation ranged from 0.853 to 0.891.

Table 6.8. CCB Bottom Flange Strain Scale Error and Correlation.

Girder	1	2	3	4	Average
Scale Error	1.7	5.0	0.3	0.9	2.0
Correlation	0.875	0.853	0.861	0.891	0.870

In an attempt to decrease the overall scale error, the strains near the supports were removed from the bridge optimization model. The previous optimized strains were input into a model that had only the midspan girder strains in an attempt to quantify the effect of the bearing transducers on the scale error. This model was analyzed and resulted in a scale error of only 2.0%, a 7.5% reduction from the original optimization model using all of the steel girder strains. The correlation values provided in Table 6.8 did not change in the new analysis.

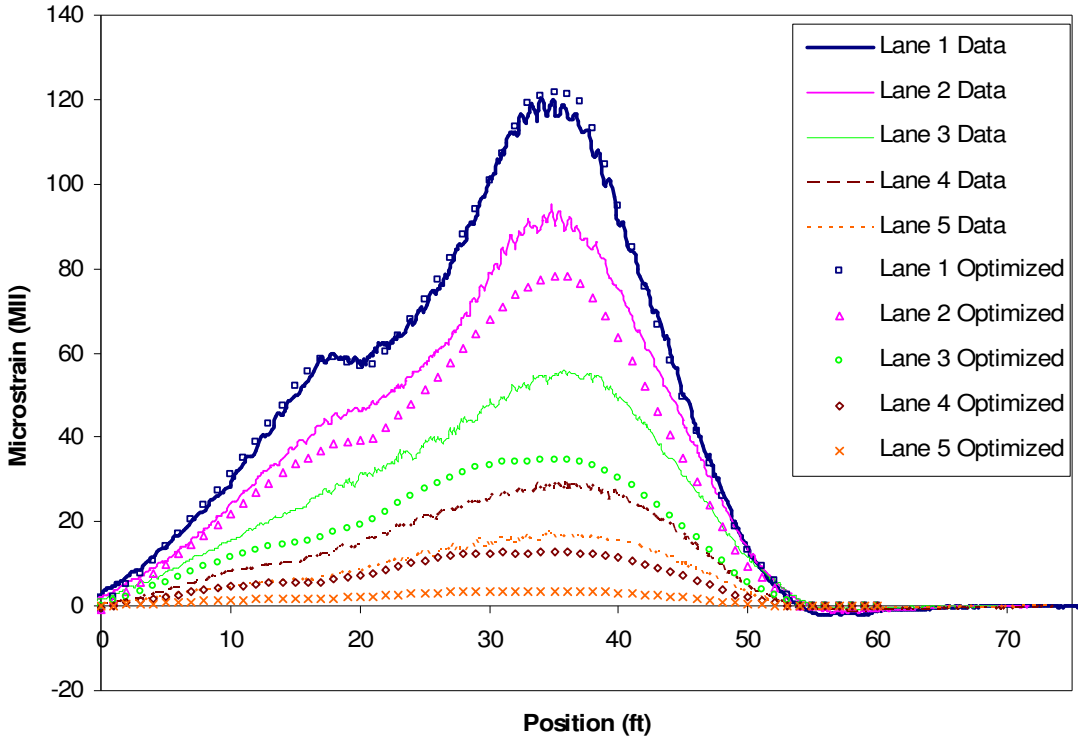

Figure 6.16. CCB Girder 1 Optimized Strain Comparison.

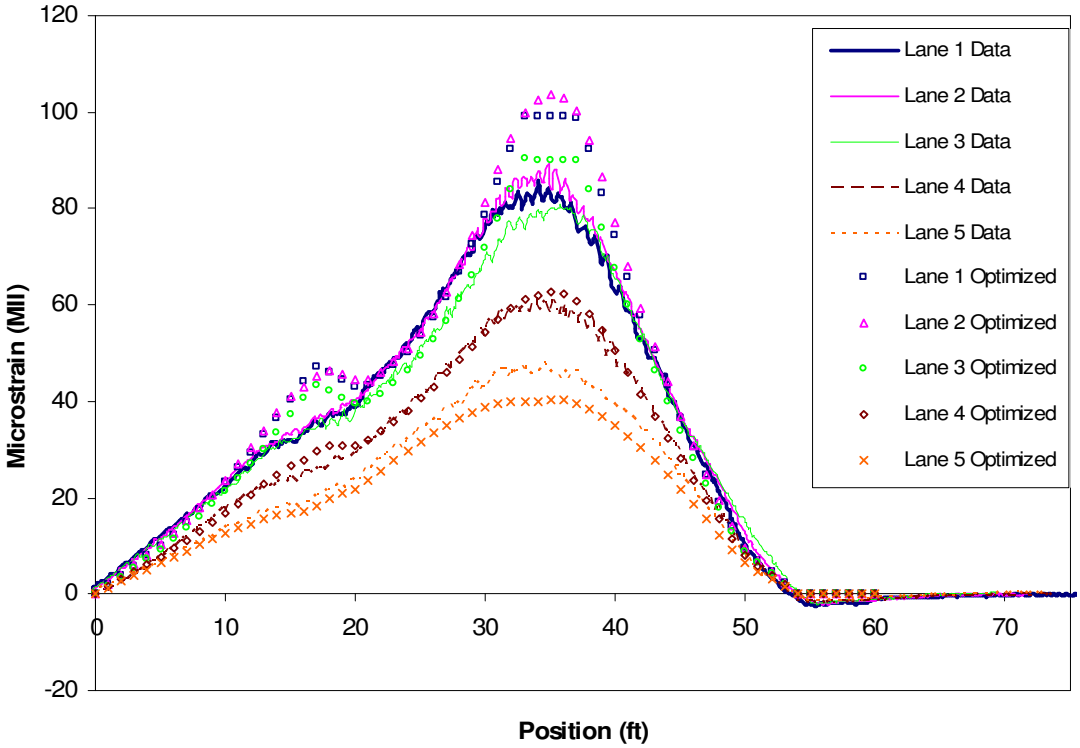

Figure 6.17. CCB Girder 2 Optimized Strain Comparison.

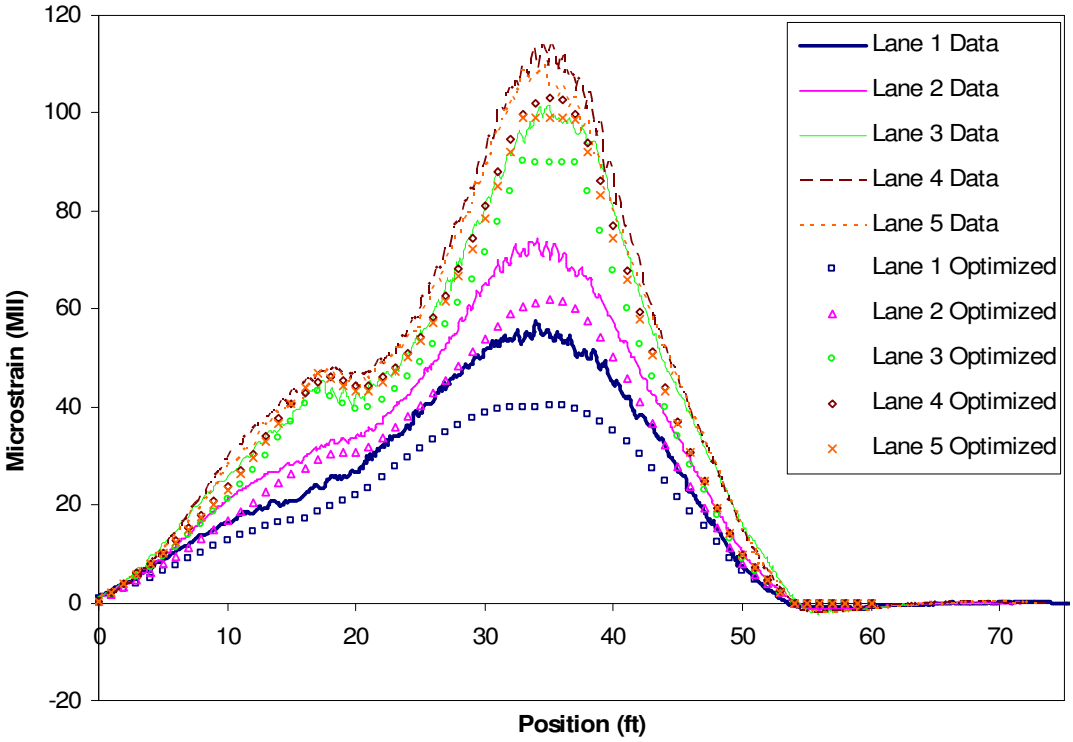

Figure 6.18. CCB Girder 3 Optimized Strain Comparison.

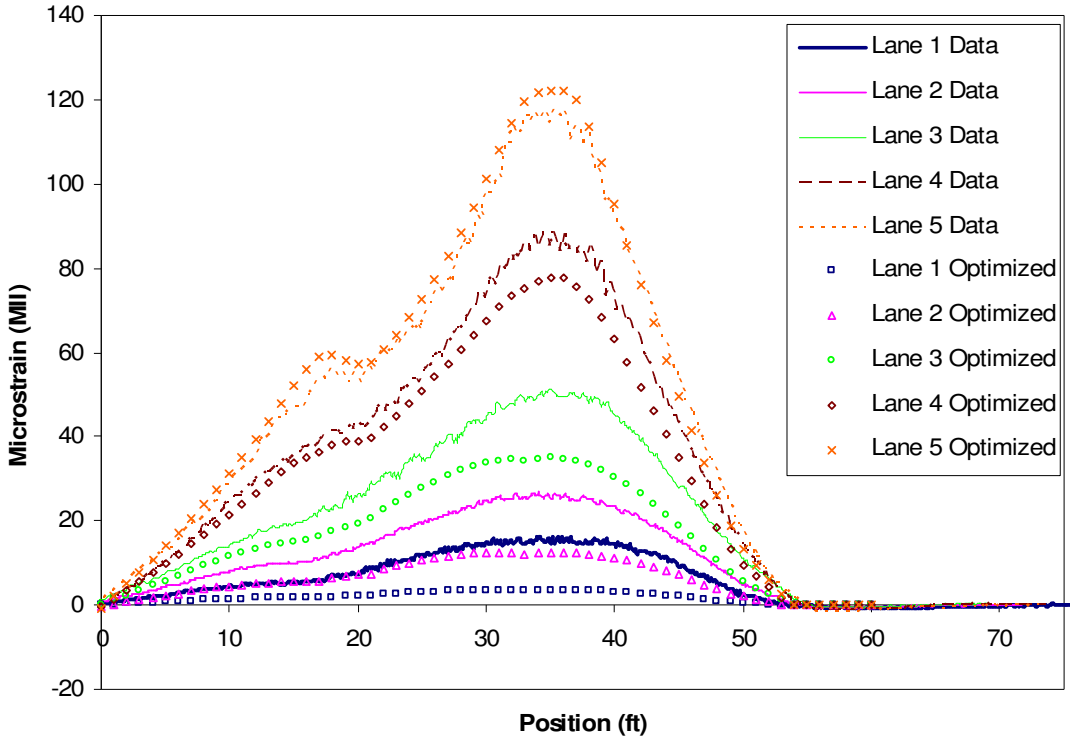

Figure 6.19. CCB Girder 4 Optimized Strain Comparison.

6.5 Bridge Rating

6.5.1 Conventional Rating

The bridge was rated using the Load Factor Rating (LFR) approach. This analytical rating, in which both the interior and exterior girders were rated, was performed assuming a non-composite design with simple support conditions. The bridge was also independently rated by both the Iowa DOT and PCF. Ratings calculated by the three different rating agencies are provided in Table 6.9.

Table 6.9. CCB Analytical Ratings.

Interior Girders						
	ISU		PCF		Iowa DOT	
Vehicle	Operating	Inventory	Operating	Inventory	Operating	Inventory
HS20 (36 ton)	59.3	35.5	57.4	34.4	51.7	31.0
Type 4 (27.25 ton)	47.2	28.3	46.7	28.0	43.2	25.9
Type 3-3 (40 ton)	84.2	50.5	84.2	50.5	78.0	44.8
Type 3S3 (40 ton)	71.7	43.0	71.9	43.1	66.6	39.9
Exterior Girders						
	ISU		PCF		Iowa DOT	
Vehicle	Operating	Inventory	Operating	Inventory	Operating	Inventory
HS20 (36 ton)	30.7	18.4	28.2	16.9	23.0	13.7
Type 4 (27.25 ton)	24.5	14.7	23.0	13.8	19.1	11.4
Type 3-3 (40 ton)	43.7	26.2	41.4	24.8	34.4	20.4
Type 3S3 (40 ton)	37.2	22.3	35.3	21.2	29.2	17.6

The rating values from PCF correspond very closely to those values determined by ISU; however the calculated ratings from ISU tend to be slightly less conservative than those calculated by PCF. The Iowa DOT once again found the serviceability criterion to govern the bridge rating and as a result, have more conservative ratings than the other two rating agencies. The operating ratings calculated by all three rating agencies determined that the interior girders are sufficient for the legal loads and would not require posting, however the exterior girders fall slightly below the legal loading for the operating ratings and would require postings for three of the four rating vehicles.

6.5.2 Rating Using Optimized Parameters From BDI Software

Utilizing the strains measured during the load test, the BDI software (WinGEN) was once again utilized to determine the bridge rating using the optimized parameters. Using the modified bridge model, the bridge was rated using the same rating vehicles as were used in the analytical ratings. The rating vehicles were input into the WinGEN software and moved across the bridge in pre-selected lanes to produce maximum strains in the girders. Both single and double lane loading cases were analyzed using the WinSAC software. With the optimized moments of inertia for each girder being different, each girder was rated separately using the BDI software. The load factor rating method was once again used for the ratings using the

optimized bridge parameters. The operating and inventory ratings were calculated for each girder and are summarized in Table 6.10.

Even though the analytical rating equations resulted in bridge ratings less than the legal loads for the exterior girders, all of the ratings calculated using the optimized model were above the legal loads for the bridge. After optimization, the limiting girder was Girder 1 having the lowest operating rating with a limit of 81.7 tons for a HS20 rating vehicle, more than double the legal weight of 36 ton. The inventory ratings were also larger than the legal loads for the rating vehicles with Girder 1 again having the lowest rating. The percentage increase from the ISU analytical ratings to the optimized ratings for the operating level is provided in Table 6.11. The range for the increased ratings after optimization for the HS20 rating vehicle was 73% for interior Girder 2 to 167% for exterior Girder 4.

Table 6.10. CCB Optimized Ratings.

Operating Rating (ton)				
	Girder			
Vehicle	1	2	3	4
HS20 (36 ton)	81.7	102.6	102.2	82.1
Tandem (25 ton)	47.8	59.5	59.5	47.8
Type 3 (25 ton)	68.8	86.3	86.3	69.0
Type 4 (27.25 ton)	64.3	83.4	83.1	64.6
Type 3-3 (40 ton)	117.2	152.0	152.0	117.6
Type 3S3 (40 ton)	98.0	126.0	126.0	98.4
Type 4S3 (48 ton)	115.2	148.3	148.3	115.7
Inventory Rating (ton)				
	Girder			
Vehicle	1	2	3	4
HS20 (36 ton)	49.0	61.5	61.3	49.2
Tandem (25 ton)	28.6	35.7	35.7	28.6
Type 3 (25 ton)	41.2	51.7	51.7	41.3
Type 4 (27.25 ton)	38.5	50.0	49.8	38.7
Type 3-3 (40 ton)	70.2	91.1	91.1	70.5
Type 3S3 (40 ton)	58.7	75.5	75.5	59.0
Type 4S3 (48 ton)	69.0	88.9	88.9	69.3

Table 6.11. CCB Operating Rating Percent Increase After Optimization.

	Girder			
Vehicle	1	2	3	4
HS20 (36 ton)	166	73	72	167
Type 4 (27.25 ton)	162	77	76	164
Type 3-3 (40 ton)	168	81	81	169
Type 3S3 (40 ton)	163	76	76	163

7. MAHASKA (380) COUNTY BRIDGE (KCB2)

7.1 Bridge Description

The fifth bridge that was load tested, shown in Figure 7.1, is located in Mahaska County, IA on Osborn Avenue approximately 3 miles northeast of Oskaloosa, IA. The bridge (FHWA ID: 237380), henceforth referred to as KCB2, is a 37.67-foot, simple-span, non-composite bridge with five steel girders, a concrete deck, and no skew crossing a creek. The substructure consists of five timber piles, a double C-channel cap, and a timber back wall. Currently posted at 20 ton for a straight truck and 30 ton for a truck and trailer combination vehicle, the bridge was given a sufficiency rating of 43 when it was last inspected in March of 2005.

Figure 7.1. KCB2 Alignment View Looking Northwest.

The superstructure was in relatively good condition with only minor rust on the girders. Shown in Figure 7.2 is the minimal rust on the girders and the most significant substructure damage in which at least two of five piles on the northeast abutment have significant deterioration or splitting. The guard rail on the southwest corner of the bridge, as shown in Figure 7.3, was also heavily damaged.

The superstructure, a cross section of which is shown in Figure 7.4, consists of five W24x76 girders with a 7.5-inch thick concrete deck. There are C-channel diaphragms at the 1/3 points of the bridge, concrete curbs eight inches wide by one foot tall and steel railing on both sides of the bridge.

Figure 7.2. KCB2 Pile Deterioration.

Figure 7.3. KCB2 Railing Damage.

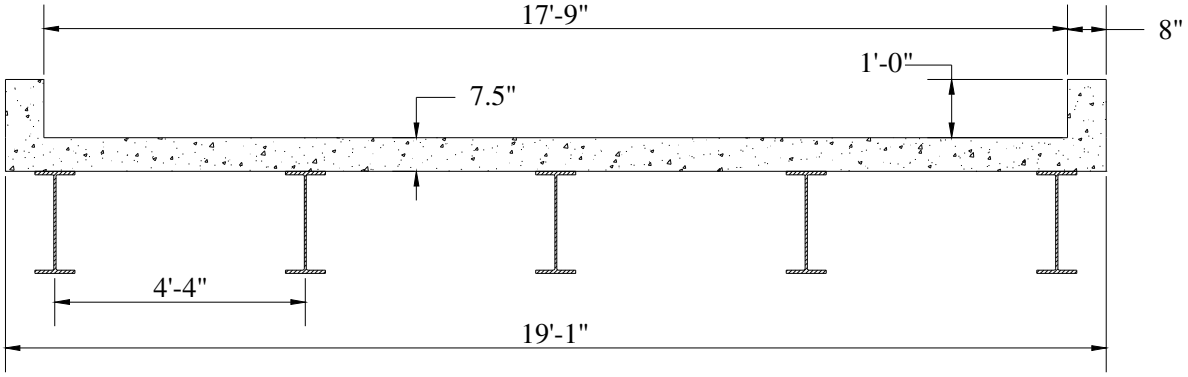

Figure 7.4. Cross Section of KCB2 Looking Northwest.

7.2 Test Setup

7.2.1 Test Truck

Two incremental loads, referred to as a half full truck and a full truck, were selected for the bridge test. The truck used for the load test was provided by the county and was a standard maintenance tandem dump truck. A photograph of the test truck as it is crossing the bridge during a load test is shown in Figure 7.5, axle weights are presented in Table 7.1, and dimensions are presented in Figure 7.6.

Figure 7.5. KCB2 Test Truck.

Table 7.1. KCB2 Truck Weights.

Truck Loading	Axle Weights (kip)			Gross Weight (kip)
	A	B	C	
Half Full	16.60	12.20	12.50	41.30
Full	16.45	17.45	16.90	50.80

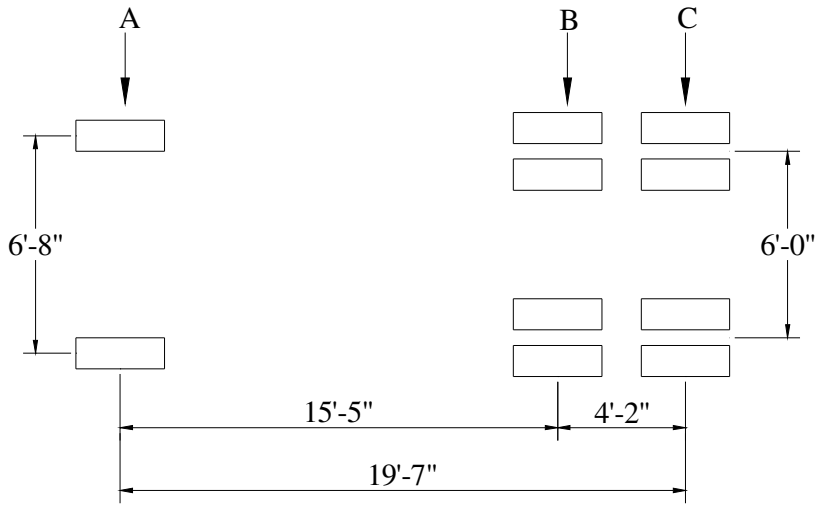

Figure 7.6. KCB2 Test Truck Dimensions.

7.2.2 Testing Plan and Instrumentation

There were five lanes, shown in Figure 7.7, selected for the truck to follow as it crossed the bridge. Each lane was loaded twice for each load increment to check repeatability of the test results. Measurements (strains and deflections) were taken when the centroid of the tandem was at the centerline of each end bearing and at each quarter point (see Figure 7.7). Lanes 2 and 4 were selected to create the largest possible strains in Girders 2 and 4, respectively by placing a wheel load directly over these girders.

The bridge was instrumented 24 inches from the edge of the bearing at each abutment, at the southeast quarter point, and at the midspan. Strain transducers were installed on the top and bottom flanges of Girders 1, 2, and 3 near the northwest abutment, near the southeast abutment, and at the quarter point as shown in Figure 7.8. At the midspan, strain transducers were attached on the top and bottom flanges of each of the girders as well as on the underside of the concrete deck near Girder 5 and directly between Girders 4 and 5 as shown in Figure 7.9. Also shown in Figure 7.9 is the location of the deflection transducers installed at the midspan. One strain transducer was located on the top of each curb at the midspan as well. Thus, there were a total of 32 strain transducers and five deflection transducers installed on the bridge for the load tests.

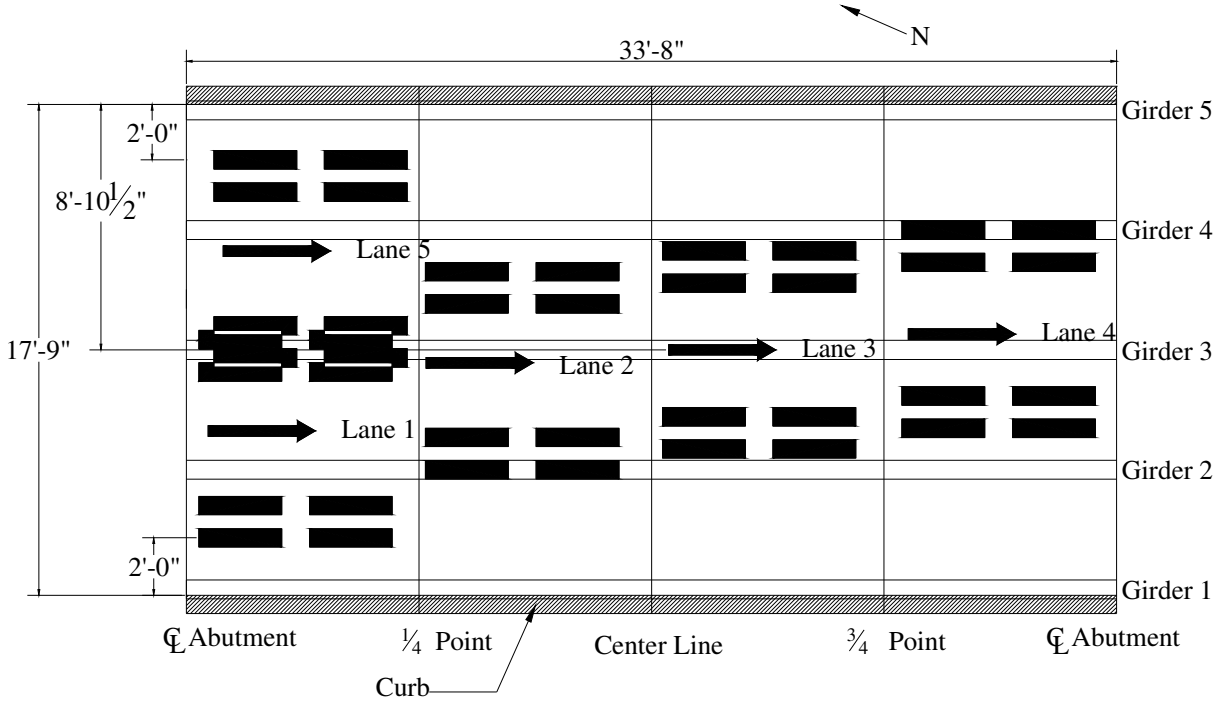

Figure 7.7. Plan View of Loading Lanes Used in KCB2 Test.

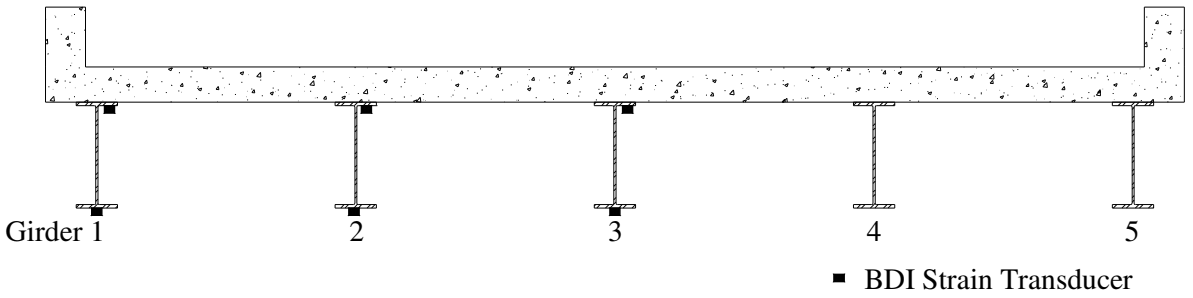

Figure 7.8. KCB2 Northeast, Southwest, and Quarter Point Transducer Locations Looking Northwest.

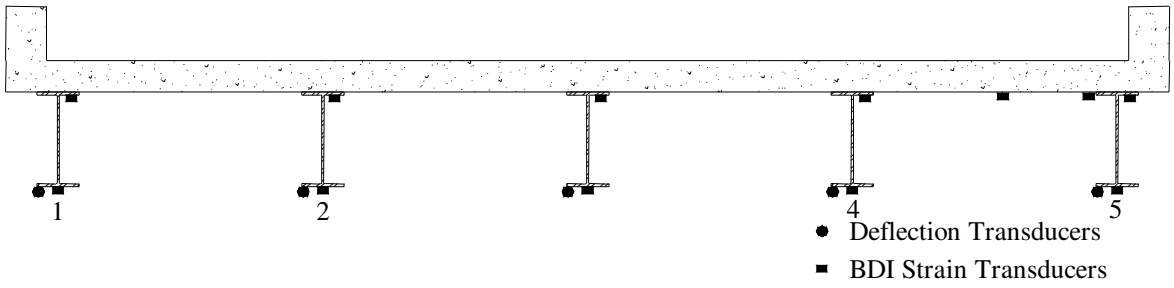

Figure 7.9. KCB2 Midspan Transducer Locations Looking Northwest.

7.3 Bridge Analysis

7.3.1 Neutral Axis and Partial Composite Action

The bridge was designed as a non-composite simple span bridge and common with most bridges of this type, there were some details that could increase the flexural capacity of the bridge. Shown in Figure 7.10 through Figure 7.14 are the top and bottom flange strains and deflections with the loading in Lane 1 through Lane 5, respectively. In the figures described above, TF and BF refers to the top and bottom flange strains, respectively. The deflection profiles do not follow the same shape as the bottom flange strain profiles for any of the five lanes. Deflections for Girder 4 from the Lane 5 loading are approximately 1/3rd the deflections in Girder 2 with the loading in Lane 1. The deflection in Girder 3 was the largest for Lane 5 loading but the maximum strain was observed in Girder 5 under the same loading. Girder 4 deflections were lower than the Girder 2 deflections under symmetrical loading whereas the strain profiles maintained symmetry under symmetrical loading as shown in Figure 7.12b. Both the top and bottom flange strain profiles exhibited symmetry as can be observed in Figure 7.12 as well as in Figure 7.10 and Figure 7.14 which are mirror images of each other. As was the case with the KCB1 Girder 2 deflections, it was not determined why the KCB2 Girder 4 deflections were so much smaller than the other girders but was likely due to poor instrumentation.

The neutral axis locations, shown in Figure 7.15, were determined by interpolating between the top and bottom flange strains to determine the location on the girder where the strain was equal to zero. Partial composite action, shown simply by the location of the neutral axes between the theoretical composite and non-composite neutral axis locations, was observed in all of the girders for each of the lanes loaded. The amount of partial composite action deteriorated with increased loading; this can be seen in Figure 7.15 where the neutral axis location shifts toward the non-composite neutral axis location with increased loading. This deterioration was the most noticeable in Girder 3 and the least noticeable in both exterior girders. The neutral axes of Girders 2 and 4 are also much closer to the non-composite neutral axis location than in the other girders.

The neutral axis locations for this bridge were not as close to the non-composite neutral axis locations as in the KCB1 but the general variation in the profiles was similar. Neutral axis locations in the exterior girders were also not as high as in the previously tested bridges but were higher than the interior girder neutral axis locations, thus displaying the edge stiffening effect that was prevalent in the previously tested bridges. The increased edge stiffness can be attributed to the concrete curb and steel railing which were not included in the calculation of the composite neutral axis location. All of the neutral axis profiles are nearly identical indicating that the location of the neutral axis was not dependent upon the load distribution.

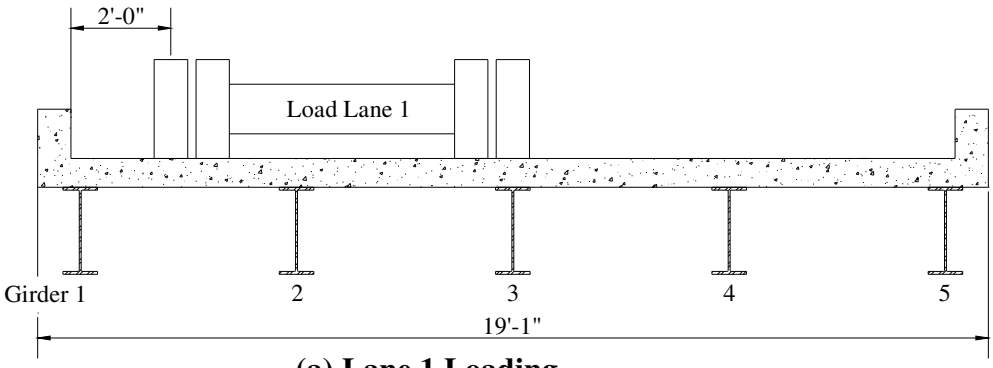

(a) Lane 1 Loading

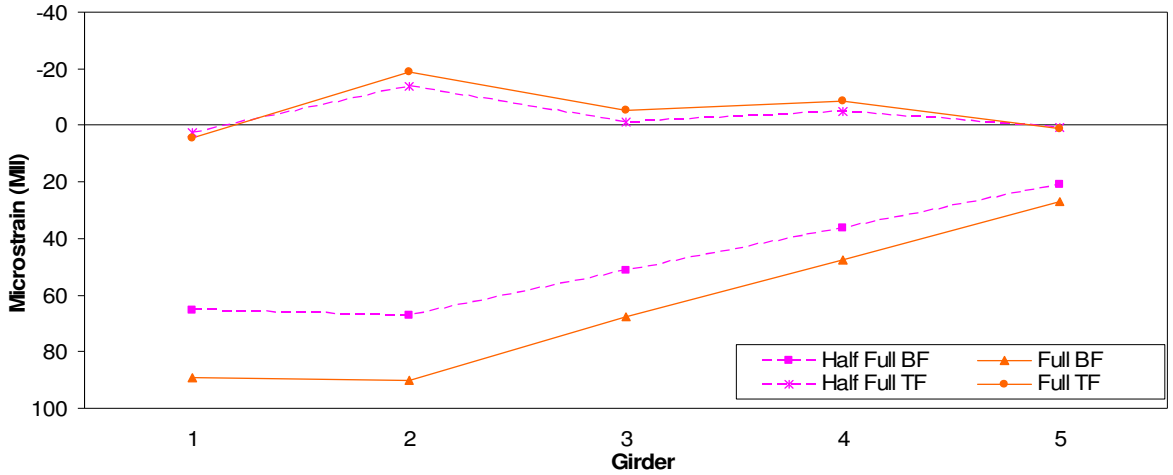

(b) Strain Profile

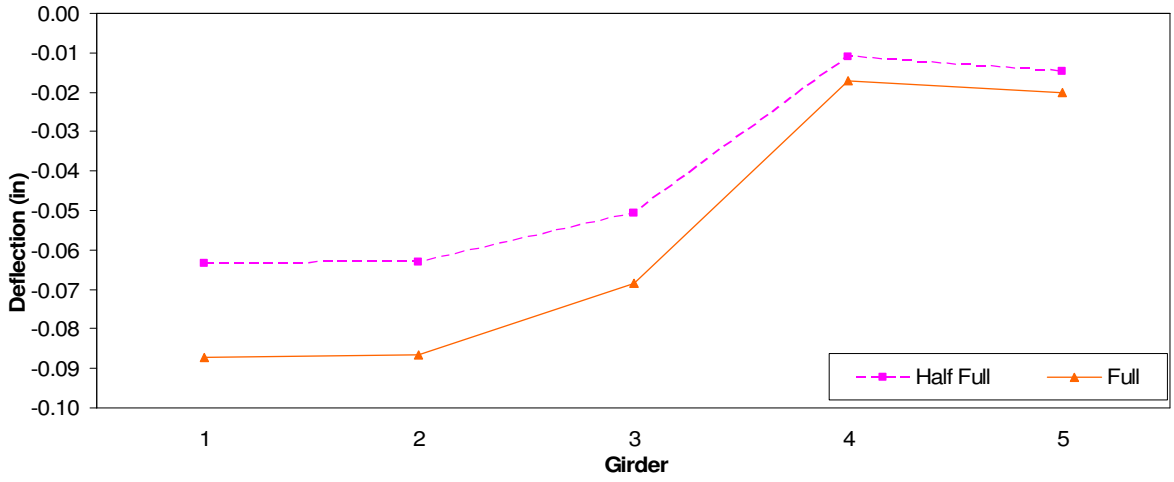

(c) Deflection Profile

Figure 7.10. KCB2 Lane 1 Strains and Deflections.

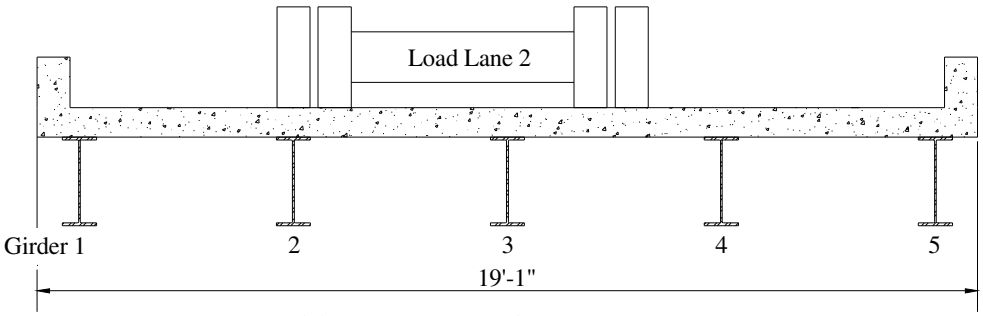

(a) Lane 2 Loading

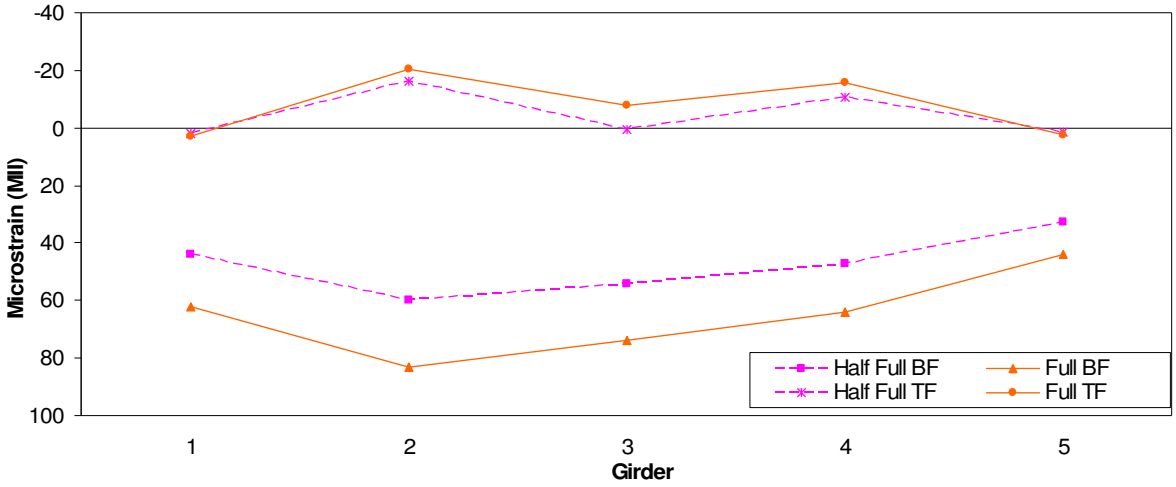

(b) Strain Profile

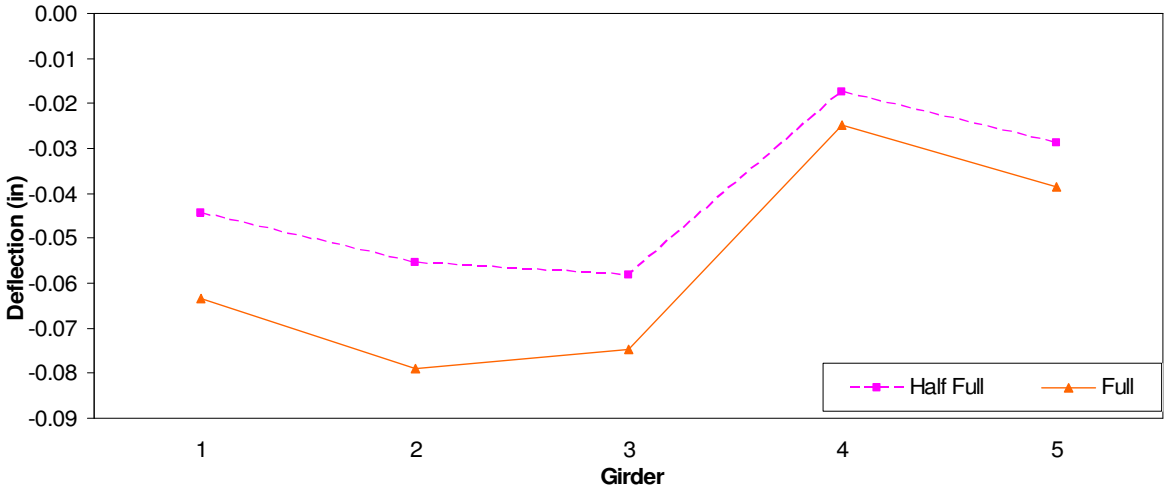

(c) Deflection Profile

Figure 7.11. KCB2 Lane 2 Strains and Deflections.

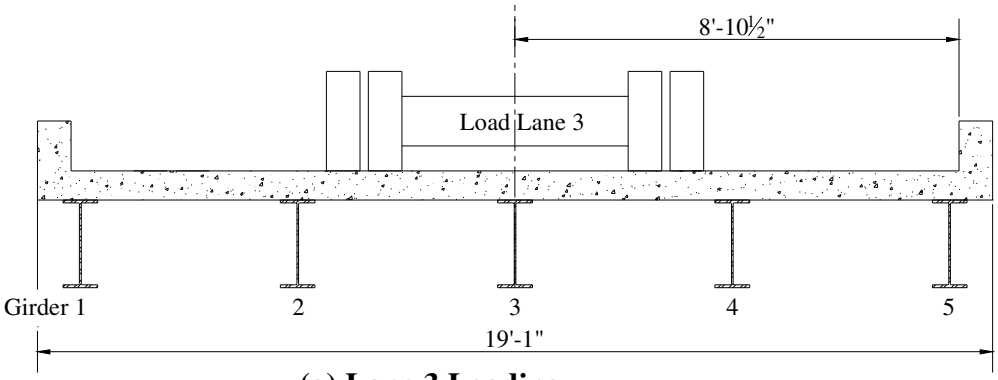

(a) Lane 3 Loading

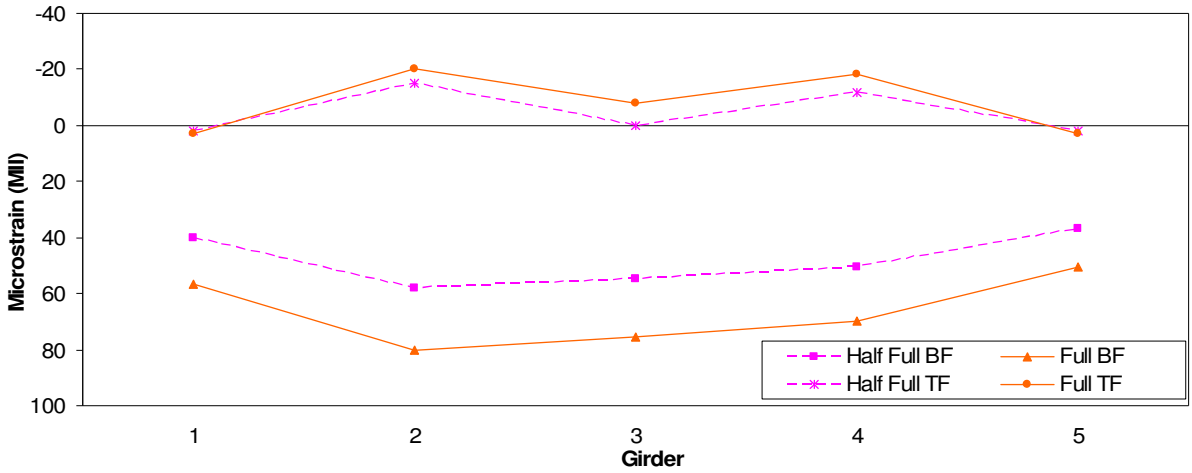

(b) Strain Profile

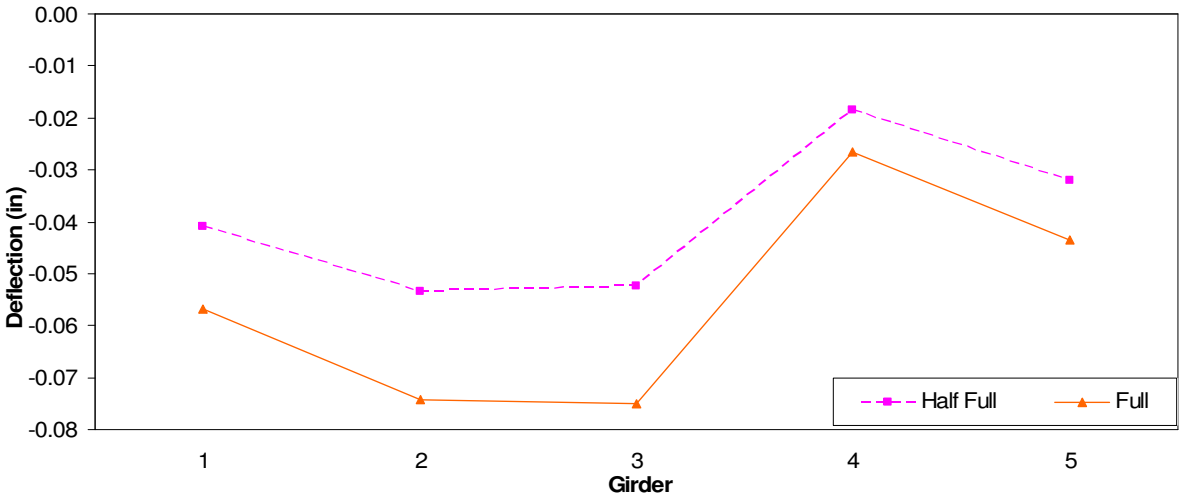

(c) Deflection Profile

Figure 7.12. KCB2 Lane 3 Strains and Deflections.

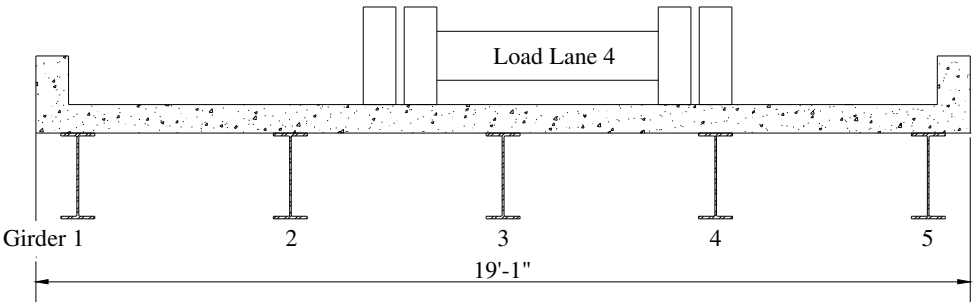

(a) Lane 4 Loading

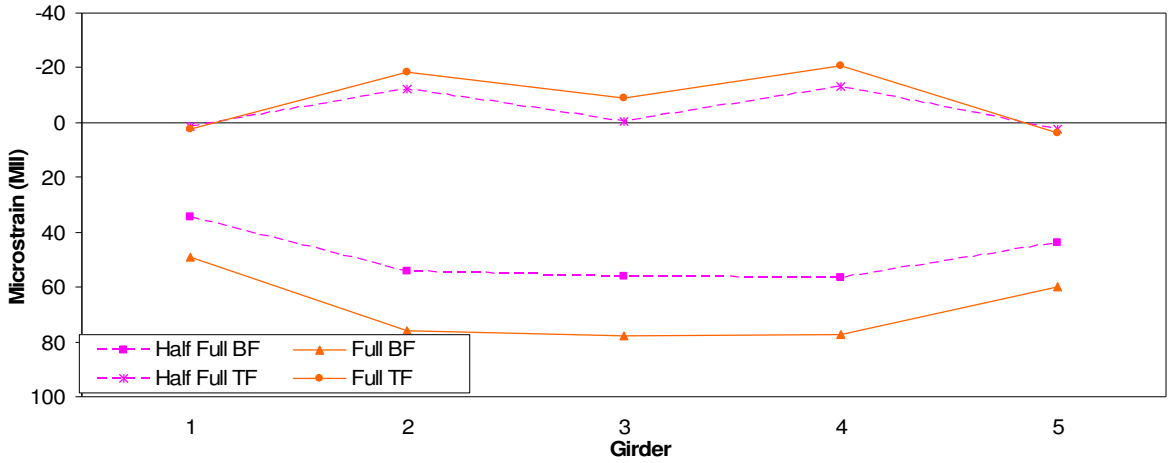

(b) Strain Profile

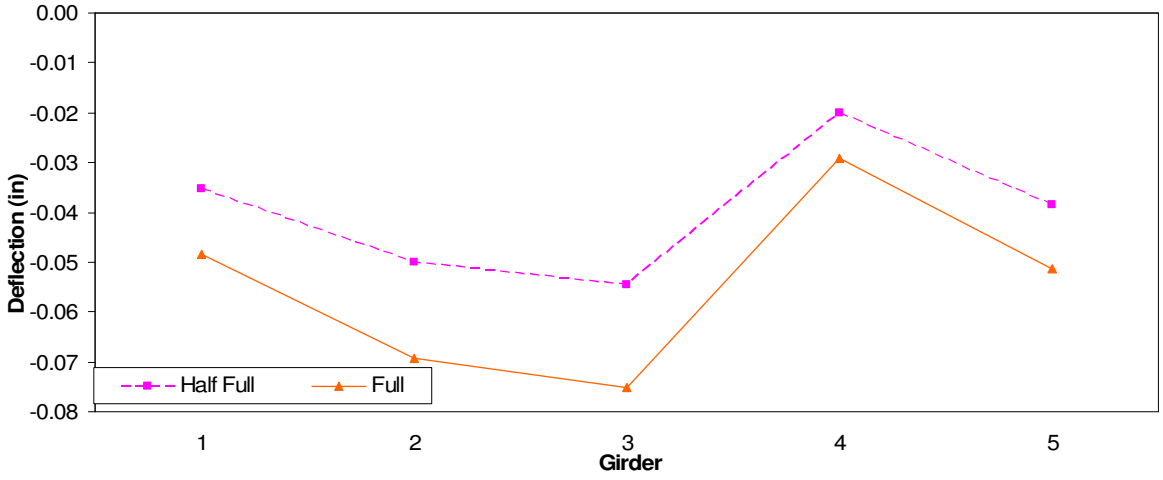

(c) Deflection Profile

Figure 7.13. KCB2 Lane 4 Strains and Deflections.

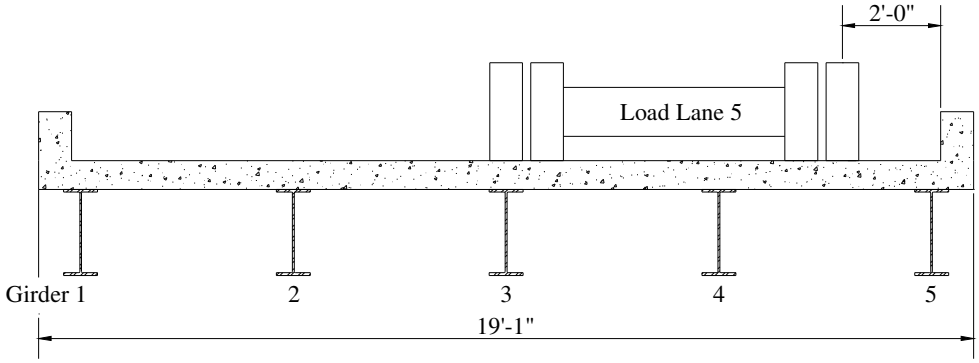

(a) Lane 5 Loading

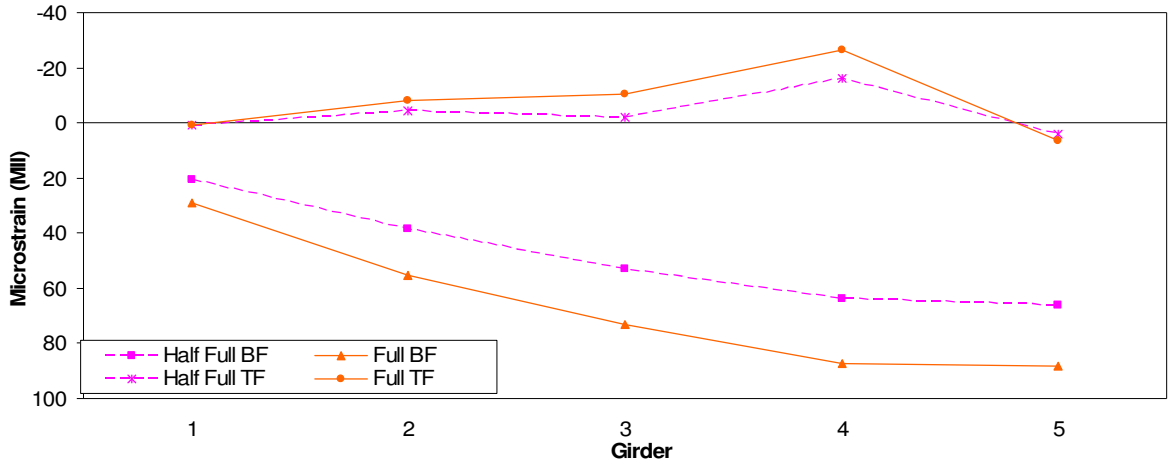

(b) Strain Profile

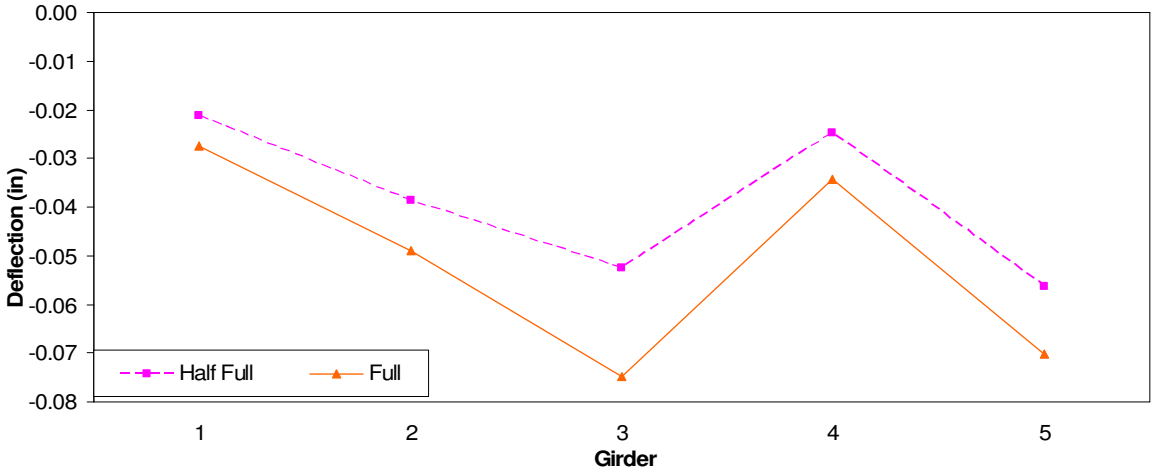

(c) Deflection Profile

Figure 7.14. KCB2 Lane 5 Strains and Deflections.

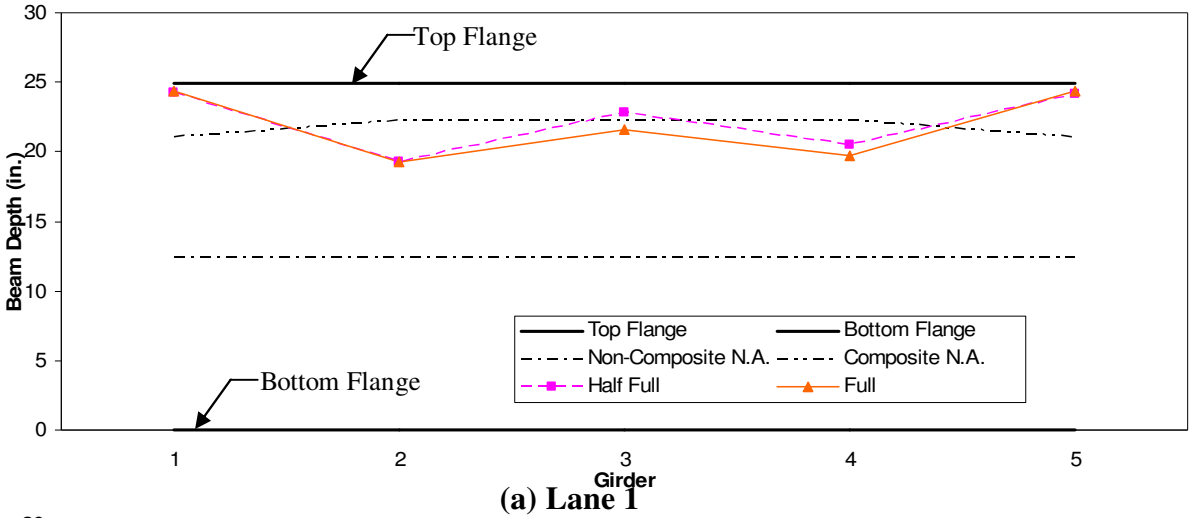

(a) Lane 1

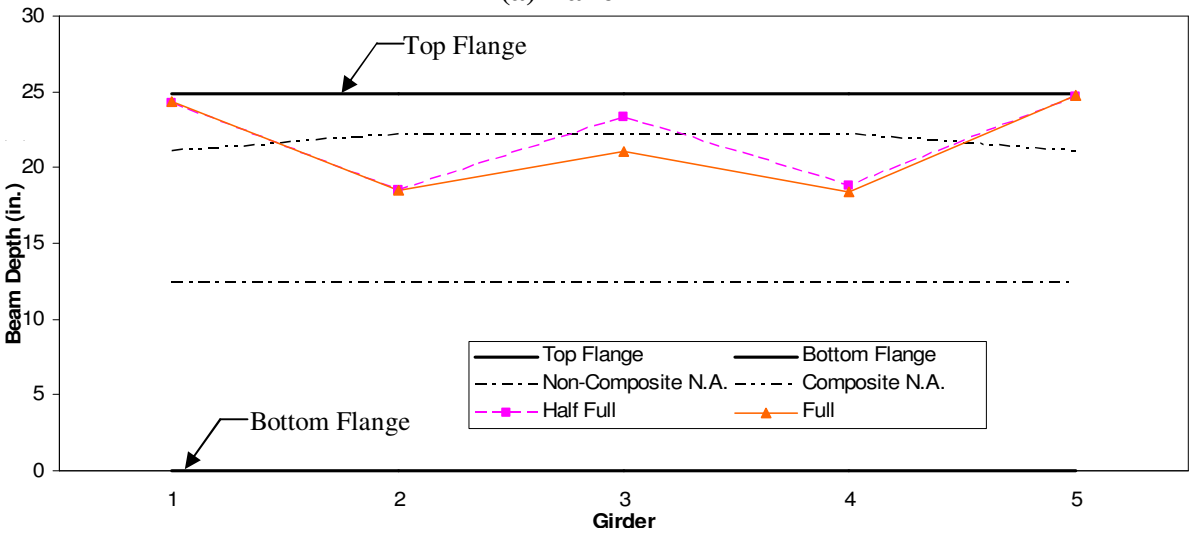

(b) Lane 3

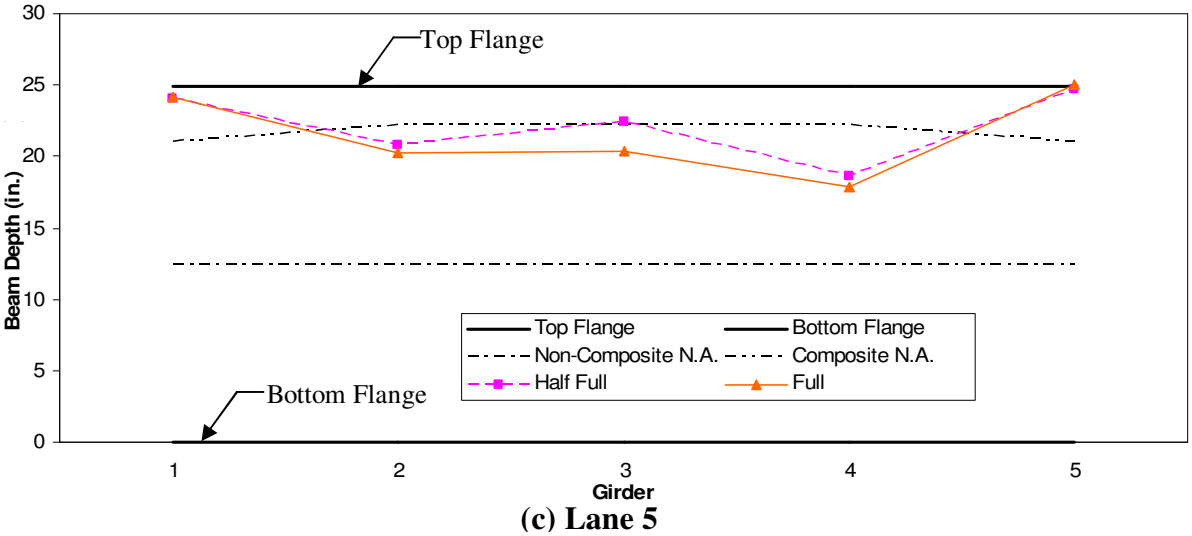

(c) Lane 5

Figure 7.15. KCB2 Neutral Axis Locations.

7.3.2 Load Distribution

Using the previously described truck locations, the theoretical moment induced in the bridge, assuming simply supported conditions, was calculated for each loading; these are presented in Table 7.2. As may be seen in this table, there was a 36% increase in moment from half full to full.

Table 7.2. KCB2 Induced Truck Moments.

Load	Moment (in-k)
Half Full Truck	2665
Full Truck	3625

Using the bottom flange strains, the distribution percents were calculated as the ratio of the individual girder strains to the sum of the five girder strains. With both of the load increments producing slightly different load distribution percentages, the maximum values, summarized in Table 7.3, were selected for each of the three lanes. Note that the values are the maximum percentage values of the three load cases and therefore do not sum to 100%. As may be seen, the maximum distribution percentages occurred in the exterior girders when directly loaded. Girders 2 and 4 had distribution percentages very close to each other for Lane 3 loading which demonstrates symmetry in the bottom flange strains. Symmetry in the bottom flange strains can be observed by comparing the Girder 1 distribution for Lane 1 loading to the Girder 5 distribution for Lane 5 loading.

Table 7.3. KCB2 Maximum Single Lane Percent Distributions.

Lane \ Girder	1	2	3	4	5
1	27.8	28.0	21.3	15.1	8.6
2	19.0	25.4	22.7	19.8	13.8
3	16.9	24.1	22.8	21.1	15.4
4	14.5	22.3	22.9	23.0	18.0
5	8.7	16.6	22.0	26.4	27.3

As previously noted, the percent distributions are provided in Table 7.3; however in order to compare them to the AASHTO distribution factors the values must be multiplied by two to obtain the distribution of a single wheel line. The maximum distribution factors from the percent distributions summarized in Table 7.3 are provided in Table 7.4. The bridge was too narrow for there to be two lanes loaded simultaneously so only single lane distribution factors were calculated.

The maximum distribution factors for the interior and exterior girders for the single lane loading are both 0.56 while the AASHTO distribution factor for the single lane loading with a girder spacing of 4'-4" using the aforementioned equation of S/7.0 is 0.62 for the interior girders. AASHTO stipulates that distribution factor for the exterior girders shall not be less than S/5.5 even though there is only one lane on the bridge which gives a distribution factor of 0.79 for the exterior girders. Values obtained by dividing the AASHTO distribution factors by the experimental distribution are summarized in Table 7.5.

Table 7.4. KCB2 Calculated Single Lane Distribution Factors.

Lane \ Girder	1	2	3	4	5
1	0.56	0.56	0.43	0.30	0.17
2	0.38	0.51	0.45	0.40	0.28
3	0.34	0.48	0.46	0.42	0.31
4	0.29	0.45	0.46	0.46	0.36
5	0.17	0.33	0.44	0.53	0.55

Table 7.5. KCB2 Distribution Ratios.

	Single Lane
Interior Girder Distribution	0.56
Exterior Girder Distribution	0.56
AASHTO Interior Distribution Factor	0.62
AASHTO Exterior Distribution Factor	0.79
Interior Factor Ratio	1.10
Exterior Factor Ratio	1.42

As can be seen, the distribution ratios for the single lane indicate that the AASHTO equations are slightly conservative as the ratios exceed 1.0. Load distribution factors calculated using the AASHTO equation are larger than the experimental distribution by 40% for the exterior girders. If the AASHTO equation for the interior girders of S/7 was used on the exterior girders, the exterior factor ratio would be 1.10, resulting in a much closer correlation. In general, the AASHTO distribution factors are verified by the field test results.

7.3.3 Moment of Inertia

The calculated moments of inertia prior to the model optimization for previous bridge tests did not correlate with the optimized moments of inertia. For this reason, the theoretical moments of inertia for this bridge are not provided. The moment of inertia will instead be optimized using the BDI software.

7.4 BDI Optimization

The bridge was once again modeled using software (WinGEN) provided by Bridge Diagnostics Inc. that utilizes the actual test data to create a model that is close to the actual bridge based on the response of the structure due to the truck loadings. This bridge model consisted of modeling each girder separately so that the moments of inertia for each girder could be optimized. This was important due to the partial composite action differences in each of the girders. As noted before, the deck was modeled using plate elements, while the girders were modeled using beam elements. Rotational springs were attached to the ends of each of the girders: one for the north end of the exterior girders, one for the north end of the interior girders, and two more for the interior and exterior girders on the south end of the bridge.

The initial values for the moments of inertia in each girder were assumed to be equal to the theoretical composite moment of inertia. The initial value for all of the spring constants was 1000 kip-in/rad, while the initial value for the modulus of elasticity for concrete was 3,200 ksi.

Only the steel girder strains were input into the model; concrete slab strains were not included in the model because there were large variations in their magnitudes due to cracks. After the model was generated using WinGEN, it was then analyzed using WinSAC. WinSAC compares the actual strains induced by test truck to those produced by a theoretical truck with the same dimensions and wheel loads as the test truck.

With a large initial scale error, the model needed to be optimized. The parameters that were optimized for the bridge included the moments of inertia for each girder, the rotational spring stiffness, and the modulus of elasticity for the concrete in the deck. Upper and lower bounds for the optimization parameters are presented in Table 7.6. The upper and lower bound for the moment of inertia of the girders corresponded to 133% of the composite and 80% of the non-composite neutral axis locations, respectively. Optimizing the bridge using the parameters in Table 7.6 still yielded a scale error of 10.1%; the optimized values are provided in Table 7.7.

Table 7.6. KCB2 Optimization Parameters.

Optimization Parameter	Lower Bound	Upper Bound
Moment of Inertia (in^4)	1680	7885
Rotational Spring Stiffness (kip-in/rad)	0	1,000,000
Modulus of Concrete (ksi)	2500	5700

Table 7.7. KCB2 Optimized Parameters Using All Steel Transducers.

Optimized Parameter	Initial Value	Optimized Value
Girder 1 I_y (in^4)	6080	6430
Girder 2 I_y (in^4)	6550	7730
Girder 3 I_y (in^4)	6550	7800
Girder 4 I_y (in^4)	6550	4460
Girder 5 I_y (in^4)	6080	7770
North Exterior Rotational Spring (kip-in/rad)	1000	50,760
North Interior Rotational Spring (kip-in/rad)	1000	642,700
South Exterior Rotational Spring (kip-in/rad)	1000	238,000
South Interior Rotational Spring (kip-in/rad)	1000	519,500
Deck Modulus (ksi)	3200	5545

The apparent symmetry observed in the neutral axis, deflection profile and strain profile plots previously presented was not observed in the optimized girder moments of inertia. Comparing the optimized moment of inertia in the geometrically symmetric Girders 2 and 4

shows that the optimization was not symmetrical as the optimized values were 7,730 and 4,460 in^4, respectively. Optimized values obtained for the interior spring constants were relatively close to each other but were not very close to the values for the exterior spring constants. The upper bound for the deck modulus of elasticity was increased to 5,700ksi because the initial optimization yielded a modulus of elasticity very close to the initial upper bound of 5,500 ksi. As shown in Table 7.7, the optimized concrete modulus of elasticity was slightly larger than the initial upper bound. A graphical comparison of the optimized strains for each loading path are compared to the actual strains induced by the test truck in Girder 1 through Girder 5 are presented in Figure 7.16 through Figure 7.20, respectively.

In almost all cases, the optimized strains were close to the actual strains from the test truck. The correlation between the optimized strains and the actual strains are summarized in Table 7.8. The scale error ranged from 0.3 to 4.2 and the correlation ranged from 0.917 to 0.935.

Table 7.8. KCB2 Bottom Flange Strain Scale Error and Correlation.

Girder	1	2	3	4	5	Average
Scale Error	2.8	0.4	7.4	4.2	0.3	3.0
Correlation	0.917	0.923	0.925	0.919	0.935	0.924

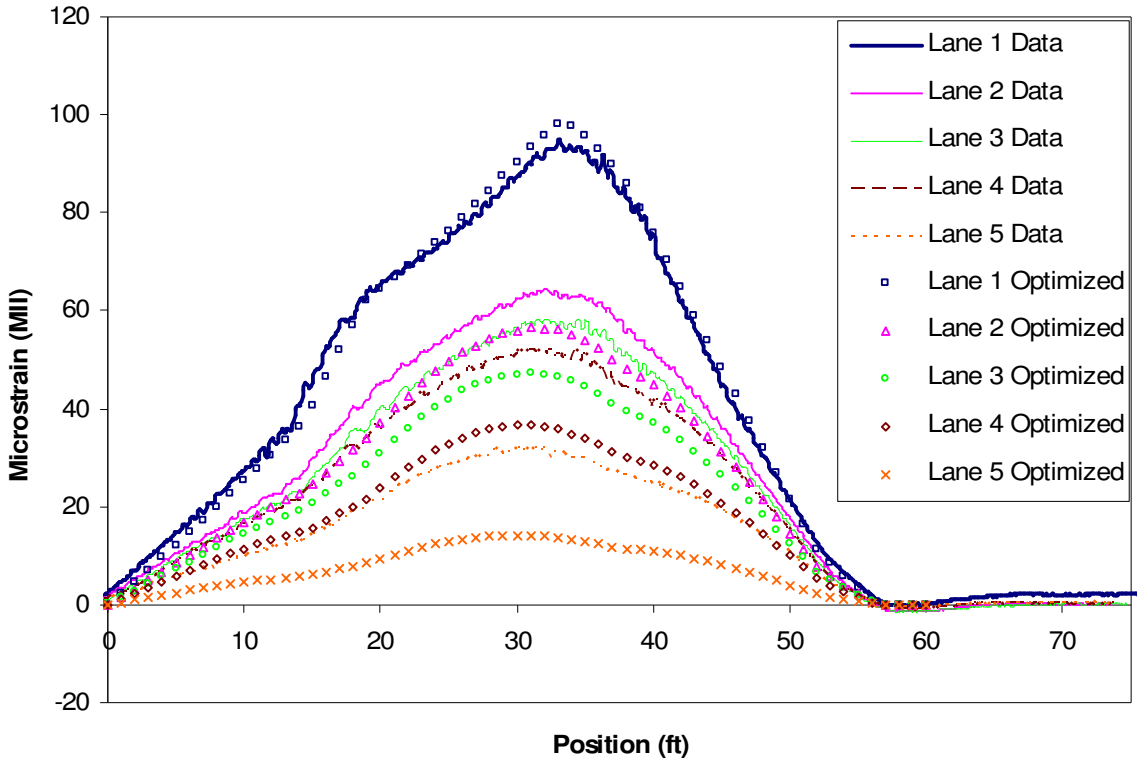

Figure 7.16. KCB3 Girder 1 Optimized Strain Comparison.

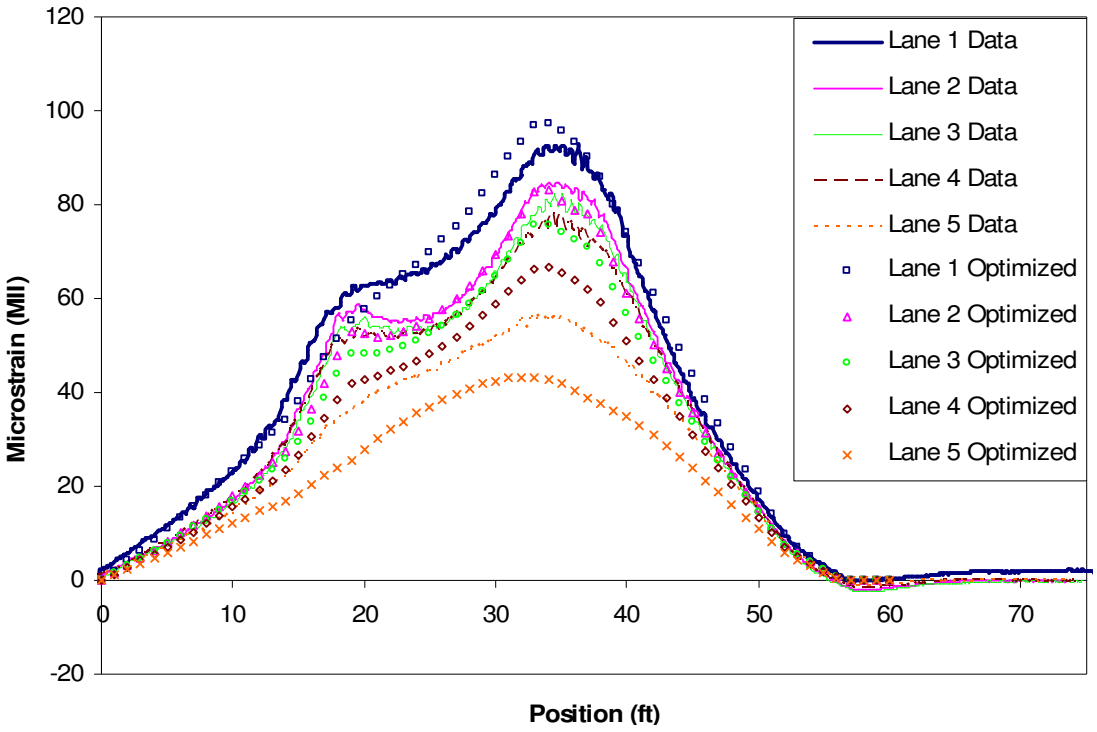

Figure 7.17. KCB2 Girder 2 Optimized Strain Comparison.

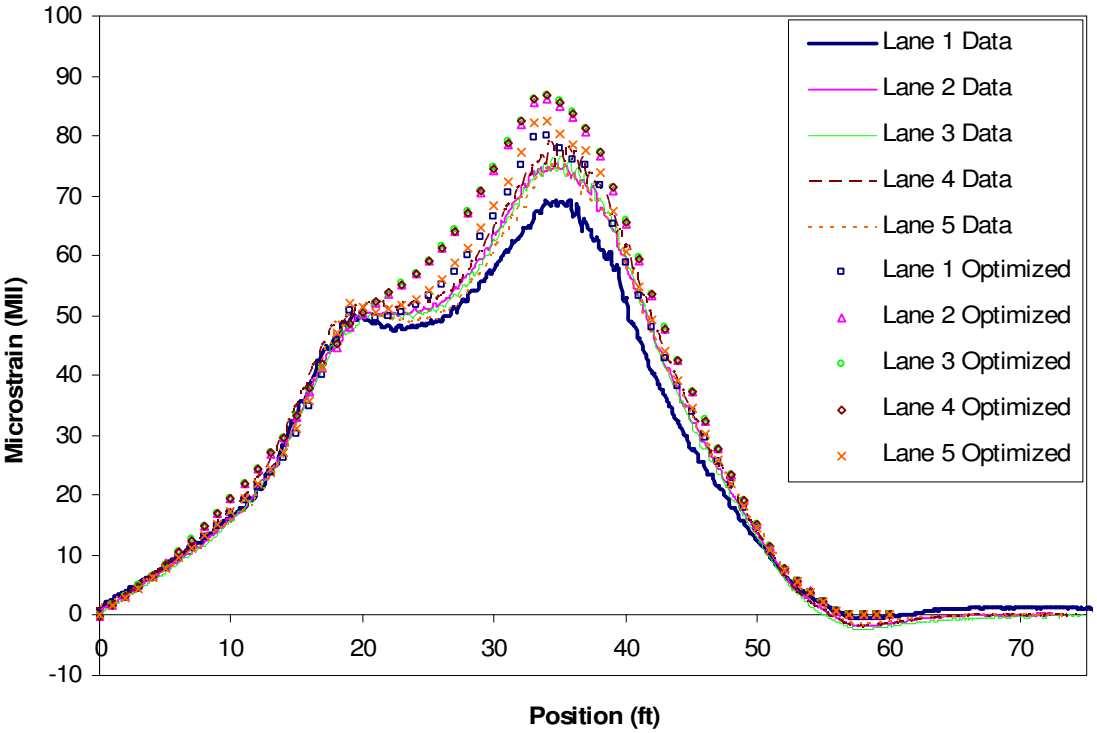

Figure 7.18. KCB2 Girder 3 Optimized Strain Comparison.

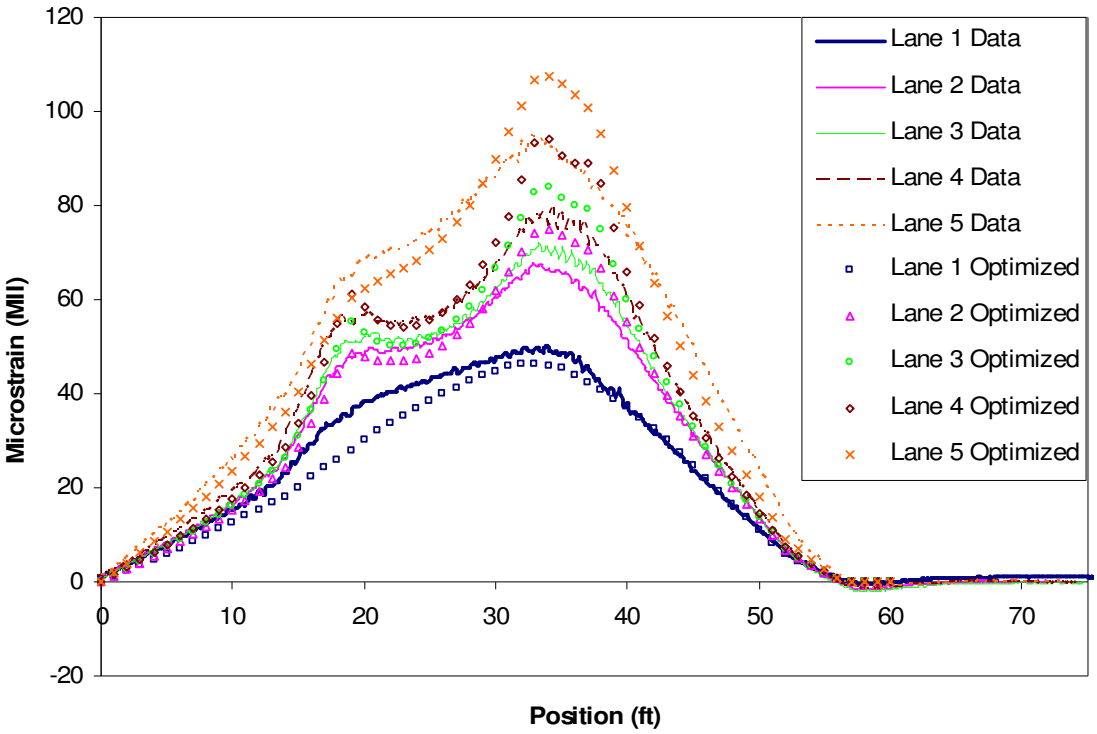

Figure 7.19. KCB2 Girder 4 Optimized Strain Comparison.

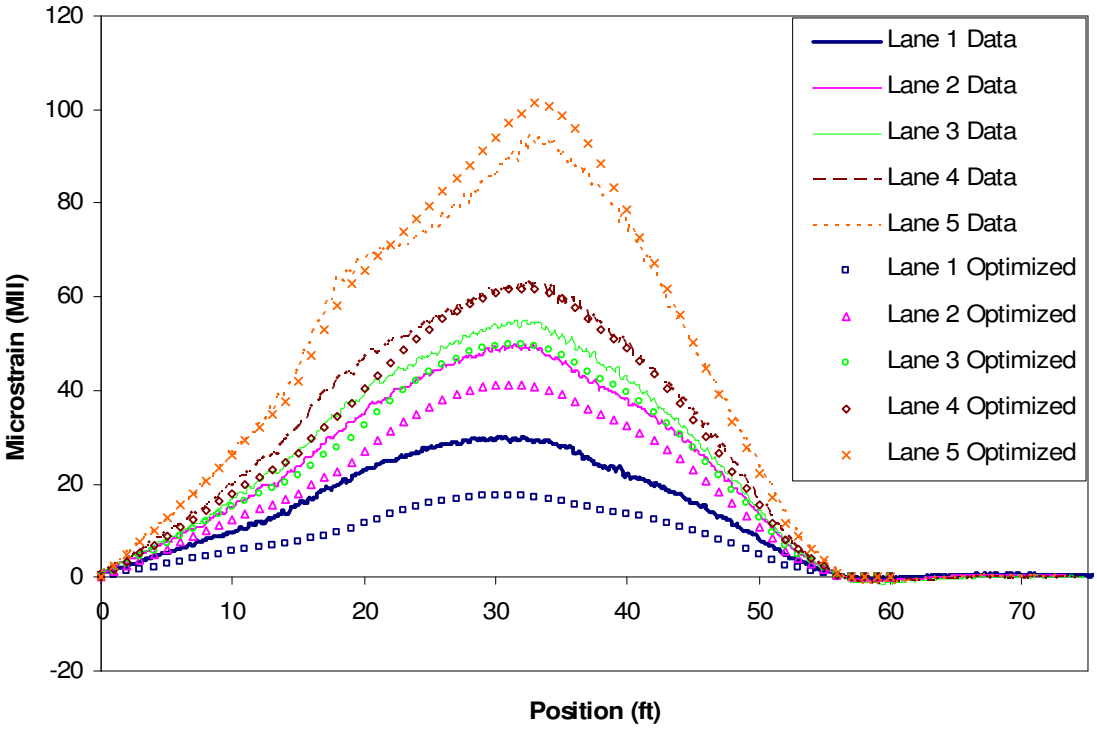

Figure 7.20. KCB2 Girder 5 Optimized Strain Comparison.

In an attempt to decrease the overall scale error, the strains measured near the supports were removed from the bridge optimization model. The previous optimized values were input into a model that had only the midspan girder strains in an attempt to quantify the effect of the bearing strains on the scale error. This model was analyzed and resulted in a scale error of only 3.0%, a 7.2% reduction from the original optimization model using all of the strain transducers located on the steel girders. The correlation values provided in Table 7.8 did not change in the new analysis.

7.5 Bridge Rating

7.5.1 Conventional Rating

The bridge was rated using the Load Factor Rating (LFR) approach. This analytical rating, in which both the interior and exterior girders were rated, was performed assuming a non-composite design with simply supported conditions. The bridge was also independently rated by both the Iowa DOT and PCF. Ratings calculated by the three different rating agencies are provided in Table 7.9.

Table 7.9. KCB2 Analytical Bridge Ratings.

Interior Girders						
	ISU		PCF		Iowa DOT	
Vehicle	Operating	Inventory	Operating	Inventory	Operating	Inventory
HS20 (36 ton)	80.8	48.4	70.7	42.3	68.9	41.4
Type 4 (27.25 ton)	67.0	40.1	59.5	35.7	57.3	34.4
Type 3-3 (40 ton)	117.2	70.2	104.8	62.8	100.8	60.5
Type 3S3 (40 ton)	105.2	63.0	94.8	56.8	91.2	54.7
Exterior Girders						
	ISU		PCF		Iowa DOT	
Vehicle	Operating	Inventory	Operating	Inventory	Operating	Inventory
HS20 (36 ton)	63.5	38.0	58.4	35.0	50.4	30.2
Type 4 (27.25 ton)	52.6	31.5	49.2	29.5	42.0	25.1
Type 3-3 (40 ton)	92.1	55.7	86.6	51.9	73.6	44.4
Type 3S3 (40 ton)	82.7	49.5	78.3	46.9	66.8	40.0

The rating calculations from ISU are significantly larger than those calculated by PCF and the Iowa DOT. The section for the girders that was used by ISU was a W24x80 which is no longer made and its properties are not in the latest AISC Steel Construction Manual. The bridge was a standard V5 series bridge that was built in 1948. The plan set for the V5 series bridge provides possible sections that could be used for different span lengths. Using the span length of this bridge and the V5 series plan set, as well as corresponding measurements from the field, it was determined that the W24x80 section was in fact the section used for this bridge. The nearest section to the W24x80 that is produced today is the W24x76. PCF and the Iowa DOT used the properties for the slightly smaller section and therefore their ratings

are more conservative. Taking the ratio of the plastic section modulus for the W24x80 to that of the W24x76 and multiplying by the HS20 operating rating of 70.7 ton produces an operating rating of 74. 9 ton. This neglects the increase in dead load of four plf between the two sections, but the ratings do become closer with an increase in the plastic section modulus.

The operating ratings for the bridge are sufficient for the legal loads and would not require any posting. The exterior girders fall slightly below the legal loading for the inventory ratings on the HS20 vehicle performed by PCF and the Iowa DOT but are above the legal loading for the same ratings calculated by ISU. Similar to KCB1, the reason this bridge was posted was due not due to the superstructure elements but due to the deteriorated substructure elements. According to the inspection report from 2003 obtained from the county, the northwest abutment piles were "decayed" and the timber back wall was "bowed", thus the aforementioned bridge posting was recommended.

7.5.2 Rating Using Optimized Parameters From BDI Software

Utilizing the strains measured during the load test, the BDI software (WinGEN) was once again utilized to determine the bridge rating using the optimized parameters. Using the modified bridge model, the bridge was rated using the same rating vehicles as the analytical ratings. The rating vehicles were input into the WinGEN software and traversed across the bridge in pre-selected lanes to produce maximum strains in the girders. Only a single lane loading was analyzed using the WinSAC software. With the optimized moments of inertia for each girder being different, each girder was rated separately using the BDI software. The load factor rating method was once again used for the ratings using the optimized bridge parameters. The operating and inventory ratings were calculated for each girder and are summarized in Table 7.10**.**

The optimized operating ratings for all of the rating vehicles were well above the legal loads for the bridge. The limiting girder was Girder 5 having the lowest operating rating with a limit of 103 tons for a HS20 rating vehicle, well above the legal weight of 36 ton. The inventory ratings were larger than the legal loading for the rating vehicles with Girder 5 having the lowest rating. The inventory rating for Girder 5 with the HS20 rating vehicle was 61.7 ton, also well above the vehicle weight of 36 ton. Girders 2 and 5 were very close in rating with Girder 5 being less than 1 ton below the rating for Girder 2. A table presenting the percentage increase from the ISU analytical ratings to the optimized ratings for the operating level is produced in Table 7.11. The range for the increased ratings after optimization for the HS20 rating vehicle was 29% for interior Girder 2 to 110% for interior Girder 4.

Table 7.10. KCB2 Optimized Ratings.

Operating Rating (ton)					
	Girder				
Vehicle	1	2	3	4	5
HS20 (36 ton)	132.5	104.4	113.8	169.9	103.0
Tandem (25 ton)	85.8	65.8	70.0	107.3	66.8
Type 3 (25 ton)	115.0	90.3	97.5	148.5	89.8
Type 4 (27.25 ton)	108.5	86.9	93.7	144.7	84.2
Type 3-3 (40 ton)	191.2	157.6	170.4	262.4	149.2
Type 3S3 (40 ton)	171.6	134.0	144.0	221.6	133.2
Type 4S3 (48 ton)	194.4	155.0	167.5	253.4	151.2
Inventory Rating (ton)					
	Girder				
Vehicle	1	2	3	4	5
HS20 (36 ton)	79.4	62.5	68.2	101.8	61.7
Tandem (25 ton)	51.4	39.4	41.9	64.3	40.0
Type 3 (25 ton)	68.9	54.1	58.4	89.0	53.8
Type 4 (27.25 ton)	65.0	52.1	56.2	86.7	50.4
Type 3-3 (40 ton)	114.5	94.4	102.1	157.2	89.4
Type 3S3 (40 ton)	102.8	80.3	86.3	132.8	79.8
Type 4S3 (48 ton)	116.5	92.9	100.4	151.8	90.6

Table 7.11. KCB2 Operating Rating Percent Increase After Optimization.

	Girder				
Vehicle	1	2	3	4	5
HS20 (36 ton)	109	29	41	110	62
Type 4 (27.25 ton)	106	30	40	116	60
Type 3-3 (40 ton)	108	34	45	124	62
Type 3S3 (40 ton)	107	27	37	111	61

8. HUMBOLDT COUNTY BRIDGE (HCB)

8.1 Bridge Description

The last bridge that was load tested, shown in Figure 8.1, is located in Humboldt County, IA on 200th Street approximately two miles north of the Humboldt, IA. The bridge (FHWA ID: 029070), henceforth referred to as HCB, is a 34.4-foot simple-span, non-composite bridge with four steel girders, a concrete deck, and no skew crossing a drainage channel. The substructure consists of seven timber piles, a double C-channel cap, and a timber back wall. Currently not posted, the bridge was given a sufficiency rating of 37 when it was last inspected in July of 2005.

Figure 8.1. HCB Alignment View Looking West.

Originally designed as a single span bridge, the HCB had a pier added near the midspan of the bridge sometime during the 1970's. The pier was added by driving two piles on each side of the bridge and placing a beam supporting each of the four girders as shown in Figure 8.2. The additional support changed the bridge from one single span to a two span continuous structure so that the bridge could support legal loads.

Figure 8.2. HCB Elevation View of Bridge Looking North.

The superstructure, a cross section of which is shown in Figure 8.3, is a four girder system with two W24x74 girders on the exterior and two W24x94 girders on the interior. There is an eight inch thick cast in place concrete deck and an asphalt overlay of five inches. There are C-channel diaphragms at the 1/3 points of the bridge, concrete curbs eight inches wide by one foot tall, and railings on both sides of the bridge.

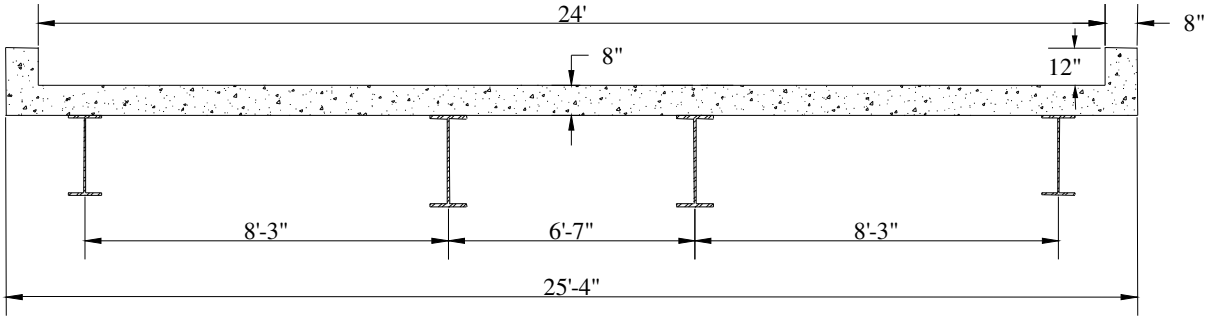

Figure 8.3. Cross Section of HCB Looking West.

8.2 Test Setup

8.2.1 Test Truck

Two incremental loads, referred to as a half full truck and a full truck, were selected for the bridge test. The truck used for the load test was provided by the county and was a standard maintenance tandem dump truck. A photograph of the test truck crossing the bridge during a load test is provided in Figure 8.4, its axle weights are presented in Table 8.1 and its dimensions are presented in Figure 8.5. Note, as shown in Figure 8.4, the pier had been removed prior to testing.

Figure 8.4. HCB Test Truck Crossing Bridge After Pier Removal.

Table 8.1. HCB Truck Weights.

Truck Loading	Axle Weights (kip)			Gross Weight (kip)
	A	B	C	
Half Full	15.20	11.80	11.40	38.40
Full	15.30	18.75	18.25	52.30

8.2.2 Testing Plan and Instrumentation

There were five lanes, shown in Figure 8.6, selected for the truck to follow as it crossed the bridge. Each lane was loaded twice for each load increment to check the repeatability of the test results. Measurements (strains and deflections) were taken when the centroid of the tandem was at the centerline of each end bearing and at each quarter point (see Figure 8.6). Lane 3, HCB test truck centered on the bridge, had the truck wheel lines very close to the centerlines of the two interior girders as shown in Figure 8.7.

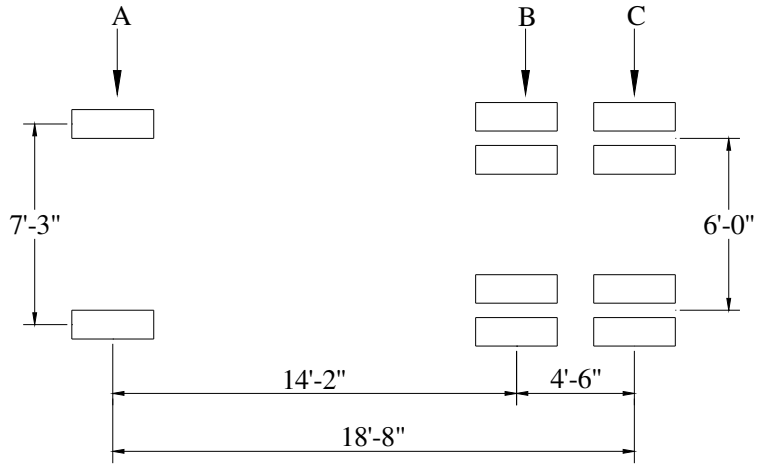

Figure 8.5. HCB Test Truck Dimensions

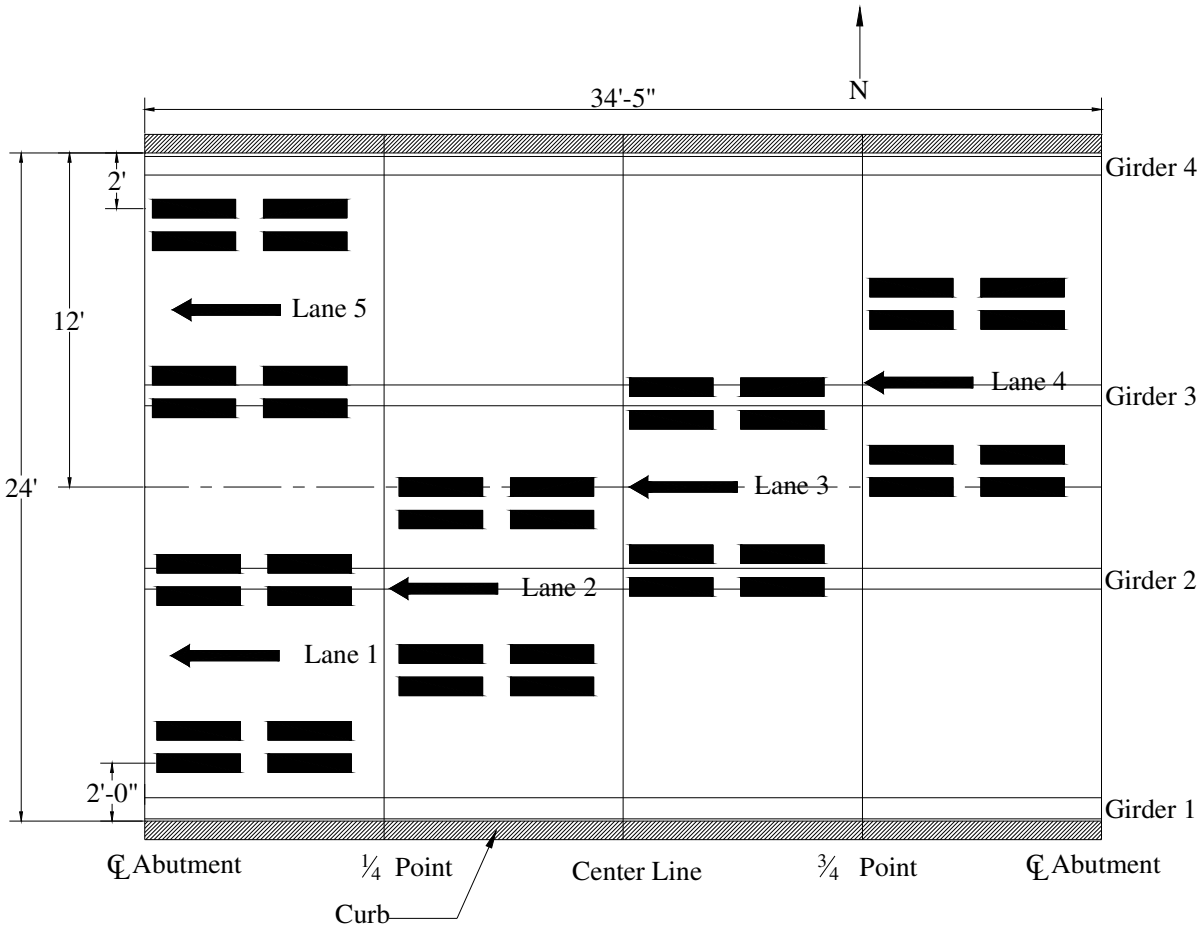

Figure 8.6. HCB Plan View Loading Lanes

Figure 8.7. HCB Test Truck in Lane 3.

The bridge was instrumented 24 inches from the edge of the bearing at each abutment, at the east quarter point, and at the midspan. To determine the rotational restraint due to end conditions of the girders, the strain transducers near the abutment were moved from six inches away from the edge of the abutment cap to 24 inches from the abutment cap in an attempt to reduce the measurement of stress concentrations near the girder bearing.

Strain transducers were installed on the top and bottom flanges of each girder near the east abutment and at the east quarter point as shown in Figure 8.8. Two strain transducers were located on the concrete at the midspan next to Girders 1 and 2. The strain and deflection transducer locations at the midspan for each girder and on the concrete are shown in Figure 8.9. Strain transducers were only installed on the top and bottom flanges of Girders 1 and 3 near the west abutment as shown in Figure 8.10. One strain transducer was located on the top of each of the two railings at the midspan as well. In total, there were 32 strain transducers and four deflection transducers installed on the bridge.

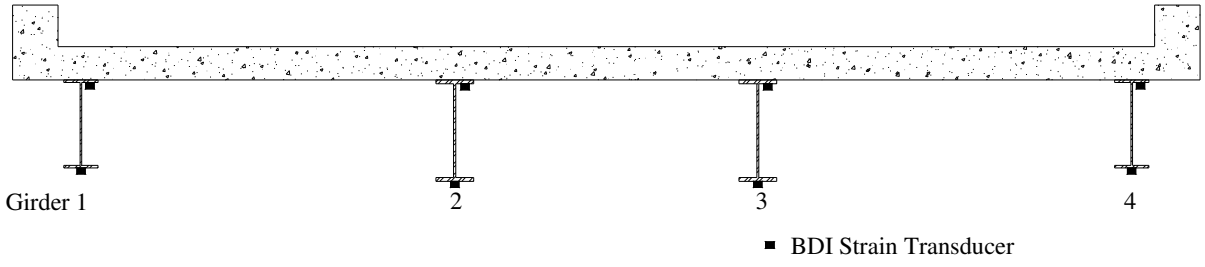

Figure 8.8. HCB East End and Quarter Point Transducer Locations Looking West.

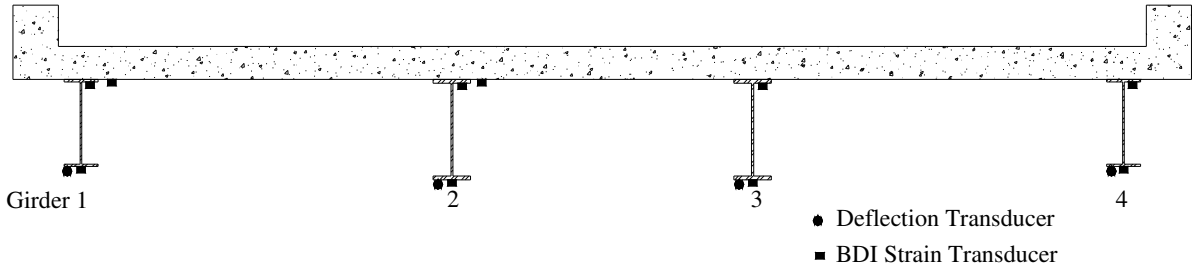

Figure 8.9. HCB Midspan Transducer Locations Looking West.

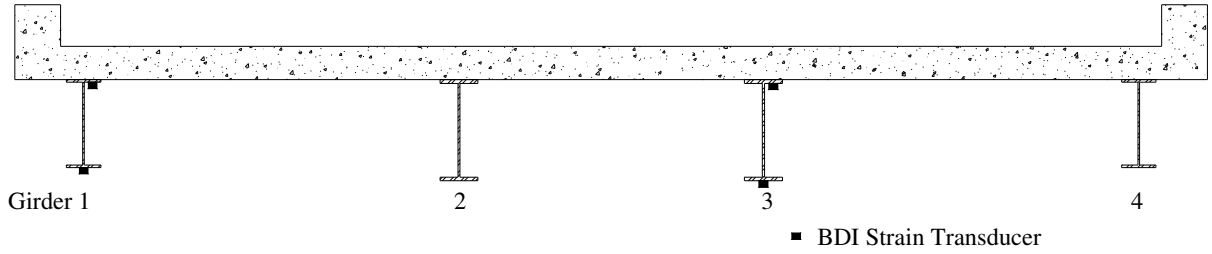

Figure 8.10. HCB West End Transducer Locations Looking West.

8.3 Bridge Analysis

8.3.1 Neutral Axis and Partial Composite Action

The bridge was designed as a non-composite simple span bridge and common with most bridges of this type, there were some details that could increase the flexural capacity of the bridge. Shown in Figure 8.11 through Figure 8.15 are the top and bottom flange strains and deflections with the loading in Lane 1 through Lane 5, respectively. In the figures described above, TF and BF refers to the top and bottom flange strains, respectively. All of the deflection profiles followed the same general shape as the bottom flange strain profiles; recall that this was not the case for the CCB.

There was very good symmetry shown in both the top and bottom flange strain profiles. This symmetry can be observed in Figure 8.13 with both sets of girders, Girders 1 and 4 as well as Girders 2 and 3, having similar strain values under symmetrical loading. Symmetry can also be observed in the two sets strain profiles, Lanes 1 and 5 as well as Lanes 2 and 4, having mirror images of each other.

The neutral axis locations, shown in Figure 8.16, were determined by interpolating between the top and bottom flange strains to determine the location on the girder where the strain was equal to zero. Partial composite action, shown simply by the location of the neutral axes being located between the theoretical composite and non-composite neutral axis locations, was observed in all of the girders for each of the lanes loaded. The amount of partial composite action deteriorated with increased loading for all of the girders.

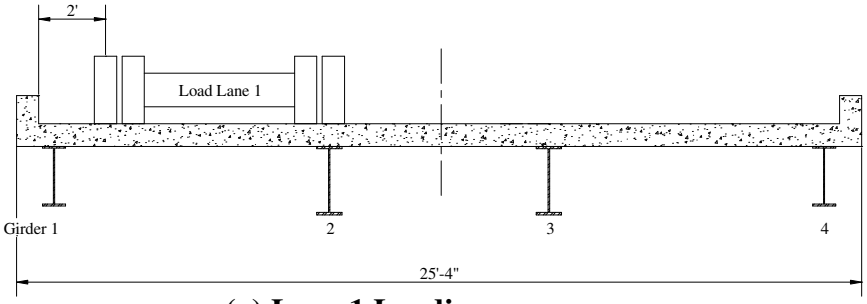

(a) Lane 1 Loading

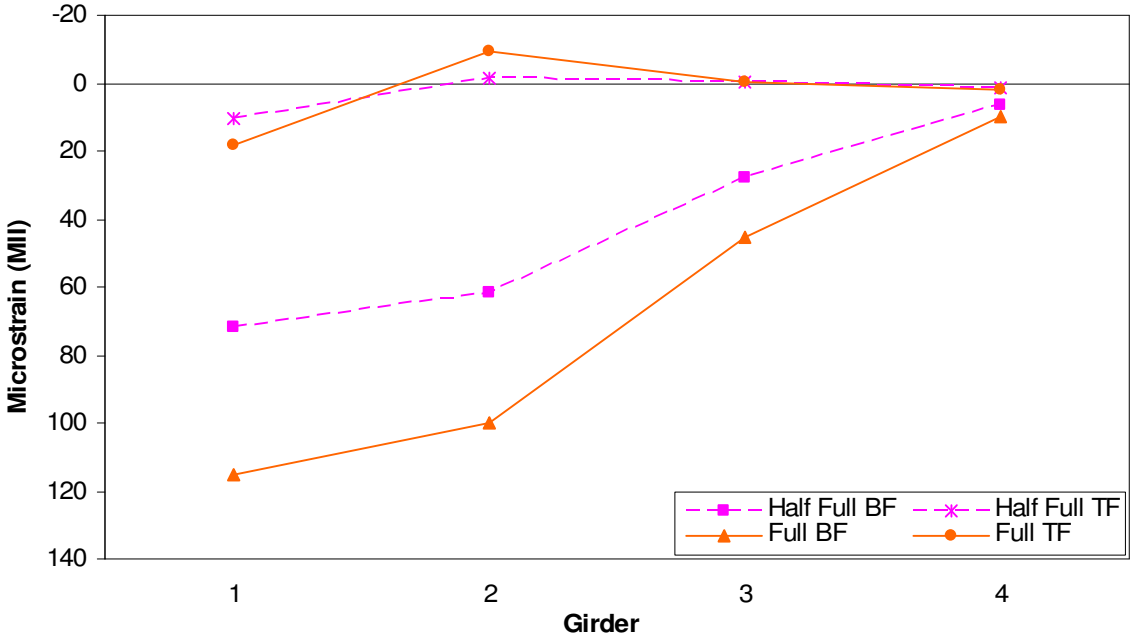

(b) Strain Profile

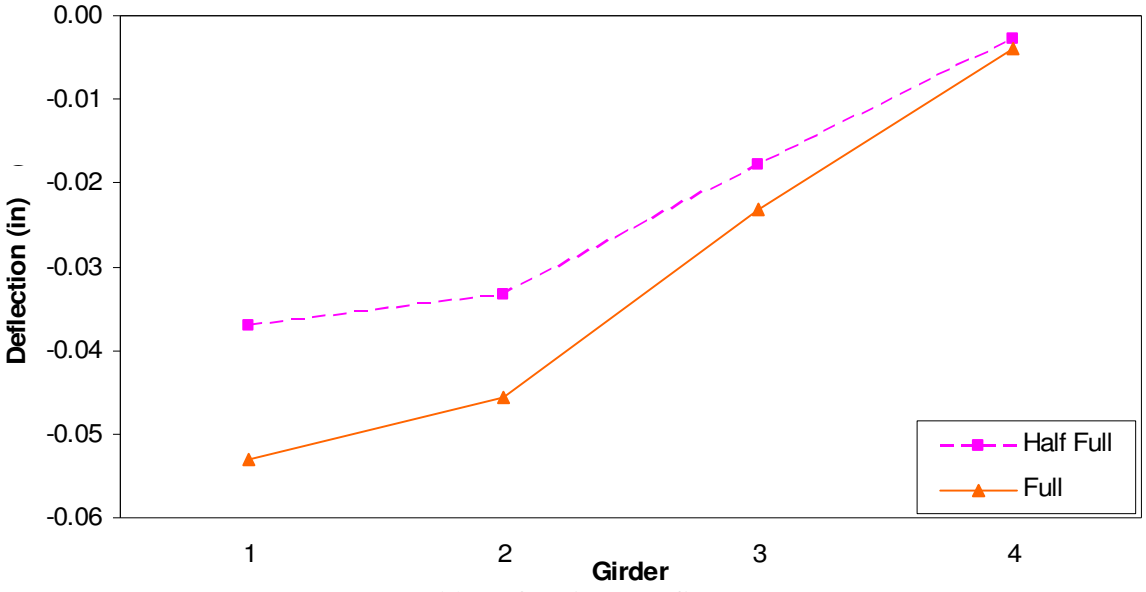

(c) Deflection Profile

Figure 8.11. HCB Lane 1 Strains and Deflections.

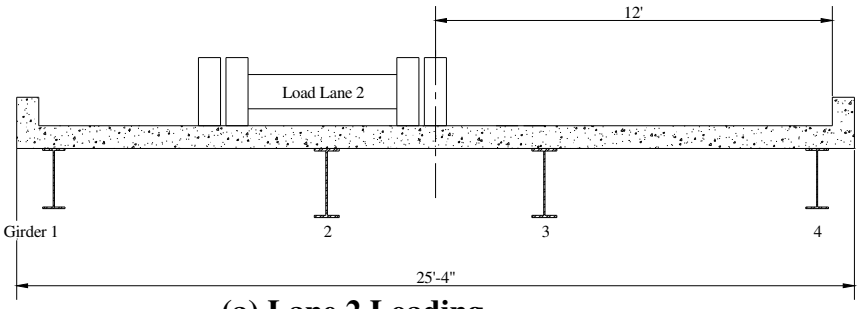

(a) Lane 2 Loading

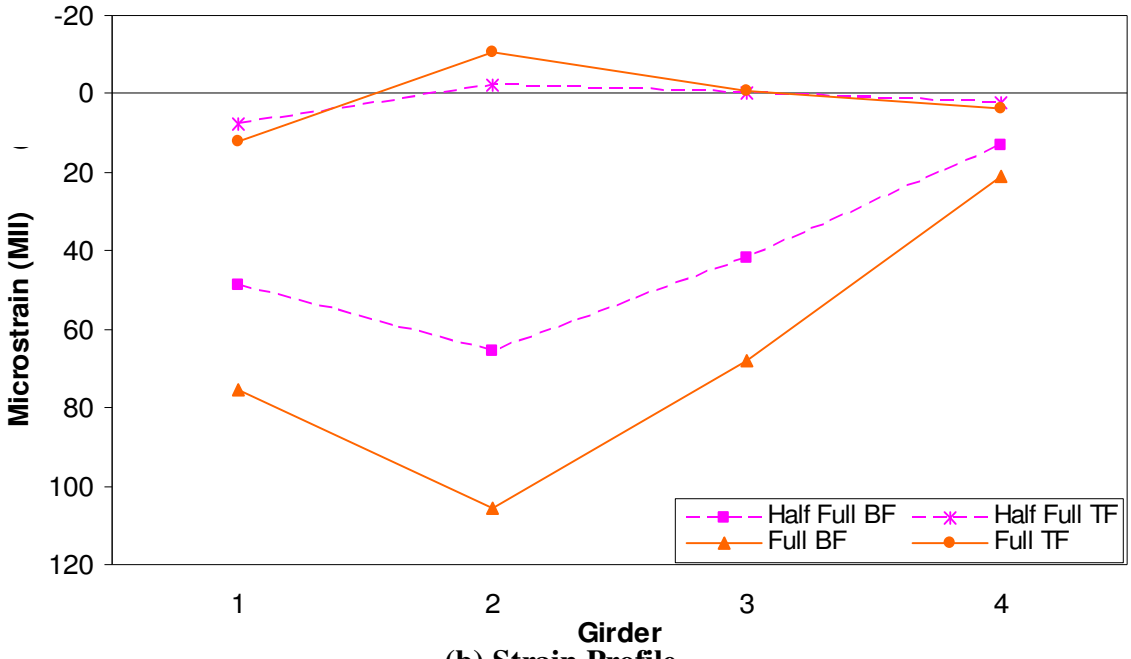

(b) Strain Profile

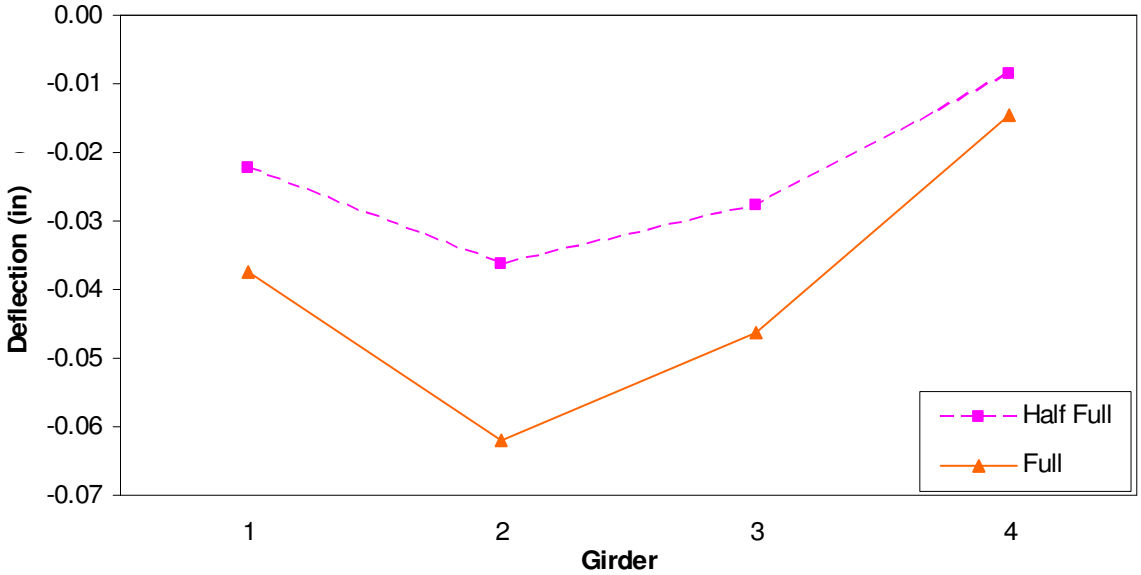

(c) Deflection Profile

Figure 8.12. HCB Lane 2 Strains and Deflections.

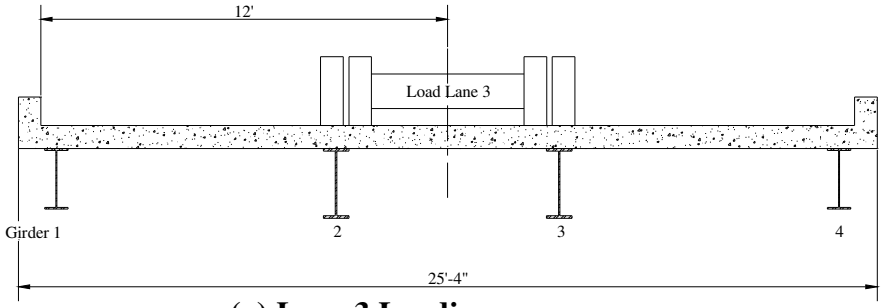

(a) Lane 3 Loading

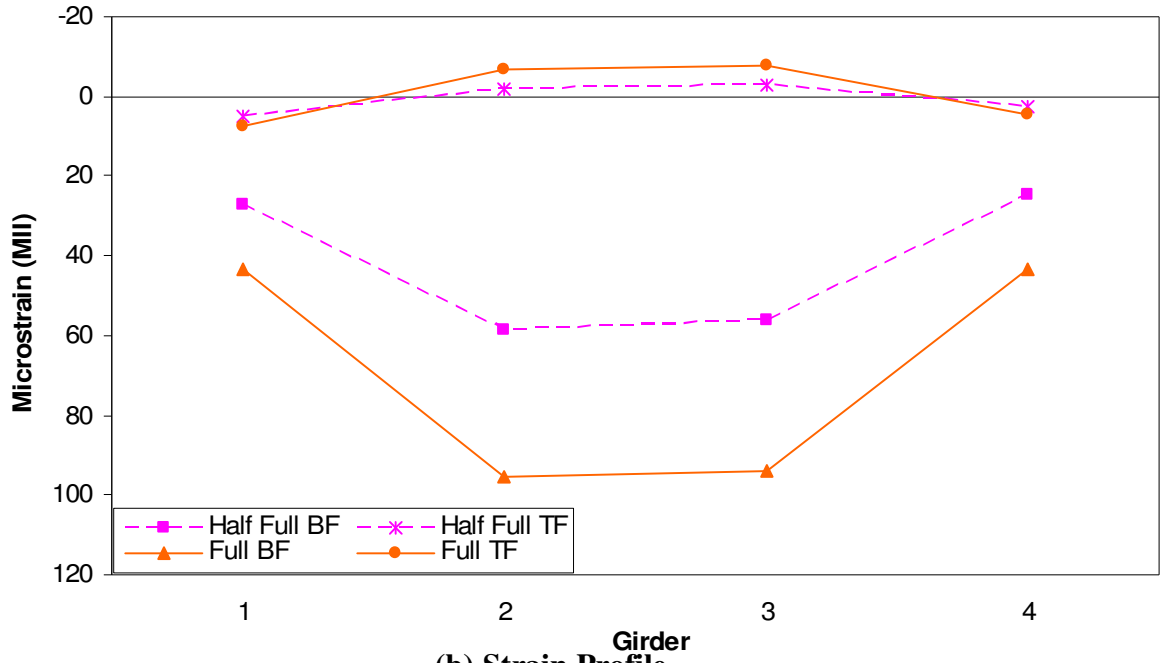

(b) Strain Profile

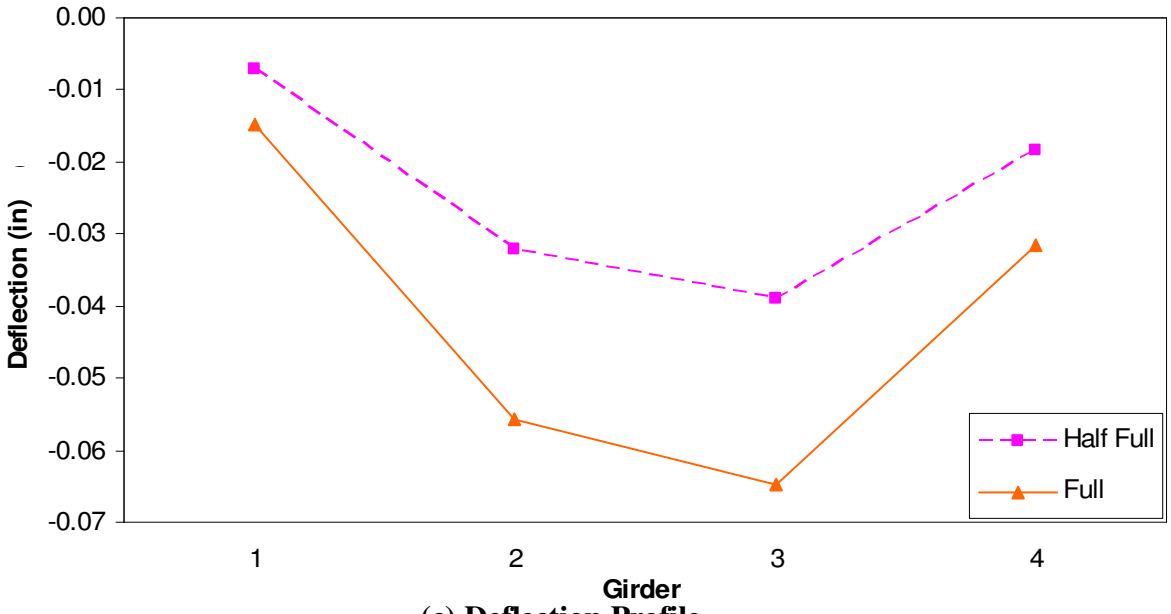

(c) Deflection Profile

Figure 8.13. HCB Lane 3 Strains and Deflections.

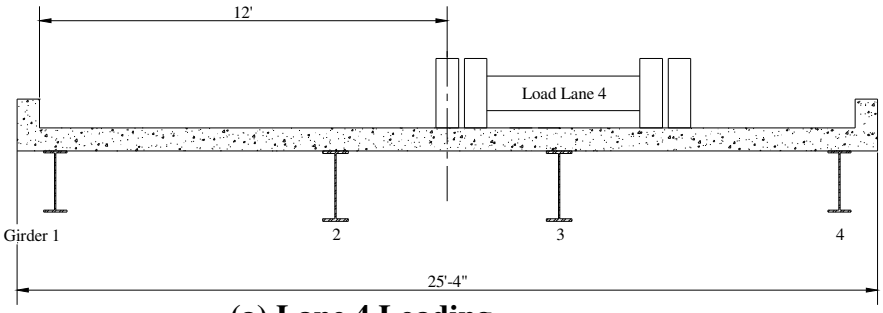

(a) Lane 4 Loading

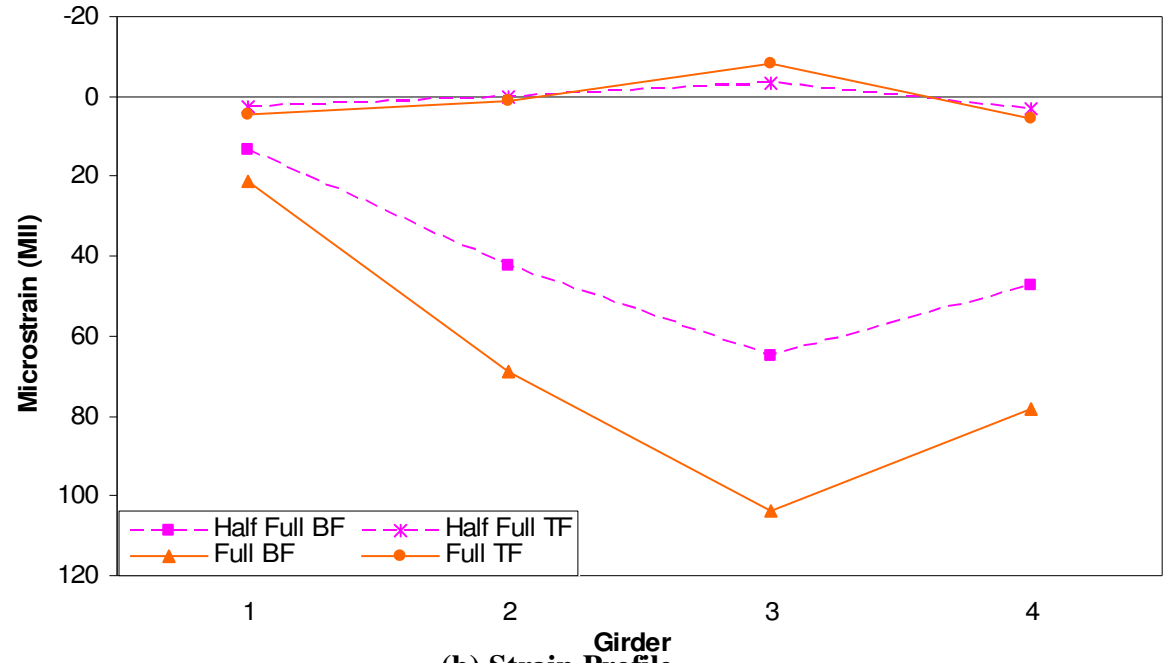

(b) Strain Profile

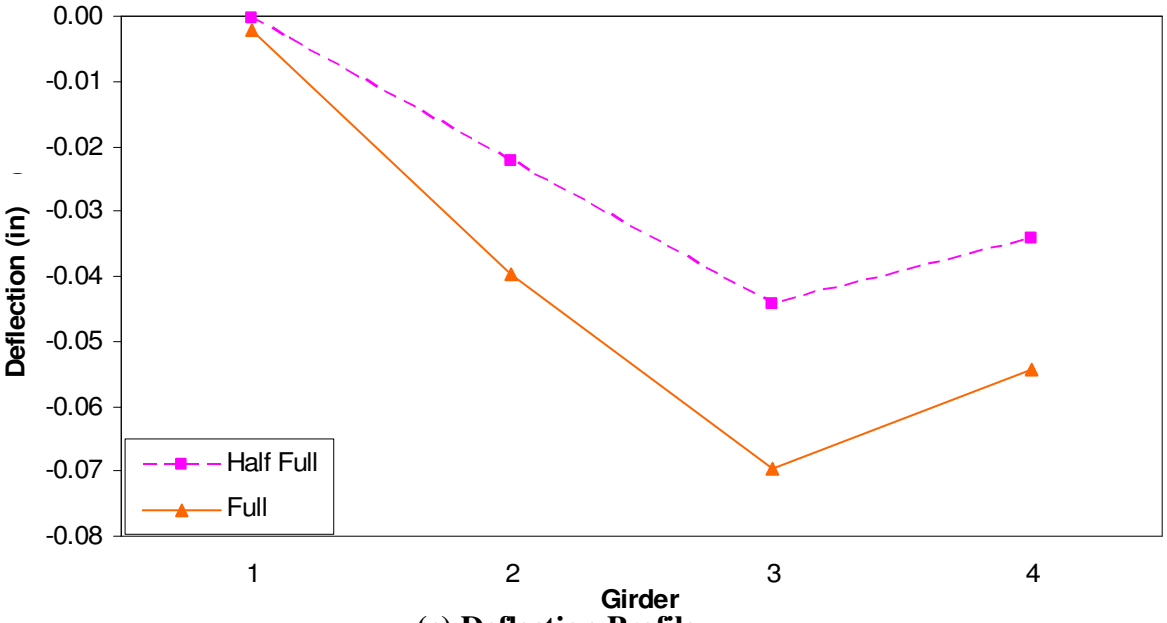

(c) Deflection Profile

Figure 8.14. HCB Lane 4 Strains and Deflections.

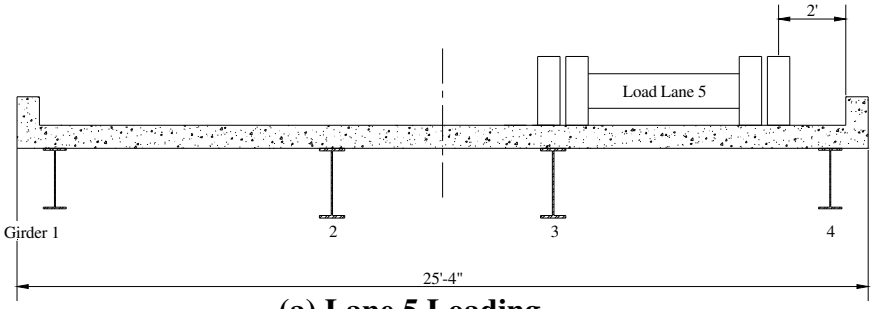

(a) Lane 5 Loading

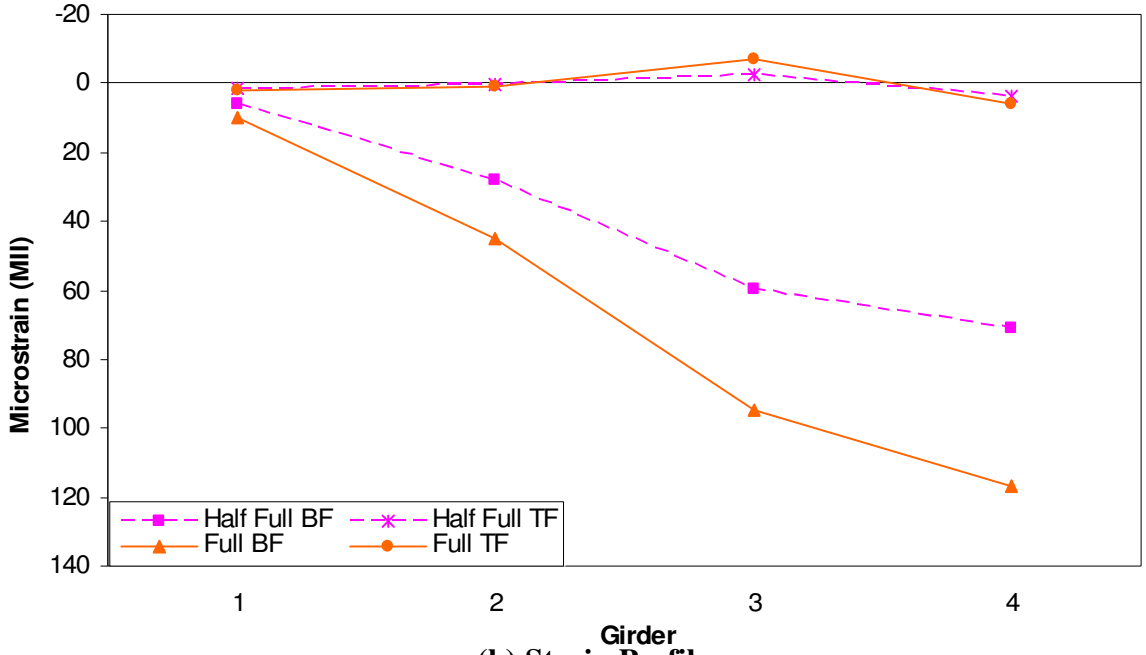

(b) Strain Profile

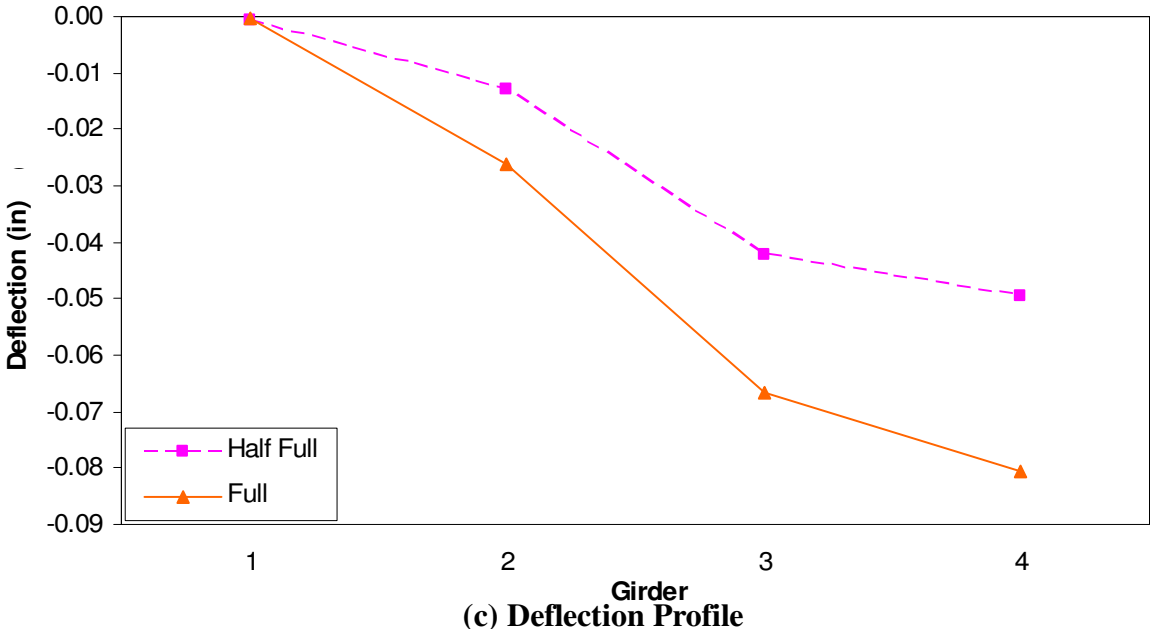

(c) Deflection Profile

Figure 8.15. HCB Lane 5 Strains and Deflections.

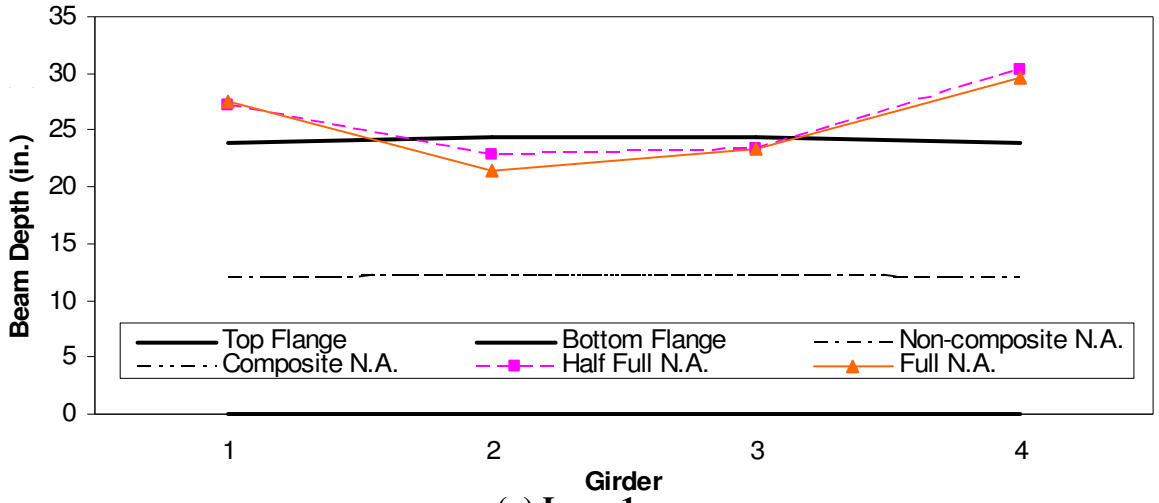

(a) Lane 1

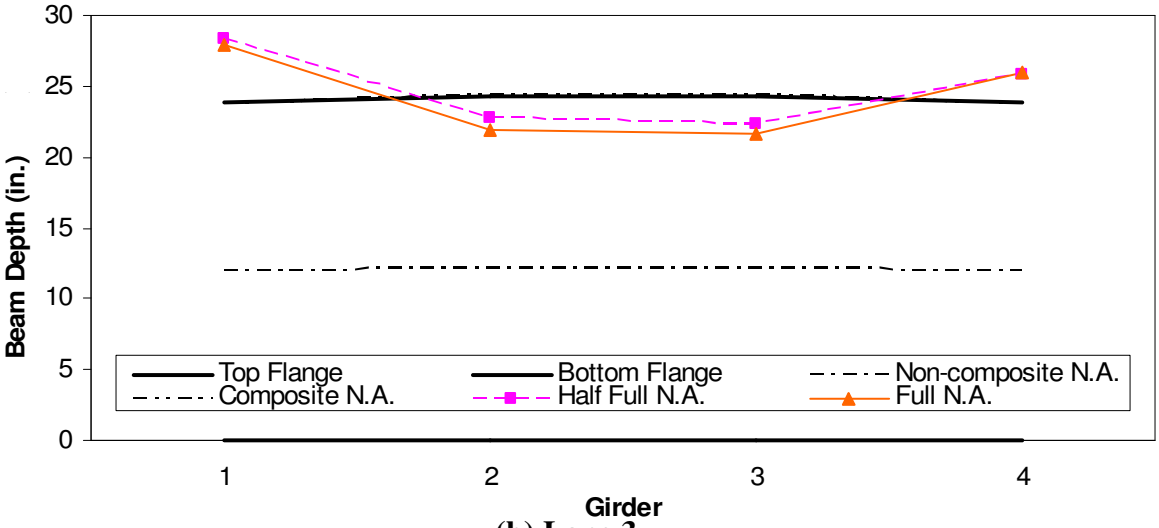

(b) Lane 3

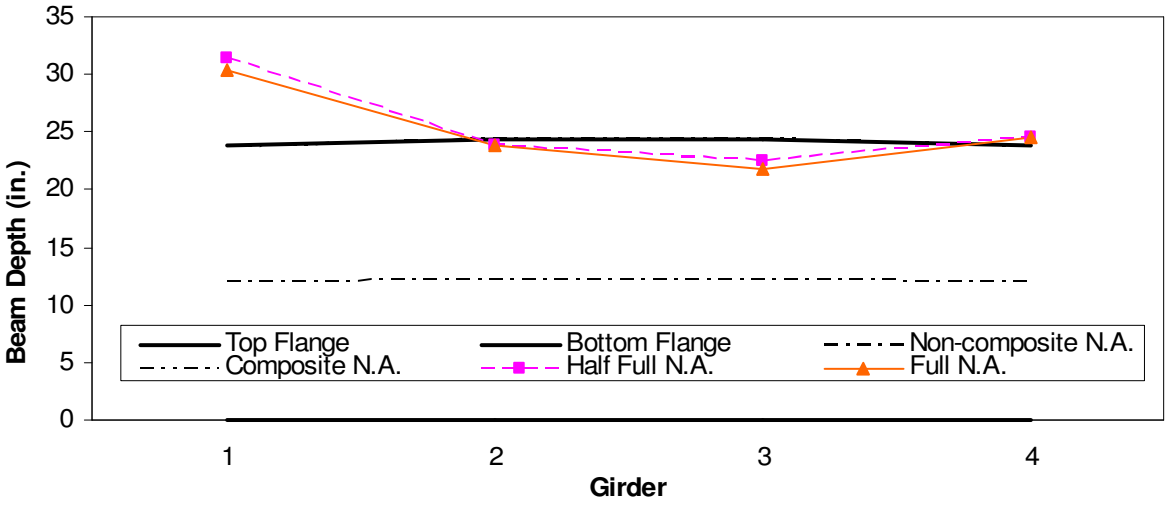

(c) Lane 5

Figure 8.16.HCB Neutral Axis Locations.

Neutral axis locations in the exterior girders were well within the concrete deck; this displays the edge stiffening effect that was prevalent in the previously tested bridge. The increased edge stiffness can be attributed to the concrete curb and steel railing which were not included in the calculation of the composite neutral axis location. The theoretical composite neutral axis locations, shown in Figure 8.16, were located within the concrete deck and within the top flange of the girder for the exterior and interior girders, respectively. As discussed for the BCB, the high neutral axis locations result from very small strain measurements in the top flange. The neutral axis profiles were fairly symmetric; the exterior girder neutral axis locations varied based on the transverse location of the test truck but the neutral axis locations for the two interior girders remained relatively unchanged.

8.3.2 Load Distribution

Using the previously described truck locations, the theoretical moment induced in the bridge, assuming simply supported conditions, was calculated for each loading; these are presented in Table 8.2. As may be seen in this table, there was a 58% increase in moment from half full to full.

Table 8.2. HCB Induced Truck Moments.

Load	Moment (in-k)
Half Full Truck	2150
Full Truck	3390

Using the bottom flange strains, the percent distributions were calculated as the ratio of the weighted individual girder strains to the weighted sum of the four girder strains. The ratio was weighted to account for the different sections that were used for interior and exterior girders. With both of the load increments producing slightly different load distribution percentages, the maximum values, summarized in Table 8.3, were selected for each of the three lanes. Note that the values are the maximum percentage values of the two load cases and therefore do not sum to 100%. As may be seen, the maximum distribution percentages occurred in the exterior girders when directly loaded. Girders 2 and 4 had distribution percentages very close to each other for Lane 3 loading which demonstrates symmetry in the bottom flange strains. Symmetry in the bottom flange strains can be observed by comparing the Girder 1 distribution for Lane 1 loading to the Girder 5 distribution for Lane 5 loading.

Table 8.3. HCB Maximum Single Lane Percent Distributions

Lane \ Girder	1	2	3	4
1	33.8	43.6	19.7	3.1
2	21.8	44.3	28.5	5.9
3	12.1	39.2	37.9	11.7
4	6.1	28.8	43.8	21.9
5	3.0	20.2	42.7	34.8

As previously noted, the percent distributions are provided in Table 8.3; however in order to compare them to the AASHTO distribution factors the values must be multiplied by two to obtain the distribution of a single wheel line. The maximum distribution factors from the percent distributions summarized in Table 8.3 are presented in Table 8.4. Using superposition, Lanes 1 and 4 and Lanes 2 and 5 were used to determine the distribution factors for two lanes which are also presented in Table 8.4.

Table 8.4. HCB Calculated Lane Distribution Factors.

Lane \ Girder	1	2	3	4
1	0.68	0.87	0.39	0.06
2	0.44	0.89	0.57	0.12
3	0.24	0.78	0.76	0.23
4	0.12	0.58	0.88	0.44
5	0.06	0.40	0.85	0.70
1 & 4	0.80	1.45	1.27	0.50
2 & 5	0.50	1.29	1.42	0.82

The maximum distribution factors for the interior and exterior girders for the single lane loading are 0.89 and 0.70, respectively, while the AASHTO distribution factor for the single lane loading with an average girder spacing of 7'-5" using the aforementioned equation of S/7.0 is 1.06 for the interior girders and for a the exterior girders, with a spacing of 8'-3" is 1.18. The AASHTO distribution factors for the two lane loading case for the exterior girders are 1.25 and 1.36, respectively. Values obtained by dividing the AASHTO distribution factors by the experimental distribution are summarized in Table 8.5.

Table 8.5. HCB Distribution Ratios.

	Single Lane	Double Lane
Interior Girder Distribution	0.89	1.45
Exterior Girder Distribution	0.70	0.82
Interior AASHTO Distribution Factor	1.06	1.18
Exterior AASHTO Distribution Factor	1.07	1.36
Interior Factor Ratio	1.20	0.81
Exterior Factor Ratio	1.54	1.67

The distribution ratio for the single lane interior girders is greater than one; however the distribution ratio for the double lane interior girders is less than 1.0 indicating that the field test results yielded a distribution factor higher than theoretically determined using the AASHTO equations. The exterior girder distribution ratios are both very large indicating the AASHTO distribution factors are conservative. Calculated exterior girder distributions based on the weighted girder strains are much lower than the distribution factors calculated using the ASHTO equations because the AASHTO equations do not allow for a change in the distribution factor based on the different girder sections.

8.3.3 Moment of Inertia

Using the previous method of determining a theoretical moment of inertia by back calculating the effective width of a transformed section of the concrete slab produced very large and unrealistic moments of inertia for the exterior girders. This observation has been discussed in the previously tested bridges when there was very small strains in the top flange of the girders which in turn produced high neutral axis locations. The calculated moments of inertia prior to the model optimization for previous bridge tests did not correlate with the optimized moments of inertia. For these two reasons, the theoretical moments of inertia for this bridge are not provided.

8.4 BDI Optimization

The bridge was once again modeled using software (WinGEN) provided by Bridge Diagnostics Inc. and the actual test data was used to create a model that is close to the actual bridge based on the response of the structure due to the truck loadings. This bridge model consisted of modeling each girder separately so that the moment of inertia for each girder could be optimized. This was important due to the partial composite action differences in each of the girders. As for all bridges, the deck was modeled using plate elements, while the girders were modeled using beam elements. Rotational springs attached to the ends of each of the girders: one for the east end of the exterior girders, one for the east end of the interior girders, and two more for the interior and exterior girders on the west end of the bridge.

The initial moments of inertia in each girder were assumed to be equal to the theoretical composite moment of inertia. The initial value for all of the spring constants was 1000 kip-in/rad, while the initial value for the modulus of elasticity for concrete was 3,200 ksi.

Only steel girder strains were input into the model; concrete slab strains were not included because of cracking. There were large variations in these strains. After the model was generated using WinGEN it was then analyzed using WinSAC. WinSAC compares the actual strains induced by test truck to those produced by a theoretical truck with the same dimensions and wheel loads as the test truck.

The initial model parameters produced a large scale error and the strains did not correlate very well with the actual strains obtained from the load tests; therefore, the bridge was optimized. The parameters that were optimized for the bridge included the moment of inertia for each girder, the rotational spring stiffness, and the modulus of elasticity of concrete in the deck. Upper and lower bounds for the optimization parameters are presented in Table 8.6. The upper and lower bound for the moment of inertia of the girders corresponded to 120% of the composite and 80% of the non-composite neutral axis locations, respectively. Optimizing the bridge using the parameters in Table 8.6 yielded a scale error of 8.35%; the optimized values are provided in Table 8.7.

Table 8.6. HCB Optimization Parameters.

Optimization Parameter	Lower Bound	Upper Bound
Exterior Moment of Inertia (in^4)	1425	7310
Interior Moment of Inertia (in^4)	2160	10255
Rotational Spring Stiffness (kip-in/rad)	0	1,000,000
Modulus of Concrete (ksi)	2500	5700

Though there was symmetry observed in the neutral axis profile and strain profile plots, there was not symmetry observed in the optimized girder moments of inertia for the interior girders; the optimized moments of inertia for the exterior girders were symmetrical though with the exact same optimized value. Comparing the optimized moment of inertia in the geometrically symmetric Girders 2 and 3, did not show symmetry with the values differing by 2480 in^4. Optimized values obtained for the spring constants also did not maintain symmetry ranging from about 380,000 to 820,000 kip-in/rad. A graphical comparison of the optimized strains for each loading path are compared to the actual strains induced by the test truck for Girder 1 through Girder 4 are presented in Figure 8.17 through Figure 8.20, respectively.

Table 8.7. HCB Optimized Parameters Using All Steel Transducers.

Optimized Parameter	Initial Value	Optimized Value
Girder 1 I_y (in^4)	6320	7190
Girder 2 I_y (in^4)	8315	7530
Girder 3 I_y (in^4)	8315	10,010
Girder 4 I_y (in^4)	6320	7190
North Exterior Rotational Spring (kip-in/rad)	1000	380,400
North Interior Rotational Spring (kip-in/rad)	1000	693,100
South Exterior Rotational Spring (kip-in/rad)	1000	468,400
South Interior Rotational Spring (kip-in/rad)	1000	821,700
Deck Modulus (ksi)	3200	5390

In almost all cases, the optimized strain values were close to the actual strain values from the test truck. The correlation between the optimized strain values and the actual strain values are summarized in Table 8.8. The scale error ranged from 1.4 to 6.3 and the correlation ranged from 0.776 to 0.864.

Table 8.8. HCB Bottom Flange Strain Scale Error and Correlation.

Girder	1	2	3	4	Average
Scale Error	2.3	6.3	5.9	1.4	4.0
Correlation	0.848	0.776	0.777	0.864	0.816

In an attempt to decrease the overall scale error, the strains near the supports were removed from the bridge optimization model. The previous optimized values were input into a model that had only the midspan girder strains included in an attempt to quantify the effect of the bearing transducers on the scale error. This model was analyzed and resulted in a scale error of only 4.0%, a 4.2% reduction from the original optimization model using all of the steel

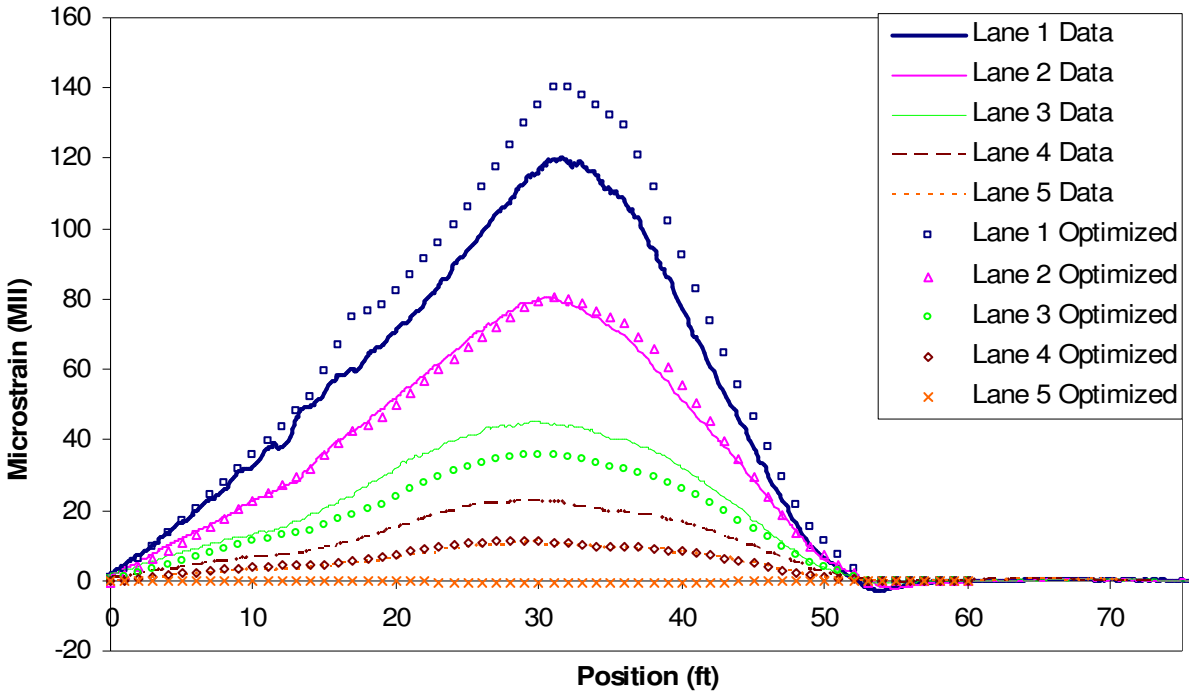

Figure 8.17. HCB Girder 1 Optimized Strain Comparison.

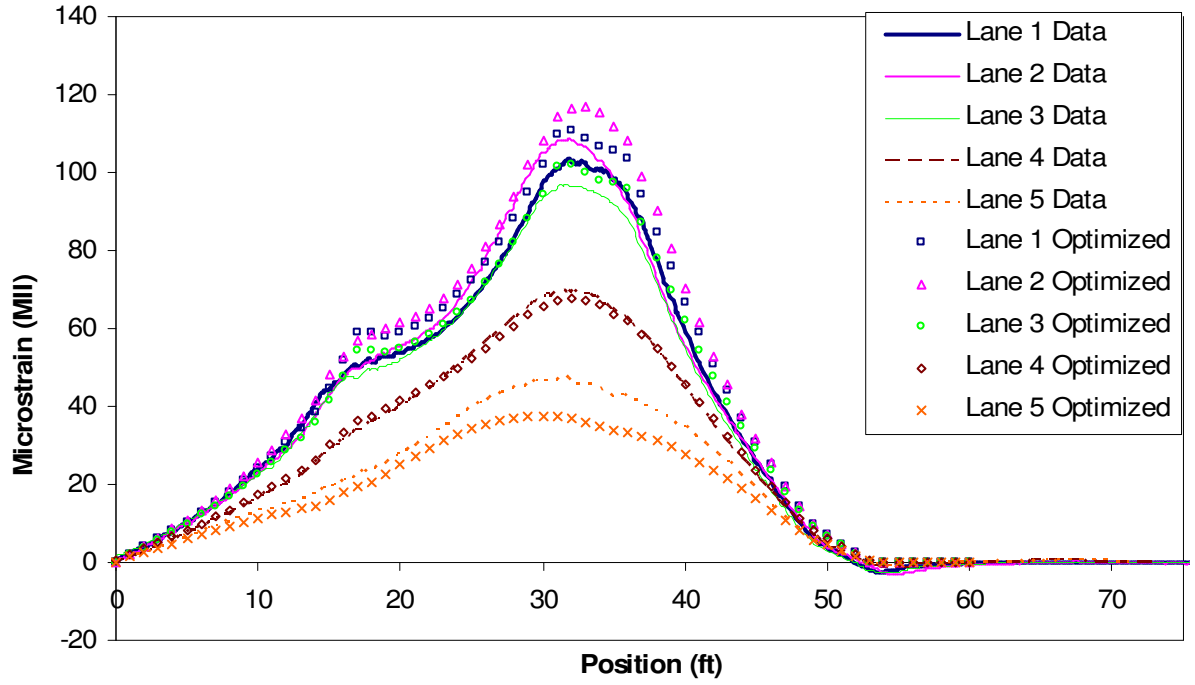

Figure 8.18. HCB Girder 2 Optimized Strain Comparison.

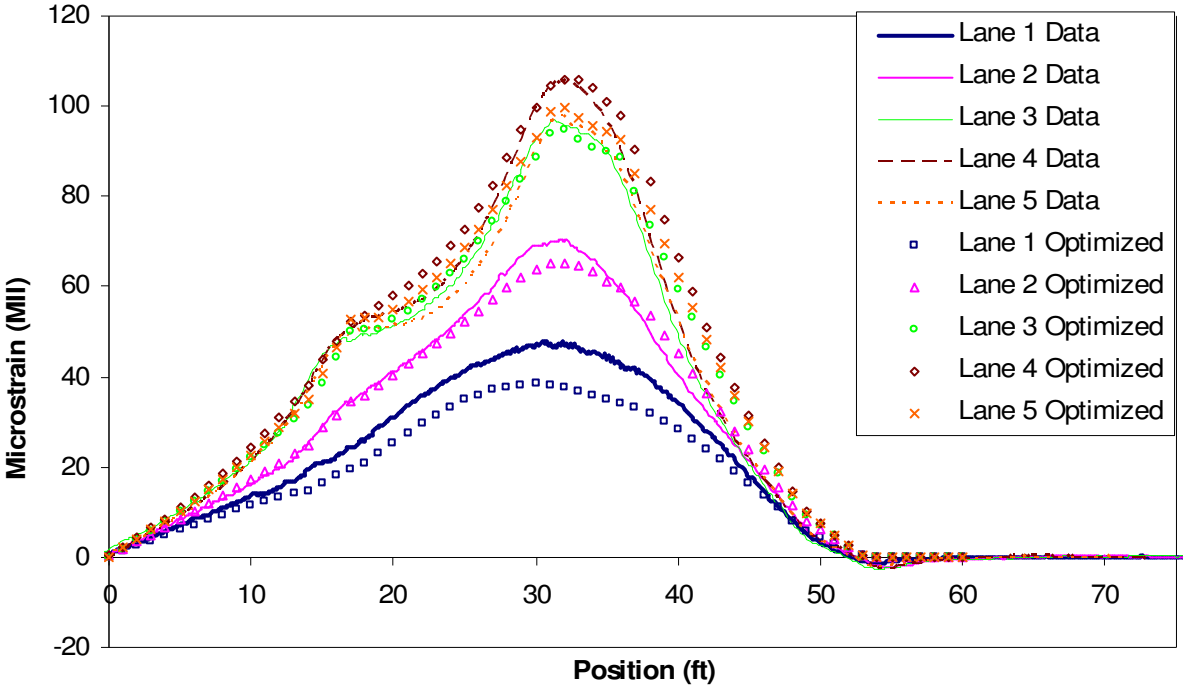

Figure 8.19. HCB Girder 3 Optimized Strain Comparison.

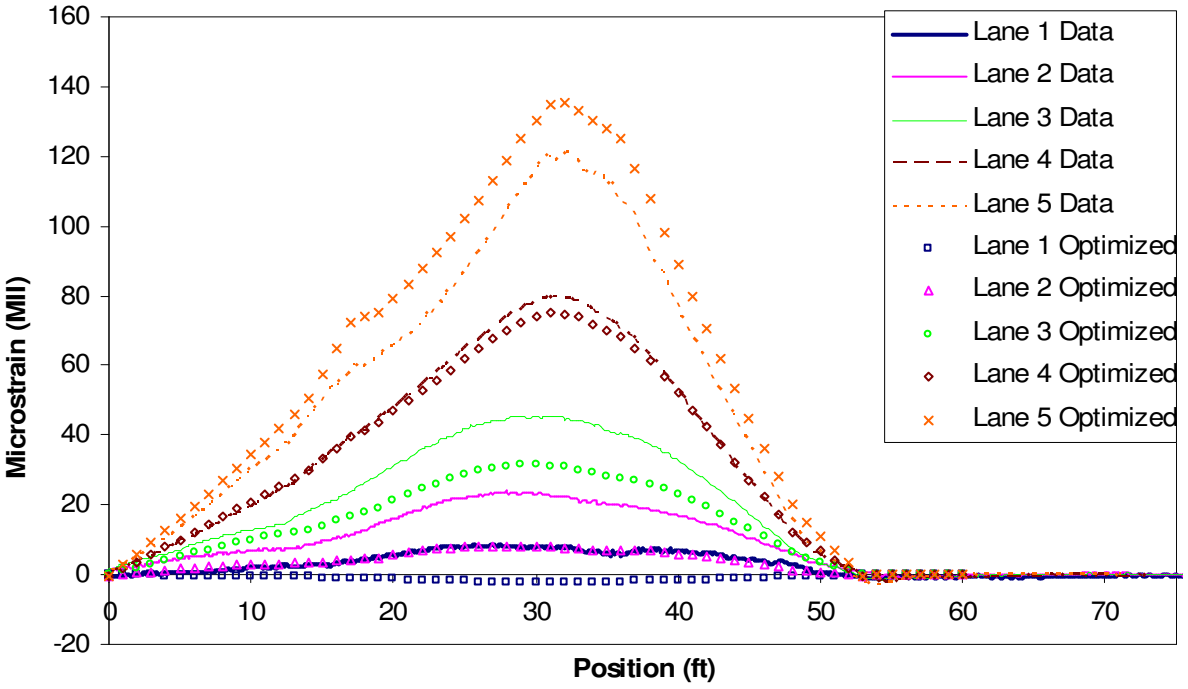

Figure 8.20. HCB Girder 4 Optimized Strain Comparison.

girder strains. The correlation values provided in Table 8.8 did not change in the new analysis.

8.5 Bridge Rating

8.5.1 Conventional Rating

The bridge was rated using the Load Factor Rating (LFR) approach. This analytical rating, in which both the interior and exterior girders were rated, was performed assuming a non-composite design with simply supported conditions. The bridge was also independently rated by both the Iowa DOT and PCF. Ratings calculated by the three different rating agencies are provided in Table 8.9.

Table 8.9. HCB Analytical Bridge Ratings

Interior Girders						
	ISU		PCF		Iowa DOT	
Vehicle	Operating	Inventory	Operating	Inventory	Operating	Inventory
HS20 (36 ton)	41.2	24.7	39.5	23.7	35.3	21.2
Type 4 (27.25 ton)	33.2	19.9	32.3	19.4	29.5	17.7
Type 3-3 (40 ton)	59.4	35.6	58.3	35.0	53.2	31.9
Type 3S3 (40 ton)	50.9	30.5	50.1	30.0	45.7	27.4
Exterior Girders						
	ISU		PCF		Iowa DOT	
Vehicle	Operating	Inventory	Operating	Inventory	Operating	Inventory
HS20 (36 ton)	30.7	18.4	28.2	16.9	21.6	13.0
Type 4 (27.25 ton)	24.5	14.7	23.0	13.8	18.0	10.9
Type 3-3 (40 ton)	43.7	26.2	41.4	24.8	32.4	19.6
Type 3S3 (40 ton)	37.2	22.3	35.3	21.2	28.0	16.8

The rating calculations from PCF correspond very closely to those calculated by ISU. The calculated ratings from ISU tend to be slightly less conservative than those calculated by PCF. The Iowa DOT ratings were once again governed by the serviceability criterion described in previous bridge tests. The exterior girders controlled the rating of this bridge with all three rating agencies rating them below the legal loads. The operating ratings for the interior girders calculated by ISU and PCF are sufficient for the legal loads and would not require any posting but are slightly below the legal loading of an HS20 load for the Iowa DOT rating.

8.5.2 Rating Using Optimized Parameters From BDI Software

Utilizing the strains measured during the load test, the BDI software (WinGEN) was once again utilized to determine the bridge rating using the optimized parameters. Using the modified bridge model, the bridge was rated using the same rating vehicles as the analytical ratings. The rating vehicles were input into the WinGEN software and traversed across the bridge in pre-selected lanes to produce maximum strains in the girders. Only a single lane loading was analyzed using the WinSAC software. With the optimized moments of inertia for

each girder being different, each girder was rated separately using the BDI software. The load factor rating method was once again used for the ratings using the optimized bridge parameters. The operating and inventory ratings were calculated for each girder and are summarized in Table 8.10**.**

Even though the analytical rating equations resulted in bridge ratings less than the legal loads for the exterior girders, all of the ratings calculated using the optimized model were above the legal loads for the bridge. After optimization, the limiting girder was Girder 3 having the lowest operating rating with a limit of 54 ton for a HS20 rating vehicle, well above the legal weight of 36 ton. The inventory ratings for Girder 3 were below the legal loading for the HS20 loading vehicle by about four tons. Girders 1, 2, and 4 had inventory ratings above the legal loading for all of the rating vehicles. A table presenting the percentage increase from the ISU analytical ratings to the optimized ratings for the operating level is provided in Table 8.11. The range for the increased ratings after optimization for the HS20 rating vehicle was 30% for interior Girder 3 to 143% for exterior Girder 4.

Table 8.10. HCB Optimized Ratings.

Operating Rating (ton)				
	Girder			
Vehicle	1	2	3	4
HS20 (36 ton)	74.5	71.3	53.6	80.6
Tandem (25 ton)	45.5	42.8	32.5	49.0
Type 3 (25 ton)	64.3	60.8	46.0	69.3
Type 4 (27.25 ton)	60.0	57.5	43.3	64.6
Type 3-3 (40 ton)	103.2	93.2	93.2	104.0
Type 3S3 (40 ton)	86.8	78.0	78.0	87.2
Type 4S3 (48 ton)	101.8	91.2	91.7	102.2
Inventory Rating (ton)				
	Girder			
Vehicle	1	2	3	4
HS20 (36 ton)	44.6	42.7	32.1	48.3
Tandem (25 ton)	27.3	25.6	19.5	29.4
Type 3 (25 ton)	38.5	36.4	27.6	41.5
Type 4 (27.25 ton)	35.9	34.5	26.0	38.7
Type 3-3 (40 ton)	61.8	55.8	55.8	62.3
Type 3S3 (40 ton)	52.0	46.7	46.7	52.2
Type 4S3 (48 ton)	61.0	54.6	54.9	61.3

8.6 Superstructure Response to Destructive Substructure Testing

With the cooperation of Humboldt County and the contractor hired to replace the bridge, ISU was provided the opportunity to perform some destructive testing on some substructure elements to determine the load distribution in the pile elements due to loading. The substructure results are provided in Volume II of this report. The superstructure was also instrumented to determine if there was any change in the strain pattern in the girders due to the removal of pile elements.

Table 8.11. HCB Operating Rating Percent Increase After Optimization.

	Girder			
Vehicle	1	2	3	4
HS20 (36 ton)	143	73	30	163
Type 4 (27.25 ton)	145	73	30	164
Type 3-3 (40 ton)	136	57	57	138
Type 3S3 (40 ton)	133	53	53	134

8.6.1 Test Setup

The same loading vehicle was used for the destructive testing as was used for the non-destructive testing previously described. Both substructure and superstructure elements were instrumented simultaneously, thus there were a limited number of BDI transducers available for installation on the superstructure. The superstructure was instrumented with BDI transducers on the bottom flanges at the midspan of each girder and two feet from the edge of the east abutment. There were a total of 8 BDI transducers installed on the superstructure. Only Lanes 1, 3, and 5 from the rating process (refer to Figure 8.6 for clarification) were used in the destructive testing. The test truck was the same geometry as the test truck provided in Figure 8.5 and was fully loaded with a gross weight of 51,640 lbs. A cross section of the east abutment is provided in Figure 8.21 showing the seven piles. Only sections of piles in the east abutment were removed.

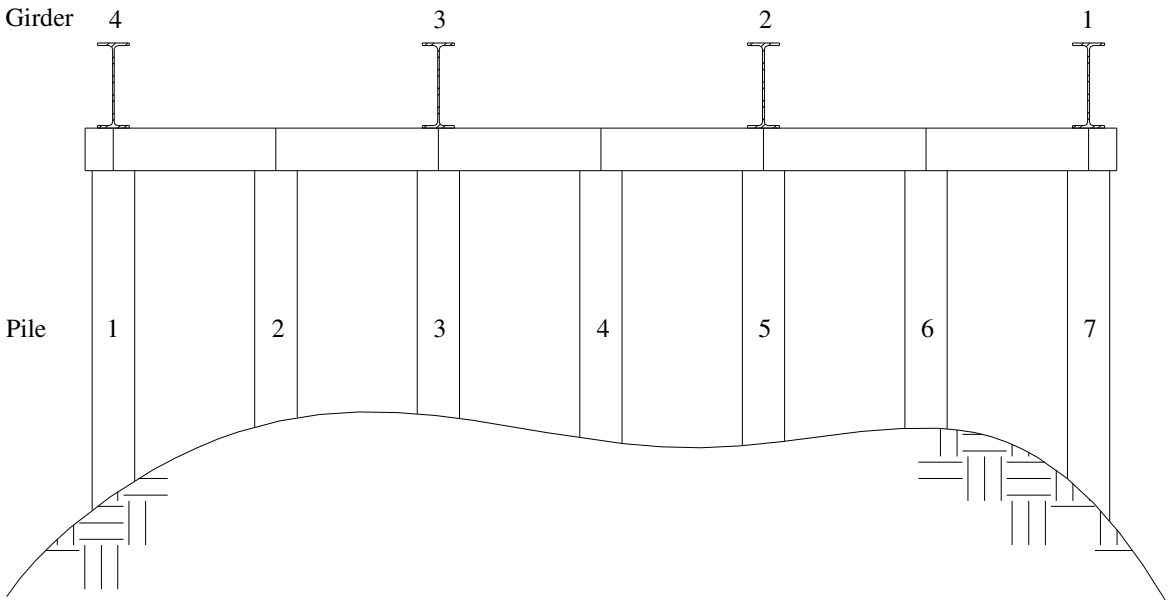

Figure 8.21. HCB East Abutment Cross Section.

8.6.2 Destructive Testing Sequence

The axle weights for the destructive testing sequence were not exactly the same as any of the previous tests; so before any of the destructive testing, a load test was conducted on the in tact bridge to determine a base line for the subsequent destructive processes. Once the base line was established, a section of Pile 7 was removed. Lanes 1, 3, and 5 were each loaded twice with a portion of Pile 7 removed. A screw jack was placed in the cut out section of Pile 7 to create a transfer of the axial load for further testing. Next, a section of Pile 3 was removed and the bridge was once again tested.

The reason for the installation of the screw jack into the voided section of Pile 7 was to isolate the response of the removing a portion of Pile 3. After a test with the removed section of Pile 3, the jack was removed from Pile 7 and the bridge was once again tested to determine the response due to the two piles being removed. Finally, a section of Pile 6 was removed and the bridge tested once more but this time the jack was not installed in the removed pile sections but rather the test was conducted with sections of Piles 3, 6, and 7 removed. Pile 6 was already heavily deteriorated and assumed to be carrying vary little load; however to ensure that it was not carrying any load a section of it was removed. The five loading stages are as follows: Stage 1 – all piles in tact, Stage 2 – section of Pile 7 removed, Stage 3 – section of Pile 3 removed with a jack supporting Pile 7, Stage 4 – sections of Piles 3 and 7 removed, and Stage 5 – sections of Piles 3, 6 and 7 removed. A photograph showing sections of Piles 3 and 7 removed is provided in Figure 8.22. A close up of the removal of the deteriorated section of Pile 6 is provided in Figure 8.23.

Figure 8.22. Photograph Showing Sections of Piles 3 and 7 Removed from HCB.

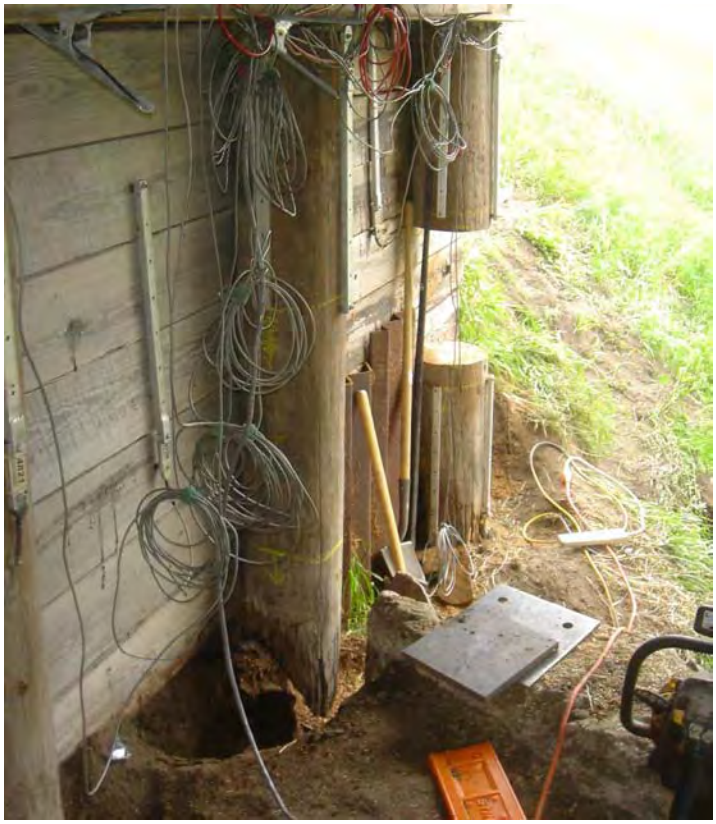

Figure 8.23. Photograph Showing Sections of Piles 6 and 7 Removed from HCB.

8.6.3 Destructive Test Results

The strain profile results due to the removal of various pile elements are summarized in Figure 8.24 through Figure 8.26. There was a problem with the strain transducer on the bottom flange of Girder 1. After the first two test stages, the transducer malfunctioned and would not zero properly and the strain transducer located on Girder 2 near the abutment was moved to the midspan of Girder 1. There was a small change in strains (a difference of about 10 microstrain) due to substituting a second transducer for the original transducer. The change was not noticeable in the other two lane loadings.

As shown in Figure 8.24 through Figure 8.26, the removal of the piles on the east abutment had essentially no effect on the critical midspan strains. To determine whether the removal of the piles may have had an effect on the bearing restraint, data from the transducers located near the abutment were also investigated. The maximum strain in the bottom flange of the girders near the abutment varied slightly from girder to girder but the maximum occurred when the centroid of the rear tandem axles on the test truck was located at approximately the 1/8 span location in the bridge. The strain distribution located near the east abutment are presented in Figure 8.27 through Figure 8.29. Note, as previously mentioned, the transducer located on the bottom flange of Girder 2 was moved to the midspan of Girder 1 after Stage 2.

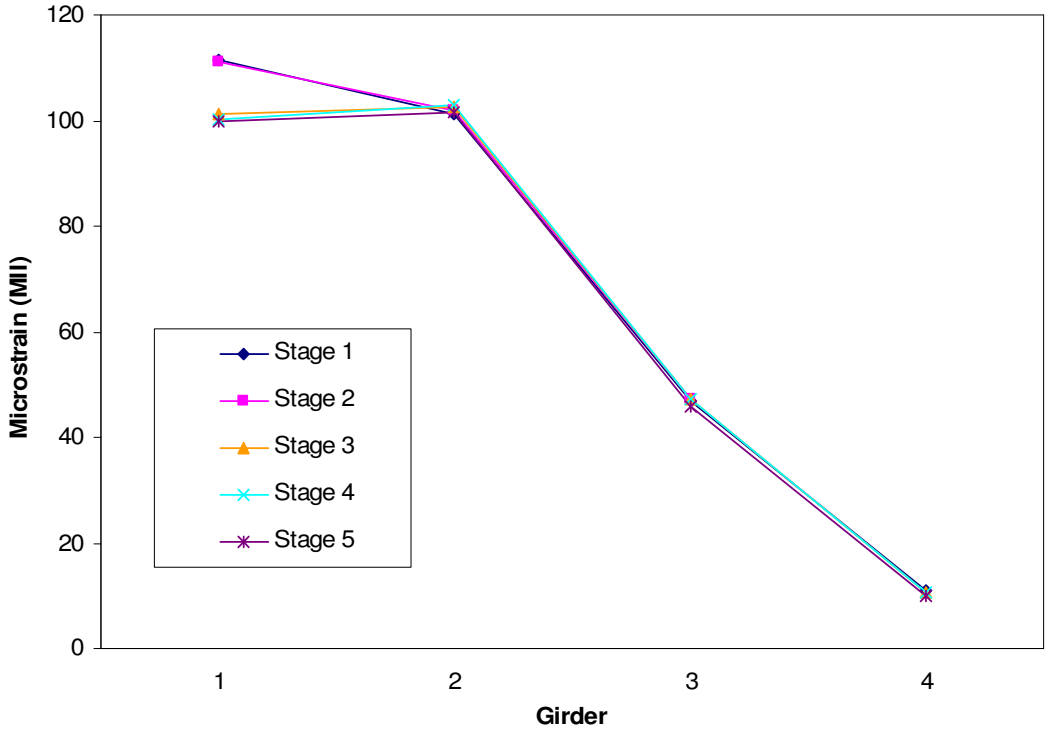

Figure 8.24. HCB Lane 1 Destructive Testing Strain Profile at Midspan.

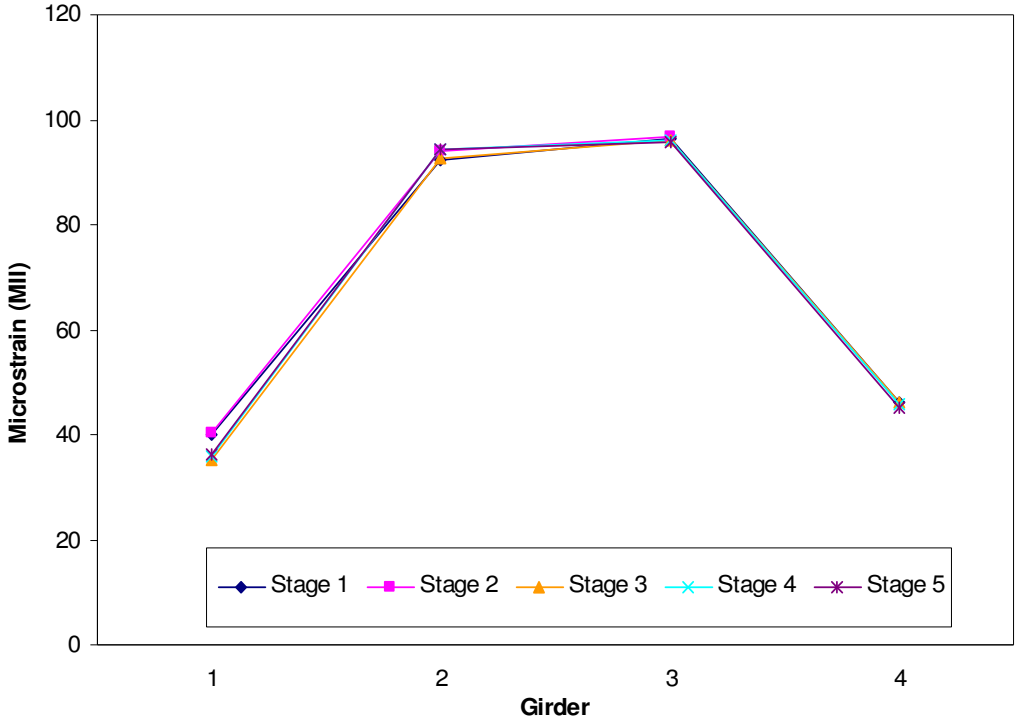

Figure 8.25. HCB Lane 3 Destructive Testing Strain Profile at Midspan.

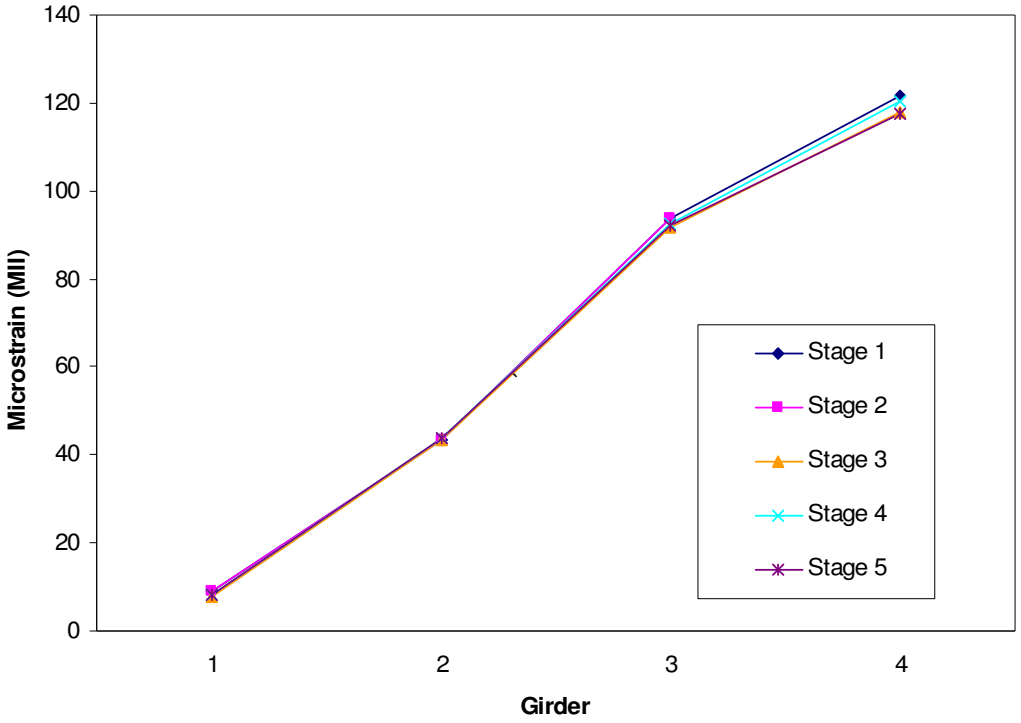

Figure 8.26. HCB Lane 5 Destructive Testing Strain Profile at Midspan.

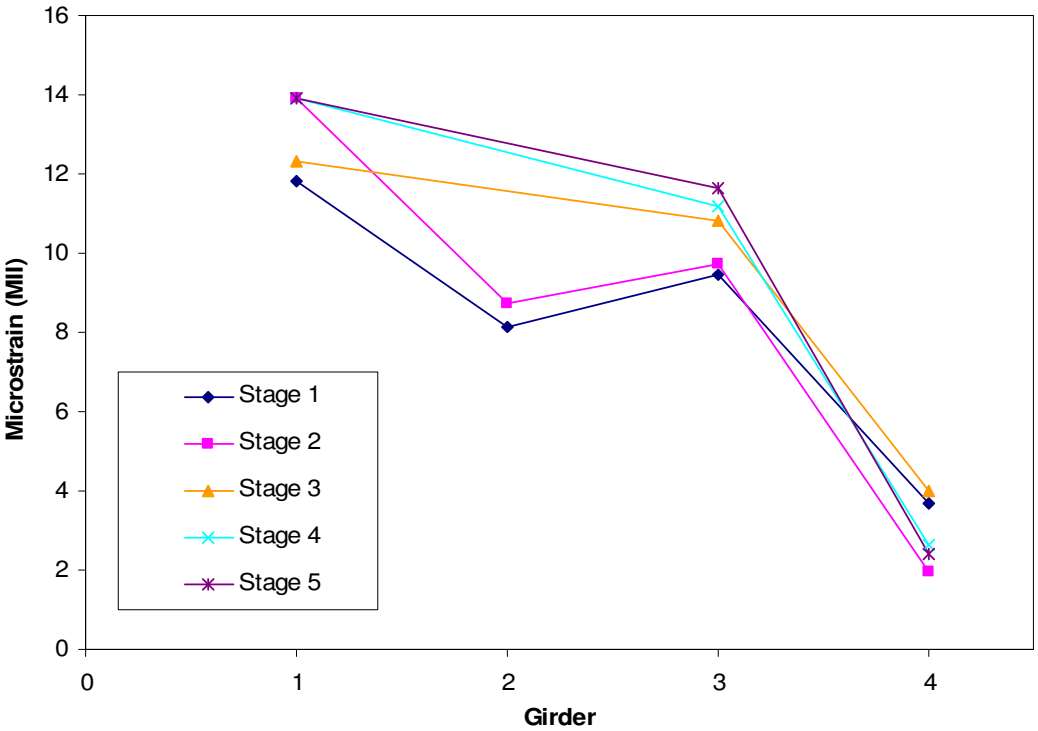

Figure 8.27. HCB Destructive Testing Lane 1 Strain Profile at East Abutment.

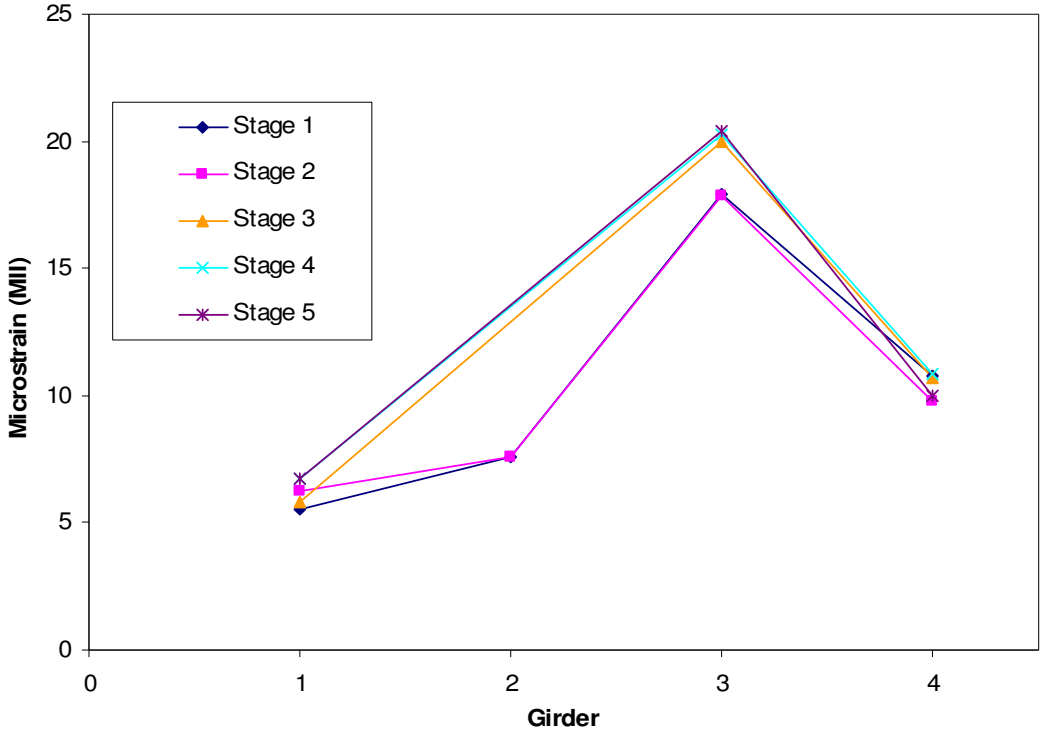

Figure 8.28. HCB Destructive Testing Lane 3 Strain Profile at East Abutment.

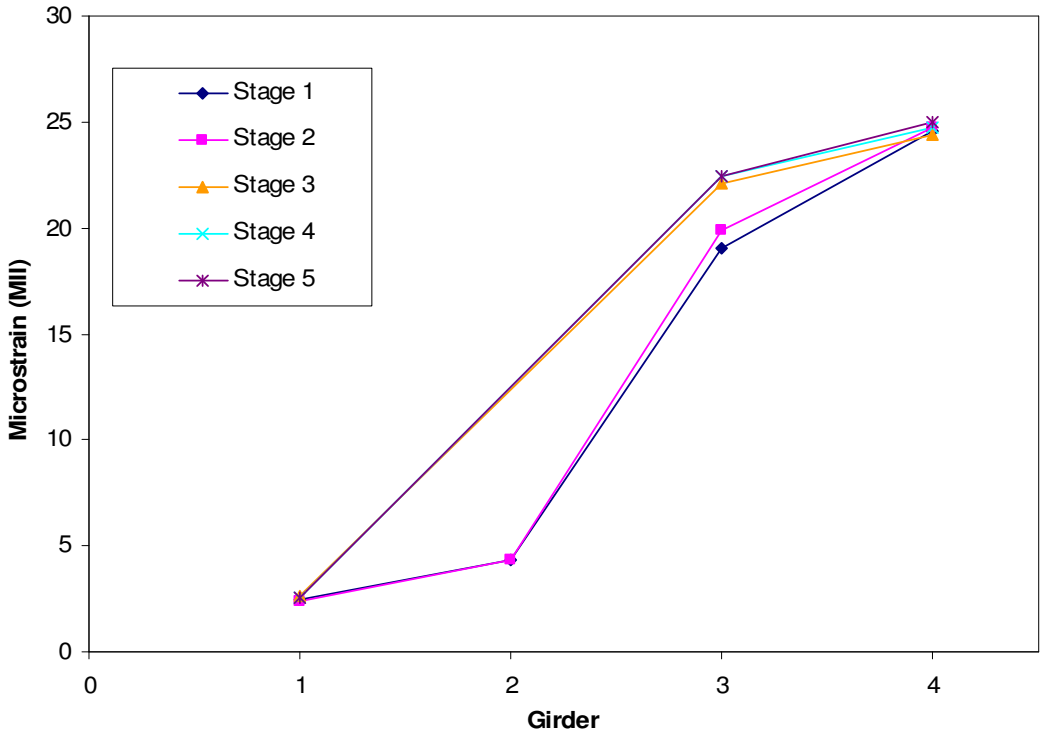

Figure 8.29. HCB Destructive Testing Lane 5 Strain Profile at East Abutment.

The difference in strains observed when the truck tandem centroid was located at the 1/8 span location for each girder was very minimal and therefore determined to be negligible. The fact that the strains observed at both the midspan and near the east abutment did not change with the removal of the pile elements indicated that the bearing restraint initially observed also remained essentially unchanged.

9. SUMMARY OF LOAD TESTING RESULTS

9.1 Factors Influencing Bridge Response and Ratings

There are many factors that influence a bridge rating; in an attempt to quantify an increased rating for the particular family of bridges investigated in this study, three main factors were investigated: live load distribution, partial composite action, and bearing restraint. The live load distribution was found to be very closely approximated using the analytical equations provided by AASHTO. Partial composite action was observed in each girder of the six bridges that were tested, however the degree of partial composite action not only varied from bridge to bridge but also from girder to girder in a given bridge. Finally, bearing restraint resulting from the support conditions of the girders was found to reduce the live load effect at the midspan of all of the bridges.

9.1.1 Live Load Distribution Summary

Differences in the live load distribution calculated using a codified approach and the actual live load distribution determined through load testing has been found to be a significant source of increased capacity. For the six bridges tested in this family though, the live load distribution was found to be very closely approximated using the AASHTO distribution equations. A summary of the live load distribution comparisons, the ratio of the actual live load distribution to the live load distribution factor determined using the AASHTO equations as described in the previous six chapters, is provided in Table 9.1. The average and standard deviation values for the live load distribution ratios provided in Table 9.1 are provided in Table 9.2. As shown in this table, the average single lane distribution factors calculated using the field test results were 11% and 33% higher than the live load distribution calculated using the AASHTO equations for the interior and exterior girders, respectively. The average exterior distribution factor ratios for the single and double lane loadings indicate nearly a 35% increase in the live load distribution compared to the AASHTO distribution equations.

Table 9.1. Summary of Live Load Distribution Ratios.

	BCB		MCB		KCB1	CCB		KCB2	HCB	
Girder	Single Lane	Two Lanes	Single Lane	Two Lanes	Single Lane	Single Lane	Two Lanes	Single Lane	Single Lane	Two Lanes
Interior	1.17	0.89	1.07	0.96	1.13	0.98	0.75	1.10	1.20	0.81
Exterior	1.00	1.03	1.11	1.14	1.31	1.60	1.68	1.42	1.54	1.67

Table 9.2. Live Load Distribution Ratio Average and Standard Deviation.

	Single Lane		Two Lanes	
Girder	Average	Standard Deviation	Average	Standard Deviation
Interior	1.11	0.08	0.85	0.09
Exterior	1.33	0.24	1.38	0.34

The interior live load distribution determined from the field test results was found to be less than that determined using the AASHTO equations for the two lane loading case as shown with an average ratio of 0.85. For all four bridges that were capable of carrying two lanes of traffic and thus rated accordingly, the actual live load distribution determined through field testing was more conservative than the live load distribution factors calculated using the AASHTO equations. Standard deviations for the exterior girders are indicative of a high degree of variability; however the interior girder standard deviations are indicative of a good correlation. Because of the differences in the average live load distribution ratios for the different girders and loading conditions (single and double lane loading), applying a factor to the AASHTO equations for the determination of the live load distribution of a previously untested bridge based on the field test results is not recommended at this time.

9.1.2 Partial Composite Action Summary

Partial composite action, defined simply as a girder having a neutral axis location somewhere between the non-composite and composite neutral axis locations, was observed in all six bridges tested. From the neutral axis locations calculated for each bridge, determined by interpolating between the top and bottom measured flange strains, there were some bridges, BCB, MCB, and HCB, that displayed symmetry and had similar neutral axis locations for all of the interior girders and for the two exterior girders. The neutral axis locations were similar across the bridge section but were not similar from bridge to bridge. The other three bridges: KCB1, CCB, and KCB2, did not have symmetry in their neutral axis locations across the cross section. This observed disparity in the neutral axis locations from girder to girder shows the high degree of variability in the degree of composite action.

Comparing the moment of inertia for each girder after optimization confirms the variability in the degree of composite action. The moment of inertia for each girder was optimized for each girder individually in each of the six bridges tested. An optimized moment of inertia similar to the moment of inertia for the girder alone would indicate non-composite action in the girder and an optimized moment of inertia similar to that of a girder and concrete deck acting together to resist bending would indicate composite action in the girder. The differences in the optimized girder moments of inertia confirm the high degree of variability observed in the neutral axis locations. Shown in Table 9.3 are the maximum and minimum degrees of partial composite action and the resulting difference in composite action determined from the optimized moments of inertia for each bridge. The percentages in this table are based on computed composite moment of inertia for each girder.

Table 9.3. Summary of Partial Composite Action

	BCB	MCB	KCB1	CCB	KCB2	HCB
Maximum	95%	116%	104%	122%	132%	118%
Minimum	39%	54%	43%	102%	75%	88%
Range	56%	62%	61%	20%	57%	30%

9.1.3 Bearing Restraint Summary

All of the bridges were designed assuming simply supported end conditions but the ends of each of the girders were cast into a concrete diaphragm, restraining the rotation of the girders. The bearing restraint induces an end moment on each end of the girder and thus reduces the midspan moment allowing for a potential increase in the live load carrying capacity of the bridge. To account for the bearing restraint, each bridge was modeled using rotational springs attached to the ends of each girder. Each spring was optimized but determining the degree of restraint based on solely the optimized rotational spring stiffness requires some additional analysis. To determine the degree of bearing restraint, the spring stiffness representing a fixed end condition must be determined. Using the results of this analysis on the BCB, a spring stiffness of about 10 million kip-in/rad represented a condition of approximately 95% fixity. The upper bound that was selected for the optimization of the spring constants was set at 1 million kip-in/rad, or about 65% fixed. There was a large range of values for the optimized spring constants for the six bridges ranging from 50,760 to 876,600 kip-in/rad. With the combination of a high degree of variability in the amount of bearing restraint and the relatively small value for the minimum optimized spring constant, relying on the bearing restraint to provide a viable factor for increasing a bridge rating is not recommended.

9.2 Bridge Rating Summary

Three different rating agencies, each using the Load Factor Rating method, calculated ratings for the six bridges using a codified approach. The three agencies produced slightly different ratings but provided a good correlation for the superstructure ratings. Using bridge optimization models that utilize the field test strain results for model calibration, Load Factor Ratings were calculated for the six bridges. As expected, the bridge ratings determined using the optimized models were larger than those calculated using the codified approach. A comparison of the percentage increases for both the interior and exterior girder ratings for the HS20 rating vehicle, for all six bridges, are displayed in Table 9.4. The smallest increase in rating from the codified approach to the optimized model approach observed in the interior girders on HCB was 29%.

Table 9.4. Percent Increase in Operating Bridge Ratings.

Bridge	Exterior Girder	Interior Girder
BCB	55	89
MCB	51	45
KCB1	68	130
CCB	166	72
KCB2	62	29
HCB	143	30

The previously discussed behavior characteristics could be predicted but their magnitude would require testing of a statistically significant sample of bridges. A factor that could be applied to previously untested bridges to modify their ratings could be determined through

further testing and analyses of bridges in this family. The fleet management concept for this fleet of bridges shows potential with all of the bridges having an increased rating after load testing.

10. CONCLUSIONS AND RECOMMENDATIONS

10.1 Summary

Diagnostic load tests were performed on six low volume bridges located on rural Iowa roads. Each of the six bridges that were tested were simple-span, zero degree skew, non-composite bridges with steel girders supporting a concrete deck. This bridge family was selected because they are often found to have a better live load response than determined theoretically which can result in an increase in their ratings. The results of the diagnostic load tests were used to calibrate analytical models of the bridges for rating purposes. All of the bridges were independently rated by three rating agencies using a codified approach. Those ratings were then compared to ratings calculated using a bridge model calibrated to the actual response of the bridge due to the load test. All of the bridges had an increase in ratings based on the results from the load tests.

An investigation of the effect of section loss in pile elements on the midspan strains was also conducted on a bridge that was scheduled for removal. Further investigation on the development of a load testing procedure for the substructure was also conducted in conjunction with the superstructure testing. The results for that aspect of testing can be found in Volume II of this report.

10.2 Conclusions

The following conclusions can be deduced from the load testing and analysis of six single span, non-composite concrete-steel bridges:

- All six bridges exhibited partial composite action without the presence of a mechanical shear connection between the steel girders and the concrete deck. The degree of partial composite action varied from bridge to bridge and even from girder to girder in each bridge. The degree of partial composite action from girder to girder for a given bridge ranged from 28% to 114%.
- There was significant end restraint observed in all of the bridges tested. With the ends of the girders cast into a concrete diaphragm, the degree of bearing restraint was a significant factor in reducing the induced moment at the midspan of the bridge for some of the bridges but was not consistent in all of the bridges.
- The live load distribution factors calculated using data from the field tests showed that the AASHTO equations for a single lane loading were slightly conservative but for the interior girders of the two lane loading case the actual live load distribution was less conservative than that predicted using the AASHTO equations.
- The experimental location of the neutral axis in exterior girders in all of the bridges were very close to and often higher than the composite neutral axis location. The curbs and railings were not included in the calculations for the theoretical composite neutral axis locations, which is probably the reason for the higher neutral axis locations in the exterior girders.
- Strains obtained from the optimized bridge models correlated very well with the strain data obtained from the bridge tests. A scale error between the strains from the

optimized model and those obtained from the load test was less than 10% and thus considered to be a good correlation.

- For the most part, there was transverse symmetry observed in the bottom flange strains in all the bridges when the test truck was centered on the bridge, but the optimized bridge parameters did not produce transverse symmetry across the girders. There was a high degree of variability in the girder moments of inertia.
- Based on the field data, all of the bridges were determined to have load ratings greater than those calculated using a codified approach. The BCB, KCB1, KCB2, and CCB had ratings that were limited by the exterior girders whereas, the MCB and HCB had ratings that were limited by the interior girders after optimization.
- The substructure condition did not appear to affect the load rating of the superstructure. Removal of pile elements in the HCB demonstrated that the girder strains were not affected at either the midspan or the abutment locations.
- Diagnostic load testing can be utilized to increase the load ratings for this family of bridges. All of the bridges had increased ratings due to the results of the load test with the smallest increase being an increase of 29%.
- Due to the variability of the optimized properties, particularly the girder moments of inertia, a reliable factor that could be applied to analytical ratings could not be determined. In addition, the sample size of six bridges was determined to be not large enough to produce a statistically reliable factor that could be applied to the theoretical ratings of additional bridges in this family without the aid of a diagnostic load test.

10.3 Recommendations

Recommendations for further investigation of the superstructures of non-composite steel girder bridges through diagnostic load testing are as follows:

- The testing of additional bridges in this family could help to refine the analysis and potentially produce a load factor that could be applied to bridges with similar geometries. The potential for the production of a load factor appears to be the greatest with the narrow, (single lane) five-girder bridges similar to KCB1 and KCB2 as those two bridges had very similar test results.
- Narrowing the family to include bridges with a given number of girders would assist in the development of a load factor that could be applied with confidence to similar untested bridges.

REFERENCES

American Association of State Highway and Transportation Officials, Manual for Maintenance Inspection of Bridges with Interim Revisions for 1985, 1986, 1987, 1988, 1989, and 1990, Washington D. C., American Association of State Highway and Transportation Officials, 1983.

American Association of State Highway and Transportation Officials, Guide Specifications for Strength Evaluation of Existing Steel and Concrete Bridges, Washington D. C., American Association of State Highway and Transportation Officials, 1989.

American Association of State Highway and Transportation Officials, Guide Specifications for Fatigue Evaluation of Existing Steel Bridges with Interim Revisions of 1993 and 1995, Washington D. C., American Association of State Highway and Transportation Officials, 1990.

American Association of State Highway and Transportation Officials, Manual for Condition Evaluation and Load and Resistance Factor Rating (LRFR) of Highway Bridges, Washington D. C., American Association of State Highway and Transportation Officials, October 2003.

American Association of State Highway and Transportation Officials, Manual for Condition Evaluation of Bridges with Interim Revisions for 1995, 1996, 1998, 2001, and 2003, Washington D. C., American Association of State Highway and Transportation Officials, 1994.

American Association of State Highway and Transportation Officials, LRFD Bridge Design Specifications, 2004, Washington D. C., American Association of State Highway and Transportation Officials, 2004.

Bakht, Baidar, Leslie G. Jaeger, "Bridge Testing-A Surprise Every Time," Journal of Structural Engineering, ASCE, Vol. 116, No. 5, May, 1990, pp. 1370-1383.

Bakht, Baidar, Leslie G. Jaeger, "Ultimate Load Test of Slab-On-Girder Bridge," Journal of Structural Engineering, ASCE, Vol. 118, No. 6, June, 1992, pp. 1608-1624.

Barker, Michael G., "Quantifying Field-Test Behavior for Rating Steel Girder Bridges," Journal of Bridge Engineering, ASCE, Vol. 6, No. 4, July/August, 2001, pp. 254-261.

Barker, Michael G., Cory M. Imhoff, W. Travis McDaniel, Troy L. Frederick, "Steel Girder Bridge Field Test Procedures," Proceedings 78th Transportation Research Board Meeting, Washington, D. C., 1999.

Bridge Diagnostics, Inc., "Load Testing and Load Rating Eight State Highway Bridges in

Iowa," Report submitted to Iowa Department of Transportation, November 1999.

Cai, Chun S., Mohsen Shahawy, " A Few Issues of Capacity Rating of Bridges From Field Measurements," Proceedings 80th Annual Transportation Research Board Meeting, January 7-11, 2001.

Chajes, Michael J., Dennis R. Mertz, Brett Commander, "Can Economical Bridge Testing Reduce Posting?" Better Roads, August, 1996, pp. 29-32/

Jauregui, David V., Joseph A. Yura, Karl H. Frank, Sharon L. Wood, "Field Evaluation of Deocmmissioned Non-Composite Steel Girder Bridge," Journal of Bridge Engineering, ASCE, Vol. 7, No. 1, January 1, 2002, pp. 39-49.

Klaiber, F. W., T. J. Wipf, C. M. Streeter, "Testing of Old Reinforced Concrete Bridges," Iowa Department of Transportation Project HR-390, Iowa State University, December, 1997.

Lichtenstein, A. G., "Bridge Rating Through Nondestructive Load Testing." National Cooperative Highway Research Program Project 12-28 (13)A, Transportation Research Board 1993.

Lichtenstein, A. G., "Bridge Rating Through Nondestructive Load Testing." Technical Report National Cooperative Highway Research Program Project 12-28 (13)A, Transportation Research Board 1993.

Moses, Fred, Jean Paul Lebet, Rolf Bez. "Applications of Field Testing to Bridge Evaluation." Journal of Structural Engineering, ASCE, Vol. 120, No. 6, June, 1994, pp. 1745-1761.

National Bridge Inventory, NBI Report, 2004, Online: nationalbridgeinventory.com, Available FTP: http://www.nationalbridgeinventory.com/nbi_report_200414.htm.

National Bridge Inventory, 2003 NBI Data, Online: midwestbridges.com, Available FTP: http://www.midwestbridges.com/2003-ia.html.

Pinjarkar, Suresh G., Otto C. Guedelhoefer, Barbara J. Smith, Robert W. Kritzler. "Nondestructive Load Testing for Bridge Evaluation and Rating." Final Report Raths, Raths, and Jonson, Inc., Willowbrook, Illinois, February 1990.

Schiff, Scott D., Terrence W. Philbrick, "Load Testing for Assessment and Rating of Highway Bridges," Phase I: Review of Current and Experimental Technologies and Practices, Clemson University Civil Engineering Department, South Carolina Department of Transportation: Research and Development Committee, September, 1999.

Schiff, Scott D., Terrence W. Philbrick, Thomas S. Peake, Joshua B. Hamby, "Load Testing for Assessment and Rating of Highway Bridges," Phase II: Development of a Highway

Bridge Load Rating and Assessment Program, Clemson University Civil Engineering Department, South Carolina Department of Transportation: Research and Development Committee, June, 2004.

Schultz, Jeffery L., Brett C. Commander, George G. Goble, "Determining Bridge Responses to Overweight Loads," Bridge Diagnostics, Inc., Wyoming Department of Transportation, March, 1998.